Interactive effects of vertical mixing, solar radiation and microbial activity on oceanic dimethylated sulfur cycling

Martí Galí Tàpias

23 d'octubre de 2012

Tesi presentada per obtenir el títol de Doctor per la Universitat Politècnica de Catalunya, Programa de Doctorat en Ciències del Mar.

Director: Rafel Simó Martorell

Universitat Politècnica de Catalunya (UPC),
Departament d'Enginyeria Hidràulica, Marítima i Ambiental
Institut de Ciències del Mar (CSIC)
Departament de Biologia Marina i Oceanografia

El Doctorand,
Martí Galí Tàpias

El Director
Rafel Simó Martorell

Abstract

Microscopic plankton thriving in the sunlit upper ocean play a key role in the biogeochemical functioning of the biosphere. The production and subsequent emission of volatile compounds is one of the numerous ways by which they participate in the cycling of elements and influence the Earth's climate. Dimethylsulfide (DMS), produced by enzymatic decomposition of the algal intracellular compound dimethylsulfoniopropionate (DMSP), is the more abundant organic volatile in the upper ocean. Its global emission amounts ca. 28 Tg S per year, and represents the main biogenic source of sulfur to the troposphere and about 30% of the total S emission (anthropogenic, biogenic and volcanic). Atmospheric oxidation of DMS contributes to atmospheric acidity, and is believed to promote the formation and growth of aerosols. Furthermore, DMS-derived sulfate aerosols have been suggested to cool the climate by reducing the amount of shortwave solar radiation reaching the Earth's surface by scattering solar radiation and, more important, by acting as cloud condensation nuclei. The 'CLAW' hypothesis postulates that, if oceanic DMS emission was in turn stimulated by solar radiation, a regulatory feedback mechanism could operate between marine plankton and the radiative budget over the oceans.

However, the relationship between DMS emission and solar radiation is not straightforward, since a number of biochemical and photochemical transformations come into action from the moment DMSP is synthesized by phytoplankton until DMS is emitted. These transformations are intimately linked to the physical environment, the ecological setting and the microbial interactions, rendering the picture of dimethylated sulfur cycling a lot more complicated. Surprisingly, though, the seasonal cycle of seawater DMS concentration seems to follow that of solar radiation in the majority of oceanic regions, regardless their productivity regimes. This characteristic feature of oceanic DMS, while broadly accepted, is not yet well understood. The premise of this thesis is that, to understand this emerging pattern, we need to understand what regulates the DMS production and consumption processes and

their balance (that is, DMS budgets). To this end, we have studied the response of biotic and abiotic DMS cycling to solar radiation by means of incubation experiments. At another level, we have studied the response of ecosystem DMS budgets to different radiation climates, and from polar to subtropical areas. Since the depth of the upper mixed layer regulates the amount and spectral composition of the 'light' seen by the cells and molecules, our studies have been backed by a careful characterization of underwater radiation fields and vertical mixing dynamics.

Our results show that solar radiation has a stimulating effect on gross DMS production. Moreover, the stimulation is more effective at shorter and more energetic wavelengths, particularly in the ultraviolet (UV) region. Among the potential explanations, direct DMS production and/or increased DMSP release by UV-stressed phytoplankton is the most plausible mechanism, and fits with the putative antioxidant function of DMS and its metabolites. In such stress conditions, the role of bacterial metabolism and microzooplankton grazing on DMS production seems to be secondary. At the ecosystem level, we have shown that vertical mixing-mediated solar exposure regulates whether DMS is preferentially oxidized by bacteria or by photochemical reactions. The outcome of this competition between DMS sinks is that total DMS loss rate constants vary little across oceanic biomes. As a result, the seasonal and also the short-term variability in DMS concentrations respond mainly to gross DMS production. The stress response occurs at different temporal scales: seasonally, through the succession of microbial communities towards stronger DMSP producers and higher DMS yields in summer stratified waters; and across day-night cycles, where short-term radiative stress modulates DMSP to DMS conversion yields. The thesis is closed by a literature meta-analysis, which places our results among the existing literature, and improves our current understanding of the distinct DMS(P) cycling regimes and their links with the ecological geography of the sea.

Contents

List of Figures

List of Tables

Introduction

0.1 Climate, biogeochemical fluxes and feedbacks

Solar radiation drives the dynamics of the fluid envelopes of our planet and supplies the external energy required to sustain the biosphere (Margalef, 1997). The latitudinal gradient in solar heating, influenced by the Earth's rotation and constrained by the continental masses, produces the planetary-scale patterns of coupled oceanic and tmospheric circulation as a response seeking to restore physical equilibrium (Mann and Lazier, 2006). The ensuing geophysical fluxes of heat, freshwater and momentum conform what we know as the climate system. The way solar radiation is transmitted, reflected or absorbed by the atmosphere, water bodies and land -the Earth's radiative budget-, has a profound influence on the climate system.

The appearance of life on Earth revolutionized the fluxes of materials among the gaseous, aquatic, and solid compartments of the planet, due to the evolution of enzymes capable of accelerating the kinetics of chemical reactions by several orders of magnitude (Schlesinger, 1997). This resulted in a highly active circulation of the elements that form living tissues or that participate in biochemical reactions, what we call the *biogeochemical cycles*. Microbial activity modified the chemical composition of the outer covers of the planet and drove them away from thermodynamic equilibrium by means of sustained energy dissipation (Lovelock and Margulis, 1974). The most prominent example is found in the chemical composition of the atmosphere, which became oxidant when photosynthetic cyanobacteria started releasing molecular oxygen. In turn, the availability of oxygen was key to the posterior evolution of more complex eukaryotic and metazoan organisms that further influenced the conditions on the Earth's surface.

The climate system is characterized by its pulsating nature, which occurs at different timescales: day-night cycles, seasonal cycles, decadal or centennial oscillations, all the way up to to the millennial changes in solar forcing that cause glacial-interglacial cycles. Biological

activity, from organisms to ecosystems, couples to these fluctuations and can act to dampen or amplify them. This can cause the conditions on the Earth's surface to oscillate around a stable state or, occasionally, to shift to a different state. A timely example of a positive or self-accelerating feedback is the greenhouse effect produced by anthropogenic CO_2 release, and the multiple side-effects and feedbacks it generates (IPCC, 2007). On the other hand, feedback mechanisms can also tend to restore the original conditions, being then called negative or self-regulating feedbacks. The Gaia theory (Lovelock, 1995) goes a step further and postulates that the entire biosphere (the entity formed by the Earth's biota and the atmosphere, oceans, sediments, soils and crustal rocks) forms a self-regulating system that keeps the planet in an habitable state.

In the original Gaia hypothesis, the homeostasis of the biosphere was achieved mainly by regulating the composition of the atmosphere (Lovelock and Margulis, 1974). In 1987, Charlson *et al.* proposed that a negative feedback could operate between the emission of the gas dimethylsulfide (DMS) by marine plankton and its effects on the Earth's radiative budget, through the formation of aerosols and clouds. This hypothesis, known as CLAW after the author's initials, became an emblematic Gaian mechanism that boosted research on both its marine and atmospheric sides. This thesis is largely based on its legacy.

0.2 Microbes in motion: pelagic ocean biogeochemistry

Oceanic currents do not only carry heat and salt, but also an endless list of inorganic and organic compounds and a myriad of microorganisms. Despite being small-sized and relatively diluted, the fact that the oceans cover more than two thirds of the planet grants planktonic microorganisms a globally important role. For example, marine phytoplankton account for about half of the global annual carbon (C) fixation into biomass -net primary production (Field et al., 1998). The regional and seasonal distribution of phytoplankton depends on the supply of nutrients by turbulent vertical mixing to the sunlit upper layers. It can be said that hydrodynamics drive pelagic productivity and plankton biogeography, a feature that was soon recognized by early oceanographers (Sverdrup et al., 1942; Longhurst, 2007) (Fig. 1). Along with primary producers, bacterioplankton, zooplankton, and virioplankton complete this somewhat sketchy picture of pelagic food webs, which are globally responsible for at least half of the biospheric respiration, transforming organic carbon back into energy, water and CO_2 (del Giorgio and Duarte, 2002). The pelagic ecosystem leaves a deep imprint on the biogeochemical

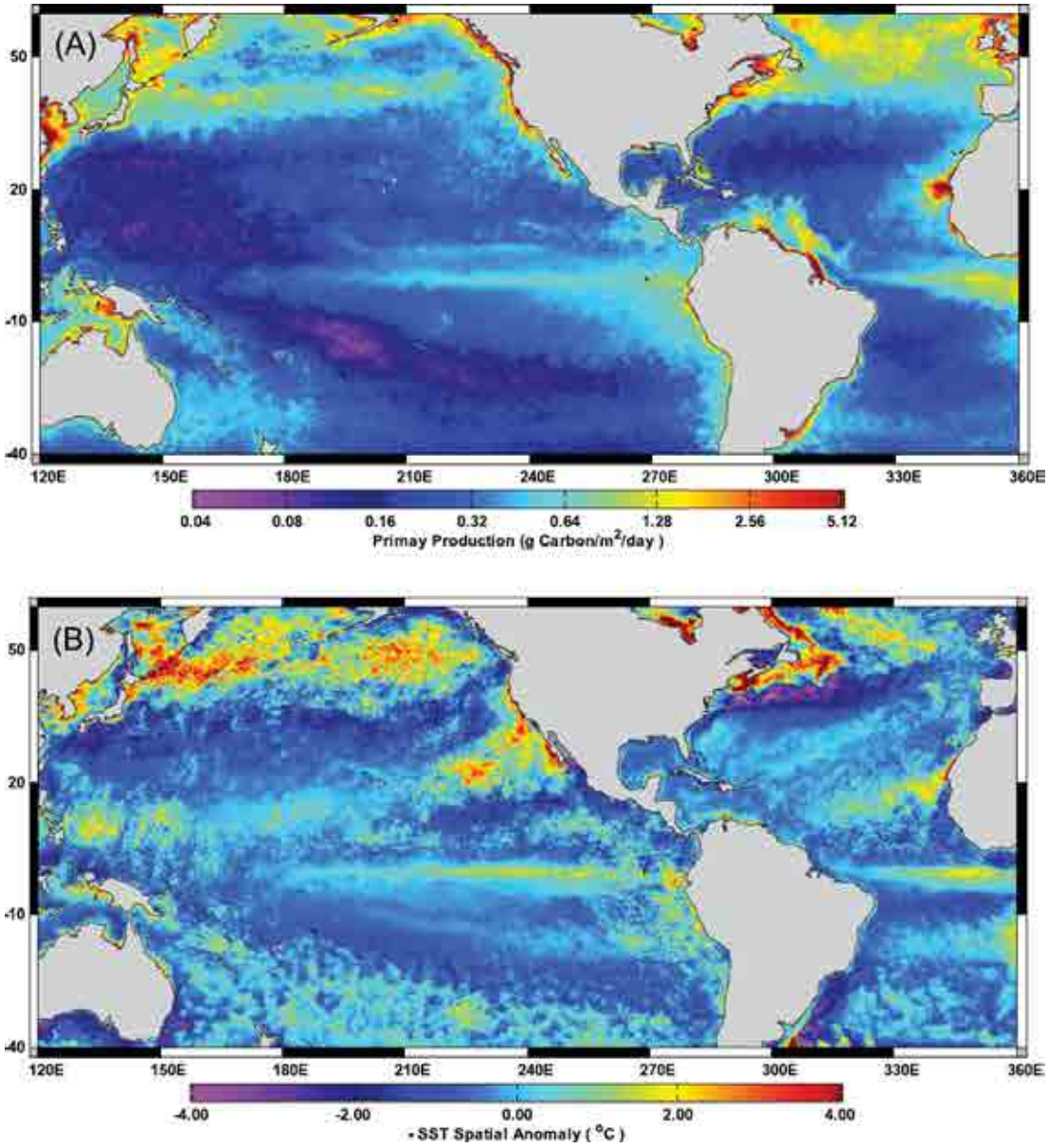

Figure 1: **Hydrodynamics drive phytoplankton productivity** - (A) Patterns of primary production in the Pacific and Atlantic oceans in July 2006, calculated from remotely-sensed chlorophyll (SeaWIFS) with the algorithm of Behrenfeld and Falkowski (1997); (B) spatial sea surface temperature anomaly; from Kolber (2007).

processing of elements other than carbon, like the major constituents of living biomass (N, P, and S, plus H and O), the elements forming the mineral shells of some organisms (Si, Ca Mg and Sr), and micronutrients like Fe and other trace metals.

The upper mixed layer (UML) of the ocean is the scenario for energy and matter exchanges between the atmosphere, the deep ocean, and the continents (Fig. 2). Many of these processes are mediated to a variable extent by microorganisms and, very often, they are promoted or affected by sunlight. Photosynthesis-derived organic matter that escapes from being utilized in the UML sinks to the dark mesopelagic waters, where it is remineralized to inorganic nutrients that will eventually return to the surface. Dissolved organic matter carried by continental runoff is microbially and photochemically processed in the UML, being finally mineralized or transformed into recalcitrant molecules and transported to the deep ocean. Inorganic gases (CO_2, O_2, N_2, N_2O) but also organic volatiles (DMS, isoprene, acetone, methanol, organohalogens, and a long list) are exchanged across the sea-air interface before or after being utilized or produced by microorganisms (Simó, 2011). A variety of particles are also actively exchanged across this interface: bubble burst ejects droplets tat contain sea salt, hydrophobic organic compounds, entire cells, detrital particles, and colloidal material (Leck, 2005; Orellana et al., 2011). Continental air masses can carry onto the ocean surface pollution-derived compounds as well as dust rich in Fe, which is the element that limits primary production in vast areas of the ocean (Boyd et al., 2007). In turn, trace metals suffer UV-catalyzed redox reactions that modify their bioavailability (or toxicity). The depth of the UML, together with underwater light attenuation, determine the average radiation field seen by the cells and materials and thus many of the processes listed above.

The role of microorganisms in biogeochemical models has been traditionally represented by rate constants in bulk equations. Emerging molecular tools are now allowing to open the black box of microbial diversity and function. However, the revolution brought by the different '-omics', and the overwhelming amount of information associated, is far from being implementable into biogeochemical models (Doney et al., 2004; Gasol et al., 2008). In the field of phytoplankton ecology, though, our knowledge of fundamental processes, rooted in earlier works (Margalef, 1978; Chisholm, 1992; Reynolds, 1994), is starting to yield sensible predictions of the organism's biogeography and functional diversity (Le Quéré et al., 2005; Follows et al., 2007). Bridging the gap between genotypes, phenotypes, ecological interactions, and actual biogeochemical rates, as modulated by environmental forcing, is one of the most exciting tasks ahead for

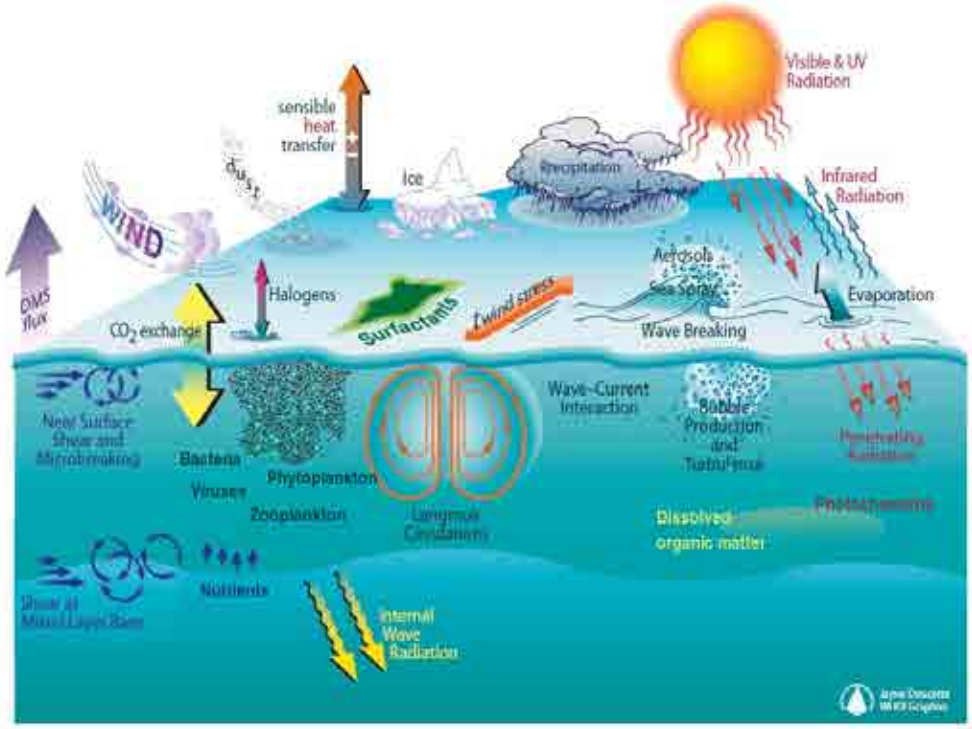

Figure 2: **The key role of the upper mixed layer** - The UML regulates the energy and matter fluxes between the atmosphere and the ocean's interior; modified from McGillis (2005).

biogeochemists. Dimethylated sulfur cycling provides an outstanding example of how specific ecosystem functions are intertwined with microbial food web dynamics and physical forcing.

0.3 Vertical mixing, radiation climate, and microbial activities in the upper ocean

0.3.1 Vertical mixing in the upper ocean

Planetary boundary layers are turbulent layers that form at the interface between the ocean and the seafloor, the atmosphere and emerged land, and at both sides of the ocean-atmosphere interface. Their thickness is defined by the maximum vertical penetration of boundary layer eddies. Differently said, eddy diffusivity and the rate of kinetic energy dissipation are much higher within such layers than in the fluid interior (Large et al., 1994). The depth of the oceanic UML reflects the balance between stabilizing and destabilizing forcing, mainly of atmospheric origin. Stabilizing forcing results from turbulence dissipation and positive buoyancy fluxes (heat

or freshwater gains), whereas destabilizing forcing results from wind stirring (shear stress) and negative buoyancy fluxes (heat or freshwater losses). Other processes that affect UML dynamics by causing shear instability are breaking internal waves, tides, fronts, and bottom roughness.

Wind shear stress (τ), or the rate of momentum transport at the air-water interface, is usually parameterized as the product of air density (ρ_a), a drag coefficient (C_{10}), and the squared wind velocity (U_{10}), the latter two normalized to 10 m above sea level:

$$\tau = \rho_a C_{10} U_{10}^2 \tag{1}$$

where the product $C_{10}U_{10}^2$ is named the friction velocity (U^*). The net buoyancy flux (B_{net}) results from the balance between the heat flux (B_{heat}) and the salinity flux, the latter determined by the balance between precipitation (P) and evaporation (E) rates:

$$B_{net} = B_{heat} + B_{precip} - B_{evap} \tag{2}$$

or

$$B_{net} = \alpha(C_p\rho_w)^{-1}Q_{net} + \beta S_0(P - E) \tag{3}$$

where α and β are the thermal and haline coefficients of expansion of water, C_p is the heat capacity, ρ_w is the density of seawater, S_0 is the reference surface salinity, and Q_{net} is the net radiative flux (Anderson et al., 1996). In turn, the net radiative flux depends on a number of processes (Fig. 3):

$$Q_{net} = Q_{SW} + Q_{LW} + Q_S - Q_L + Q_V \tag{4}$$

where Q_{SW} is the shortwave energy flux (absorbed irradiance), Q_{LW} is the net flux of longwave (infrared) radiation from the sea, Q_S is the sensible heat flux out of the sea due to conduction, Q_L is the latent heat carried away by evaporated water, and Q_V is the heat advected by currents.

Depending on the relative strength of wind shear and buoyancy fluxes, mixing will be mostly driven by wind stirring or by convection. Although average global wind fields are quite predictable, local wind forcing will depend on the passage of atmospheric fronts, on wind-current interactions at the ocean's surface and, in small marine basins, on local conditions, adding an important stochasticity in wind forcing. Instead, the radiative flux is rather predictable from the daily cycle of solar irradiance. During the day, absorption of shortwave radiation heats

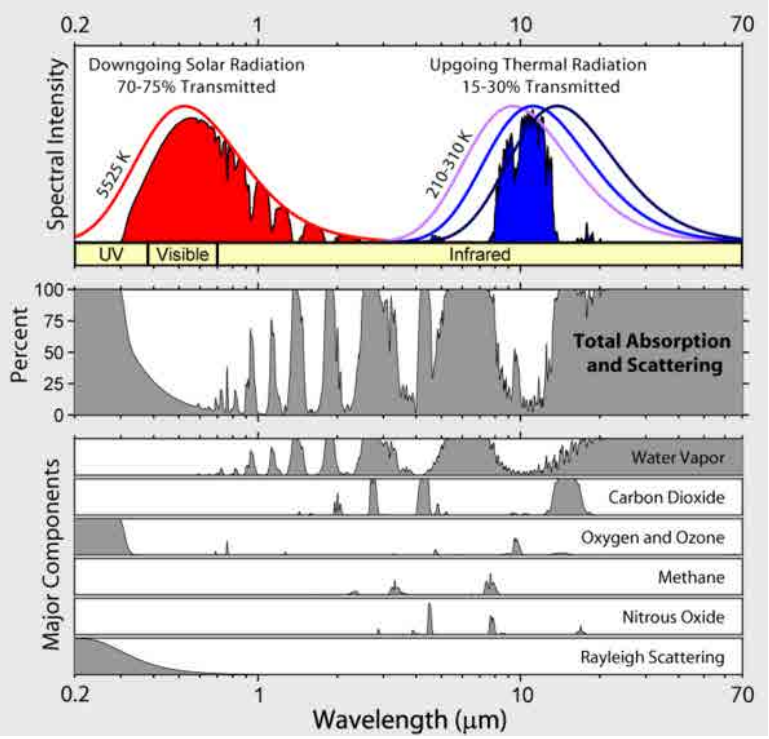

Figure 3: **Spectra of incoming and outgoing solar radiation** - Solar radiation is absorbed and scattered by atmospheric gases and particles before being abosrbed by land and ocean surfaces and partially re-emitted; modified from Wikipedia.

surface water to the point that mixing is frequently suppressed. At night, the sea surface is cooled by radiative losses in form of infrared radiation and sensible and latent heat. When surface waters become denser than the water below the water column becomes unstably stratified, triggering convective overturning (Fig. 4). Physical measurements of turbulence in the UML have shown that mixing is a rather intermittent phenomenon (Brainerd and Gregg, 1995; Piera, 2001; DAsaro, 2002). Most of the time, turbulence in the UML may be at lower (background) levels. This means that, even when uniform vertical profiles of temperature, salinity, density or other properties are observed, the homogeneous layer needs not be undergoing active mixing.

Different definitions of mixed layer may be useful depending on which time frame is more relevant to the processes under study. It is common to distinguish between the actively mixing layer (the 'depth horizon that is being mixed at present'), and the mixed layer (defined as the 'deepest penetration of surface mixing during a given time frame') (Fig. 4). In practice, though , it is difficult to identify an actively mixing layer (if any) from conventional temperature-salinity CTD profiles (Brainerd and Gregg, 1995). The distinction between mixing and mixed layers,

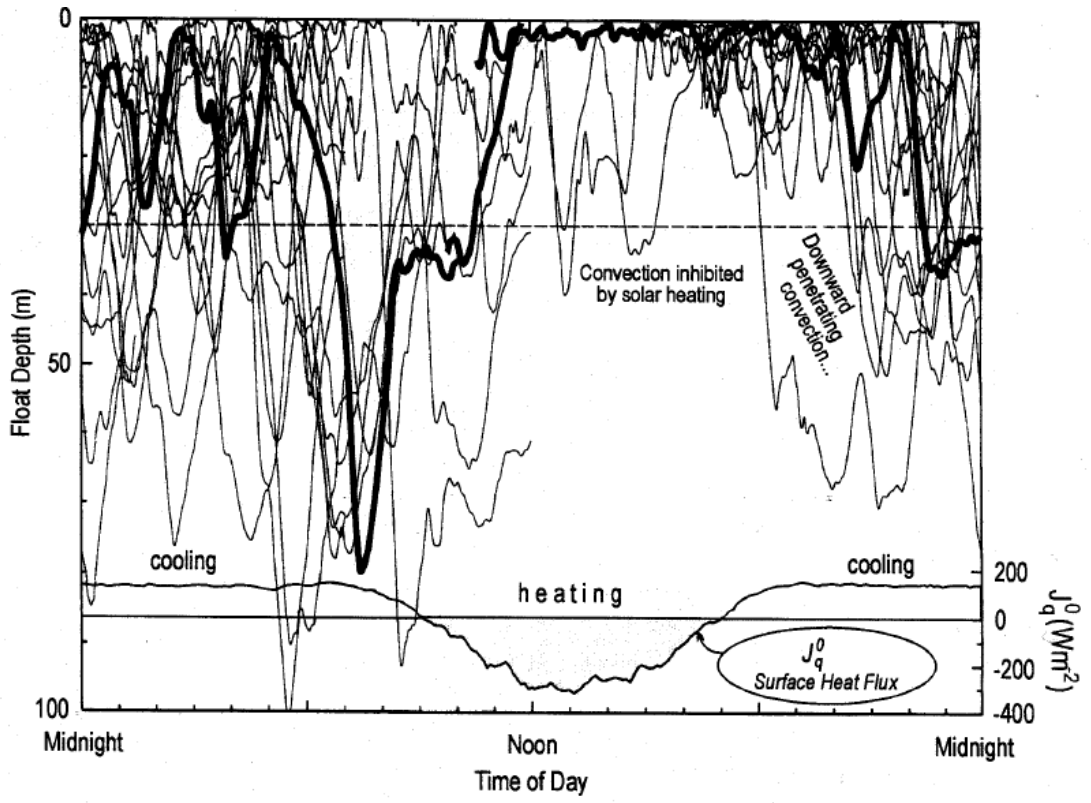

Figure 4: **Diurnal cycles of vertical mixing** - Schematic of the time vs. depth distribution of floats released at various times during a diel cycle of nocturnal mixing and diurnal stratification in the Labrador Sea. Since the floats have near-neutral buoyancy, their trajectories track the turbulent movement of water parcels within the mixing layer, resembling the possible trajectories of non-motile plankton; from Neale et al. (2003), after unpublished data by D'Asaro and Dairiki).

and the different time scales they have associated, will be relevant when discussing the effects of mixing on photobiological and photochemical processes.

The depth of the mixed layer changes seasonally in conjunction with solar irradiance and meteorological forcing (Fig. 5), and shapes the seasonal cycles of pelagic productivity (Longhurst, 1995). Below the seasonal mixed layer there is a permanent pycnocline which, depending mainly on the latitude, will be salinity- or temperature-stratified: "because low-latitude oceans gain heat while high-latitude oceans loose heat, and because water inexorably evaporates in warm regions and condenses in cold, the upper layers of subtropical seas are permanently stratified mainly by temperature, while the upper layers of high-latitude seas (and the equatorial belt) are permanently stratified mainly by salinity" (Carmack, 2007). These modes of permanent stratification shape climate processes like sea-ice formation (which cannot occur in

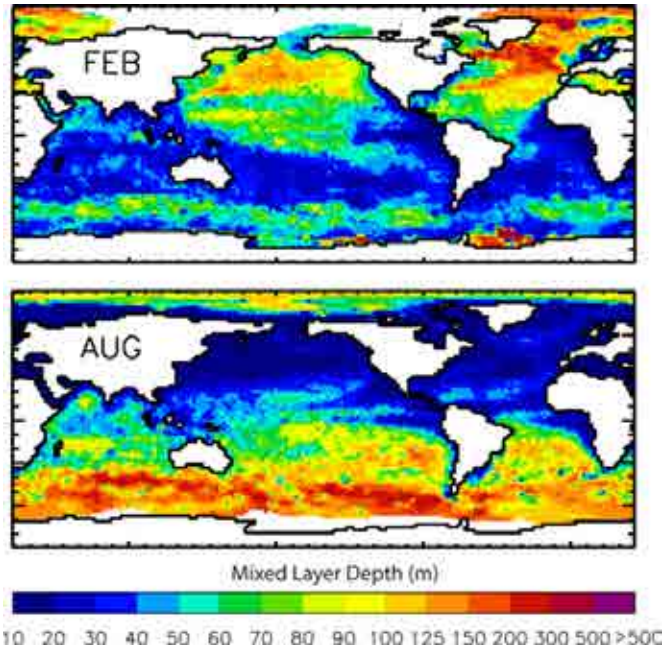

Figure 5: **Global mixed layer depth climatology** - Mean monthly values of the MLD in the global ocean for the months of February and August; modified from de Boyer Montégut (2004).

thermally-stratified oceans) or ocean ventilation by deep convection (which cannot occur in salinity-stratified oceans) and, in consequence, affect plankton biogeography.

0.3.2 What governs underwater light extinction?

The radiation climate in the surface layer of the ocean depends on atmospheric radiative transfer, reflection and refraction at the air-water interface, and underwater radiative transfer, all of which are tightly dependent on the solar elevation with respect to the ocean's surface. The solar spectrum is well described by that of a black body emitting at 5000 K, with a peak at around 500 nm, and extends between 250 and 3000 nm (Fig. 3). At the top of the atmosphere, the energy reaching a surface perpendicular to the radial direction from the sun is approximately 1394 W m^{-2}. For practical purposes, the solar spectrum is divided in three major regions that are associated to different processes: ultraviolet (UV, 200-400 nm), visible (VIS, 400-700 nm; named *photosynthetically available radiation* -PAR- by the photosynthesis research community), and infrared (IR, >700 nm), sorted from more to less energetic. In the stratosphere, the most energetic UV (UVC, 200-280 nm) and the shortwave portion of UVB (280-320 nm) are absorbed by photochemical reactions in the ozone layer, so that only radiation with wavelengths longer

than 300 normally reaches the Earth's surface. Since shorter wavelengths suffer proportionally more molecular (Rayleigh) scattering, they have a bigger chance of being absorbed before completely crossing the atmosphere. For this reason, solar radiation is enriched in the shortwave fraction at high solar elevations (that is, small zenith angles). In the IR, significant atmospheric absorption occurs at different bands due to water vapor and other 'greenhouse' gases like CO_2 (with smaller contributions of methane and nitrous oxide). The overall effect of all these processes is that solar radiation is relatively enriched in the VIS region after crossing the atmosphere (Fig. 3). Cloudiness is another important factor affecting the intensity and spectral distribution of solar energy. Although clouds generally cause an overall decrease in radiation intensity, different types of clouds with different geometries and microphysical properties can cause a relative enrichment in UV wavelengths, or even enhance sea-level irradiance (Bordewijk et al., 1995; Calbó et al., 2005).

At the water surface, the amount of photons being reflected increases sharply from about 2% with a vertical sun to almost 100% at low solar elevations, according to Fresnel's law. At intermediate to low solar elevations, sea-surface roughness acts to decrease reflectance (Kirk, 1994). According to Snell's law of diffraction, the angle of the solar 'beam' becomes more vertical after crossing the air-water interface. Once in a water body "there are only two things that can happen to photons: they can be absorbed or they can be scattered" (Kirk, 1994). Absorption and scattering of photons can be described by relatively simple physical laws (like the Lambert-Beer law of absorption), and are therefore called the *inherent optical properties* (IOPs), which depend solely on the optical properties of seawater and the concentration of dissolved, colloidal and particulate constituents it carries. The IOPs include the absorption coefficient and, since scattering is a tridimensional proces, the volume scattering functions (from which the scattering coefficient is derived). On the other hand, due to the tridimensional nature of light fields, knowing the IOPs is not enough for determining the photon flux received at a point from each direction of the space. The *apparent optical properties* (AOPs) are those describing the light field in a statistical manner; for example, the *radiance reflectance* (R), which describes the fraction of radiation being reflected in one direction of the space, or the the *mean radiance cosine* (μ), which describes the mean angular distribution of photons.

Different variables can be used to describe the underwater photon flux: the *radiance* (L) is the photon flux in a direction of the space (through an infinitesimal solid angle). Integration of radiance over all directions about a point yields *scalar irradiance* (E_o), which has units of photon flux per surface area. Scalar irradiance gives equal weight to photons coming from all

directions of space and, in consequence, is the variable of interest for modeling photochemical processes, including photosynthesis. When the integration is done over the upper or lower hemisphere, it yields *downwelling* or *upwelling* scalar irradiance, respectively. Furthermore, irradiance is often expressed as the photon flux received on a flat surface, which is called *cosine irradiance* (E_d, if downwelling). Unlike scalar irradiance, E_d gives a different weight to the photons depending on their direction with respect to the plane. The average cosine of the light field (μ) is the parameter relating cosine and scalar irradiance (Kirk, 1994).

Depending on the wavelength considered and the amount of attenuating components, the downwards penetration of solar radiation can vary between few centimeters and down to 200 m. The *attenuation coefficient of downwelling irradiance* (K_d) is the variable that describes the vertical extinction of irradiance, which approximately follows an exponential decay:

$$K_d = \frac{d(ln(E_{d,z}))}{dz} \tag{5}$$

where z is depth and $E_{d,z}$ is downwelling irradiance at depth z. Although K_d is a property of the light field (Kirk, 1994) it bears a direct relationship with the total attenuation coefficient, which is an IOP (Gordon, 2008). The total attenuation coefficient (c) is the sum of absorption coefficients (a) and the backwards component of scattering -backscattering (b_b): $c = a + b_b$. The absorbing components include pure water (a_w); colored (or chromophoric) dissolved organic matter -CDOM (a_{CDOM}); and particles. Particulate absorption is frequently split in two components: phytoplankton pigments (a_{phy}) and detritus (a_{det}). Scattering is caused by particles ($b_{b,p}$) and by water itself ($b_{b,w}$). Absorption and scattering generally have a strong spectral dependence: photons of different wavelengths will be preferentially absorbed by different molecules, and scattered by particles of different size and geometry (Fig. 6).

The relative importance of radiation attenuation by algal particles, non-algal particles and CDOM has led scientists to develop optical classifications of oceanic waters. A first classification with several categories was proposed by Jerlov (1976). However, the simpler classification with two categories proposed by Morel and Prieur (1977) is the more widely used at present. This classification roughly distinguishes between oceanic and continentally-affected waters, respectively named case 1 and case 2. Waters with continental influence have a proportionally higher content of CDOM and non-algal particles while, in oceanic waters, attenuation is dominated by algal particles and their pigments. These classifications are largely based on the visible domain because, when they appeared, precise underwater UV measurements suffered from technological

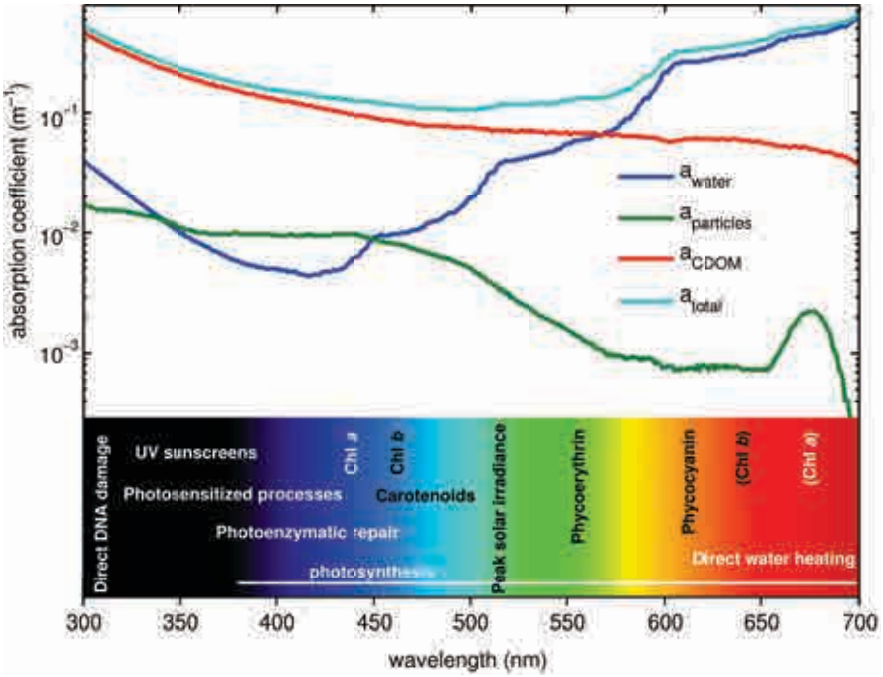

Figure 6: **Absorption of solar radiation in the ocean** - Spectral absorption coefficients: absorption due to water, colored dissolved organic matter (CDOM), particles (mainly phytoplankton), and the sum of them. The a_{CDOM} and $a_{particles}$ spectra are real data from the Mediterranean in late summer (September 2011, SUMMER I cruise, provided by G. Pérez). Relevant processes promoted by each radiation band are shown in the lower bar together with the absorption peaks of some algal pigments.

limitations. Besides, the visible region is more relevant than the UV for remote sensing applications. Other classifications including the UV region, where absorption by CDOM generally prevails, might be useful regarding biogeochemical processes promoted by UVR.

0.3.3 Importance of light exposure and mixing regimes for microbial plankton activity

The microorganisms thriving in the surface ocean have evolved in a sunlit environment, and have developed adaptations to make the most out of light and its changing availability. The most extensively studied process among those mediated by light is photosynthesis. In marine and freshwater phytoplankton, the tradeoffs between cell size and morphology, growth rates, and light and nutrient acquisition strategies have led to different evolutionary solutions, which are intimately connected to ecological niches defined by vertical mixing (Margalef, 1978; Litchman and Klausmeier, 2008). But solar radiation is used as a resource by organisms other than

phytoplankton. Good examples are the photoheterotrophic metabolisms of bacteria that possess proteorhodopsin (Béjà et al., 2000; Gómez-Consarnau et al., 2007) or bacteriochlorophyll (Kolber et al., 2000; Hojerová et al., 2011). As knowledge progresses, the frontiers between auto- and heterotrophic metabolisms are blurring. For example, it has been known for a long time that many phytoplankton are not strict photoautotrophs: some are actually mixotrophs (that prey on other phytoplankton or bacteria; (Bird and Kalff, 1986; Unrein et al., 2007) or display photohereotrophic activity (they take up organic molecules to supplement their diet; (Hellebust and Lewin, 1972)). For organisms that do not use light as a primary resource, it still constitutes a key environmental cue that regulates their physiology and behavior (Bell-Pedersen et al., 2005).

Exposure to high PAR irradiance generally co-occurs with exposure to more energetic UV wavelengths. UVB radiation is strongly absorbed by nucleic acids, thereby causing direct damage to organisms through mutation and by interfering with replication and transcription (Vincent and Neale, 2000). UVB and UVA (320-400 nm) absorption by pigments and certain protein sites results in a chain of reactions that produce short-lived oxygen radicals and longer-lived hydrogen peroxide (H_2O_2). These molecules are collectively named *reactive oxygen species* (ROS) because they can cause indirect oxidative damage to proteins and lipids. Damage to proteins will severely impair some cellular functions (like photosynthesis), while damage to lipids will 'compromise' cell membranes, that is, make them 'leaky' and thus unable to regulate cell-environment exchanges. The strategies evolved by organisms to cope with radiative stress caused by elevated PAR and UVR include behavioral avoidance, physiological protection, repair, and acclimation (Roy, 2000). Among plankton, avoidance through vertical migration is only possible in motile organisms that are big enough to overcome the viscous force of water, like some zooplankton and dinoflagellates. By means of circadian clocks (Bell-Pedersen et al., 2005), the organisms can anticipate radiative stress and conduct sensitive functions like cell division at night, in what can be seen as a more passive kind of avoidance. In the end, though, microbial plankton have to rely on protection and repair mechanisms.

Photoprotection can be achieved by means of antioxidant enzymes like catalase, superoxide dismutase, or ascorbate peroxidase; sunscreen compounds like mycosporine-like aminoacids (Garcia-Pichel, 1994; Sinha et al., 2007); and ROS-scavenging compounds like ascorbic acid, glutathione, tocopherol, carotenoids (that also participate in photosynthesis and in excess energy dissipation processes like the xantophyll cycle) (Lesser, 2006), or dimehtylsulfoniopropionate plus its metabolites (Sunda et al., 2002). Sunscreens and some ROS scavengers can be acquired

through the diet by organisms that cannot synthesize them de novo (Tartarotti et al., 2001; Lesser, 2006). Repair mechanisms involve the replacement of damaged molecules (proteins and lipids) and the fixture of damaged nucleic acids. Interestingly, DNA repair by the enzyme photolyase uses radiation in the UVA range (photoenzymatic repair; (Li et al., 2010)). While some repair processes may preferentially take place at night, in some cases a constant (even immediate) turnover of some molecules is required: this is the case of the D1 protein in the photosystem II, which has to be replaced so that photosynthesis can proceed (Neale and Kieber, 2000).

The relationship between plankton physiological performance and solar radiation is a matter of timescales: it is to be expected that characteristic response times of microbial plankton match the temporal variability of light exposure. In fact, bio-optical properties of phytoplankton can be used as tracers of mixing dynamics (Estrada, 1996; Dusenberry et al., 1999). Short-term light fluctuations elicit fast and reversible reactions. A more continued exposure may bring about permanent physiological changes like up-regulation of antioxidants and repair mechanisms, i.e., photoacclimation. In some cases, the damage can be too harsh to be repaired, triggering programmed cell death and also unregulated cell necrosis (Bidle and Falkowski, 2004). In summary, 'light' history seems to be important in determining the response of microorganisms to subsequent exposure. Although UV tolerance is generally assumed to increase after exposure to non-lethal PAR and UVR (Roy, 2000), the response can sometimes be counterintuitive (Murik and Kaplan, 2009). All these organismic responses regarding cell performance and viability will have their translation into population dynamics, interspecific interactions, and biogeochemical processes.

Turbulent mixing in the UML causes that microbial plankton (and dissolved material) experience variable radiation fields, both in intensity and spectrum, as they are carried up and down in the water column. The layer where photochemical processes are fastest and where UVR-induced damage prevails over repair processes is called the *photoactive layer*, and its limit is frequently defined by the depth of 10% UVB penetration. Depending on underwater light attenuation (spectral K_d's), the mixed layer depth (MLD), and the mixing rates, the cells will spend more or less time in the photoactive layer with respect to the time spent in UV protected layers where recovery can occur. The overall effect of the exposure on biogeochemical rates (like primary production or bacterial production) integrated in the UML will depend on the dynamic balance between photoinhibiton and recovery (Neale et al., 2003). It is also important to bear in mind that thresholds for the onset of irreversible damage may exist, further

complicating the study of microbial activity under dynamic exposure to radiation. Despite the numerous complications, the dynamic nature of light exposure is an important aspect of upper ocean biogeochemistry and should not be overlooked.

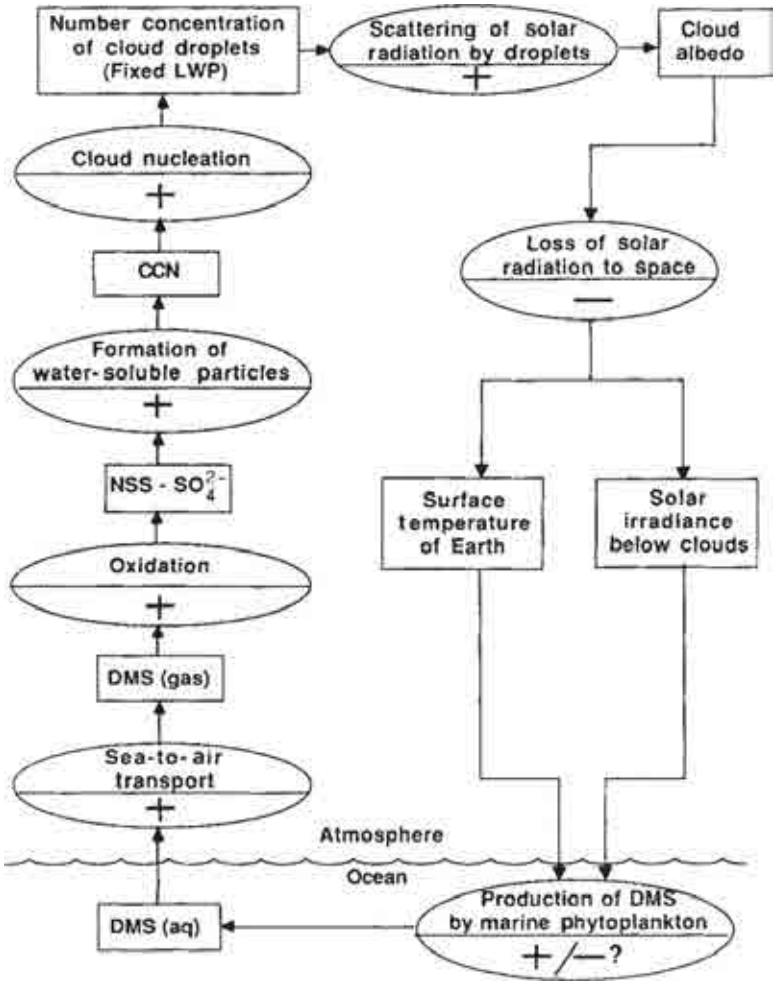

Figure 7: **The CLAW hypothesis as proposed by Charlson et al. (1987)** - "The rectangles are measurable quantities, and the ovals are the processes linking the quantities. The sign of the oval indicates the effect of a positive of the quantity in the preceding rectangle on that in the succeeding rectangle. The most uncertain link in the loop is the effect of cloud albedo on DMS emission; its sign would have to be positive in order to regulate the climate".

0.4 Dimethylated sulfur cycling in the ocean: more than climate feedbacks

0.4.1 The CLAW hypothesis

Dimethylsulfide (DMS, CH_3-S-CH_3) is a biogenic trace gas produced by the enzymatic breakdown of its algal precursor dimethylsulfoniopropionate (DMSP) by microbial food webs (Simó, 2001; Yoch, 2002; Stefels et al., 2007). The concentration of DMS dissolved in seawater (generally 0.5-10 nmol L^{-1}) is about one order of magnitude smaller than that of its precursor DMSP (roughly 5-100 nmol L^{-1}). Still, its concentration is one to two orders of magnitude above that of most trace gases in the upper ocean (Liss, 2007; Simó, 2011) (Fig. 8). In the early 70's the environmental importance of DMS was realized for the first time, when Lovelock et al. (1972) gathered evidence that oceanic DMS emission and its subsequent transport and deposition on land could balance the sulfate deficiency of the continents due to runoff. Until then it had been believed that hydrogen sulfide (H_2S), which is highly unstable in oxygenated waters, accounted for most of the (insufficient) flux of S to the atmosphere and the continents (Fig. 7).

As a result of Lovelock et al. findings, marine and atmopsheric DMS biogeochemistry gained interest as a research subject and more data were collected, which resulted in the release of the CLAW hypothesis (Charlson et al., 1987). In the original CLAW, atmospheric oxidation of ocean-emitted DMS would promote the formation of new particles -sulfate aerosols- in the marine troposphere. These aerosols would not only scatter sunlight, but further enhance the formation of cloud condensation nuclei. This would result in more, brighter, and longer-lived clouds in the oceanic troposphere, due to the higher concentration of cloud droplets of smaller size. The increase in cloud albedo would in turn diminish the irradiance reaching the oceans' surface. If, in turn, DMS production by plankton was a function of irradiance or sea surface temperature, a negative feedback loop would be established: an increase in DMS emission would increase the planetary albedo, which would act to decrease DMS emission, decreasing the albedo again. This groundbreaking hypothesis caused a burst in all aspects of DMS research, rendering the DMS(P) cycling scheme a lot more complicated (Fig. 9). Below, we will briefly review some of developments occurred on the marine side of the story.

0.4.2 Lost from complexity

The complexity in the marine dimethylated sulfur cycle begins with the synthesis of DMSP [$(CH_3)_2$-S^+-CH_3-CH_3-COO^-]. Chemically, DMSP is a zwitterionic tertiary sulfonium com-

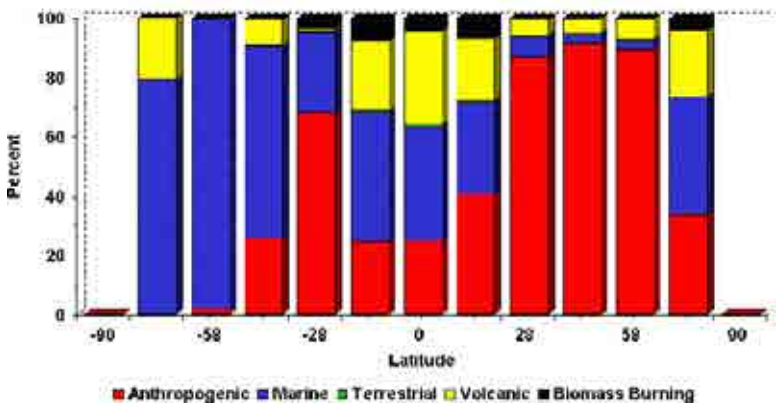

Figure 8: **Global sulfur emissions by latitude bands** - Anthropogenic includes biomass burning; biogenic includes marine and terrestrial, and ~90% of it corresponds to marine DMS; from Bates et al. (1992).

pound analogue to the nitrogen-based betaines, like glycine betaine (Keller et al., 1999a,b). All algae (and almost all bacteria) are believed to be capable of *assimilatory sulfate reduction*, the process by which the abundant sulfate ion is incorporated into biomass. It seems that DMSP biosynthesis routes, which have methionine as the pivotal molecule, may have evolved independently in algae and in the few higher plants that also produce it (Gage et al., 1997). Intracellular DMSP concentrations vary across five orders of magnitude among phylogenetic groups (Stefels et al., 2007). Within algal classes, DMSP production is species-specific or even clone-specific, and is additionally modulated by environmental conditions, owing to its multiple potential functions in the algal cytosol. Although it is believed to work primarily as an osmoregulator, it has been suggested to act as cryoprotectant (Malin and Kirst, 1997), methyl donor in metabolic reactions (Kiene et al., 1999), overflow compound (Stefels, 2000), and radical scavenger (Sunda et al., 2002). In summary, it can be said that DMSP is an anti-stress molecule.

DMSP is not only appreciated by its algal producers, which can invest in DMSP as much as $> 30\%$ of their cellular C (Berdalet et al., 2011) and $> 90\%$ of their cellular S (Matrai and Keller, 1994). Bacteria acquire it by osmotrophic uptake (Kiene et al., 1998) and protozoan grazers mainly through the diet (Saló et al., 2009). It is not surprising that DMSP exuded by healthy algal cells, or released upon grazing, viral lysis, or phytoplankton cell death acts as a strong chemoattractant for these heterotrophic organisms (Seymour et al., 2010). Phytoplankton that are moderate DMSP producers seem to save some of the energy required to reduce sulfate by taking up dissolved DMSP, which seems to remain untransformed in their cytosol (Saló

et al., 2009; Spielmeyer et al., 2011). Interestingly again, it seems that the same membrane transport system works for DMSP and glycine betaine uptake (Kiene et al., 1998; Vila-Costa et al., 2006b). Another interesting facet of DMSP ecology is its apparently important role in photosymbiotic interactions, like those in corals (Broadbent and Jones, 2004; Van Alstyne et al., 2006), flatworms (van Bergeijk et al., 2002) and the planktonic protists Acantharia (Decelle et al., 2012), which might be related to its antioxidant function.

Some DMSP-producing phytoplankton can enzymatically cleave DMSP to DMS and acrylate, either intracellularly or extracellularly (Stefels and Dijkhuizen, 1996). In some species, DMSP and its cleaving enzymes appear to be spatially segregated, so that cell disruption is a condition for DMS production (Wolfe and Steinke, 1996). The fact that not all DMSP producers can cleave it, and the variable location of the enzymes and their activity, make DMSP cleavage an enigmatic cellular function (Stefels, 2000; Simó, 2001; Sunda et al., 2002). The picture is not simple either regarding bacterial DMSP metabolism. A major portion of bacterially consumed DMSP enters the central sulfur metabolism through the demethylation pathway (*dmd* metabolism; (Howard et al., 2006). After a few metabolic steps (Reisch et al., 2011) the sulfur moiety is converted to methanethiol and, finally, can be incorporated into proteins as methionine or cysteine, while the C3 moiety may finally enter the tricarboxylic acid cycle (Krebs cycle). A minor portion of the DMSP consumed by bacteria is cleaved by extra- or intracellular enzymes (*ddd* metabolism; (Yoch et al., 1997), and thus produces DMS. This process can occur through at least two biochemical pathways (Todd et al., 2007), and be carried out by at least 6 different enzymes (Curson et al., 2011) present in variable number, location and specific activity in different strains. In the end, it seems that DMS produced by algal or bacterial enzymes is just a byproduct of the more central DMSP metabolism.

Once in seawater, the fate of most DMS is being photooxidized or utilized by bacteria (Simó, 2004). Only a minor fraction is vented to the atmosphere where, at high concentrations, it can serve as a foraging cue for some birds and mammals (Cunningham et al., 2008; Nevitt, 2008) before being oxidized and causing accretion of sulfate aerosols. Although the function of bacterial DMS utilization is still debated, it seems that its oxidation, presumably catalyzed by a monooxygenase, may generally supply a small energetic surplus rather than being used as S or C source (Vila-Costa et al., 2006a; Schäfer, 2007; Hatton et al., 2012). DMS photolysis in the water column is a photosensitized process, meaning that DMS does not absorb light but reacts with the radicals (Brimblecombe and Shooter, 1986) produced upon light (UVR) absorption by CDOM and nitrate. Similarly, DMS can also be oxidized by ROS inside algal cells before

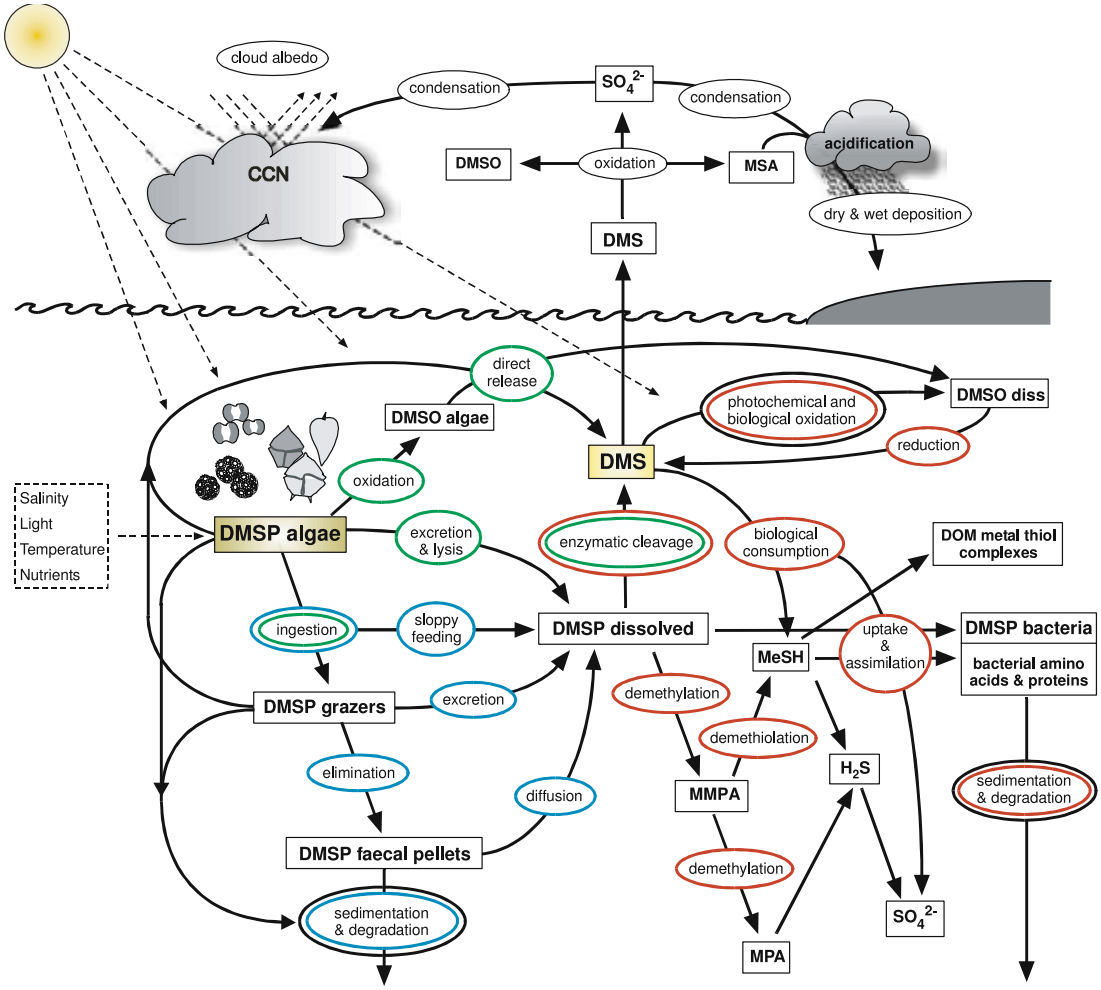

Figure 9: **Current view of DMS(P,O) cycling processes** - Dominant role of functional groups is indicated by colored ellipses: green, phytoplankton; blue, zooplankton; red, bacteria; black, abiotic factors. CCN, cloud condensation nuclei; DOM, dissolved organic matter; MeSH, methanethiol; MPA, mercaptopropionate; MMPA, methylmercaptopropionate; MSA, methanesulfonic acid; see text for other abbreviations; from Stefels et al. (2007).

diffusing across the cell membrane (Sunda et al., 2002). Dimethylsulfoxide (DMSO) appears to be the major end product of the different DMS oxidation pathways, and accumulates at notable concentrations inside algal cells (Simó et al., 1998; Lee and de Mora, 1999; Simó and Vila-Costa, 2006; Hatton and Wilson, 2007) and dissolved in seawater. The widespread capability of bacteria to reduce DMSO back to DMS (Hatton et al., 2004) has led to speculations about its potential pivotal role both as a sink and source of DMS (Spiese et al., 2009). However, until DMSO reductase activity was recently reported in Antarctic waters (Asher et al., 2011), it had

never been observed in the pelagic environment. From this section, it is easy to conclude that dimethylated sulfur cycling by microbial plankton is a multifaceted problem, which requires it being tackled from different sides.

0.4.3 Emergent properties

It is a common goal of ecology to find regularities emerging from the (usually tangled) network of interactions between the organisms and the environment. In the case of dimethylated sulfur cycling, the analysis of global scale patterns has yielded valuable insights, which owe a lot to the creation of a global surface seawater DMS database (Kettle et al., 1999), maintained at NOAA/PMEL (http://saga.pmel.noaa.gov/dms/) and in continuous expansion. In the monthly 1°x1° Kettle climatology no significant correlation was found between sea surface DMS and physical and variables like sea surface temperature, salinity, nutrients, or chlorophyll. Yet, subsequent works tried to find shortcuts for predicting DMS from the different combinations of biogeochemical or physical parameters, with different underlying hypotheses and also different success (reviewed by Belviso et al. (2004)). Recently, the DMS climatology was updated by Lana et al. (2012) (Fig. 10).

There is one feature of DMS variability which has remained difficult to capture by most algorithms and prognostic models (Le Clainche et al., 2010): the seasonal decoupling between DMS and plankton biomass (i.e. chlorophyll) at low latitudes, showing its maximum intensity at the cores of most anticyclonic subtropical gyres (named the 'summer DMS paradox' by Simó and Pedrós-Alió (1999b). A line of evidence showing an inverse relationship between DMS concentrations and MLD in oligotrophic regions (Simó and Pedrós-Alió, 1999a; Simó and Dachs, 2002) produced the first algorithm capable of capturing the summer paradox. The work of Toole and Siegel (2004) went a step further in conceptualizing oceanic DMS cycling regimes, and introduced the distinction between the stress regime (occurring in summer paradox regions) and the bloom regime, occurring at high latitudes where DMS and chlorophyll covary. More recently, Vallina and Simó (2007) found a linear relationship between the daily solar radiation dose (SRD) in the UML and DMS concentrations on regional and monthly bases, effectively synthesizing with a single indicator the interplay between mixing and light at different latitudes. Such relationship had been hinted by Bates et al. (1987) with the few data available 25 years ago, and has been further revisited by Lana et al. (2012). Nevertheless, the clear emergent relationship between sunlight (plus its derived effect: stratification) and DMS cycling is not yet

underpinned by a solid mechanistic understanding. This hampers the progress of prognostic DMS models, which ultimately rely on experimental data.

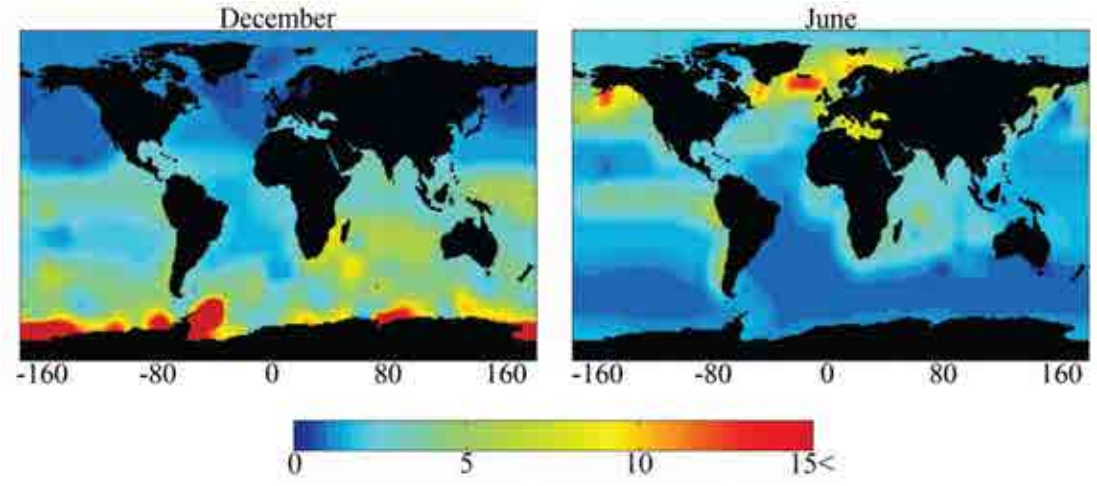

Figure 10: **Global DMS climatology: the seasonal beat** - Monthly average concentrations (nmol L^{-1}) at the ocean's surface in the summer solstice of both hemispheres. The 'summer intensification' occurs from subtropical to polar latitudes regardless their productivity regimes; modified from Lana et al. (2011).

Aims and outline of the thesis

In this thesis, the response of dimethylated sulfur cycling to environmental forcing has been addressed at the ecosystem level by combining knowledge generated in the areas of microbial ecology, photochemistry and photobiology, underwater optics, and the physics of vertical mixing. The thesis contains six chapters that are organized around the following aims:

1. **Identify distinct DMS cycling regimes in the coastal and open ocean, as modulated by vertical mixing and underwater optics, microbial plankton community succession, and seasonal to daily meteorological forcing.** Chapters 1, 5 and 6.

2. **Investigate the effect of solar radiation on community gross DMS production and explore its photobiological bases.** Chapters 2, 3 and 4.

The results presented in the first five chapters have been obtained by the author and by other members of the research group, in the framework of five oceanographic cruises in polar and subtropical oceans and two seasonal sampling programs in the coastal Mediterranean. These chapters are structured as scientific papers, which can result in some reiteration but allows them being read as independent pieces. Chapter 6 is both a literature meta-analysis and the general discussion of the thesis, where the results of the previous chapters are analyzed in a wider context. A brief introduction of each chapter and the hypotheses (in **bold**) that were tested is presented below.

Chapter 1: *Occurrence and cycling of dimethylated sulfur compounds in the Arctic during summer receding of the ice edge.* Marginal ice zones provide the environment where phytoplankters like colonial *Phaeocystis* can bloom. Currently, global warming is changing the extent and seasonality of this ecosystem at an accelerated pace. Here we hypothesize that **the shallow stratification induced by sea-ice melt is the key factor modulating DMS production-consumption budgets**. Besides improving the understanding of a particular *bloom regime* ecosystem, this study became the seed for the following three chapters, after observing that DMS budgets were apparently unbalanced when biological processes were measured in dark incubations. This work is based on the ATOS I Arctic cruise that took place during July 2007, a record ice melt summer.

Chapter 2. *Stimulation of gross dimethylsulfide (DMS) production by solar radiation.* Previous research had shown that gross DMS production is enhanced in summer stratified conditions, largely driven by succession towards DMS(P) producing phytoplankton. In this work we test the hypothesis that **direct solar exposure stimulates gross DMS production**, which until present has been routinely measured in dark incubations. The hypothesis is tested in contrasting oceanic settings, from the coastal Mediterranean to the subtropical gyre of the southern Indian ocean.

Chapter 3. *Sunlight-stimulated gross dimethylsulfide (DMS) production: Interactive effects of spectral irradiance, the microbial community and its light history.* After observing that gross DMS production is stimulated by sunlight, we test the hypothesis that **the intensity and spectral composition of solar radiation modulates gross DMS production**. This requires a careful characterization of the radiation field experienced by the samples, both before and during the experimental exposure. The response to a spectral irradiance gradient is better understood if the composition and activity of the microbial plankton community are assessed simultaneously.

Chapter 4. *Differential response of planktonic primary production, bacterial production, and dimethylsulfide production to vertically-moving and static incubations in UV-transparent summer stratified waters.* Going a step further, we compare the response of gross DMS production, plus microbial autotrophic and heterotrophic activities, to static and dynamic light exposure. The underlying hypothesis is that **vertical mixing can change the balance between UVR-induced damage and the repair processes that counteract it, thereby altering C and S cycling rates**.

Chapter 5. *Diel patterns of oceanic dimethylsulfide (DMS) cycling: microbial and physical drivers.* In this chapter we return to the ecosystem-level study of DMS budgets. We resolve the sub-daily variability in DMS cycling, with the hypothesis that **sunlight modulates biotic and abiotic DMS sources and sinks and this leads to observable diel patterns of DMS cycling**. Such modulation can occur either directly or through the indirect effects of stratification. This time we focus on the *stress regime*, exemplified by the Sargasso and Mediterranean seas in summer, with the counterpoint of the coastal Mediterranean in late winter.

Chapter 6. *General discussion: A meta-analysis of oceanic DMS(P) cycling.* Twenty-five years after the CLAW hypothesis was put forward, the number of process studies and their spatial and temporal coverage may be sufficient to conduct a meta-analysis. We will try to find regularities in DMS(P) cycling across oceanic biomes, and to refine our current representation of DMS(P) cycling regimes, integrating the findings reported in the previous chapters.

Chapter 1

Occurrence and cycling of dimethylated sulfur compounds in the Arctic during summer receding of the ice edge

Galí, M., and Simó, R. (2010). *Marine Chemistry*, 122:105 – 117.

Abstract

The distribution and cycling of dimethylsulfide (DMS), dimethylsulfoniopropionate (DMSP) and dimethylsulfoxide (DMSO) were studied in the Greenland Sea and Arctic Ocean during July 2007. The concentration of these compounds was analyzed in vertical profiles of the top 100 m of the water column, with special emphasis on the subsurface (1 m) and the immediate subsurface waters (0.1 m). Seawater incubations were conducted in order to measure the rates of biological DMS cycling, as well as DMS photolysis rates. DMS ventilation rates were calculated from the hourly meteorological time series. Moderate concentrations of DMS (0.1 to 18.3 nM), DMSP (1.4 to 163.6 nM) and DMSO (9.0 to 84.7 nM) were found, considering that elevated biomasses of the haptophyte *Phaeocystis pouchetii* dominated in the study area. The overall situation was characterized by a tight coupling of biological DMS production and consumption, and a fast biological turnover of DMS (0.5 to 4 days). Bacterial consumption was the dominant sink for DMS, accounting for 9–73% of its loss in the upper mixed layer (UML). However, the shallow stratification encountered (mixed layer depth between 1.5 and 11 m) enhanced DMS photolysis, which accounted for 12–65% of the total DMS loss and, at some stations, became the dominant sink. DMS production followed phytoplankton biomass (and DMSP concentration) in surface waters, while bacterial DMS consumption was controlled by the depth of the UML (presumably through exposure to solar radiation). Ice melt drove surface stratification, regulating the entrainment of cells and materials into the upper layer from the more productive waters below, and eventually the fraction of DMS escaping to the atmosphere.

1.1 Introduction

Dimethylsulfide (DMS) is the most abundant volatile sulfur compound in the surface ocean, and represents the major natural source of reduced sulfur to the global troposphere (Andreae and Crutzen, 1997). DMS is mainly produced by the enzymatic cleavage of its biological precursor dimethylsulfoniopropionate (DMSP), an abundant and widespread intracellular compound found in marine microalgae (Keller, 1989) and in other halophytic plants.

Research on DMS was first stimulated by the realization that this gas could account for the 'missing' flux of sulfur from the oceans to the atmosphere that closes the budget of this essential element at the global scale (Lovelock et al., 1972), and was further encouraged when its involvement in a climatic regulatory feedback was proposed (Charlson et al., 1987). The latter authors hypothesized that the oxidation of DMS in the atmosphere would modify the albedo of clouds through the development of cloud condensation nuclei, thus altering the radiative budget over the oceans. If, in turn, DMS production by the marine microbiota was dependent on sea surface irradiance or temperature, the loop would be closed, establishing a negative plankton-climate feedback.

Since this hypothesis was postulated, our knowledge of the marine cycle of DMS and DMSP has rapidly increased, either from the physiological, ecological or the biogeochemical point of view. Several physiological functions have been proposed for DMSP: osmoregulator and cryoprotectant (Malin and Kirst, 1997; Welsh, 2000), methyl donor in metabolic reactions (Kiene et al., 1999), overflow mechanism for excess reducing power under conditions of unbalanced growth (Stefels, 2000), and the initial compound in a cascade of oxidations (involving its breakdown products DMS, acrylate, dimethylsulfoxide (DMSO) and methane sulfinic acid) that would prevent oxidative stress in cells (Sunda et al., 2002). Moreover, DMSP plays a critical role in marine microbial food webs, both as a chemical signal (Wolfe, 2000; Zimmer-Faust et al., 1996), and as the main carrier of reduced S and a significant carrier of C within and among trophic levels (Kiene et al., 2000; Simó and Dachs, 2002).

DMSP production by phytoplankton displays a large variability, both across taxonomic groups (Keller, 1989) and within taxa depending on environmental conditions (Stefels et al., 2007). The cleavage of DMSP to DMS can proceed through different enzymatic pathways in the microbial food web, generally referred to as 'DMSP lyases'. These are found in some algal and bacterial taxa, and can be intra- or extracellular (Stefels and Dijkhuizen, 1996; Yoch et al., 1997). DMSP release to the dissolved phase, eventually promoting DMS production,

takes place upon grazing, viral lysis and phytoplankton autolysis (Simó, 2001). However, a competing, non DMS-producing pathway for DMSP degradation ubiquitously exists, by which bacteria demethylate DMSP and eventually assimilate its sulfur (Kiene et al., 2000; Howard et al., 2006). The widespread uptake of DMSP by marine phytoplankton (Vila-Costa et al., 2006b) further complicates the picture.

Once in seawater, DMS has three dominant fates: ventilation to the atmosphere, photooxidation, and microbial (bacterial) consumption, which usually represents its major sink (Simó, 2004). In the latter two processes dissolved dimethylsulfoxide (DMSO) is one of the products (del Valle et al., 2007; Kieber et al., 1996). Phytoplankton can also produce and release DMSO (Simó et al., 1998), but its possible physiological roles remain uncertain, although functions similar to those of DMSP have been proposed (Lee and de Mora, 1999; Sunda et al., 2002). In summary, DMSO is a major pool of organic sulfur in the ocean (Hatton et al., 2004; Simó and Vila-Costa, 2006), and its pivotal role in dimethylated sulfur cycling is progressively being unveiled.

Due to the complexity and number of interactions explained above, fully mechanistic models often fail to predict seawater DMS concentrations (Simó and Dachs, 2002). Comprehensive field studies, therefore, are of great importance as they provide further gains in understanding as well as the grounds against which hypotheses, laboratory results and model outputs can be validated. In the context of climate change, studies on the biogeochemical functioning and air-sea interactions of marine ecosystems already undergoing visible changes are very relevant, especially if existing data for the area under study are relatively scarce. The Arctic Ocean is predicted to be among the areas most affected by the ongoing climate change (IPCC, 2007; Johannessen et al., 2004; Moritz et al., 2002). In addition, in the late summer of 2007 the lowest ice extent was observed since the start of satellite records in 1979 (Stroeve et al., 2008). The aim of our study is to provide a better understanding of the distribution and cycling of dimethylated sulfur compounds in open-ocean and ice-margin waters during the Arctic ice melt, and the processes controlling the fraction of biologically produced DMS that ends up in the atmosphere.

1.2 Methods

1.2.1 Sample collection and CTD profiles

During the ATOS1 Arctic cruise, carried out in July 2007, a total of 49 stations were occupied, of which 17 were sampled for dimethylated sulfur compounds. Deck board incubation experiments were conducted in 8 of these. Most stations were located NW of the Svalbard archipelago, between 80º N – 81º N and 5ºE – 20º E, except for the initial stations that covered the transect from the north of Iceland to NW Svalbard, across the East Greenland Current (EGC) and the Fram Strait.

Samples for DMS(P,O) profiles were collected every morning at 8 am from 5 depths in the top 200 m of the water column, using Niskin bottles attached to a CTD rosette (Seabird SBE 911). Silicone tubing was used to fill 120 ml glass vials to the top (without head space), allowing some overflow and taking care to avoid bubbling. An additional Niskin bottle was deployed to sample at 1 m depth. At some stations, an extra sample from 0.1 m depth was taken from a Zodiac inflatable boat by pumping seawater through acid-cleaned Teflon tubing to a 0.25 L Teflon bottle. All bottles were cleaned with hydrochloric acid before the cruise started, and from then on they were rinsed several times with MQ water after each use, and with sample seawater before they were filled.

At 4 stations in the Fram Strait area, DMSP and DMSO were also analyzed in sea ice samples obtained with a coring device (Mark III, Kovacs Enterprise Inc.). Only the top and bottom 20 cm of the ice cores (which were 1 m long and 7.25 cm in diameter) were used after melting overnight in acid-washed Teflon (PFA) bags at room temperature. The ice melt water was sampled with a syringe from the Teflon bags and analyzed like seawater samples.

In addition to temperature, conductivity (salinity) and pressure (depth), the variables measured in CTD profiles included fluorescence of chlorophyll *a*, beam attenuation (c_p) at 660 nm (a proxy for total biogenic particle mass, i.e. particulate organic carbon) and turbidity. Vertical profiles were binned and averaged in 1 m intervals. Density σ_t was calculated from temperature and salinity with the built-in algorithm of the *Ocean Data View* software. The mixed layer depth (MLD) was defined as the maximum depth before a step in density bigger than 0.02 kg m^{-4} was encountered. At all stations (except Stn. 1), shipborne CTD profiles of the uppermost water column were checked against the more reliable temperature and salinity profiles obtained from the zodiac boat, which covered the 3 upper meters of the water column.

Both fluorescence and extracted Chl *a* are poor indicators of algal biomass, for they are affected by photoadaptation and nutrient stress (Behrenfeld and Boss, 2003). Consequently, we chose beam attenuation (c_p) as our reference variable for planktonic microbial biomass. Even though c_p also accounts for heterotrophic bacterial biomass (Oubelkheir et al., 2005), the proportion of autotrophic biomass is expected to increase as we move towards eutrophic conditions (Gasol et al., 1997) and will probably dominate during strong phytoplankton bloom conditions.

1.2.2 Analysis of sulfur compounds

Dimethylated sulfur compounds were analyzed by purging, cryotrapping and sulfur-specific gas chromatography followed by flame photometry (Simó et al., 1996). The detection limit was ca. 3 pmol S. To analyze DMS, 3-5 ml of seawater were gently filtered through a GF/F syringe filter and immediately sparged in a crimp glass vial. A larger volume of sample (40 ml) was stored in crimp glass vials, where two pellets (45 mg each) of NaOH were added. DMS was analyzed within 1 h after collection. Total DMSP (DMSPt) was analyzed the following day, except for a few samples that were run on land within 2 months after the cruise had finished. Total DMSO (DMSOt) was analyzed within a few months in the same vials, after purging with N_2 the DMS evolved from alkaline DMSP cleavage. DMSO was measured as DMS after reduction by $NaBH_4$, added in its cobalt-doped form to skip the neutralization step (Simó and Vila-Costa, 2006). All samples were analyzed in duplicate, and the median coefficient of variation between replicates was 5.2, 6.3 and 3.5% for DMS, DMSPt and DMSOt respectively.

The attempts made to measure dissolved DMSP (DMSPd) by the small-volume gravity drip filtration method (Kiene and Slezak, 2006) repeatedly failed, due to the presence of the colony-forming haptophyte *Phaeocystis*. The colonies and even the solitary cells of this small flagellate easily break down upon filtration, releasing the intracellular content (Schoemann et al., 2005). For this same reason, a prefiltering step through a 50 μm mesh was carefully applied when filling the vials destined for DMS analysis. This step prevents artifacts in the measurement of DMS, caused by the elevated concentrations of DMSP and DMSP lyases in solution.

Table 1.1: Main characteristics of stations occupied during the cruise. Only Stn. 18 and 19 were on the continental shelf. Water masses are defined as Atlantic Water (AW, West Svalbard Current), Polar Surface Water (PSW) and PSW with highest or more recent ice influence (PSWi). Temperature, salinity, σ_t and c_p are UML averages, practically equivalent to surface values. Irradiance and wind speed are the average for the 24 h prior to sampling. The asterisk (*) denotes stations where sea ice was close to the ship during sampling (up to 60% ice cover). Sulfur data available: Is = surface water (1m) incubation; Id = fluorescence maximum incubation; p = complete profile; (p) = profile with less than 6 depths; photo = photochemistry; surface = surface DMS, DMSPt and DMSOt measured.

Station	Date Jul 2007	Latitude (N)	Longitude (E)	Water mass	T UML (°C)	Sal UML	σ_t (kg m^{-3})	MLD (m^{-1})	$K_{d,PAR}$ (m^{-1})	c_p (m^{-1})	E_d (W m^{-2}	Wind speed (m s^{-1}	Sulfur data available
1	7/1	68 28.81	-19 30.30	PSW	2.4	32.7	25.9	6	0.11	0.36	NA	NA	Is, Id, p
2	7/2	70 43.26	-17 08.17	PSW	2.0	31.7	25.3	2	0.11	0.28	118	4.9	p
3	7/3	72 57.23	-12 39.67	PSW	2.3	31.8	25.4	2	0.11	0.33	113	3.0	Is, Id, p
5	7/5	77 23.23	-1 39.82	AW	2.7	33.8	26.9	6	0.29	0.90	134	4.3	(p)
9	7/7	78 43.72	2 58.49	AW*	2.6	33.7	26.9	5	0.24	0.78	210	7.8	Is, Id, (p)
12	7/8	79 30.80	7 29.64	AW*	1.4	32.8	26.2	3	0.20	0.57	145	5.7	Is, Id, p
18	7/10	80 26.96	13 37.59	PSW	1.6	33.3	26.5	11	0.11	0.79	274	10.3	surface
19	7/11	80 29.28	16 53.28	PSW*	1.5	33.6	26.9	7	NA	0.62	147	3.7	Is
20	7/12	80 13.99	10 11.44	AW*	0.1	32.3	25.9	5	0.17	0.52	222	3.3	Is, Id, p, photo
23	7/13	79 22.18	6 49.54	AW	5.3	34.3	27.1	7	0.21	0.61	268	5.6	surface
26	7/14	80 09.93	8 05.16	AW*	1.6	32.3	25.8	1.5	0.13	0.41	238	4.6	Is, (p), photo
30	7/16	80 19.12	10 17.70	PSWi*	0.5	32.2	25.8	9	0.13	0.36	360	7.1	surface
33	7/17	80 23.61	12 26.15	AW*	2.0	33.2	26.5	6	0.13	0.52	242	5.9	surface
36	7/18	80 46.47	13 21.11	PSW*	0.0	31.9	25.6	2	0.11	0.31	159	6.4	surface
39	7/19	80 49.57	13 14.22	PSWi*	0.3	32.0	25.7	9	0.11	0.36	82	7.8	Is, p, photo
42	7/20	80 47.16	12 32.04	PSWi*	-0.9	32.1	25.8	10	0.13	0.38	93	8.0	Is, photo
43	7/21	80 22.72	7 52.70	PSW	0.7	33.2	26.6	11	0.18	0.68	99	8.4	surface

1.2.3 Biological process incubations

For the determination of gross DMS production by the whole microbial community and bacterial DMS consumption, water from 1 m depth and from the depth of the fluorescence maximum was incubated in the dark at the in situ surface temperature ± 1 °C. For that purpose, amber glass bottles (2.9 L) were directly filled from the Niskin bottles. One unamended bottle was incubated as a control, along with a second bottle that was amended with ca. 250 nM of dimethyldisulfide (DMDS), an effective inhibitor of bacterial DMS consumption (Wolfe and Kiene, 1993a; Simó et al., 2000). The duration of the incubations was around 20 h, during which the inhibitory effect generally held. Otherwise, only the part of the incubation with a linear DMS accumulation was used for the calculations. The slope of the linear regression between DMS concentration and incubation time in the control bottles provided the net DMS production rate. The slope of the DMDS amended treatment yielded the rate of the community gross DMS production. The bacterial DMS consumption rate was obtained as the difference between gross and net DMS production rates. DMSPt was also monitored in the control incubations. At Stn. 42, surface seawater was also incubated in the light under the same irradiance as the photochemistry incubations using 2.3 L Teflon bottles (see *Results, Dark versus light incubation*).

1.2.4 DMS photolysis

1.2.4.1 Incubation setup

DMS photolysis rates were measured at stations 20, 26, 39 and 42 in either 75 ml quartz flasks or 250 ml Teflon bottles (Stn. 42) incubated on board. Seawater from 1 m depth was gravity filtered through GF/F, and then syringe filtered through 0.2 μm Nylon membranes. DMS was added to concentrations of 20-70 nM in order to ensure that photooxidation of DMS was detectable within incubation times, and the water was transferred to the bottles leaving no head space. Duplicate light and dark bottles (the latter wrapped in aluminum foil) were kept for 7 – 12 h in a bath with running seawater from the ship's underway intake, while solar radiation and bath temperature were recorded continuously. The incubation tank was covered with a neutral screen that attenuated 52% of the solar radiation in the ultraviolet (UV) and in the photosynthetically active radiation (PAR) regions.

1.2.4.2 Rate constant calculation

The photolysis rate constant (k_{photo}, d^{-1}) was calculated assuming a pseudo first-order kinetics (Brimblecombe and Shooter, 1986; Kieber et al., 1996; Brugger et al., 1998; Hatton, 2002). Concentrations from duplicate bottles were averaged, and final concentrations in the light were corrected for any changes happened in the dark. The natural logarithms of initial and final DMS concentrations were plotted against time after dark correction, and the slope was taken as the k_{photo}. A correction factor was applied at Stn. 42 to account for the slightly lower transmittance of Teflon bottles in the UV range compared to quartz.

1.2.4.3 CDOM measurements

Absorption spectra of chromophoric dissolved organic matter (CDOM) were measured in the GF/F filtrates used for DMS photolysis before and after the incubations. Spectrophotometric scans (280 to 800 nm) were performed in a 1 cm pathlength (r) quartz cuvette, and spectral absorption coefficients were calculated from spectral absorbance ($A_{CDOM,\lambda}$) after subtracting the absorbance of MQ water, as $a_{CDOM,\lambda} = 2.303 A_{CDOM,\lambda} r^{-1}$. Analysis of 0.2 μm filtrates showed minor differences with GF/F filtrates. The spectral slope of CDOM ($S_{300\text{-}400}$) was computed from the linear regression between the natural logarithm of $a_{CDOM,\lambda}$ and wavelength, in the range 300 – 400 nm. In some samples, marked absorption peaks occurred around 330 nm, which were attributed to mycosporine-like aminoacids. In those occasions, the peaks were excluded from the linear regression.

1.2.5 Upper mixed layer-averaged solar radiation and optical calculations

1.2.5.1 Attenuation coefficients (K_d) and UML-averaged solar radiation

Diffuse attenuation coefficients for downward radiation (k_d) were calculated as the slope of the linear regression between the natural logarithm of downwelling irradiance and depth. Only the UML, or alternatively, a deeper and optically homogeneous surface layer, were used for k_d calculation, so that the R^2 of the regression was above 0.98 at all stations considered. The minutely time series from the ship's meteorological station was used to calculate the mean irradiance during the 24 h prior to sample collection. This value was converted to subsurface irradiance ($E_{d,o-}$) with a 10% surface reflectance applied, based on mean wind speed and solar zenith angle (Kirk, 1994), and then the average depth-integrated solar radiation in the UML was calculated following Vallina and Simó (2007).

1.2.5.2 Averaged spectral irradiance in photolysis experiments

A PAR-UV radiometer (Biospherical PUV 2500) was placed in the center of the incubation tank to keep a continuous record of the solar radiation reaching the samples. Downwelling cosine irradiance was measured at a frequency of 5 s^{-1} in six bands in the UV region (centered at 305, 313, 320, 340, 380 and 395 nm) and one integrated band in the visible region (PAR). The mean spectral irradiance during the incubation was obtained for each UV band, and the total energy received in the UVB and UVA was computed as the integral of mean spectral irradiance over a given spectral interval and time.

The time series from the meteorological station of the ship was used to calculate the time-integrated total irradiance reaching the samples after successively crossing the neutral screen (52% attenuation) and the water surface (10% reflectance). The K_{photo} obtained in bottle experiments were converted to in situ mixed layer photolysis rate constants ($k_{photo,UML}$) according to the following steps: first, a subsurface in situ rate constant was obtained as the product of the experimental k_{photo} by the average in situ subsurface irradiance divided by the averaged incubation irradiance; second, a depth-averaged $k_{photo,UML}$ was calculated in the same manner as $E_{d,UML}$, but assuming that k_{photo} decayed exponentially with the K_d of 340 nm radiation. Our calculations indicated that 340 nm was the wavelength at which maximum DMS photolysis occurred in surface waters, according to the product of light absorption (CDOM spectra) by the apparent quantum yield of DMS photolysis obtained by Deal et al. (2005) in the Bering Sea.

1.2.6 Sea-air DMS flux

Hourly DMS fluxes were calculated using the subsurface DMS concentration (1 m depth, and 0.1 m depth when available) and the hourly wind speeds from the ship's meteorological station, and were then averaged on a daily basis. The parameterization of Nightingale et al. (2000) was used to obtain $k_{w,DMS}$, the transfer or piston velocity of DMS (cm h^{-1}): $k_{w,DMS} = (5.88U_{10}^2 + 1.49U_{10})Sc^{-1/2}$, where U_{10} = wind speed at 10 m height (m s^{-1}); Sc = Schmidt number of DMS, calculated from the sea surface temperature according to Saltzman et al. (1993). Emission fluxes (F_{DMS}) were then obtained as the product of DMS in seawater (C_w, which drives the flux) and the transfer velocity: $F_{DMS} = 0.24k_{w,DMS}C_w$. Finally, ventilation rate constants in the UML ($k_{vent,UML}$) were obtained as the surface flux divided by DMS concentration and MLD.

1.2.7 Statistical analysis

1.2.7.1 Grouping of stations

Vertical profiles of CTD variables were used to construct a classification of the 17 stations where sulfur data were available. Briefly, profiles of each variable between 0 and 30 m were grouped using cluster analysis (cityblock, cutoff = 1). The resulting groups had characteristic depth profiles of the selected variable. This rendered as many different classifications as variables used. However, salinity and c_p showed a strong agreement, and were therefore used as the defining criteria (see *Results*). The average profiles (± SE) of representative CTD variables were calculated for each group (Fig. 1.1).

1.2.7.2 Vertical profiles

A correlation matrix (Pearson correlation) allowed the exploration of the relationships between sulfur compounds and biotic and abiotic parameters measured from CTD casts. In addition, stepwise regression was performed in order to find the most significant predictors for DMS, DMSPt and DMSOt. Stepwise regression was judged a convenient technique to prevent collinearity artifacts in the multiple regression, that is, artifacts caused by highly correlated variables within the predictor matrix. The initial model included no terms, and the entrance tolerance for additional terms was $p < 0.05$.

1.2.7.3 Surface distribution and biological cycling

Surface distribution of dimethylated sulfur compounds, planktonic biomass and related abiotic parameters, and biological sulfur cycling were explored by means of correlation analysis. Given the low number of data points available (< 20), the non-parametric Spearman correlation method was used.

1.3 Results

1.3.1 Oceanographic setting

1.3.1.1 Physical features

The transect from Iceland to the north of Svalbard archipelago is characterized by the interaction between warm and salty Atlantic Water (AW), which flows northwards forming the West Svalbard Current (WSC), and the southwards overflow of Arctic Water through the Fram Strait (between Svalbard and Greenland) and along the Greenland shelf, forming the East Greenland

Current (EGC; Rudels et al. (2005); Fig. 1.1A, B). In the Fram Strait and on the Yermak Plateau (NW of Svalbard) mixing between these water masses occurs, and recirculated AW is entrained into the EGC which, further south, progressively loses the low temperature and salinity characteristic of Polar Surface Water (PSW). In our cruise, the AW end member showed a temperature maximum of ca. 7 °C in the UML, while PSW had a temperature minimum of almost -1.8 °C at around 40 m depth (Fig. 1.1C). Sea surface temperature ranged from -1 to 7 °C. Salinity usually decreased from a value of 35 at 100 m to reach values between 31 and 35 at surface (Fig. 1.1D).

1.3.1.2 Classification of the stations

According to vertical profiles of salinity and its grouping with cluster analysis (see *Methods*), stations were divided in AW and PSW (Fig. 1.1, Table 1.1). Additionally, the latter group included a subgroup of stations that showed a stronger influence of ice melt, which will be referred to as PSWi. These groups showed distinct vertical profiles of physical variables, but also a distinct pattern of biomass distribution with depth. The cluster based on c_p profiles was highly consistent with that based on salinity, with only 3 out of 17 stations misclassified. This means that, despite the spatial variability induced by ice melt and mixing between water masses, there was consistency between the physical setting and the timing and extent of the phytoplankton bloom. Schematically, it can be said that the bloom was triggered by ice melt-induced stratification of nutrient-rich AW as it moved northwards. The progressive input of meltwater pushed down the biomass maximum, which occurred deepest at those stations most influenced by ice (PSWi). Finally, the bloom progressively declined as nutrient-exhausted waters were recirculated south by the EGC.

1.3.1.3 Biological features

Elevated productivity and biomass were widespread features throughout the cruise. Compared to vertical profiles of either fluorescence or Chl *a*, c_p profiles did not display such a sharp decrease in biomass towards the surface (Fig. 1.1E). Biomass at the c_p maximum was around 1 m^{-1} in AW and PSWi stations, which approximately corresponded to a chlorophyll *a* concentration of 4 μg L^{-1}. Biomass in the UML was lower at PSW and PSWi stations (< 0.5 m^{-1}, chlorophyll < 1 μg L^{-1}) while it remained high (> 0.5 m^{-1}, chlorophyll > 1 μg L^{-1}) at those stations less influenced by ice (AW). Phytoplankton biomass was generally dominated by

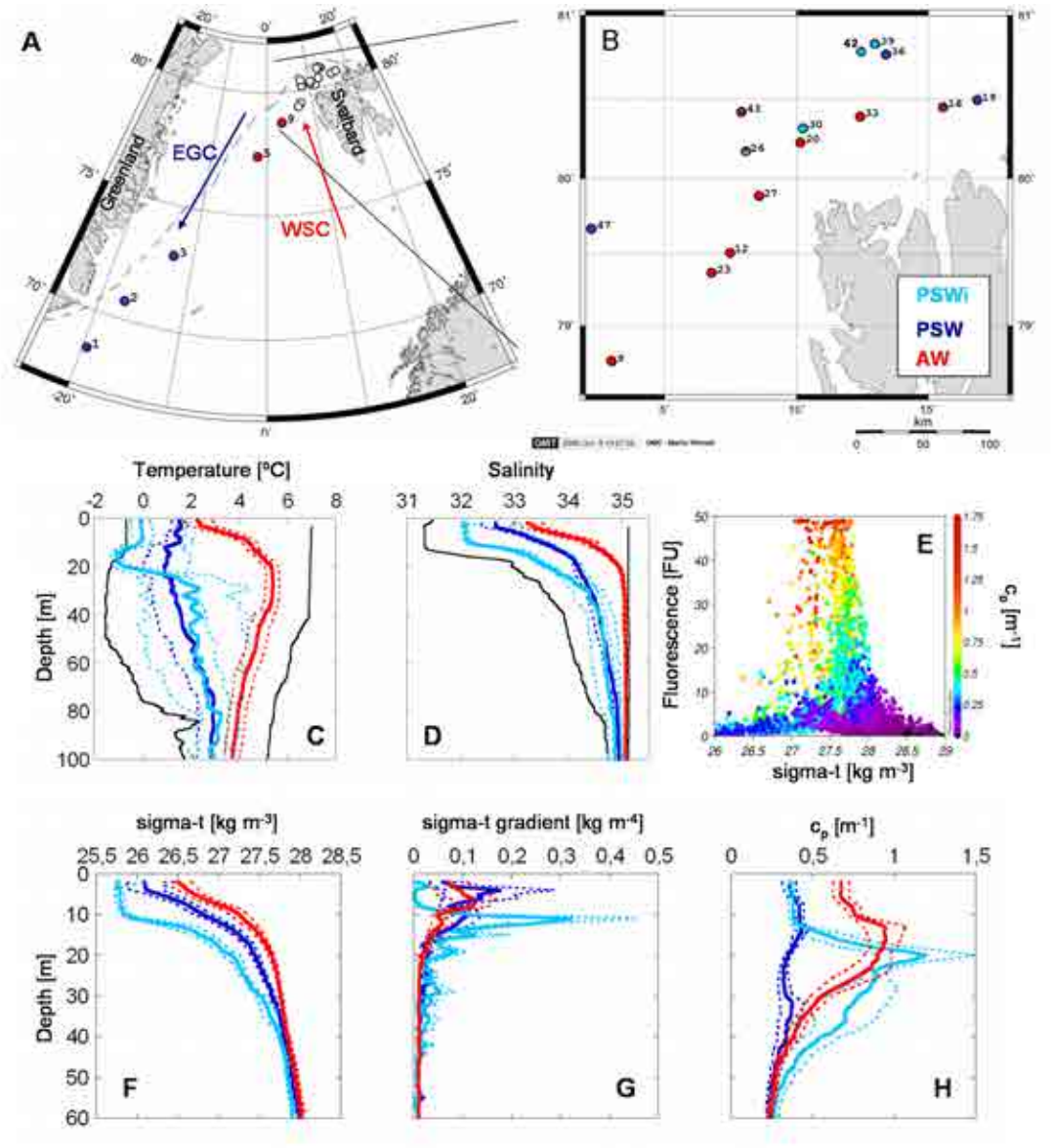

Figure 1.1: **Biogeochemical setting in the East Greenland current and Fram Strait** - Map of the stations where sulfur measurements were performed and synthesis of the oceanographic setting. (A) whole study area and main currents: EGC (East Greenland Current) and WSC (West Svalbard Current) with the approximate location of the sea ice edge (dashed line); (B) closer look to the Fram Strait Area. Note that non-sampled Stns. 27 and 47 are added as references of water mass end members. Red circles denote AW, dark blue squares PSW and light blue squares denote PSWi. Symbols in two colors represent those stations where classifications based on salinity (upper) and c_p (lower) disagreed; (C) temperature and (D) salinity, with the end member stations in black; (E) diagram showing the occurrence of the deep fluorescence maximum on a well constrained isopycnal surface, and the complementary information given by c_p; (F) density, (G) density gradient and (H) c_p for the aforementioned three groups. Vertical profiles are average $\pm$ SE.

the haptophyte *Phaeocystis pouchetii*, although dinoflagellates, diatoms and other nanoflagellates made significant contributions at some stations (Lasternas and Agustí, 2010). A highest proportion of heterotrophic biomass was found at EGC stations, supporting our view of the temporal-spatial progression of the bloom. *Phaeocystis pouchetii* , like its close relatives *P. globosa* and *P. antarctica*, is known for its ability to form quasi-monospecific blooms, and for the production of a mucilaginous polysaccharide matrix in which cells are embedded, forming large colonies (Schoemann et al., 2005). A relevant feature of bloom-forming *Phaeocystis* species is their elevated intracellular DMSP concentration (generally well above 100 mM) and DMSP lyase activity (Stefels and van Boekel, 1993; Stefels and Dijkhuizen, 1996), which can give rise to elevated concentrations of DMS and acrylate in seawater.

1.3.1.4 Radiation climate in the UML

As a result of ice thaw (together with light winds) a strong and shallow stratification of the surface water column was found during our cruise: the MLD ranged from 1.5 to 11 m (mean of 6 m). Due to the vertical distribution of microorganisms, the UML was more transparent than the waters beneath. The vertical diffuse attenuation coefficient for downwelling PAR (K_d) was on average 0.15 m^{-1} (with values spanning between 0.11 - 0.29 m^{-1}). Light extinction in the UML was governed by biogenic materials, as demonstrated by the positive correlation between K_d and c_p ($R^2 = 0.59$, $p < 0.001$, $n = 17$). Consequently, the differences in surface biomass translated into different PAR and UV transparency between AW and PSW(i) (Table 1.1). Overcast and misty skies predominated in the beginning and the end of the cruise, so that a low mean surface irradiance of 180 W m^{-2} was recorded (total solar spectrum). However, the combination of very shallow and moderately clear mixed layers with 24 h of continuous sunlight rendered notable daily UML averaged irradiances (mean 119, range 43 – 217 W m^{-2}). These values fall in the mid- upper range of values found in the world oceans (Vallina and Simo 2007). According to the calculated vertical attenuation coefficients for downward irradiance, the UML was exposed, on average, to >10% and >1% of subsurface UVA and UVB radiation (respectively) in most stations.

1.3.2 Dimethylated sulfur concentrations

1.3.2.1 Vertical profiles

DMSPt concentrations in the study area closely followed phytoplankton biomass, generally peaking at the c_p maximum (Fig. 1.2, and see Matrai et al. (2007)). In the upper 40 m of the

water column (roughly, the euphotic zone) DMSPt was 65.5 ± 50 nM (average ± SD), with a maximum of 163 nM, and below that depth it was never above 15 nM. DMS concentrations had a vertical pattern different from that of its precursor compound. It generally decreased from the subsurface to the deepest waters analyzed (85 m), although at some stations a second DMS peak was found at the depth of the c_p maximum. In the euphotic zone, DMS was typically around 5.3 ± 4 nM, reaching up to 18.3 nM. Below 40 m depth, DMS concentrations rarely exceeded 1 nM. Despite varying in a narrower range than the preceding compounds, DMSOt also exhibited a clear vertical pattern, with a mean of 51 ± 13.6 nM in surface waters and down to 5 m depth, and 27 ± 10.5 nM below that depth. DMSOd accounted for 58 ± 8% of DMSOt in surface waters where it was measured (n = 9, data not shown). In the context of *Phaeocystis* blooms, the DMSPt and DMS concentrations we report fall in the mid-low range (Stefels et al., 2007). To our knowledge, no review exists on DMSO pools and dynamics during *Phaeocystis* blooms. Integrating vertically the concentrations in the euphotic zone, we obtain that DMSPt, DMSOt and DMS accounted for 67 ± 5%, 28 ± 5% and 5 ± 2% of the total dimethylated sulfur, respectively. Due to shallow mixing, only a minor fraction of the sulfur pools was in the UML: approximately 20% of DMS and DMSOt, and only 10% of DMSPt.

1.3.2.2 Surface concentrations and sea ice

The highest spatial variability for the three sulfur compounds was encountered in subsurface waters (0.1 and 1 m depth, Fig. 1.3). DMS concentrations spanned one order of magnitude (1.5 to 18.3 nM), and were slightly lower at 0.1 m (mean 5.3 nM) compared to 1 m (mean 6.3 nM). DMSPt concentrations had an even broader span (5.6 to 163.6 nM), but were not different at 1 m or 0.1 m (overall mean around 70 nM). DMSOt concentrations varied between 19 and 85 nM, with a mean of 51 nM and slightly more disperse values at 0.1 m. Consistent with the differences found in surface biomass between station types, surface DMSPt was clearly higher at AW stations (102.5 ± 31.3 nM) than those at PSW and PSWi (18.8 ± 6.8 nM). However, no significant differences were found for DMS and DMSOt between station types (Fig. 1.3).

DMSOt (range of 7.9 – 12.2 nM) but no DMSPt were found in snow and surface ice, which supports an atmospheric origin of DMSO (Andreae, 1980). At two stations, higher amounts of DMSPt and DMSOt were found in bottom ice, with maximum concentrations of 90 and 24 nM respectively. In this case, a biological origin was feasible, but the concentrations were very low compared to the μM levels reported by Levasseur et al. (1994), or the hundred nM levels reported by Bouillon et al. (2002). Our results indicate that sea ice was not a major source

of dimethylated sulfur in the region at that time of the year, and therefore they will not be discussed.

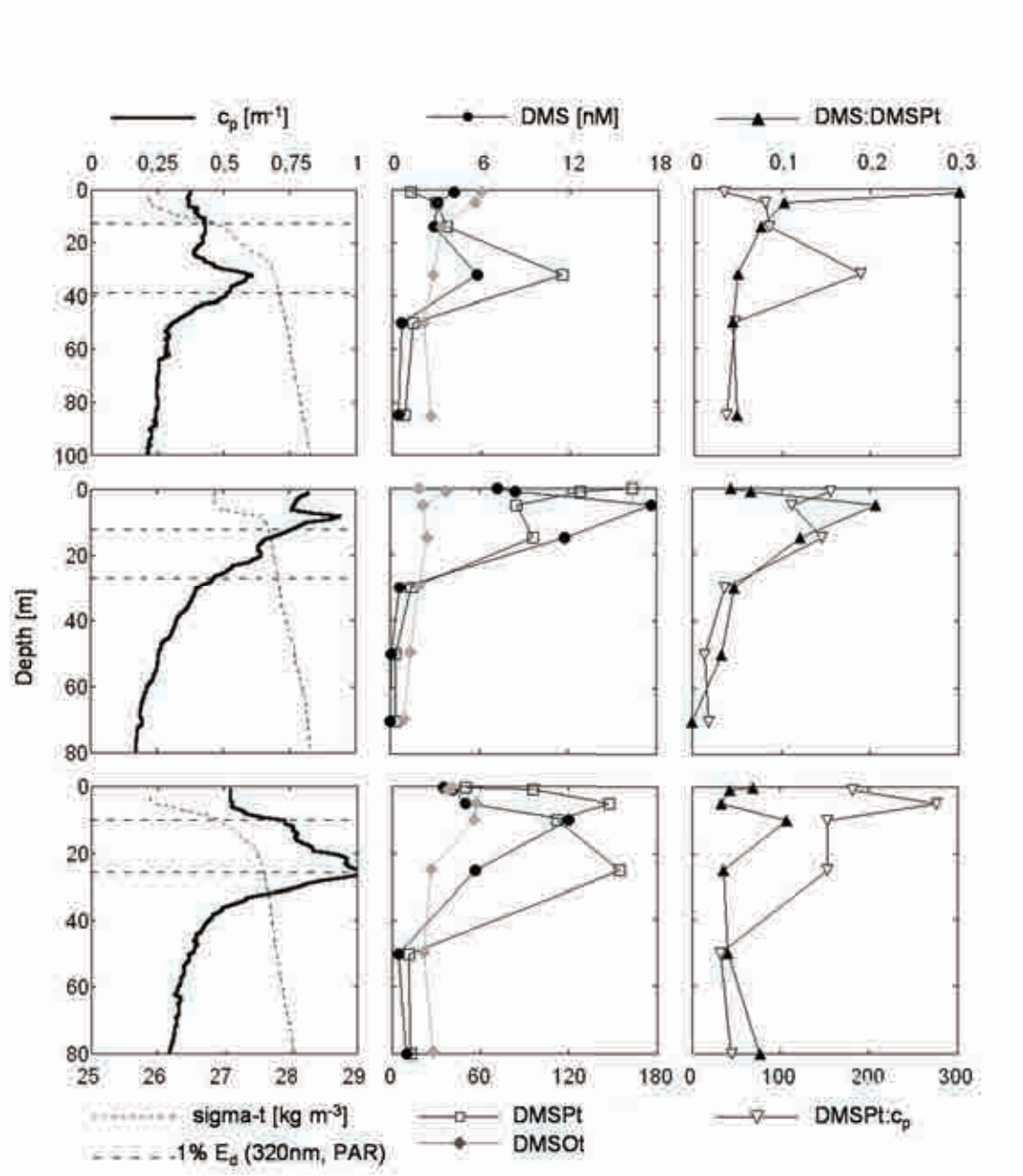

Figure 1.2: **Vertical profiles showing distinct biomass and dimethylated sulfur distributions with depth** - Stn. 1 (PSW, EGC; top panels), 9 and 20 (AW, Fram Strait area; middle and bottom panels). These stations are suggested to represent different stages of the bloom: early (9) middle (20) and late (1).

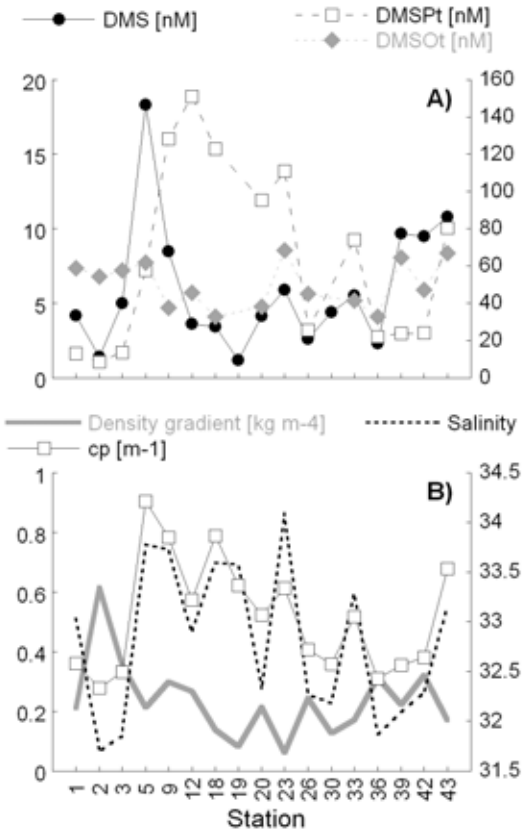

Figure 1.3: **Influence of stratification on surface DMS(P,O) concentrations** - Surface water properties at all 17 stations and day of sampling (July 2007): (A) concentration of dimethylated sulfur compounds; and (B) ice-induced stratification, salinity and planktonic microbial biomass. All values correspond to 1 m depth except the σ_t gradient (depth of the maximum gradient at the pycnocline).

1.3.3 Biological turnover of DMS

1.3.3.1 Production and consumption rates

DMDS amended incubations in all cases caused accumulation of DMS over that in non-amended incubations (Fig. 1.4). Gross DMS production rates at the surface (1 m) ranged between 1.4 nM d^{-1} (Stn. 1) and 14.8 nM d^{-1} (Stn. 42, Table 1.2). The stations belonging to the PSW group (EGC) showed the lowest gross production rates (<1.5 nM d^{-1}), while in strongly blooming waters and in the vicinity of the ice (AW and PSWi) gross production rates were higher (mean of 6.4 nM d^{-1}). At the fluorescence maximum, gross DMS production was also lowest at PSW stations (<1 nM d^{-1}) with an absolute minimum at Stn. 3 (0.4 nM d^{-1}). The maximum

was found at Stn. 12, with 12.7 nM d^{-1}. Bacterial DMS consumption at the surface had its minimum at Stn. 26 (0.37 nM d^{-1}) and its maximum at Stn. 42 (12.9 nM d^{-1}). At the fluorescence maximum, DMS consumption ranged between 0.8 nM d^{-1} (Stn. 3) and 16.8 nM d^{-1} (Stn. 20). No clear differences were found in DMS consumption between water masses and/or ice influence at either depth. The overall mean of bacterial DMS consumption in surface waters was 4.3 nM d^{-1}, slightly below the mean gross production of 5.5 nM d^{-1} (Table 1.2). At the fluorescence maximum, conversely, DMS consumption was 7.4 nM d^{-1}, slightly above the mean gross production of 5.9 nM d^{-1}.

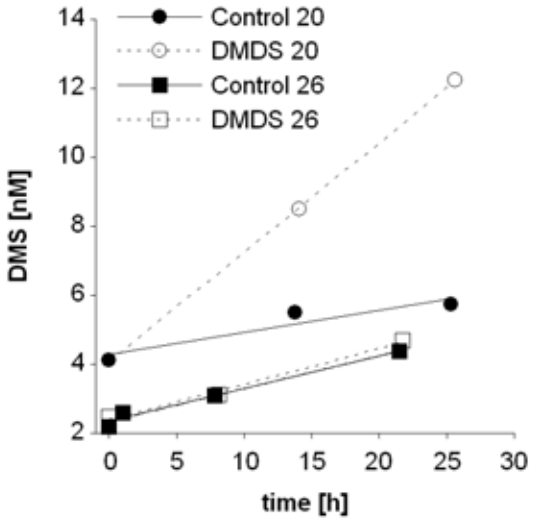

Figure 1.4: **Measuring gross DMS production with the inhibitor technique** - Examples of DMS evolution during biological process incubations at Stns. 20 and 26 (1 m depth).

1.3.3.2 Consumption and production rate constants

The rate constants (k's) of the biological process incubations were calculated as the process rate (nM d^{-1}) divided by the initial DMS concentration (nM). The Ks of gross DMS production (K_{gp}) in both surface and fluorescence maximum samples lay between 0.30 d^{-1} (Stn. 3) and 2.2 d^{-1} (Stn. 19 surface and Stn. 12 fluorescence maximum, Table 1.2). DMS consumption rate constants (k_{BC}) were in the same range, from 0.14 d^{-1} (Stn. 26 surface) to 2.2 d^{-1} (Stn. 19 surface). The mean rate constants in surface samples were 1.2 d^{-1} for production and 0.9 d^{-1} for bacterial consumption, while at the fluorescence maximum the mean Ks were 1.3 and 1.7 d^{-1} for production and consumption respectively (Table 2).

Table 1.2: Gross DMS production (GP) and biological DMS consumption (BC) rates for the UML (1 m) and fluorescence maximum samples, with the corresponding rate constants (k_{gp} and k_{bc}). The standard error of the slope (or the propagated SE when required) is shown in parenthesis. [a]Determined from GP in the light and NP in the dark. Not included in the means

Station	Sample depth (m)	GP rate (nM d^{-1})		BC rate (nM d^{-1})		k_{gp} (d^{-1})		k_{bc} (d^{-1})	
UML (1 m depth)									
1		1.4	(0.89)	2.9	(1.5)	0.32	(0.21)	0.70	(0.37)
3		1.5	(0.74)	1.3	(0.77)	0.30	(0.15)	0.26	(0.15)
9		6.8	(0.60)	6.6	(0.87)	0.80	(0.07)	0.78	(0.10)
12		6.9	(0.16)	1.6	(0.43)	1.9	(0.04)	0.45	(0.12)
19		2.6	(0.19)	2.5	(0.19)	2.2	(0.16)	2.2	(0.17)
20		7.6	(0.12)	6.1	(0.56)	1.8	(0.03)	1.5	(0.14)
26		2.5	(0.22)	0.4	(0.31)	0.95	(0.08)	0.14	(0.12)
42		ND		17.1[a]	(0.91)	ND		1.8[a]	(0.10)
42 light		14.8	(0.50)	12.9	(0.84)	1.6	(0.05)	1.4	(0.09)
Mean		5.5		4.3		1.2		0.9	
Fluorescence maximum									
1	34	0.62	(1.18)	3.90	(1.92)	0.3	(0.57)	1.9	(0.93)
3	25	0.41	(0.36)	0.82	(0.46)	0.27	(0.24)	0.54	(0.31)
9	15	5.2	(0.67)	5.1	(1.6)	1.8	(0.23)	1.7	(0.57)
12	9	12.7	(2.7)	16.8	(2.8)	2.3	(0.48)	3.0	(0.50)
20	25	10.6	(1.1)	10.4	(1.3)	1.7	(0.18)	1.6	(0.20)
Mean		5.9		7.4		1.3		1.7	

1.3.3.3 Dark versus light incubation

At Stn. 42, dark and light incubations were performed with the same surface water sample, to investigate whether solar radiation affected biological production and consumption. Duplicate bottles were incubated with the following treatments: DMDS-light, control-light and control-dark. In incubations kept under the sunlight, DMS evolution was corrected using the photochemical rate constant obtained from parallel photochemistry incubations. Net biological DMS production in the light (1.9 nM d^{-1}) was clearly higher than in the dark (-2.3 nM d^{-1}), but the lack of dark DMDS incubations obscures the interpretation of these results (see *Discussion*).

1.3.4 DMS photolysis

The rate constants of DMS photolysis in photochemistry experiments ranged from 0.50 d^{-1} (Stn. 42) to 1.14 d^{-1} (Stn. 20), with a mean of 0.81 d^{-1}. Once extrapolated to the whole UML, the photolysis rate constant ($k_{photo,UML}$) was on average 0.72 d^{-1}, equivalent to a mean in situ photolysis rate of 3 nM d^{-1} (Table 1.3).

1.3.5 Sea-air DMS flux

1.3.5.1 Sea surface fluxes

DMS emission fluxes at the sea surface varied between 0.5 μmol m^{-2} d^{-1} (Stn. 19) and 22.5 μmol m^{-2} d^{-1}(Stn. 42), with a mean flux of 6.5 μmol m^{-2} d^{-1}. Volumetric ventilation rates in the ML ranged from 0.07 nM d^{-1} (Stn. 19) to 2.77 nM d^{-1} (Stn. 36), averaging 1.12 nM d^{-1}. The corresponding range of ventilation rate constants ($k_{vent,UML}$) was 0.056 – 0.69 d^{-1}(mean 0.23 d^{-1}).

Table 1.3: Integrated irradiance during deck board incubations, CDOM characteristics (absorption coefficient at 300 nm and spectral slope in the 300 – 400 nm range), and K_{photo} obtained from the experiments and calculated for the entire UML. The sky was clear at Stn. 20 and 26 and heavily overcast at Stn. 39 and 42. Incubations generally started at 14:00 and ended between 21:00 and 02:00.

Station	Experiment							UML		
	UVB (kJ m^{-2})	UVA(kJ m^{-2}) (kJ m^{-2})	PAR (mol photons m^2)	$a_{CDOM,300}$ (m^{-1})	$S_{300-400}$ (nm^{-1})	k_{photo} (d^{-1})	k_{photo}/UVR (m^{-2} kJ^{-1} d^{-1})	$K_{d,340}$ (m^{-1})	$k_{photo,UML}$ (d^{-1})	Photo. rate (nM d^{-1})
20	5.0	160	6.9	0.94	0.010	1.14	0.007	0.40	1.05	4.43
26	5.6	200	8.7	0.38	0.023	0.69	0.003	0.44	1.04	2.6
39	1.8	59	2.3	0.43	0.026	0.93	0.015	0.35	0.55	3.01
42	2.6	85	3.2	0.58	0.014	0.5	0.006	0.29	0.23	1.85

1.4 Discussion

1.4.1 Factors controlling DMS(P,O) concentrations

1.4.1.1 Vertical profiles

The statistical analysis of dimethylated sulfur compounds concentration together with CTD variables revealed a different pattern for each of the compounds (Table 1.4). DMSPt was strongly correlated to indicators of algal biomass (especially to c_p) and negatively correlated with depth. The stepwise regression indicated that c_p was the only predictor worth including in the regression model, that is, with a slope significantly different from zero at the 0.05 level ($R^2 = 0.67$, $p < 10^{-7}$). Forcing the addition of the next most significant term in the model (fluorescence) increased the variance explained only to 70% ($R^2 = 0.70$). The high predictability of DMSPt from c_p probably stemmed from the abundance of *Phaeocystis pouchetii* during our study.

Intracellular DMSP concentrations in *Phaeocystis* are roughly 10 to 100 times higher than in diatoms, and in the same order of magnitude than in dinoflagellates (Hatton and Wilson, 2007; Stefels et al., 2007). The dominance of *Phaeocystis* and the elevated DMSPt:Chl *a* during our cruise (38.6 nmol μg^{-1}), a value in the upper edge of those found in *Phaeocystis* blooms (Stefels et al., 2007), suggests that *Phaeocystis* was the dominant species in terms of its contribution to the DMSPt pool. Assuming that almost all DMSP was particulate (after Kiene and Slezak (2006), the DMSPt:c_p ratio can be taken as a biomass-specific DMSP concentration, that is, a proxy for intracellular DMSP concentration. Even more, the evidence of low feeding rates on *Phaeocystis* by zooplankton, supported by field data from our cruise (Calbet *et al.*, submitted) and reported in the literature (review by Nejstgaard et al. (2007)), suggests that most DMSP was algae-bound. In Fig. 1.2 it can be observed that the DMSPt:c_p ratio had a vertical pattern somewhat different from that of DMSPt alone. Whether this distinct pattern resulted from differences in community composition or in physiological status with depth (and bloom phase) remains an open question.

In the case of DMS, only correlations with c_p and DMSPt (positive) and depth (negative) were significant individually. DMSPt was the only predictor accepted in the stepwise regression model ($R^2 = 0.42$, $p < 10^{-4}$), and forcing the addition of depth in the predictor matrix (the second most significant term) increased the explained variance only to 46%. Not surprisingly, DMS was less predictable than its precursor DMSP, due to the greater weight of physical forcing on its cycling (Simó and Pedrós-Alió, 1999c). DMS concentrations and, most important, the

Table 1.4: Correlation table for oceanographic variables and sulfur compounds in vertical profiles. The values are Pearson correlations, and are marked in bold when $p < 0.01$. The maximum number of XY pairs available has been used in each variables combination. N is 61, 54 and 51 for DMS, DMSPt and DMSOt respectively.

	DMSOt	DMS	DMSPt
Depth	**-0.65**	**-0.47**	**-0.40**
Temperature	-0.25	0.19	0.24
Salinity	**-0.71**	-0.14	-0.04
σ_t	**-0.76**	-0.23	-0.13
σ_t gradient	**0.48**	0.04	0.02
O_2	-0.25	-0.09	-0.01
c_p	0.09	**0.52**	**0.81**
Fluorescence	-0.33	0.16	**0.50**
DMSPt	0.07	**0.47**	
DMS	0.27		

DMS:DMSPt ratio, were highest in surface waters (Fig. 1.2). This might indicate that, despite greater rates of DMS photooxidation and ventilation close to the surface, an elevated exposure to solar irradiance favored a more efficient conversion of DMSP to DMS by the microbial food web.

Compared to the other sulfur species, DMSOt concentrations were strongly related to abiotic parameters such as density (or salinity) and depth, and increased clearly towards the surface. Interestingly, water density (σ_t) was the only predictor admitted in the stepwise regression model ($R^2 = 0.49$, $p < 10^{-3}$). This means that this parameter did the best at summarizing the environmental conditions that led to DMSOt accumulation. Production of dissolved and particulate DMSO through light-mediated biotic and abiotic processes is relatively well documented. Those processes include (a) DMSO production due to DMS photochemistry (Hatton, 2002; Kieber et al., 1996) and algal DMSP and DMS oxidation (del del Valle et al., 2007; Hatton and Wilson, 2007; Simó et al., 1998; Sunda et al., 2002), and (b) bacterial DMS oxidation, with a tendency towards higher DMSOd yields in the UML, (where lower bacterial DMS consumption rates normally occur), and higher DMS carbon utilization and sulfate production in deeper waters (del Valle et al., 2007; Delvalle et al., 2009). In the stably stratified surface waters of the Arctic, lower water density implies a higher exposure to solar radiation in the mid or long term. In fact, a correlation existed between the strength of the stratification and DMSOt concentrations. Finally, DMSOt concentrations could be interpreted in terms of bloom phase,

with higher values being associated with late bloom stages: at Stn. 9, where a situation of early bloom was found, DMSOt concentrations integrated over the top 100 m were 40% lower than at Stn. 1 or 20.

1.4.1.2 Surface concentrations

The amount of DMSPt, DMS and DMSOt at the immediate subsurface (0.1 m) compared to 1 m depth was very similar, with a ratio that approached 1, on average, for all three compounds. The existing variability, however, can tell us about the factors controlling each of the sulfur species. An overall higher variability was found for DMS (34% of the range about the mean) than for DMSPt (24%) or DMSOt (23%).

When we plotted DMSPt concentrations together with physical variables and biomass data at the surface, a clear picture of the factors explaining its surface distribution emerged (Fig. 1.3). Salinity and temperature at 1 m depth were positively correlated (Spearman's $r = 0.68$, $p < 10^{-3}$) illustrating the effect of ice melting. In turn, both variables were negatively correlated with the density gradient at the base of the mixed layer (r = -0.77, $p < 10^{-4}$, and r = -0.5, $p < 0.05$, for salinity and temperature, respectively), which means that ice melting controlled the strength of surface stratification. In addition, plankton biomass (c_p) varied inversely with salinity (r = -0.87, $p < 10^{-6}$) and the density gradient (r = -0.47, $p < 0.05$). This illustrates that recent meltwaters were not a good growth medium for DMSP producers (*Phaeocystis*), an inference supported by measurements of primary production and phytoplankton cells viability done in the same cruise (Lasternas et al., 2010). Indeed, surface DMSPt and c_p were highly correlated ($r = 0.87$, $p < 10^{-4}$). The higher concentrations of algal biomass and DMSPt in less isolated surface waters suggest that the DMSP stock at the surface was fed by living cells and detrital algal material entrained from waters below.

In the case of DMS, the picture was somewhat different. It seemed to follow DMSPt and biomass concentrations at some stations, while at others much of the DMS expected from its precursor had vanished. Indirect evidence that solar radiation was the main factor accounting for the 'missing' DMS at those stations is provided in Fig. 1.5. If we examine the relationship between the DMS:DMSPt ratio and the mean solar irradiance during the 24 h previous to sampling, a significant negative correlation exists (r = -0.82, $p < 10^{-3}$). Further evidence is found in the fine-scale DMS vertical gradient (previously normalized to the mean surface DMS concentration to account for the more pronounced gradients found at high-DMS stations), which also appears related to the previous surface irradiance (r = -0.73, $p < 0.01$, after removing one

outlier). Generally the DMS concentrations increased towards the surface when the daily mean irradiance was below 200 W m^{-2}. Conversely, if the daily mean irradiance was greater, then the DMS concentrations decreased towards the surface, indicating that DMS photolysis was able to counteract biological DMS production. Finally, lower UML-averaged DMS concentrations were associated with higher UML-averaged irradiances (r = -0.60, $p < 0.05$). Adding wind speed did not help explain more of the variance of the DMS variables, indirectly indicating an overall minor impact of sea-air flux in DMS cycling compared to solar radiation.

Surface DMSOt displayed less variability across stations than its precursor compounds (Fig. 1.3). It was correlated to DMS (r = 0.58, $p < 0.05$) but not to DMSPt (r = -0.22, $p > 0.05$) or c_p (r = 0.02, $p > 0.05$). This points to DMS photochemistry and bacterial DMS consumption as the main sources of DMSO(d), with algal production playing a secondary role. With a mean UML DMS of 5.5 nM, a mean $k_{photo,UML}$ of 0.7 d^{-1} with a DMSOd yield of 50%, and a mean k_{BC} of 0.9 d^{-1} with a DMSOd yield of 20% (yields taken from Delvalle et al. (2009), the DMSOd produced daily by DMS photochemistry (2 nM d^{-1}) would be twice that produced by microbial DMS oxidation. This would imply a turnover time of 10 d for the mean surface DMSOd of 30 nM in our study area. These figures are in quite good agreement with those presented in Delvalle et al. (2009) for the Ross Sea. Particularly, the calculated DMSOd turnover time falls between those found for the early and late phase of the *Phaeocystis antarctica* bloom in that work. Surprisingly, we found a negative correlation between DMSOt and the UML-integrated irradiance (r = -0.67, $p < 0.01$). This seems to contradict the statements made above, but could also indicate a solar radiation induced removal of DMSO. Our knowledge of DMSO removal pathways in oceanic waters is too poor to make better inferences.

1.4.2 Factors controlling biological DMS cycling

Biological DMS cycling was very fast, with turnover times as short as half a day encountered both in the UML and in the fluorescence maximum. On average, biological turnover occurred in 2.2 d and was never longer than 4 d (except at Stn. 26, where an extremely low bacterial consumption rate was observed). This range is very similar to that found by (Wolfe et al., 1999) in the Labrador Sea. In the following paragraphs we will examine what factors controlled the rates and rate constants (k's) of biological DMS cycling, with emphasis on those taking place in the UML.

DMSP cleavage in our study area was probably dominated by algal lyases. *Phaeocystis* species have been shown to dominate DMSP lyase activity in blooms where they occur in large

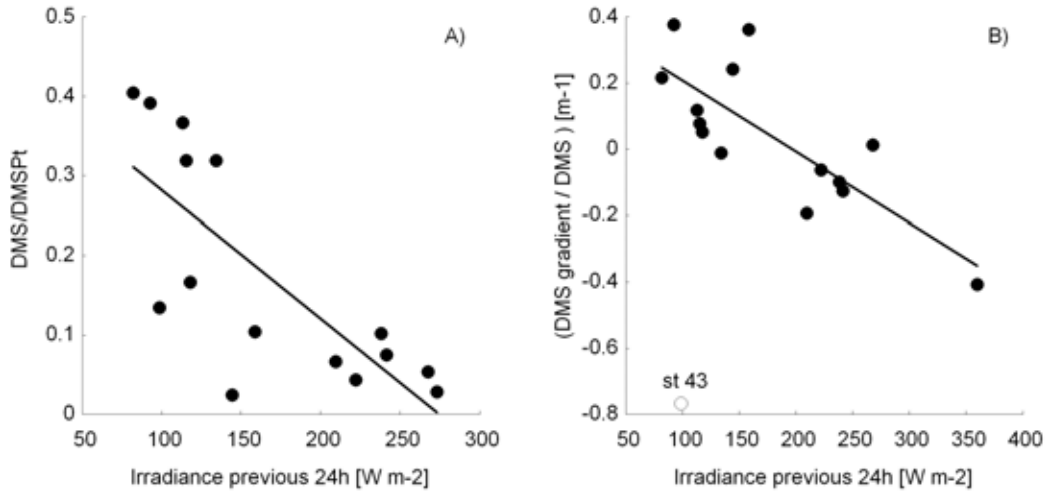

Figure 1.5: **Indirect evidence of the impact of photochemistry on surface DMS concentrations** - Relationship between the mean surface irradiance during the previous day and (A) the ratio DMS:DMSPt at 1 m depth; and (B) the gradient of DMS concentration in the first meters of the water column.

numbers (Stefels et al., 1995). In the Labrador sea, Cantin et al. (1999) found that most DMSP lyase activity occurred in the 2 – 11 and > 20 μm size fractions, although they could not refute that part of the DMSP lyase activity was due to attached bacteria. We could not quantify how much of the gross DMS production was grazing-mediated, but a low impact of micro- and mesozooplankton grazing on algal biomass was inferred from dilution experiments (Calbet *et al.*, submitted). This suggests that much of the DMSP might be directly cleaved after lysis of damaged cells, or upon DMSP exudation, which occurs at high rates in *Phaeocystis* compared to other phytoplankton (Laroche et al., 1999). In any case, most DMSP cleavage would be done by either membrane-bound enzymes of healthy algal cells (Stefels and Dijkhuizen, 1996) or by free (dissolved) lyases from lysed cells. The good correlation between gross community DMS production rates and in situ DMSPt concentrations ($r = 0.75$, $p < 0.01$, Stn. 42 excluded) supports this suggestion.

The above correlation includes data from both the surface (UML) and the fluorescence maximum, which did not seem to behave differently in terms of gross DMS production. The exception was Stn. 42 (surface), where a DMS production rate disproportionately high for the in situ DMSPt concentration was obtained. The ratio of gross DMS production (GP) to

the DMSPt stock gives an estimate of the DMSPt fraction that was transformed daily by the cleavage pathway. GP/DMSPt was between 0.01 and 0.16 d^{-1} at all stations, except at Stn. 42 (0.54 d^{-1}), where incubations were done in the light. Enhancement of DMS production as a result of high light or UV stress has been previously suggested by experimental results (Hefu and Kirst, 1997; Stefels, 2000; Sunda et al., 2002), and by model simulations (Toole et al., 2008; Vallina et al., 2008). Such stimulation by sunlight might have a strong impact on DMS budgets, but still awaits a clear experimental confirmation.

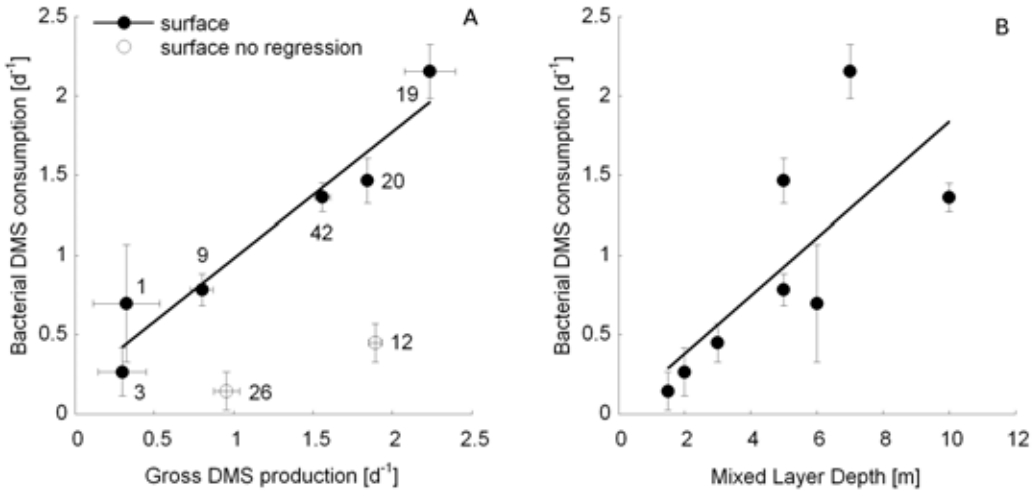

Figure 1.6: **Factors controlling bacterial DMS consumption in the UML** - (A) relationship between DMS production and consumption (1 m depth samples). Only points represented by the filled squares are used in the linear least squares fit, which has a slope of 0.79 $\pm$ 0.3. The station number is indicated adjacent to each point; and (B) relationship between DMS consumption and the MLD.

Pooling together surface and fluorescence maximum incubations, gross DMS production and bacterial consumption rates appeared tightly coupled at most stations ($r = 0.76$, $p <$ 001). From a temporal point of view, the rise in DMS production and, therefore, in DMS concentrations, would trigger the response of DMS consumers. DMS consumption rates did not seem to saturate at the highest DMS concentrations observed, and represented around 100% or more of the DMS produced in the fluorescence maximum (Table 1.2), and 80% in the UML (Fig. 1.6A). This coupling is a common feature of DMS cycling (see review by Simó (2004)) and has been observed in diverse systems and with varied methodological approaches. Looking

Table 1.5: Factors potentially controlling DMS production and removal in the UML. The values are Spearman correlations, and the asterisks denote significance at the $p < 0.05$(**) or $p < 0.10$ (*) level.

	k_{gp}	k_{bc}
Temperature	-0.67*	-0.38
Salinity	0.40	0.40
MLD	0.32	0.81**
σ_t gradient pycnocline	-0.48	-0.43
E_d previous 24 h	0.04	-0.11
DMS	-0.40	0.02
DMSPt	0.75*	0.21
c_p	0.62	0.45
Bacterial production (1 m)	-0.13	-0.05
k_{gp}		0.57

at surface rates, however, we can see that some stations deviated from the general coupling pattern (Stn. 12 and 26; Fig. 1.6A). To explore which factors could explain this decoupling, a correlation table was calculated including k_{GP}, k_{BC}, and environmental variables (Table 1.5). Among the factors considered, we found a strikingly good correlation between k_{BC} and MLD ($r = 0.81$, $p < 0.05$, Fig. 1.6B). Considering that the MLD regulates the exposure of plankton to solar radiation, we hypothesize that bacterial DMS consumers were inhibited by sunlight at the stations with the shallowest MLD (Stn. 3, 12 and 26), thus decoupling DMS consumption rates from gross production rates. This agrees with previous works reporting severe photoinhibition of DMS consumption in different oceanic regions (Toole2006). However, if that was the case, why was k_{BC} not strongly correlated ($r =$ - 0.11, $p > 0.10$) to the previous 24 h solar exposure?

A possible response lies in the timespan used to calculate the UML-integrated irradiance, that is, how long we go back in time to define the radiative history of the microbial community. Taking into account that our incubations were conducted in the dark, and that bacterial recovery from photodamage can take place over hourly time scales (Kaiser and Herndl, 1997), the observed effects should have occurred through succession in the bacterioplankton community. Selection of photoresistant bacteria would operate in a time scale of days by reducing the numbers of the less photoresistant bacterial populations, eventually affecting the DMS consumers. However,limited knowledge on the taxonomy of DMS consumers (Vila-Costa et al., 2006a; Schäfer, 2007) hampers our understanding of their response to solar radiation. Alternatively, slow or lack of dark recovery in the biochemical machinery implicated in DMS metabolism

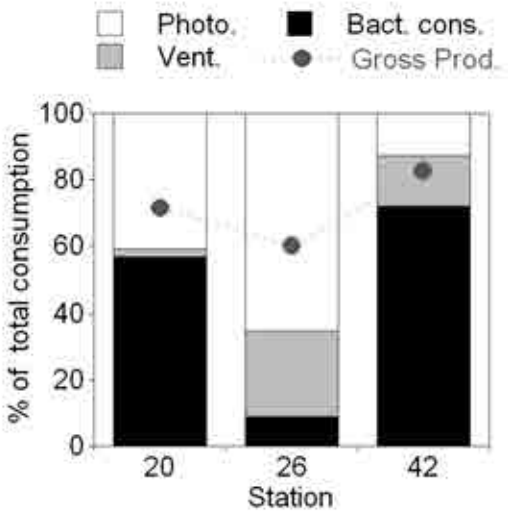

Figure 1.7: **DMS budgets in the UML** - Relative contribution of DMS loss processes to its removal from the UML, and comparison with the relative gross DMS production.

could also cause the observed effect.

1.4.3 Links between ice-induced stratification and sulfur cycling

1.4.3.1 Short term DMS budgets and sea-air flux

DMS cycling is characterized by its fast turnover. Adding up the three main processes that remove DMS from the UML in stratified conditions (that is, bacterial consumption, photolysis and degassing to the atmosphere) a mean turnover time of 0.8 d was obtained for our cruise. Based on measured k_{BC}, $k_{photo,UML}$ and $k_{vent,UML}$, we calculated that the mean relative contribution to DMS removal by bacterial consumption, photolysis and ventilation was 46%, 40% and 14% respectively. Fig. 1.7 shows that a shallower MLD (Stn. 26) caused simultaneously an increase in $k_{photo,UML}$ as a consequence of enhanced solar radiation doses, an increase of $k_{vent,UML}$ through the reduction of the volume of water exposed to wind stress, and a reduction of k_{BC} probably due to photoinhibition.

Another relevant information contained in Fig. 1.7 is that measured rates of gross DMS production were only able to supply 60 – 80% of the total DMS consumed. In our opinion, this imbalance suggests that gross DMS production was underestimated by dark DMDS-amended incubations, a fact that was also suggested by the distinct behavior of the only light incubation performed (Stn. 42), as described above. Few works exist that report oceanic DMS budgets

based on actual measurements of each of the processes involved, since normally one of them is calculated by budgeting upon assumption of steady state, a condition that approximately holds over a daily time scale. Due to methodological difficulties, gross DMS production is most frequently the indirectly calculated flux (e.g., Bailey et al. (2008)). All in all, comprehensiveness makes our data more valuable, despite methodological shortcomings related to dark incubations and the inhibitor method.

Focusing now on the sea-air DMS flux, we see that the mean value in our cruise (6.5 μmol m^{-2} d^{-1}) is above that reported for a cruise conducted in 1991 in a nearby region (2 μmol m^{-2} d^{-1}; Leck and Persson, 1996). The same authors report DMS concentrations to decline, from a maximum of ca. 10 nM in early August, at a rate of 30 % per week in the Arctic ice margin region through August and September. Thus, our cruise probably took place during the time of the year when highest DMS emissions occur in the Fram Strait area. This timing of DMS emissions is different from that reported for the Barents sea, where the peak occurs earlier in the season because of earlier sea-ice retreat (Matrai and Vernet, 1997; Gabric et al., 1999). However, the biogeochemical settings reported and simulated (respectively) in those studies differ significantly from ours, in that they found deeper mixing conditions and light limited phytoplankton growth.

Examining our flux calculations, it can be observed that seawater DMS concentrations and wind speed contributed almost equally to determinethe DMS flux. But, did wind speed exert a more indirect influence on DMS cycling? With the help of stepwise linear regression, we found that wind speed alone (over the previous 24 h) explained 52% of the variance of the MLD ($p < 0.01$, $n = 16$). Adding to the model the strength of stratification at the base of the UML, the variance of the MLD explained increased to 71% ($p < 10^{-3}$, $n = 16$), indicating that meltwater indeed helped maintain the strong and shallow stratification conditions. In the paragraphs and sections above, we have emphasized the control exerted by the pycnocline in the supply of cells and detritus from the richer waters underneath, and the importance of the mixing depth for the balance between competing DMS sinks. Since sea-air flux was generally a minor sink for DMS in the UML, it might well be that wind exerted the greatest influence on DMS cycling through partially controlling mixing depths, rather than through direct DMS emission.

The discussion hitherto has addressed the factors that seemed to modulate DMS cycling processes in the short term according to observations. Our data capture a snapshot of the DMS cycle in the Arctic ice edge in the ice melt season, as summarized in Fig. 1.8.

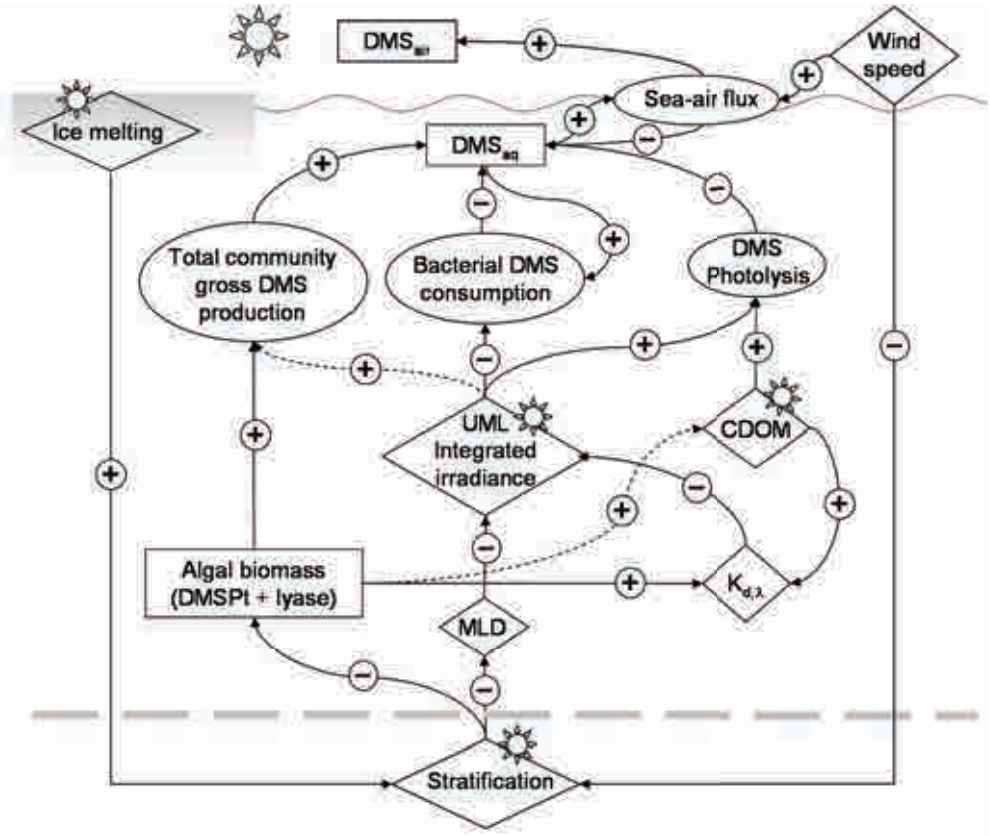

Figure 1.8: **Conceptual scheme linking dimethylated sulfur dynamics with surface stratification and ice melt dynamics during the ice-edge Phaeocystis bloom** - Rectangles: chemical and biological stocks and concentrations (measured, except $[DMS]_{air}$); diamonds: physical and chemical environmental forcings; ellipses: measured DMS fluxes (rates); round labels: sign of the interaction in the direction of the arrow; continuous lines represent connections that can be deduced from the data presented, or that were already well established; dashed lines represent proposed connections.

1.4.3.2 Mid and long term

Short term DMS dynamics in any marine environment take place within a physico-chemical setting that influences cycling processes both directly and by driving plankton community composition and succession. In our study case, physical climatic forcing (ocean circulation, ice melting) drove water productivity and exposure to solar radiation, two factors with major influence on DMS cycling. A third factor with a particularly large importance was the presence of *Phaeocystis pouchetii*. The success of this species may be due to a number of features. Among them, its ability to avoid grazers through colony formation, and its ability to thrive in shallow-mixed, ice-stratified, and highly irradiated waters seem key properties (Schoemann

et al., 2005). Our observation of marked absorption peaks around 330 nm in CDOM spectra, which probably indicates leakage of mycosporine-like aminoacids from algal cells during GF/F filtration (Jeffrey et al., 1999) supports the importance of photoprotective mechanisms in ice-stratified waters. In addition, DMSP and its degradation compounds DMS and DMSO may constitute an important physiological adaptation to cope with radiative stress (Sunda et al., 2002) or nutrient demand-unbalanced growth (Stefels, 2000). It turns out that any change in environmental conditions able to modify the strength, duration and extent of the ice-edge *Phaeocystis* bloom, will have a strong impact on sulfur biogeochemistry in the Arctic, and on its role as an atmospheric DMS source.

During summer 2007, a historical minimum of Arctic sea ice was observed, together with an abnormal atmospheric circulation pattern and a deeper northwards penetration of Atlantic Waters. A sea-ice free Arctic summer is envisaged within the next few decades (Stroeve et al., 2008). Gabric et al. (2005) predicted a 90% increase in Arctic DMS emissions (in a scenario of atmospheric CO_2 tripling by 2080) as a result of a larger ice-free area and a longer growth season. This would represent a significant DMS-derived cooling effect. However, the numerical model used in that work appears too simple to capture the complex dynamics and spatial heterogeneity of the Arctic ecosystem. In summary, great changes in Arctic biogeochemistry (including volatile sulfur emissions) are likely to occur yet remain difficult to predict.

1.5 Conclusions

During July 2007, dimethylated sulfur dynamics in the Greenland Sea and Arctic Ocean were basically driven by phytoplankton biomass, i.e., the 'bloom regime' postulated by Toole and Siegel (2004) as opposed to the (UV) stress regime found in oligotrophic regions. High potential for elevated summertime DMS concentrations and emissions did exist, owing to the dominance of *Phaeocystis pouchetii*, but they were constrained by the fast photochemical and bacterial DMS consumption in the UML. Our findings portray a highly buffered system: vertical mixing causes alternation among DMS loss processes, preventing exaggerated consumption or build up.

Differences in DMS, DMSPt and DMSOt concentrations at the ocean surface resulted from the complex interaction of biological processes and physical (ultimately meteorological) forcing. Ice melting added complexity to the usual open-sea picture of DMS cycling, and created an isolated layer of fresher and colder water that acted as a highly irradiated trap for organisms

and molecules, episodically entrained from below, and as a lid on the more productive waters underneath. This thin UML played a key role in regulating the flux of DMS to the atmosphere.

Acknowledgements

We thank the chief scientist of the ATOS1 cruise, C.M. Duarte, the marine technicians (UTM) and the crew aboard the BIO Hespérides for their assistance and cooperation. We also thank J.M. Arrieta and A. Tovar-Sánchez for collecting surface samples, and A. Calbet, D. Vaqué and S. Lasternas for sharing unpublished biological data. The work of 2 anonymous reviewers, as well as proofreading by B. Tomlinson, helped improve the manuscript. This work was supported by the Spanish Ministry of Science and Innovation through the IPY project ATOS (POL2006-00550/CTM) and the project SUMMER (CTM2008-03309). M.G. acknowledges the receipt of a JAE PhD scholarship from the CSIC. This is a contribution of the Research Group on Marine Biogeochemistry and Global Change, supported by the Generalitat de Catalunya.

Chapter 2

Stimulation of gross dimethylsulfide (DMS) production by solar radiation

Galí, M., Saló, V., Almeda, R., Calbet, A., and Simó, R. (2011). *Geophysical Research Letters*, 38(L15612).

Abstract

Oceanic gross DMS production (GP) exerts a fundamental control on the concentration and the sea-air flux of this climatically-active trace gas. However, it is a poorly constrained process, owing to the complexity of the microbial food web processes involved and their interplay with physical forcing, particularly with solar radiation. The *inhibitor method*, using dimethyldisulfide (DMDS) or other compounds to inhibit bacterial DMS consumption, has been frequently used to determine GP in dark incubations. In the work presented here, DMDS addition was optimized for its use in light incubations. By comparing simultaneous dark and light measurements of GP in meso- to ultraoligotrophic waters, we found a significant enhancement of GP in natural sunlight in 7 out of 10 experiments. Such stimulation, which was generally between 30 and 80% on a daily basis, occurred throughout contrasting microbial communities and oceanographic settings.

2.1 Introduction

Oceanic DMS is a minor volatile byproduct of the microbial cycling of dimethylsulfoniopropionate (DMSP), a multifunctional osmolyte produced by ubiquitous oceanic phytoplankton (Simó, 2001; Stefels et al., 2007). Even though only a tiny fraction (generally $< 10\%$) eventually escapes to the atmosphere, its global emission amounts ca. 28 Tg S y^{-1} (Lana et al., 2011), and comprises $> 90\%$ of the biogenic sulfur flux and around 20% of the total (man-made, volcanic and biogenic) sulfur flux to the atmosphere (Simó, 2001). Several DMS(P) cycling processes are influenced by solar radiation. This translates into a positive correlation between solar radiation and DMS concentration in most of the surface ocean, across latitudes and seasons (Vallina and Simó, 2007). This correlation provides support for the controversial CLAW hypothesis (Charlson et al., 1987), which postulates that a negative feedback between oceanic plankton and the radiative forcing could occur through the influence of DMS emissions on atmospheric aerosol chemistry and, ultimately, on the albedo of stratiform clouds.

The major DMS removal pathways in the upper mixed layer (UML) are photolysis and bacterial consumption, and their response to sunlight is relatively well understood (Toole et al., 2006). In contrast, DMS production mechanisms and their response to physical forcing are more poorly known. Microbial processes contributing to DMS production include phytoplankton release upon enzymatic cleavage of DMSP, phytoplankton autolysis, non-assimilatory microbial DMSPd metabolism, and viral lysis and zooplankton grazing on DMSP producers (Stefels et al., 2007). With current methods, the contribution of each process to bulk GP cannot be determined independently. Moreover, it could well be that the sum of the different components did not yield the actual GP rates due to unexpected interactions. Hence, DMS cycling studies have to rely on determinations of bulk GP rates.

Two distinct approaches, with their own advantages and pitfalls, exist for the determination of GP: a direct measurement, generally by use of bacterial consumption inhibitors in dark incubations (Wolfe and Kiene, 1993a; Simó et al., 2000); or an indirect estimate, which requires determining the bulk net DMS evolution over time together with all the consumption terms (Bailey et al., 2008). The latter approach can benefit from accurate radioisotope measurements of DMS loss rates, but suffers from increased uncertainty owing to error propagation, since at least three rate measurements are involved in the budget. In addition, radiolabeled DMS (e.g., ^{35}S-DMS) is not commercially available. On the other hand, the inhibitor method, though allowing direct determination of GP, is dependent on the efficiency of the inhibitor used and,

if applied under natural light conditions, requires the simultaneous measurement of the photochemical DMS loss, which also contributes error. In this work we present evidence of increased GP (as determined with the inhibitor method) due to sunlight exposure and propose alternative hypotheses to explain this observation.

2.2 Methods

2.2.1 Sampling and oceanographic data processing

Six different months throughout the seasonal cycle were sampled in the coastal NW Mediterranean, whereas the Southern Indian Ocean Subtropical Gyre and the Tasman Sea were sampled during the austral summer aboard the R/V Hespérides (Table 2.1). Vertical profiles of conductivity, temperature and photosynthetically active radiation (PAR) were obtained from CTD casts, and subsequently processed to calculate the mixed layer depth (MLD) and the diffuse attenuation coefficient of downwelling PAR ($K_{d,PAR}$). Total solar irradiance of the prior 48 h, recorded by land- or ship-based meteorological stations, was used for light history calculations. Depending on the water column stability, the previous exposure of microbial communities to solar radiation (SR_{UML}) was calculated as the UML average (Vallina and Simó, 2007), or as that found at the sampling depth (see Table 2.2, SI). Surface water samples (5 or 3 m depth) were collected in the morning and incubated on a building's roof (Mediterranean) or on the ship's deck (Indian Ocean and Tasman Sea) as described below. Further details about the procedures concerning ancillary data reported herein can be found in Calbet et al. (2008).

2.2.2 Incubations and DMS(P) analyses

DMS concentrations during the incubations were measured by purging, cryotrapping and sulfur-specific gas chromatography coupled to flame photometric detection (GC-FPD), while DMSP was measured as DMS after undergoing alkaline hydrolysis (Saló et al., 2010). Calibrations were conducted with a DMS permeation tube (Simó et al., 1998). Whole seawater samples were incubated for 24 – 29 h in a tank with continuous flow from a seawater intake to maintain the temperature close to that of the sampling site. Duplicate UV-transparent Teflon bottles of 2 L were covered by a neutral screen that decreased natural sunlight irradiance by 38%. Parallel, duplicate amber glass bottles wrapped in black plastic were set in the tank as dark incubations. All dark and light bottles were amended with 200 nmol L^{-1} dimethyldisulfide

(DMDS), an effective inhibitor of bacterial DMS consumption (Wolfe and Kiene, 1993a), to obtain dark and light gross DMS production rates (GP_D and GP_L, respectively).

In typical dark DMDS-amended incubations, DMS builds up linearly as long as DMDS inhibition holds (Galí and Simó, 2010; Saló et al., 2010), so that the slope of the linear regression of $[DMS]$ over time yields GP_D. In natural sunlight, DMS evolution is affected by non-constant photolysis over time. This sometimes results in non-linear DMS build-up, so that *apparent* GP_L (aGP_L) is more easily calculated from initial and final $[DMS]$ and elapsed time:

$$GP = \frac{[DMS]_f - [DMS]_0}{t_f - t_0} \tag{2.1}$$

Although DMS evolution with intermediate time points was monitored during all dark incubations (as well as in light incubations, though with lower frequency), we calculated GP_D with the t_f - t_0 approach for coherence with aGP_L. GP_D rates calculated in this manner differed from regression-derived GP_D by a 0 – 27% (mean 9%) excess (see Table 2,3, SI).

2.2.3 Photolysis correction and DMS photolysis in DMDS-amended incubations

Along with whole water biological process bottles, duplicate dark and light Teflon bottles containing < 0.2 μm-filtered water were incubated to measure DMS photolysis rates. In this way, aGP_L in the whole water bottles could be corrected to obtain the actual GP_L, with the assumption that photolysis follows the same kinetics in whole waters as in the filtered waters. Photolysis rate constants (units of d^{-1}) in < 0.2 μm-filtered water were calculated as

$$K_{photo,inc} = \frac{-ln([DMS]_f/[DMS]_0}{t_f - t_0} \tag{2.2}$$

where $[DMS]_f$ and $[DMS]_0$ are, respectively, the final $[DMS]$ (after being corrected for dark DMS production in filtered waters) and initial $[DMS]$. The mean DMS photolysis rate ($Photo_{inc}$) was computed from mean $[DMS]$ during the incubation ($[DMS]_{inc}$), defined as the average of $[DMS]_f$ and $[DMS]_0$

$$Photo_{inc} = K_{photo,inc}[DMS]_{inc} \tag{2.3}$$

and aGP_L was corrected following:

$$GP_L = aGP_L + Photo_{inc} \tag{2.4}$$

Table 2.1: Summary of characteristics of the initial water samples. Abbreviated phytoplankton group names are: Diat (diatoms); Crypt (cryptophytes); Hapt (haptophytes, or prymnesiophytes); Dino (dinoflagellates); Syn (*Synechococcus*); Pro (*Prochlorococcus*); Neuk (nanoeukaryotes); Peuk (picoeukaryotes). Neuk and Peuk are populations defined by flow citometry, with no taxonomic meaning a priori; nd = not determined; DMS and DMSPt in nmol L^{-1}.

Date	Lat. (°N)	Long. (°E)	Temp. (°C)	MLD (m)	Chl *a* (μg L^{-1})	Chl *a* <10 μm (%)	Dominant phyto	DMS	DMSPt
Mediterranean Sea									
11/29/05	41.22	2.13	16.1	40	0.97	61	Diat >> Crypt > Hapt	1.5	11.4
01/18/06			13.0	40	0.47	81	Crypt > Diat > Hapt	0.9	12.4
05/16/06			18.1	5	0.95	60	Diat >> Hapt ˜ Crypt	1.6	10.0
06/14/06			21.1	5	0.49	88	Dino > Hapt ˜ Crypt	7.8	71.0
07/31/06			24.4	5	0.39	79	Diat ˜ Syn > Crypt	5.2	17.5
08/29/06			24.4	nd	0.31	90	Syn > Hapt > Crypt	5.8	27.0
Indian Ocean and Tasman Sea						Chl *a* <2 μm (%)			
02/24/11	-30.05	61.46	24.9	32	0.094	63	Pro > Neuk > Peuk	0.73	6.8
02/28/11	-29.56	72.45	24.5	31	0.040	46	Neuk > Pro > Peuk	1.04	7.4
02/04/11	-29.75	86.26	22.5	26	0.033	51	Pro ˜ Neuk > Peuk	0.96	7.5
03/28/11	-38.66	150.42	21.1	46	0.34	73	Pro ˜ Syn ˜ Peuk	0.78	8.3

In addition to the simple correction, we also calculated a time-resolved photolysis that accounted for nonlinearities due to the first-order kinetics of DMS photolysis and the diel variation in irradiance. Only very small differences between the two methods were observed (smaller than the experimental error), so we used the simple correction outlined in equations 2 and 4 throughout.

The concern arose as to whether DMDS addition to whole water bottles interferes with the kinetics of DMS photolysis. To test this, we performed a series of independent DMS photochemistry experiments, where < 0.2 μm-filtered (or < 30 kDa tangential flow filtered) seawater was spiked with DMDS at concentrations ranging from 100 nmol L^{-1} to 2 μmol L^{-1}. No significant effects (compared to unamended samples) were observed at [DMDS] less than or equal to 200 nmol L^{-1}. Above this concentration, DMDS caused an increase in DMS photolysis and the departure from first-order kinetics (Fig. 2.1). Since DMDS does not appreciably absorb actinic radiation, its effect could happen through a concentration-dependent transient increase in the amount of oxidants. Therefore, a maximum [DMDS] of 200 nmol L^{-1} is recommended to avoid underestimation of GP_L.

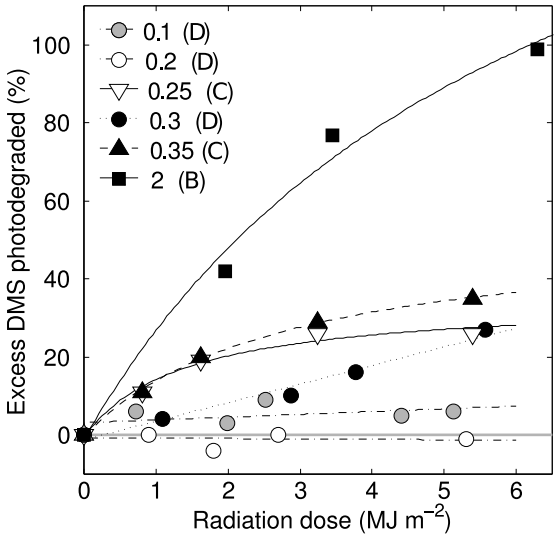

Figure 2.1: **Effects of DMDS additions on DMS photolysis.** - Different symbols and fillings in the legend denote different DMDS concentrations added, in mol L^{-1}. Letters in parentheses denote the different samples incubated (only time-course experiments shown; see SI for additional experiments). The equations fitted are Michaelis-Menten-like curves or straight lines. Initial DMS concentrations (nmol L^{-1} are: 21.1 (B); 27.8 (C); and 9.1 (D).

2.3 Results and discussion

Our study covered a wide range of environmental conditions, evident in the water column stratification parameters, phytoplankton biomass and community composition summarized in Table 2.1. In terms of sulfur cycling, this is illustrated by the extremely wide range displayed by the DMSPt:Chl *a* ratio (12 – 227 nmol μg^{-1}). In Mediterranean samples, low GP_D rates were found in the vertically mixed waters of November and January (< 1 nmol L^{-1} d^{-1}), whereas the stratified waters of May through August displayed higher GP_D rates (2.3 – 6.3 nmol L^{-1} d^{-1}). This resembles the seasonal pattern of GP_D found by Vila-Costa et al. (2008) at the nearby Blanes Bay Microbial Observatory. In the Indian Ocean and Tasman Sea, dark GP_D rates ranged 0.38 – 0.82 nmol L^{-1} d^{-1}, in accordance with the low plankton biomass and DMSPt concentrations found.

Once corrected for photochemical DMS loss, GP_L was significantly higher than GP_D in 7 out of 10 experiments ('significant' meaning that their respective error intervals -the ranges of duplicate incubations- did not overlap; Fig. 2.2). The January sample was the most responsive, with a 207% difference between GP_L and GP_D, coinciding with a severe experimental overexposure (Table 2.2, SI). The remaining 6 samples where significant stimulation occurred, which were exposed to more realistic irradiance, displayed stimulations between 30 and 78%. On the other hand, two of the samples displaying no stimulation were clearly underexposed during the incubations (Nov and Ind2). Yet, no correlation could be found between sunlight-stimulated GP and light history, experimental exposure, or any other biotic or abiotic variable.

Support for light-stimulated gross DMS production exists in the experimental literature. However, no attempts have been made at constraining its magnitude on a daily basis, a key time frame for DMS cycling studies. In the Sargasso Sea, Toole et al. (2006) observed that total DMS loss (as measured with ^{35}S-DMS) increased at higher irradiances and higher proportions of shortwave UVR mainly due to increased photochemical loss. Nevertheless, net DMS production remained very close to zero irrespective of UVR dose, indicating that an extra source of DMS must exist to compensate for the increased loss. These results also indicated some spectral dependence of DMS production, which deserves further investigation.

Stress-induced DMS release by phytoplankton is feasible based on physiology. In this regard, two non-exclusive explanations have been put forward relating it with high irradiance and nutrient starvation: the overflow hypothesis (Stefels, 2000) by which DMSP and DMS serve as an overflow mechanism when phytoplankton undergo unbalanced growth; and the antioxidant

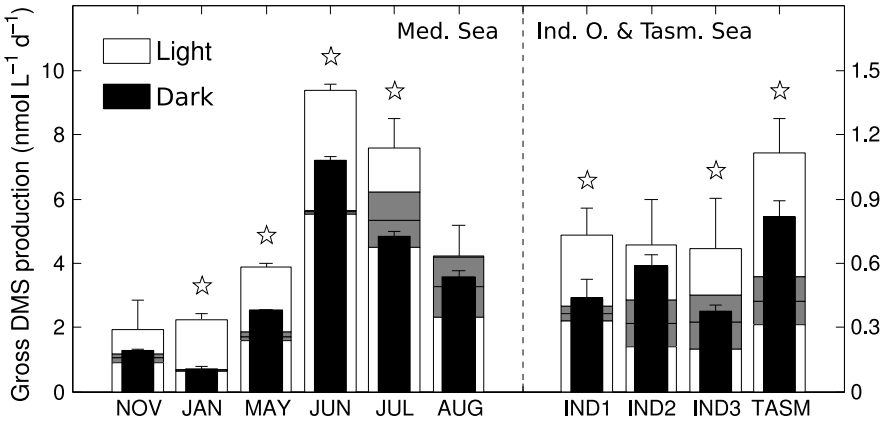

Figure 2.2: **Dark vs. light gross DMS production in 24 h incubations** - GP_D and GP_L calculated from initial and final DMS concentrations, and associated uncertainty. Grey intervals on white bars represent $aGP_L \pm$ error range, so that the relative weight of the photolysis correction on the final GP_L values can be appreciated. Stars denote experiments where the error ranges of GP_D and GP_L did not overlap.

hypothesis (Sunda et al., 2002), which states that the downstream products of DMSP cleavage, including DMS, could act as intracellular radical scavengers. Cell membrane-permeating DMS would leak from this protective cascade of antioxidant metabolites. DMS + DMSP release rates of the order of 1 to 11% d^{-1} (as % of the intracellular DMSP pool) have been reported for axenic cultures of haptophyte and dinoflagellate strains (Stefels et al., 2007). Remarkably, Archer et al. (2010b) recently found higher values during short term exposure to UV of a non-axenic *Emiliania huxleyi* strain: 8 – 14% d^{-1} for DMS and 13 – 22% d^{-1} for DMSP, which could supply a considerable fraction of the sunlight-induced GP.

In the field, and consistent with both the overflow and the antioxidant hypotheses, potential enzymatic DMSP to DMS conversion (the so-called 'lyase' activity) has been shown to correlate with radiative stress conditions (Harada et al., 2004; Bell et al., 2007). However, the relative importance of sublethal physiological responses (like the up-regulation of DMSP synthesis and/or lyase activity) compared to lethal UV damage of the most sensitive phytoplankton (Agustí and Llabrés, 2007) is unknown. UVR-induced cell membrane damage or, directly, cell disruption, would induce DMS(P) release, along with algal lyases from some phytoplankton, stimulating DMS production without any need for short-term physiological regulation.

But, is algal release the major driving mechanism behind sunlight-induced DMS production? UVR seems to enhance DMSP exudation, and a variable fraction of the dissolved DMSP (DMSPd) pool will be channeled to DMS depending on the dissolved lyase activity, the yield

of dissolved DMSPd to DMS conversion by bacteria, and the algal share of DMSPd uptake (Vila-Costa et al., 2006b). Enhancement of the bacterial yield by UVR has been proposed, but Slezak et al. (2007) obtained inconclusive results: bacterial yields did not always increase after irradiation, and when they did, they were often offset by severe photoinhibition of bacterial DMSPd uptake. Even more uncertain are the interactive effects of UVR exposure and food-web processes like viral lysis and microzooplankton grazing (Sommaruga, 2003), but they should not be overlooked. Microzooplankton grazing accounted for 63 and 72% of GP_D in our experiments of June and July, respectively (Saló et al., 2010).

The existence of a sunlight-associated DMS source is also consistent with mechanistic and diagnostic models. At low latitudes, annual maxima of DMS concentrations co-occur with the lowest plankton biomass, a feature named the 'summer DMS paradox' (Simó and Pedrós-Alió, 1999a). Reproducing this uncoupling represents a challenge for modelers (Le Clainche et al., 2010), and some recent studies (Toole et al., 2008; Vallina et al., 2008; Vogt et al., 2010) have identified stress-induced (algal) DMS release as the key mechanism allowing mechanistic models to simulate the summer paradox.

At the global scale, marine ecosystems are facing important changes in the decades to come. UVR-transparent, highly irradiated oligotrophic waters are expanding due to global warming and increased vertical stratification (Polovina et al., 2008), thus expanding the 'stress regime' areas, as depicted by Toole and Siegel (2004). Conversely, diagnostic modeling exercises suggest that DMS emission is a very resilient ecosystem function, which should undergo very little fluctuations in the near future in spite of enhanced stratification due to global warming (Vallina et al., 2007). Our work points at sunlight as an important modulator of DMS production, but further work is required to understand the physiological and ecological basis of sunlight-driven DMS production and its variability across diel to seasonal time scales.

Acknowledgments

This work was supported by the Spanish Ministry of Science and Innovation through the projects MICROROL (CTM2004 – 02575/MAR), SUMMER (CTM2008 – 03309), and the CONSOLIDER-INGENIO 2010 project Malaspina (CSD2008 – 00077), and through PhD scholarships to V.S and R.A. M.G. acknowledges the receipt of a JAE PhD scholarship from the CSIC. We thank Marta Estrada for Chl *a* data and Eva Sintes and Kerstin Olbrich for flow

citometry data. This is a contribution of the Research Group on Marine Biogeochemistry and Global Change, supported by the Generalitat de Catalunya.

2.4 Supplementary Information (SI)

Mixing depth and light history calculations

Estimation of mixed layer depth (MLD) and in situ solar exposure

MLD was defined as the depth where either temperature or σ_t (density) varied by > 0.02 °C or kg m^{-3}, compared to the respective values at the surface reference depth (fixed at 5 m). These criteria are likely to capture the actively mixing layer depth (Brainerd and Gregg, 1995). However, the water column was thermally stratified up to the surface in the coastal Mediterranean in May through August CTD profiles, and no proper mixed layer existed. According to these criteria, the previous exposure of microbial communities to solar radiation (SR_{UML}) was computed in 2 different ways. In November and January Mediterranean samples, as well as in Indian Ocean and Tasman Sea samples, UML-averaged irradiance (SR_{UML}) was calculated from downwelling irradiance at the water subsurface ($E_{d,0-,48h}$) during the 48 h prior to sampling, the MLD, and the underwater light attenuation ($K_{d,PAR}$), according to Vallina and Simó (2007). In May through August, in the Mediterranean, SR_{UML} was defined as the total irradiance received at a fixed depth of 5 m (we have used the same notation for simplicity).

Estimation of in-situ UVR exposure in the coastal Mediterranean

To calculate UVB, UVA and PAR exposure history (Table 2.2, SI), we employ the same type of calculation, after first scaling subsurface UVB, UVA and PAR to total irradiance. The respective conversion factors were obtained from a set of rooftop experiments recently performed, where UV irradiance (6 wavebands centered at 305, 313, 320, 340, 380 and 395 nm) and PAR (one integrated band) were recorded with a UV-VIS radiometer (Biospherical PUV 2500). Vertical attenuation coefficients for UVB and UVA in the water column (not measured in the experiments reported here) were calculated from the linear regression between K_d, PAR and $K_{d,UVB}$ or $K_{d,UVA}$, respectively, obtained from a time series study at the nearby Blanes Bay Microbial Observatory (BBMO) (Galí *et al.*, unpublished). The equations used are:

$$K_{d,UVB} = 1.99 K_{d,PAR} + 0.12 \tag{2.5}$$

($R^2 = 0.42$)

$$K_{d,UVA} = 1.48 K_{d,PAR} - 0.01 \quad (2.6)$$

($R^2 = 0.76$)

$K_{d,PAR}$ spanned a similar range of values at both study sites (see Table 2.2 for $K_{d,PAR}$ of this study).

Estimation of experimental UVR exposure in Mediterranean rooftop experiments

UVB, UVA and PAR exposure during the rooftop incubations (Table 2.2) were calculated similarly to in situ subsurface irradiance. The daily-averaged irradiance in each of these wavebands was corrected for the attenuation of the neutral screen placed on top of the incubator (62% transmittance at all UVR wavelengths and PAR), and for the spectral transmittance of the bottles used. The Teflon bottles (Nalgene, made of fluorinated ethylene-propylene polymer, FEP) transmitted 65%, 77% and 100% of UVB, UVA and PAR, respectively. Their spectral transmittance was measured with a USB 2000+ hyperspectral radiometer (Ocean Optics).

Photolysis correction in light incubations

The experimentally determined photolysis rate constants ($K_{photo,inc}$) integrated DMS photolysis over the duration of the whole incubation (with the corresponding daytime variation in $E_{d,0-,t}$) and over the full solar spectrum. Spectral variability in CDOM light absorption and apparent photolysis quantum yields were not a concern, since biological incubation and photolysis bottles had the same spectral transmittance. However, there is no doubt that varying $E_{d,0-,t}$ resulted in variable photolysis rates. Furthermore, given the pseudo first-order kinetics of DMS photolysis (Bouillon and Miller, 2005; Kieber et al., 1996), instantaneous photolysis rates would depend on [DMS], resulting in non linear DMS evolution over time. To check if these nonlinearities were efficiently captured by $K_{photo,inc}$ without producing too large a bias, we computed GP_L using a number of approaches with increasing levels of complexity and iterations.

Table 2.2: Underwater PAR attenuation ($K_{d,PAR,UML}$) in m^{-1}; UVR in W m^{-2}; and PAR in μmol photons m^{-2} s^{-1}. SR_{UML} and SR_{EXP}, respectively, refer to in situ and experimental exposure to total (pyranometer) solar radiation (the SRD index of Vallina and Simó (2007).

Experiment	$K_{d,PAR,UML}$	UVB_{UML}	UVB_{EXP}	UVA_{UML}	UVA_{EXP}	PAR_{UML}	PAR_{EXP}	SR_{UML}	SR_{UML}
Nov 2005	0.14	0.01	0.06	0.4	1.6	28	111	14	61
Jan 2006	0.12	0.009	0.05	0.4	1.2	24	86	13	47
May 2006	0.16	0.06	0.19	3.2	4.7	221	322	116	176
Jun 2006	0.15	0.08	0.19	4.4	4.7	294	326	155	178
Jul 2006	0.10	0.12	0.19	5.9	4.8	348	334	183	182
Aug 2006	0.10	0.082	0.10	3.8	2.4	224	168	118	92
Ind1								103	124
Ind2								129	86
Ind3								230	225
Tasm								54	70

At any time, DMS production in DMDS-amended bottles would vary according to:

$$\frac{[DMS]}{dt} = GP(t) + K_{photo}(t)[DMS] \tag{2.7}$$

As a first approach, the integrated $K_{photo,inc}$ obtained in parallel incubations of filtered water was applied to the mean $[DMS]$ of the whole-water DMDS-amended bottles ($[DMS]_{inc}$) to obtain the mean photolysis rate in those bottles. This yielded a first estimate of GP_L ($GP_{L,simple}$), which corresponds to eq. 2.4 of the article. Using that equation means assuming constant $[DMS]$ (and thus, constant photolysis rates) throughout the experiment. This was obviously not the case, because bottles were incubated for 24 h – 29 h under naturally variable sunlight, and because $[DMS]$ possibly underwent variations during the incubation. For this reason, the hourly irradiance time series from a nearby meteorological station (Badalona Museu, http://www.meteocat.com/mediamb_xemec/servmet/), in the Mediterranean experiments, or from the ship's meteorological station, was used to calculate hourly photolysis rates, assuming proportionality with irradiance:

$$k_{photo,t} = \frac{k_{photo,inc} E_{d,0-,t}}{E_{d,0-,inc}} \tag{2.8}$$

Because all incubations showed higher GP in the light (although not always significantly), GP_L could be calculated under the assumption that higher GP_L occurred during the daytime. This has been recently supported by experimental data (Gal *et al.*, unpublished). Therefore, estimates of the daily GP_L could have also been made following three different approaches according to the representation of the k_photo:

a) *Time-resolved photolysis and constant GP_L.* In this scenario $[DMS]$ is predicted with hourly resolution (Δt = 1 h), according to:

$$[DMS]_t = [DMS]_{t-1} + GP_L \Delta t + K_{photo,t-1}[DMS]_{t-1}\Delta t \tag{2.9}$$

The calculation was repeated iteratively changing GP_L (with aGP_L as the starting value), until the simulated $[DMS]$ equaled the real $[DMS]_f$ ($\pm$ 1%) at the end of the incubation. The resulting GP_L is thus the actual GP_L.

b) *Time-resolved photolysis, constant background GP and radiation driven extra-GP.* In this case, GP is split into a constant background GP, designated as dark GP (GP_D), and a

radiation driven GP_L. The latter is modulated by hourly irradiance in the same manner as photolysis in eq. 2.8:

$$GP_{L,t} = \frac{GP_L E_{d,0-,t}}{E_{d,0-,mean}} \tag{2.10}$$

and $[DMS]$ is predicted over time according to

$$[DMS]t = [DMS]_{t-1} + GP_D + GP_{L,t-1}\Delta t + K_{photo,t-1}[DMS]_{t-1}\Delta t \tag{2.11}$$

which is iterated as in (a). No integration of GP_L,t is needed, because the iterated GP_L is already the average actual GP_L (nM h^{-1}). It only has to be converted to nM d^{-1}.

c) *Time-resolved photolysis and radiation-driven GP only.* The last approach consists of setting $GP_D = 0$ in eq. S7. This way, DMS production rates are entirely a function of sunlight.

When applied to our experiments, the inclusion of any time-resolved photolysis correction (either a, b or c) did not alter the results by more than 10% (thus, within the overall experimental error), compared to the simplest correction approach (described by eq. 3 and 4 of the paper). For that reason, we adopted the simple correction.

We also checked how different ways of computing the average DMS concentration in whole water bottles during the sunlit incubations ($[DMS]_{inc}$) affected the calculation of the amount of DMS photooxidized (eq. 3 of the article). When we took into account the DMS concentrations measured at intermediate times, and interpolated linearly the missing hourly $[DMS]$ values, the resulting $[DMS]_{inc}$ differed by less than 10% (and in almost all cases by ca.$< 5\%$) from the $[DMS]_{inc}$ computed using only initial and final [DMS]. Thus, as described in the main text, $[DMS]_{inc}$ was computed from initial and final DMS concentrations only.

DMS photolysis in DMDS-amended incubations

Experiments were carried out in order to determine whether DMDS additions affected DMS photolysis rates, thereby affecting the photolysis correction described above. The potential for such an artifact was assessed both in time-course and t_f-t_0 experiments. Seawater was sampled at the BBMO (http://www.icm.csic.es/bio/projects/icmicrobis/bbmo) on four different dates between March and August. The water was filtered through a 0.2 μm polycarbonate filter or, in one occasion (experiment 3), ultrafiltered by tangential flow, which excluded molecules larger than 30 kDa. Initial DMS concentrations ranged from 8.6 to 27.8 nol L^{-1}. Along with unamended and DMDS-amended samples, dark bottles were incubated in the same conditions

Table 2.3: Comparison between GP_D rates derived from linear regression or final-initial DMS concentrations (± standard error of regression slope and range of duplicate bottles, respectively).

Experiment	Regression				Final-initial
	$GP_{D,slope}$ ± SE	R^2	p	n	GP_D ± range
Nov 2005	0.94 ± 0.18	0.79	0.0014	10	1.29 ± 0.02
Jan 2006	0.58 ± 0.11	0.75	0.00060	12	0.72 ± 0.05
May 2006	2.29 ± 0.32	0.88	0.00018	10	2.54 ± 0.01
Jun 2006	6.33 ± 0.77	0.94	7.8×10^{-8}	12	7.19 ± 0.14
Jul 2006	4.98 ± 0.53	0.96	4.6×10^{-6}	10	4.84 ± 0.14
Aug 2006	2.82 ± 0.50	0.78	0.00030	12	3.57 ± 0.11
Ind1	0.44 ± 0.05	0.93	0.00011	8	0.44 ± 0.09
Ind2	0.59 ± 0.05	0.98	0.00021	6	0.59 ± 0.05
Ind3	0.36 ± 0.05	0.93	0.0017	6	0.38 ± 0.03
Tasm	0.81 ± 0.15	0.88	0.0054	6	0.82 ± 0.07

to account for an eventual dark increase in [DMS]. When this occurred, DMS was produced at a constant rate in dark bottles (suggesting DMSPd cleavage by free lyases), and $[DMS]$ in exposed bottles was corrected accordingly. Experiment 1 was carried out under natural sunlight in a bath with running seawater from the coastal intake system (temperature ca. 23 °C); experiments 2, 3 and 4 were carried out in a solar simulator (SUNTEST CPS+, Atlas) equipped with a xenon arc lamp which closely matches solar spectral irradiance. The bottles were kept in a thermostatted bath at 20 °C.

DMS was analyzed by GC-FPD, using an activated carbon packed column (Carbopack BHT, Supelco) operated at 170 °C. Under these conditions, DMS eluted at 0.90 minutes, and DMDS at 2.30 minutes. The high temperature of the column helped minimize problems derived from transient DMDS adsorption due to its stickiness to apolar materials. DMDS 'bleeding' can increase the sensitivity of the analytical system (known as the 'doping' effect), yielding artificially higher DMS concentrations. For that reason, care was taken to calibrate the instrument with sequential injections of DMS standard (Dynacal permeation tube, VICI Metronics) before and after passing of DMDS. When necessary, single injections of standard were done to further check the performance of the GC. The analytical system was not well suited for DMDS quantification, so photochemical destruction of DMDS could not be monitored. Nevertheless, DMDS peak areas remained above our calibration range, indicating that DMDS concentrations were high throughout the irradiation (which is a condition for its use as an inhibitor). The results of the $t_f - t_0$ experiments (those not included in Fig. 2.1) are summarized in Table 2.4.

Table 2.4: Summary of DMDS addition photolysis experiments where only t_0 and t_f were sampled (letters correspond to the same water samples as in Fig. 2.1). Excess DMS photolysis at the final radiation dose has been calculated only for those [DMDS] that caused significant changes compared to the unamended bottles.

Experiment (sample code)	$[DMS]_0$ (nmol L^{-1})	[DMDS] added (nmol L^{-1})	Radiation dose (MJ m^{-2})	K_{photo} ± SE (MJ m^{-2})	Excess DMS photolysis (%)
A	9.8	0	15.48	0.030 ± 0.0004	
		200	15.48	0.032 ± 0.0005	
B	16.1	0	5.4	0.064 ± 0.004	
		200	4.6	0.069 ± 0.008	
		500	3.8	0.157 ± 0.006	22.4
		2000	2.7	0.298 ± 0.002	51.7
C	26.2	0	5.6	0.052 ± 0.007	
		200	5.3	0.055 ± 0.011	
		350	4.7	0.078 ± 0.016	10.1
		500	4.1	0.127 ± 0.034	21.9

We are not aware of any study reporting on the interaction between DMS and DMDS during aqueous photooxidation. Possible explanations could be related to a transient increase of oxidants derived from sulfenyl radicals or their derivatives, formed upon DMDS photolysis (Barnes et al., 1994; Yin et al., 1990a,b). The interaction between DMDS (or its degradation compounds) and chromophores or other DOM-bound hydrophobic moieties could also play a role, as shown for other photosensitized reactions (Zhang and Hsu-Kim, 2010).

Chapter 3

Sunlight-stimulated gross dimethylsulfide (DMS) production: Interactive effects of spectral irradiance, the microbial community and its light history

Galí, M., Ruiz-González, C., Lefort, T., Gasol, J. M., Cardelús, C., Romera-Castillo, C., and Simó, R. Accepted in *Limnology and Oceanography*.

Abstract

We investigated the short-term effect of sunlight on the gross biological production of dimethylsulfide (DMS), a trace gas with potential climatic effects, in eight experiments performed through the seasonal cycle of an oligotrophic northwest Mediterranean coastal site. Whole water samples were taken at dawn and incubated under different irradiance conditions and in the dark. Both total irradiance and ultraviolet radiation (UVR) were manipulated using different bottles and filters, and spectral irradiance conditions were monitored. The exposure was set to mimic, within a reasonable range, the in situ radiation climate at each time of the year. Experimentally determined net community DMS production, DMS photolysis, and dark microbial DMS consumption rates were used to calculate gross community DMS production by budgeting. In addition, the composition of the bacterioplankton and phytoplankton communities in the initial samples, and the photoinhibition of bulk bacterial heterotrophic activity and phytoplankton photosynthetic efficiency were monitored. Our results show that: 1) gross DMS production is irradiance-dependent, with a short-term stimulation factor of up to 6-fold compared to dark incubations; 2) its spectral shape is variable but generally similar to that of phytoplankton photoinhibition or photodamage; and, 3) the light history of the microbial community critically affects sunlight-dependent DMS production.

3.1 Introduction

Solar radiation is a major driver of biogeochemical processes. In the last decades, our understanding of how the ultraviolet (UV; 280-400 nm) region of the spectrum influences major carbon and nutrient cycling pathways (e.g., photosynthesis, heterotrophic activity, and photochemical reactions), as well as its effects on organism survival and population dynamics, has increased significantly (Häder et al., 2007; Zepp et al., 2007). In parallel, spectrally-resolved models for photochemical and photobiological processes have been developed (Neale and Kieber, 2000). Despite all these facts, routine measurements of biogeochemical processes naturally occurring under sunlight are seldom conducted under UVR-inclusive conditions.

Dimethylsulfide (DMS) is a volatile sulfur compound produced at the ocean's surface as a result of microbial cycling of dimethylsulfoniopropionate (DMSP), an ubiquitous algal osmolyte (Simó, 2004). The oceanic emission of this single volatile annually transfers ca. 28 Tg of sulfur to the atmosphere (Lana et al., 2011), and some of it back to land, balancing biospheric sulfur budgets (Lovelock et al., 1972). Atmospheric DMS oxidation influences aerosol chemistry, potentially promoting the formation of cloud condensation nuclei in remote marine regions. Twenty-five years ago, a paradigm-changing paper (Charlson et al., 1987) proposed that, if DMS emission resulted in increased cloud albedo and, in turn, it responded positively to irradiance or temperature, a negative feedback would operate between oceanic plankton and the Earth's radiative budget. Since the so-called CLAW hypothesis (after the author's initials) was postulated, several studies have unveiled the complexity of oceanic DMS cycling (Simó, 2004; Stefels et al., 2007) and, although the feasibility of the whole hypothesis remains controversial (Levasseur, 2011; Quinn and Bates, 2011), there is a growing body of evidence pointing at solar radiation as a major driver of DMS cycling (Simó, 2004; Vallina and Simó, 2007; Lana et al., 2012).

DMSP is a multifunctional zwitterion found at high concentrations in the cytosol of various phytoplankton groups, mainly prymnesiophytes, dinoflagellates, chrysophytes, prasinophytes and pelagophytes (Corn et al., 1996; Stefels et al., 2007). Some algal DMSP producers can enzymatically cleave it to DMS (and acrylate), but the cleavage activity varies widely within phytoplankton groups and even among different strains of the same 'species' (Franklin et al., 2010). In addition, a major portion of algal DMSP is released to the dissolved phase due to algal exudation, senescence or autolysis, viral lysis and microzooplankton grazing (Stefels et al., 2007). Dissolved DMSP (DMSPd) undergoes active microbial cycling (Vila-Costa et al.,

2006a; Moran et al., 2012), but only a minor fraction of microbially-consumed DMSP results in DMS production by bacterial enzymes, the remainder being diverted into microbial biomass and non-volatile compounds (Kiene and Linn, 2000; Moran et al., 2012). In turn, seawater DMS is readily oxidized, either by bacteria or by photochemical reactions, and only a minor fraction is vented to the atmosphere (Simó, 2004; Stefels et al., 2007; Vila-Costa et al., 2008).

Several processes in this dimethylated sulfur cycling scheme are influenced by sunlight. At the global scale, this seems to translate into a strong correlation between average irradiance in the upper mixed layer and DMS concentrations (Vallina and Simó, 2007; Lana et al., 2012). Algal DMSP synthesis has been interpreted as a physiological adaptation to high light and nutrient limitation. Stefels (2000) suggested that DMS(P) excretion could constitute an overflow mechanism for excess reduced compounds when phytoplankton undergo unbalanced growth. Shortly after, Sunda et al. (2002) put forward the antioxidant hypothesis, whereby intracellular DMSP cleavage would allow the scavenging of reactive oxygen species by DMS, acrylate, and subsequent DMS oxidation products (dimethylsulfoxide and methanesulfinic acid). At the ecosystem level, sunlight modulates microbial DMSPd utilization (Slezak et al., 2001, 2007), and the relative importance of heterotrophic and autotrophic DMSPd consumers (Ruiz-González et al., 2012f). On the other hand, DMS sinks are also related to sunlight: UVR inhibits bacterial DMS consumption (Toole et al., 2006; Kieber et al., 2007), and drives DMS photolysis (Toole et al., 2003).

Recently, Galí et al. (2011) reported that gross DMS production was stimulated by the exposure to full spectrum sunlight, in water samples from distinct coastal and open ocean ecosystems. However, several uncertainties remained regarding the irradiance response patterns, the specific regions of the solar spectrum promoting such response, and the interplay between solar exposure and microbial community structure and activity. In the present work we have addressed these issues by means of eight short incubation experiments, combining bulk DMS cycling budgets with an array of algal and bacterial physiological indicators. Our results improve the current understanding of ecosystem gross DMS production, which is, despite its importance, a poorly constrained term in models of dimethylated sulfur cycling.

Table 3.1: Summary of the water column conditions on the sampling dates, and initial sample characteristics. MLD stands for mixed layer depth. $K_{d,320}$ is the diffuse attenuation coefficient for 320 nm wavelength radiation (WI: winter, SP: spring, SU: summer and AU: autumn).

Experiment	Date	Temp.	Sal.	MLD	$K_{d,320}$	Chl a	Chl $a < 3$ μm	Bacteria	DMS	DMSPt
		(°C)		(m)	(m^{-1})	μg L-1	μg L^{-1}	10^5 cells mL^{-1}	nmol L^{-1}	nmol L^{-1}
WI1	18 Mar 2010	11.9	37.7	15	0.44	1.25	0.42	8.5	3.2	6.8
SP1	12 May 2009	15.2	37.8	9	0.37	0.54	0.27	6.9	3.1	46.3
SP2	26 May 2009	16.8	37.6	8	0.34	0.58	0.27	8.9	6.2	38.5
SP3	9 Jun 2009	16.5	38.0	8	0.32	0.30	0.13	12.3	3.3	14.6
SU1	9 Jul 2008	23.0	37.8	4	0.35	0.20	0.15	8.5	9.0	48.6
SU2	30 Jun 2009	17.8	38.2	6	0.28	0.12	0.06	8.8	3.6	13.2
SU3	21 Jul 2009	20.3	38.1	8	0.26	0.13	0.03	9.4	3.4	15.9
AU1	30 Sep 2008	20.2	38.3	4	0.34	0.23	0.14	7.5	1.3	18.6

3.2 Methods

3.2.1 Sampling and experimental setting

Between summer 2008 and winter 2010, surface water samples (0.5 m depth) were collected on eight occasions at the Blanes Bay Microbial Observatory (BBMO), a northwest Mediterranean coastal site (< 24 m depth; 0.5 miles offshore; 41°39.9' N, 2°48.3'E). BBMO is well characterized in terms of bacterioplankton and phytoplankton community succession (Alonso-Sáez et al., 2008; Gutiérrez-Rodríguez et al., 2011) and dimethylated sulfur cycling (Vila-Costa et al., 2008; Simó et al., 2009). One experiment was conducted in late winter (WI1), three in spring (SP1, SP2, and SP3) and summer (SU1, SU2, and SU3), and one in early autumn (AU1), covering the phytoplankton succession from bloom to low-biomass conditions (Table 3.1).

The samples were taken before sunrise to avoid prior exposure to sunlight, and brought within 2 h to the laboratory in dimmed polycarbonate carboys. In situ temperature and salinity profiles were measured with a conductivity, temperature, and depth (CTD) probe (SAIV A/S model SD204) also equipped with turbidity and chlorophyll *a*(Chl *a*) fluorescence sensors. Underwater UVR and photosynthetically-active radiation (PAR) profiles could not be measured on experiment days as we sampled before sunrise. Instead, radiation profiles obtained in the routine monthly sampling at BBMO (since 2008) were used to reconstruct the underwater radiation field, in conjunction with CTD and meteorological data (see below).

A gradient of spectral irradiance was created by manipulating total irradiance and the UV region of the spectrum, making a total of 5 treatments: Two spectral treatments, with two irradiance levels each, plus one dark treatment (Table 3.2). Total irradiance was regulated using a variable number of neutral screen layers, adjusted in each experiment to match in situ mixing conditions. Spectral manipulation was achieved using incubation bottles with different spectral transmittance: polytetrafluoroethylene bottles (Teflon®, Nalgene; abbreviated T), which transmit the full solar spectrum, and polycarbonate bottles (Nalgene; abbreviated PC), which have the 50% cutoff at 339 nm, eliminating almost all ultraviolet B radiation (UVB; 280-320 nm). Thus, the high irradiance treatments (T and PC) had their dimmed counterparts (labeled T_{dim} and PC_{dim}). Biological DMS cycling rates were measured in whole water samples, incubated in single or duplicate 2.3 L bottles. DMS photolysis was measured in duplicate or triplicate bottles (40 mL to 250 mL), filled with 0.22 μm-filtered water obtained from a sequential filtration system connected to a peristaltic pump (system routinely used for DNA collection, with 3 and 0.22 μm pore size filtration cartridges). Biotic and abiotic process bottles,

Table 3.2: Summary of experimental manipulations and their corresponding treatment code (see text for a detailed description). The irradiance transmitted by each bottle type in different wavebands is also given (see Fig. 3.2).

Treatment	Bottle material	Transmitted irradiance (%)			Neutral screens (No.)	Mean duration	
		UVB	UVA	PAR		Bio. processes	Photolysis
T	Teflon	65	77	100	0-1	5.7	3.8
Tdim					1-3	7.1	4.2
PC	Polycarbonate	11	77	100	0-1	6.7	3.8
PCdim					1-3	7.6	4.2

covered by ca. 5 cm of running seawater, were incubated in a black tank on the roof of the lab. Spectral irradiance at the water subsurface was continuously recorded with a profiling ultraviolet (PUV-2500, Biospherical) multichannel filter radiometer placed inside the tank.

The experiment work flow was as follows: when the carboy arrived at the lab, aliquots for the determination of initial parameters were withdrawn, and the black plastic bag that covered the carboy was removed to allow some degree of initial photoacclimation in room light. The biological process bottles were filled without bubbling, after gently mixing the carboy, using silicone tubing. All the materials used were cleaned with hydrochloric acid, milli-Q water and the same seawater sample. Once all biological process bottles had been filled (within 30 min), they were immediately set in the incubation tank (ca. 3 h before solar noon). DMS photolysis incubations started around 1 h after whole water incubations, and were stopped after 3 – 4 h of exposure. Biological process incubations lasted for 5 – 9 h, after which aliquots were taken to measure DMS and DMSPt, post-exposure bacterial heterotrophic activity, and the photosynthetic performance of phytoplankton (see below).

3.2.2 Sample processing and analysis

3.2.2.1 DMS and DMSP analysis

DMS and DMSP were analyzed using a purge and trap system coupled to sulfur-specific gas chromatography (GC; Shimadzu GC14A) with flame photometric detection (Simó et al., 1996). For DMS analysis (analyzed $<$ 1 h after the end of the incubation) 3-5 mL of seawater were gently passed through a syringe filter (GF/F, Whatman) and immediately sparged in a crimp glass vial for 3-5 min with 40 mL min^{-1} of high purity He. Volatiles were trapped in a 1/8 inch Teflon tube loop submerged in liquid nitrogen, from where they were re-volatilized by dipping the loop in hot water. Sulfur compounds were separated using a packed Carbopack®

60/80 mesh column (Sigma-Aldrich) maintained at 170°C. Retention time for DMS was 0.9 min, and detection limit was 3 pmol. Analytical precision was better than 5%. Calibration was performed by syringe injection into the purge vial of varying volumes of a gaseous mixture of He and DMS released by a weight-calibrated permeation tube (Dynacal, Valco Instruments Co. Inc) (Simó et al., 1998). Plots of log(nmol DMS) vs. log(peak area) yielded a straight line (usually $R^2 > 0.99$) that was used for DMS quantification in the samples. For total DMSP analysis (DMSPt) a larger volume of unfiltered sample (40 mL) was stored in crimp glass vials after adding two NaOH pellets (45 mg each, ca. 0.2 mol L^{-1} final concentration, pH > 12). The DMSPt+DMS pool was analyzed as evolved DMS after undergoing alkaline hydrolysis for at least 24 h (and always within 2 weeks). The DMSPt concentration was calculated by subtraction of the previously determined DMS concentration.

3.2.2.2 Other chemical analyses

Dissolved inorganic nutrients (only nitrate + nitrite are reported here) were analyzed in an Alliance Evolution II autoanalyzer with spectrophotometric detection. For Chl *a* analysis, 150 mL of seawater were filtered through GF/F filters (Whatman), extracted in acetone (90% v:v, 4°C, overnight), and measured in a Turner Designs fluorometer. Picoplankton Chl *a* was determined by parallel filtration onto GF/F after screening with polycarbonate 3 μm pore filters (Poretics). Samples for colored (or chromoporic) dissolved organic matter (CDOM) were measured immediately after filtration following C. Romera-Castillo (unpubl.). Seawater was filtered by an acid cleaned glass filtration system using precombusted GF/F filters. CDOM absorption was measured in a dual-beam spectrophotometer (Varian Cary 100 Bio) equipped with a 10 cm quartz cell. Spectral scans were collected between 250 and 750 nm at a constant room temperature of 20°C. Milli-Q water was used as blank. Absorption coefficients of CDOM were calculated as $a_{CDOM} = 2.303 Abs_\lambda L^{-1}$, where Abs_λ stands for absorbance at wavelengths λ, and L for the optical path length in meters (0.1 m cuvette). The spectral slope of CDOM (S_{CDOM}) was computed from the linear regression between the natural logarithm of $a_{CDOM,\lambda}$ wavelength at the range 300–400 nm.

3.2.2.3 Phytoplankton counts and carbon biomass

Picocyanobacteria (*Prochloroccus* and *Synechococcus*) and picoeukaryotic phytoplankton populations were enumerated in live samples by flow cytometry (FACScalibur, Beckton Dickinson) (Marie and Partensky, 2006). Autotrophic nanoplankton (nanoflagellates and crypto-

phytes) were counted using epifluorescence microscopy in samples stained with 4,6-diamidino-2-phenylindole (DAPI). Microphytoplankton species (dinoflagellates and diatoms) were identified and counted with an inverted microscope in samples preserved with formalin-hexamine (0.4% final concentration) and kept at 4°C. Carbon biomass was estimated using standard conversion factors for picophytoplankton (following Simó et al. (2009), or factors based on cell size for nano- and microphytoplankton (Menden-Deuer and Lessard, 2000).

3.2.2.4 Phytoplankton photosynthetic efficiency

Maximum quantum efficiency of photosystem II photochemistry ($F_v : F_m$) was measured using a Fast Repetition Rate fluorometer (FRRf; Fasttracka, Chelsea Marine Systems), and interpreted as a proxy for photoinhibtion and photodamage. Subsamples of 60 mL were withdrawn from the incubation bottles and allowed to recover from short-term photoinhibition during 5 minutes in dim light, and subsequently placed in the dark chamber of the FRRf. The protocol consisted of 100 saturation flashlets (1.3 μs duration, 2.8 μs interflash delay) followed by 20 relaxation flashlets (separated by 50 μs). 30 acquisitions were averaged for each sample, and the resulting saturation curve was fitted using the version 5 (v5) Matlab software (Laney, 2003), which allows correcting for 0.2-μm filtered-water blanks and for the instrument's response function. All samples were analyzed in duplicate. When needed, additional bottles were set in the incubator to measure $F_v : F_m$ at intermediate time points.

3.2.2.5 Particulate primary production (PPp)

Photosynthesis-irradiance curves were measured on the initial water samples, and used to estimate PPp in each experimental treatment. Thirteen 70 mL-bottles (Corning) and one dark control were filled with seawater and inoculated with 10 μCi $NaH^{14}CO_3$. The incubation was carried out in a water bath at in situ temperature in a gradient of artificial PAR (10-1000 μmol photons m^{-2} h^{-1}). After 2 h of incubation the samples were filtered at low vacuum through cellulose ester filters (Millipore 0.22 μm), which were subsequently exposed overnight to concentrated HCl fumes. Scintillation cocktail (4 mL Optiphase Hisafe 2) was then added to each filter, and the radioactivity was measured in a Beckman LS6000 scintillation counter. The photosynthesis-irradiance curves showed no photoinhibition at high PAR, so they were fitted using the model of Webb et al. (1974). Uninhibited photosynthesis rates in the incubations were calculated at 1 min resolution using the photosynthesis-irradiance curve-derived parameters (P^b_{max} and α) and the PAR measured in the tank. UVR-inhibited PPp rates were re-calculated by multiplying,

at each time step, uninhibited PPp by the relative inhibition of $F_v : F_m$ (interpolated at 1 min resolution). The rates were finally averaged over the duration of the experiment.

3.2.2.6 Bacteria counts

Samples were fixed with 1% paraformaldehyde (PFA) + 0.05% glutaraldehyde (final concentration), flash-frozen in liquid nitrogen and stored at -80 ^{o}C. Bacterial populations were enumerated with a FACSCalibur flow cytometer (Becton Dickinson) following standard procedures (Gasol and del Giorgio, 2000).

3.2.2.7 Catalyzed reporter deposition-fluorescence in situ hybridization (CARD-FISH)

Hybridization with phylogenetic probes targeting major bacterial groups allowed the determination of the bacterial community composition in the initial sample. The clades targeted were *Gammaproteobacteria*, NOR5 (within *Gammaproteobacteria*), *Bacteroidetes*, *Roseobacter*, SAR11 (the last two, members of *Alphaproteobacteria*), and *Synechococcus*, as well as *Eubacteria*. Counterstaining of CARD-FISH filters was done with DAPI. We used the protocol of Pernthaler et al. (2002). Further details can be found in Ruiz-González et al. (2012d).

3.2.2.8 Bulk bacterial heterotrophic activity

Initial and post-exposure bacterial heterotrophic activities were estimated with the ^{3}H-leucine incorporation method (Kirchman et al., 1985) in triplicate samples (plus one killed control), processed by the centrifugation method of Smith and Azam (1992).

3.2.3 Optics and spectral weighting functions

3.2.3.1 In situ radiation field

The in situ exposure regime was calculated combining UVR and PAR attenuation profiles, mixing depths obtained from the CTD casts, and the spectral irradiance at the water subsurface recorded by the PUV-2500 placed in the incubator. Diffuse attenuation coefficients of downwelling cosine irradiance ($K_{d,\lambda}$) were calculated for each of the radiation bands measured by the PUV-2500 (six in the UV, centered at 305, 313, 320, 340, 380 and 395, and one single band in the PAR) assuming an exponential extinction (after discarding the first 2 m from the surface). In addition, k_ds for the UVB and UVA (320-400 nm) bands were calculated by spectrally integrating PUV-2500 profiles. Since we had no direct measurements on the date of

sampling, each experiment was assigned the k_ds from the closest sampling, if the water column conditions were very similar. Else, k_ds were calculated as function of Chl *a* and turbidity, which were good predictors of underwater light attenuation at this site (M. Galí unpubl.). The mixed layer depth (MLD) was calculated from both temperature and density (σ_t) profiles, binned at 1 m resolution, as the depth where either temperature or density departed > 0.15°C or kg m^{-3} from the surface reference value (2 m depth). For each radiation band, subsurface irradiance, vertically-integrated irradiance in the mixed layer (Vallina and Simó, 2007), and that at the bottom of the mixed layer were computed for the duration of each experiment (Fig. 3.1).

3.2.3.2 Experimental radiation field

The calibrated UVR time series recorded by the PUV-2500 in each experiment (6 discrete bands) was spectrally interpolated with the shape of a standard, high-resolution non-calibrated spectrum. The standard spectrum was obtained by averaging several standardized spectra measured with a miniature diode array spectroradiometer (USB2000+, Ocean Optics) on sunny days around noon. Standardized spectra showed very little variation and were in good agreement with published ones (Gueymard et al., 2003). This way, an average UVR spectrum between 300 and 400 nm at the water subsurface, with 1 nm resolution, was produced for each experiment and treatment. The USB2000+ (equipped with a cosine detector) was also used to measure the spectral irradiance inside and outside the T and PC bottles to calculate their spectral transmittance (Fig. 3.2A). These measurements were corrected by transmittance measurements done with a scalar irradiance spherical PAR sensor, to better take into account the three-dimensional radiation field. Finally, the product of subsurface spectral irradiance, bottle transmittance and neutral screen attenuation yielded the actual spectral irradiance ($E_{d,\lambda}$) experimented by the samples, which is the basis of further calculations.

3.2.3.3 Spectral weighting functions

UVR-mediated reactions have a strong spectral dependence. Therefore, $E_{d,\lambda}$ was weighted with spectral functions found in the literature. All weighting functions were normalized to 1 at 300 nm, thus, they were used as a dimensionless spectral efficiency. Spectral integration (or sum, in discrete form) of weighted $E_{d,\lambda}$ yielded the weighted UV irradiance E^*:

$$E^* = \sum_{\lambda=300nm}^{400nm} E_{d,\lambda}\varepsilon_\lambda \tag{3.1}$$

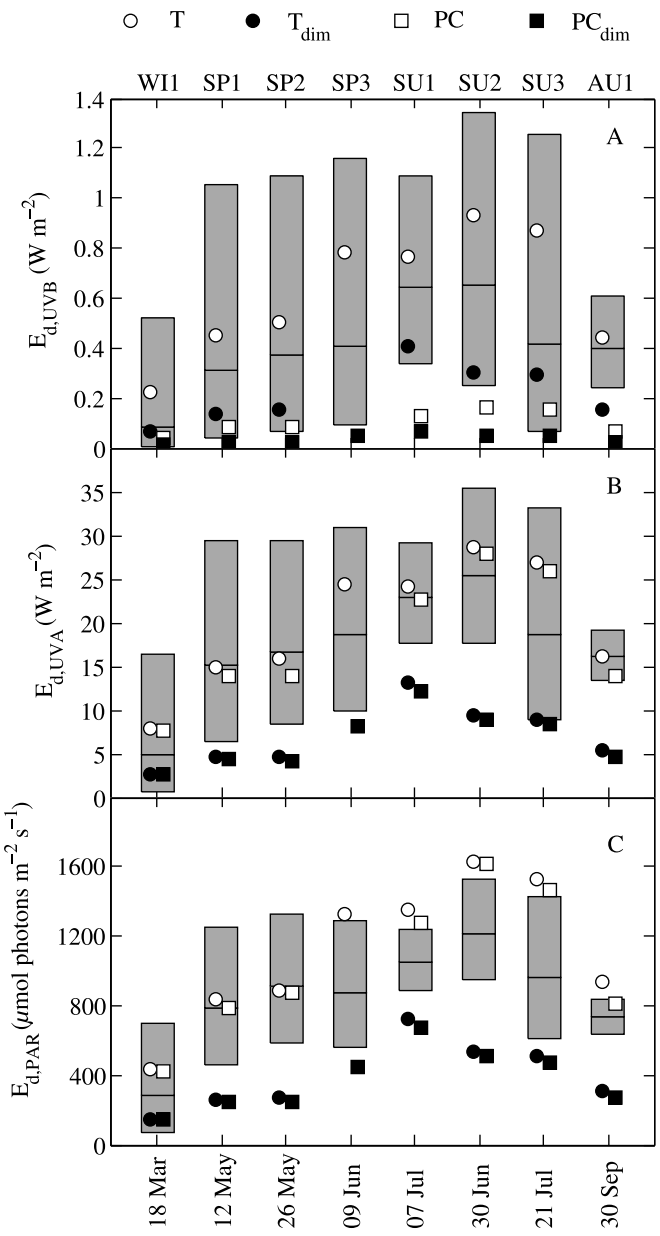

Figure 3.1: **Comparison between in situ and experimental exposure** - Grey bars encompass the hypothetical in situ irradiance at: The water subsurface; the bottom of the mixed layer; and the MLD average, resulting from applying the subsurface irradiance recorded during the experiment to the insitu mixing conditions. The symbols represent experimental exposure to each band: (A) UVB; (B) UVA; and (C) PAR. 1000 μmol photons m^{-2} s^{-1} approximately equal 220 W m^{-2}.

where ε_λ is a wavelength-dependent scaling coefficient. Since ε_λ has inverse energy units (m^2 W^{-1}) in the photobiological literature but inverse quantum units (m^2 $quanta^{-1}$ s^{-1}) in the

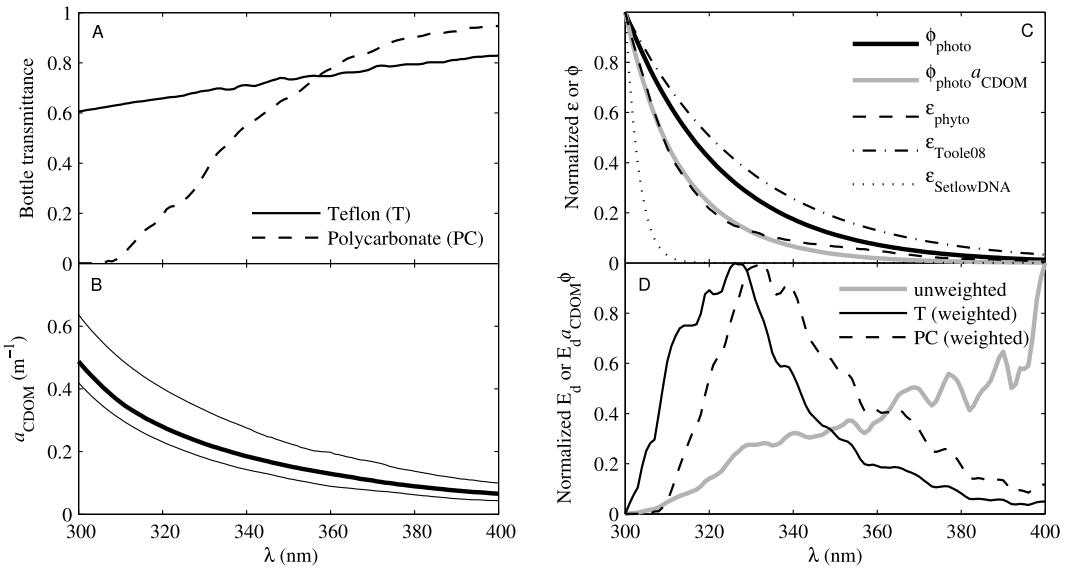

Figure 3.2: **Graphical example of how biologically or photochemicallyweighted irradiance was calculated** - (A) Spectral transmittance of Teflon and polycarbonate bottles; (B) absorption coefficient of colored dissolved organic matter (a_{CDOM}), with the median of the 8 experiments, maximum (26 May 2009) and minimum (30 September 2008); (C) average spectral quantum yield (ϕ_{photo}) and action spectrum ($\phi_{photo} a_{CDOM}$) of DMS photolysis, compared to an average biological weighting function (BWF) for the inhibition of photosynthesis (ε_{phyto}), a proposed BWF for UV-induced DMS production by phytoplankton ($\varepsilon_{Toole08}$), and a BWF for DNA damage ($\varepsilon_{SetlowDNA}$); (D) Comparison of the spectral shape of DMS photolysis in Teflon and PC bottles, and unweighted UV irradiance. (C, D) The spectra are normalized to their maximum between 300 and 400 nm.

photochemical literature, we converted $E_{d,\lambda}$ to quantum units, when necessary, using Planck's constant. E^* was converted to weighted irradiance dose H^* multiplying it by the duration of the exposure.

3.2.3.4 DMS photolysis

DMS photolysis can be described by apparent spectral quantum yields (φ_λ) that decrease exponentially with wavelength (Toole et al., 2003). An average ϕ_λ was produced by averaging four spectral slopes, obtained from two studies done at the Sargasso Sea and the Bering Sea (Toole et al., 2003; Deal et al., 2005). The resulting ϕ_λ had a spectral slope of 0.0436 nm^{-1} (with the original slopes ranging between 0.0321 and 0.0499). DMS photolysis is a photosensitized process, meaning that actinic light is not directly absorbed by DMS. Thus, ϕ_λ has to be

multiplied by the amount of light absorbed by CDOM (Fig. 3.2B-D) to obtain the photolysis-weighted irradiance as

$$E^*_{photo} = \sum_{\lambda=300nm}^{400nm} E_{d,\lambda} a_{CDOM,\lambda} \phi_\lambda \tag{3.2}$$

where the photochemical action spectrum is

$$\varepsilon = a_{CDOM,\lambda} \phi_\lambda \tag{3.3}$$

3.2.3.5 Biological weighting functions

Three biological weighting functions (BWFs), representative of different biological processes, were applied to the average spectral irradiance recorded during whole water incubations (Fig. 3.2C): one for DNA damage, which is strongly UVB-shifted (Setlow, 1974); one for phytoplankton DMS release, estimated from a diagnostic modeling study in the Sargasso Sea, with an exponential spectral slope of 0.0340 nm^{-1} that results in UVA-shifted weights (Toole et al., 2008); and a BWF representative of photosynthesis photoinhibition, with intermediate UVB vs. UVA weights. Most published BWFs for photosynthesis are biased towards large-celled phytoplankton, which are rarely dominant at the BBMO (Gutiérrez-Rodríguez et al., 2011). Therefore, the average BWF for natural plankton assemblages calculated by Neale and Kieber (2000) was further averaged with the BWF calculated for two picoplankters (Sobrino et al., 2005), which are expected to be more sensitive to UVR (Garcia-Pichel, 1994). Fig. 3.2 is a graphical summary of the optical calculations pipeline, starting with spectral irradiance entering the bottles and ending with wavelength-resolved spectra for each process and treatment.

Table 3.3: Relationship between change in DMS concentration and the weighted irradiance dose (H^*) in incubations of filtered (photochemistry) and unfiltered seawater (biological processes). Variables known to affect DMS photolysis are also included: The absorption coefficient of colored dissolved organic matter (a_{CDOM}) and its spectral slope (S_{CDOM}), and nitrate + nitrite concentration. k^*_{photo} is the slope ± standard error, (n = 3 to 5) of the linear least squares regression between the logarithm of fractional DMS loss and H^*. An analogous k has been calculated for unfiltered water incubations ('$k^*_{unfiltered}$', n = 5 except in SP3 where n = 3). The Y-intercept of the regression ($Y_{x=0}$) is reported for unfiltered water incubations only (see text); p values indicate the probability that the slope (k) is different from 0.

Experiment	Photolysis incubations					Bio. Process incubations		
	$a_{CDOM,300}$ (m^{-1})	S_{CDOM} (nm^{-1})	Nitrate + nitrite (μmol L^{-1})	$k^*_{photo} \pm SE$	p	$k^*_{unfiltered} \pm SE$	$Y_{x=0} \pm SE$	p
WI1	0.48	0.020	4.6	-27.7 ± 1.3	0.001	2.4 ± 16.9	-0.02 ± 0.10	0.90
SP1	0.52	0.018	0.12	-23.8 ± 1.3	0.01	-0.9 ± 7.8	0.56 ± 0.08	0.91
SP2	0.61	0.018	0.09	-16.4 ± 0.9	0.009	-9.7 ± 1.2	0.58 ± 0.02	0.004
SP3	0.50	0.017	0.13	na	na	0.4 ± 2.5	0.06 ± 0.04	0.90
SU1	0.48	0.021	0.21	-14.4 ± 1.1	0.11	-3.5 ± 1.2	0.26 ± 0.02	0.06
SU2	0.47	0.020	0.02	-18.7 ± 2.4	0.007	-1.7 ± 2.1	-0.03 ± 0.04	0.48
SU3	0.50	0.022	0.64	-15.9 ± 0.6	0.001	-0.8 ± 1.7	-0.09 ± 0.03	0.66
AU1	0.42	0.019	0.26	-7.1 ± 0.2	0.01	-18.8 ± 9.5	0.1 ± 0.05	0.14

3.2.4 Sulfur cycling rates

The DMS photolysis rate constant in filtered-water incubations (k^*_{photo}) was calculated assuming pseudo first-order kinetics with respect to the weighted irradiance dose (H^*) (Kieber et al., 2007) as follows: First, the natural logarithm of fractional DMS loss in the different irradiance treatments was calculated as $ln([DMS]_0/[DMS]_f)$, where $[DMS]_0$ and $[DMS]_f$ represent initial and final DMS concentrations, respectively; then, $ln([DMS]_0/[DMS]_f)$ was regressed against the weighted irradiance dose (H^*). Since the latter accounts for variations in both incubation time and spectral conditions, a linear relationship between the two variables is expected, and k^*_{photo} is the slope of the regression. The units of k^*_{photo} calculated in such a manner are those of (weighted irradiance dose)$^{-1}$.

Net DMS production rate (NP) in unfiltered water incubations was calculated as the change in DMS between the beginning and the end of the incubation (nmol L^{-1} h^{-1}). Since NP results from the balance between biological and photochemical processes, it has to be corrected by the photochemical DMS consumption (PH_{bio}) to obtain the net biological DMS production: $NP_{bio} = NP + PH_{bio}$. At any time, the photolysis rate (PH_{bio}) in whole-water bottles can be calculated as the product of k^*_{photo}, weighted irradiance E^*_{bio}, and DMS concentration. Estimating the average photolysis rate would require measuring DMS with sufficient temporal resolution. Since only initial and final DMS were measured, we assumed that the mean photolysis rate in each incubation was proportional to the average E^* and DMS concentration:

$$PH_{bio} = k_{photo} E^*_{bio} \overline{DMS}_{bio} \tag{3.4}$$

Finally, gross DMS production rates (GP) were calculated by budgeting as

$$GP = NP + PH_{bio} + BC \tag{3.5}$$

where BC stands for bacterial DMS consumption. To estimate dark bacterial DMS consumption (BC_{dark}), one of the two dark bottles (2.9 L, amber glass) was amended before the incubation with 200 – 300 nmol L^{-1} dimethyldisulfide (DMDS), an effective inhibitor of bacterial DMS consumption (Wolfe and Kiene, 1993b; Simó et al., 2000). The difference between DMS production rates in the DMDS-amended and the unamended bottle yielded $BC_{dark} = GP_{dark} - NP_{dark}$. Field studies using radioisotope additions have shown that solar radiation inhibits DMS consumption, roughly, as much as bacterial leucine incorporation (Toole et al., 2006; Kieber et al., 2007). Thus, in sunlit incubations, BC rates were calculated

as the product of BC_{dark} and the fractional inhibition of bulk bacterial leucine incorporation rates (I_{LIR}), as $BC = C_{dark}I_{LIR}$. We took this alternative approach based on bulk bacterial heterotrophic activity photoinhibition because our study, ufortunately, began before the DMDS inhibition had been optimized for its use in light incubations (Galí et al., 2011).

3.2.4.1 Sources of uncertainty

To estimate the uncertainty associated to budget-derived GP (eq. 3.5), the error in each individual measurement was propagated following standard methods (Taylor, 1997). We considered the uncertainty in BC and NP rates due to analytical error and incubation duplicates (when existing), and the error of photolysis (Table 3.3). Error was defined as the range, in the case of duplicates, or as the standard error, when triplicates or more measurements existed.

Besides the measurement error, some uncertainty in GP arose from the assumptions made in its calculation. The first assumption was that BC was photoinhibited to the same extent than microbial leucine incorporation. To address this issue we conducted sensitivity tests where two extreme scenarios were considered: no photoinhibiton of BC in sunlight, and total photoinhibiton of BC in the harshest exposure (T bottles). According to published data, both extreme assumptions are unlikely to happen (Toole et al., 2006; Kieber et al., 2007). These exercises showed that calculating BC in alternative ways would have little impact on GP rates, and that the change would be generally smaller than the measurement uncertainty.

The second assumption implied that DMS photolysis was proportional to the average of initial and final DMS concentration (eq. 3.4). This issue was addressed by calculating a time-resolved photolysis using the recorded irradiance time-series. Such calculation was repeated with different patterns of temporal DMS evolution during the incubation. This exercise showed that the bias in the photolysis term (PH_{bio}) derived from the simplification used in eq. 3.4 was $< 10\%$, and that DMS evolution could not have departed too much from linearity in most incubations (as already described in Galí et al. (2011)). This is in line with DMS measurements performed at an intermediate time in SU1 (1.5 h after solar noon), which indicated almost linear DMS evolution.

3.3 Results

3.3.1 Initial microbial communities

Phytoplankton biomass and community composition ranged from high-biomass, diatom-dominated communities in late winter (WI1) to low-biomass, picoplankton-dominated communities in late summer and early autumn (SU 1-3, AU1). Spring samples showed an intermediate position and were dominated by nanoflagellates (Table 3.1; Fig. 3.3A). Regarding bacterial communities, the SAR 11 clade dominated numerically almost all year round, with higher abundance in late summer and early autumn, while the *Gammaproteobacteria, Bacteroidetes* and *Roseobacter* clades were relatively more abundant during spring (Fig. 3.3B).

3.3.2 Phytoplankton activity and response to sunlight

Maximum, uninhibited particulate primary production rates (PPp) occurred in WI1 and SP3 samples (around 120 nmol C L^{-1} h^{-1}) and minimum in SU1-3 and AU1 (37-56 nmol C L^{-1} h^{-1}), with intermediate values in SP1-2 (64-79 nmol C L^{-1} h^{-1}). The photoacclimation parameter ($E_k = P^b_{max}/\alpha$ varied between 294 and 2280 μmol photons m^{-2} s^{-1} (median of 537), and showed no obvious relation to light levels in the field. The values of E_k indicate that, in the non-dimmed treatments, the samples spent most of the time on the PAR-saturated portion of the photosynthesis-irradiance curve. Initial $F_v : F_m$ values varied in a narrow range (0.48-0.61), indicative of good physiological condition. At the end of the experiments only slight inhibition was observed, $F_v : F_m$ being reduced to 85.9 ± 1.8% (T;), 87.6 ± 2.0% (PC), 87.1 ± 2.0% (PT_{dim}), and 91.6 ± 3.4% (PC_{dim}) of its initial values (average ± SE, $n = 5$).

In WI1 and SU1-3, subsamples for $F_v : F_m$ were taken at 2-4 intermediate times during the incubation. During the first hour of exposure, $F_v : F_m$ decreased to 38 – 73% of its initial value in T bottles. By the time peak irradiance was reached $F_v : F_m$ levels had recovered substantially (Fig. 3.4), even in bottles suffering the harshest exposure. Thus, the initial photoinhibtion (or even 'light shock') was reversible, and phytoplankton (as a bulk) were able to photoacclimate. Note that at the time when incubations started (3 h before solar noon), irradiance was on average 40 and 60% of the noontime maximum for the 305 nm and PAR bands, respectively.

3.3.3 Bacterial activity and response to sunlight

Bulk bacterial heterotrophic activity, as indicated by initial leucine incorporation rates (LIR), was highest in SP2 and SU1 (74-84 pmol leu L^{-1} h^{-1}, and lowest in WI1 (10 pmol Leu L^{-1} h^{-1}),

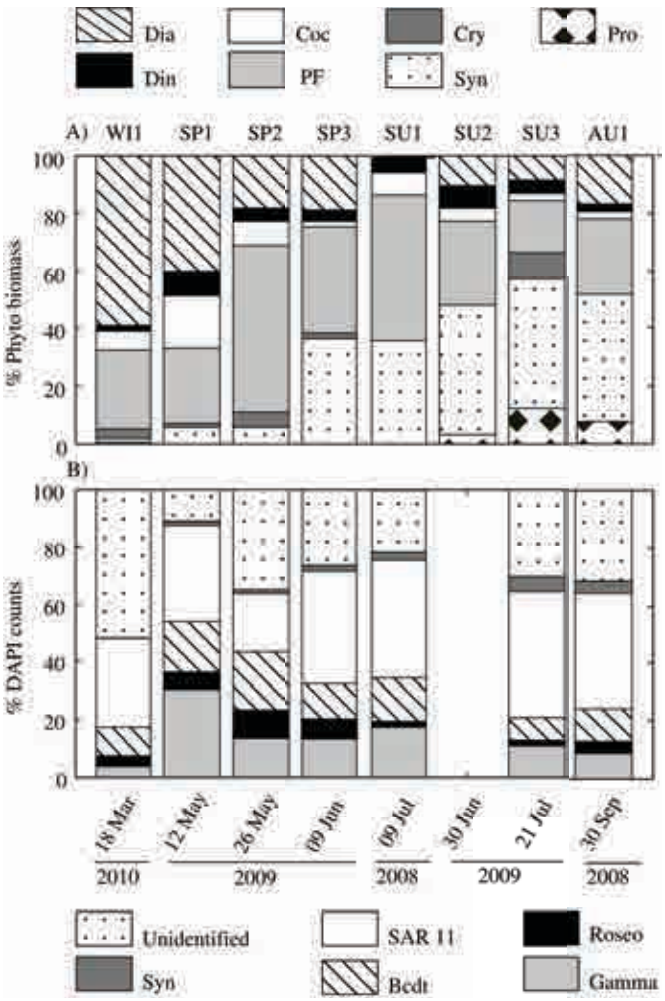

Figure 3.3: **Composition of the phytoplankton and bacterioplankton communities** - (A) Contribution of different groups to total phytoplankton carbon biomass, as assessed by flow cytometry and microscopy. Dia: diatoms (*Bacillariophyceae*); Din: dinoflagellates (*Dinophyceae*); Cry: *Cryptophyceae*; Syn: *Synechococcus*; Coc: coccolithophorids (*Prymnesiophyceae*); PF 2 – 5 μm: phototrophic nanoflagellates; Pro: *Prochlorococcus*. According to Gutiérrez-Rodríguez et al. (2011), the phototrophic nanoflagellates fraction (PF) contains high proportions of small prymnesiophytes, but also pelagophytes and, in winter, prasinophytes. (B) Contribution of different groups to total bacterial numbers, as assessed by CARD-FISH. No data were available for SU2 (30 June 2009). However, other variables indicated that that sampling took place during a smooth transition between late spring and midsummer conditions. Unidentified: unlabeled prokariotes; Syn: *Synechococcus*; SAR 11 (*Alphaproteobacteria*); Bcdt: *Bacteroidetes*; Roseo: *Roseobacter* (*Alphaproteobacteria*); Gamma: *Gammaproteobacteria*.

with intermediate values in the remaining samples (18-52 pmol Leu L^{-1} h^{-1}). Solar exposure generally inhibited leucine incorporation but, on occasions, slight stimulation was also observed

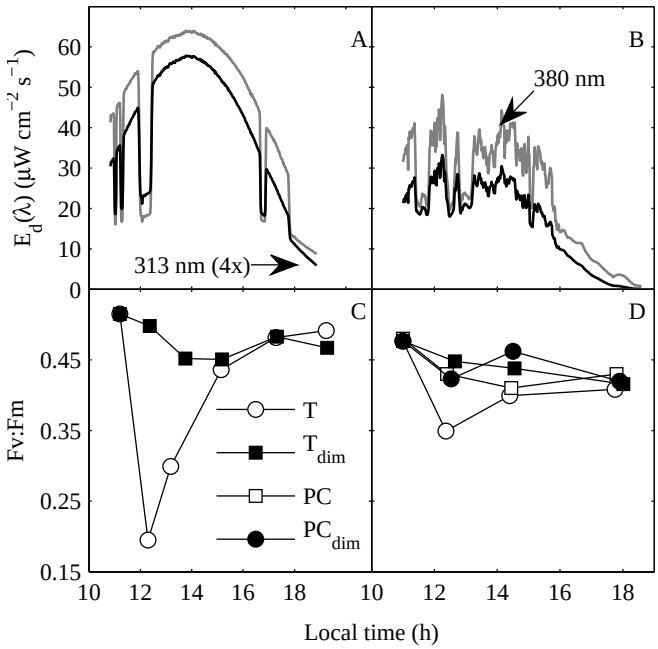

Figure 3.4: **UV irradiance and photosynthetic performance of phytoplankton** - (A, B) Time series of spectral irradiance at two representative wavebands centered at 313 nm (UVB) and 380 nm (UVA), and (C, D) corresponding time courses of phytoplankton photoinhibition. The examples correspond to two days with different solar zenith angle and cloudiness: (A, C) SU3 and (B, D) WI1.

(mostly in PC_{dim} bottles). Overall, sunlight incubations yielded LIR values (average ± SE, n = 6) that were 73.3 ± 6.1% (T), 88.6 ± 7.3 % (PC), 93.0 ± 8.3% (PT_{dim}) and 106.9 ± 8.5% (PC_{dim}) those of dark incubations. In SP3 and SU2 experiments, where no post-exposure LIR measurements were available, the average of the other experiments was used to calculate the inhibition of bacterial DMS consumption.

3.3.4 DMS photolysis

Maximum photolysis rates occurred in T bottles, followed by PC or T_{dim}, and PC_{dim}. In each experiment, the logarithm of fractional DMS loss showed a linear relationship with weighted irradiance dose (H^*). The R^2 of the regression was 0.89-0.99 (except in SU1, $R^2 = 0.83$ with $n = 3$) and the slope significantly different from 0 (Table 3.3). The intercepts of the regression were never significantly different from 0, as expected, since no photolysis occurs in the dark. For this reason, k^*_{photo} was deduced from the slope of the regression forced through 0. These observations indicate that DMS photolysis was well described by pseudo first-order kinetics,

and that the spectral weighting functions used were appropriate because they accounted for the spectral variation between T and PC bottles.

Photolysis 'yields' (k^*_{photo}) decreased by 4-fold from late winter through early autumn (Table 3.3). In fact, k^*_{photo} was significantly correlated to the day of the year (Spearman's rank correlation r = -0.93, $p < 0.01$). The highest photochemical yield occurred in WI1, coinciding with relatively high nitrate concentration (Table 3.3), in keeping with previous findings (Bouillon, 2004; Toole and Siegel, 2004). Besides the variation in photolysis yields, maximum DMS photolysis rates (T bottles) were largely driven by irradiance and DMS concentration (Eq. 4). Thus, highest photolysis rates occurred in SP2 and SU1 (0.54-0.60 nmol L h^{-1}), intermediate values in the rest of summer and spring experiments (0.21 - 0.36 nmol L h^{-1}), and lowest values in WI1 (0.14 nmol L h^{-1}) and AU1 (0.02 nmol L h^{-1}). Photolysis rates averaged over the duration of each incubation are represented in Fig. 3.5.

3.3.5 Net DMS production

The highest NP occurred in SP1, SP2 and SU1 experiments, with 0.21-0.46 , 0.43-0.53 and 0.21-0.31 nmol L^{-1} h^{-1}, respectively. All other experiments yielded lower NP rates between -0.06 and 0.05 nmol L^{-1} h^{-1}. More interestingly, NP rates displayed a rather flat response across the different treatments (Fig. 3.5 A through H). The regression between NP and radiation dose was never significantly different from 0, no matter the radiation dose was expressed as a specific band (UVB, UVA, PAR) or weighted by any of the spectral weighting functions ($p > 0.2$). In other words: across the spectral irradiance gradient, biological DMS production increased enough to (at least) compensate photochemical DMS loss. The only exception to this behavior was found in AU1 (although the low DMS concentrations and cycling rates in that experiment might have rendered noisier estimations). To provide additional evidence for this finding, we made the exercise of regressing the logarithm of fractional DMS change in unfiltered water incubations to the photolysis-weighted irradiance dose, as done for the photolysis bottles. This clearly showed that, in biological process bottles, DMS evolution departed from the kinetics dictated by DMS photolysis (Table 3.3).

The lack of treatment replicates in biological process bottles in the first five experiments might limit the strength of our conclusions. However, there are indications that the behavior we observed was robust: 1) the flat response of NP across the spectral irradiance gradient was found in several independent samples; 2) similar NP and photolysis k's were found in experiments performed with similar initial samples, i.e., on sampling dates that were close in

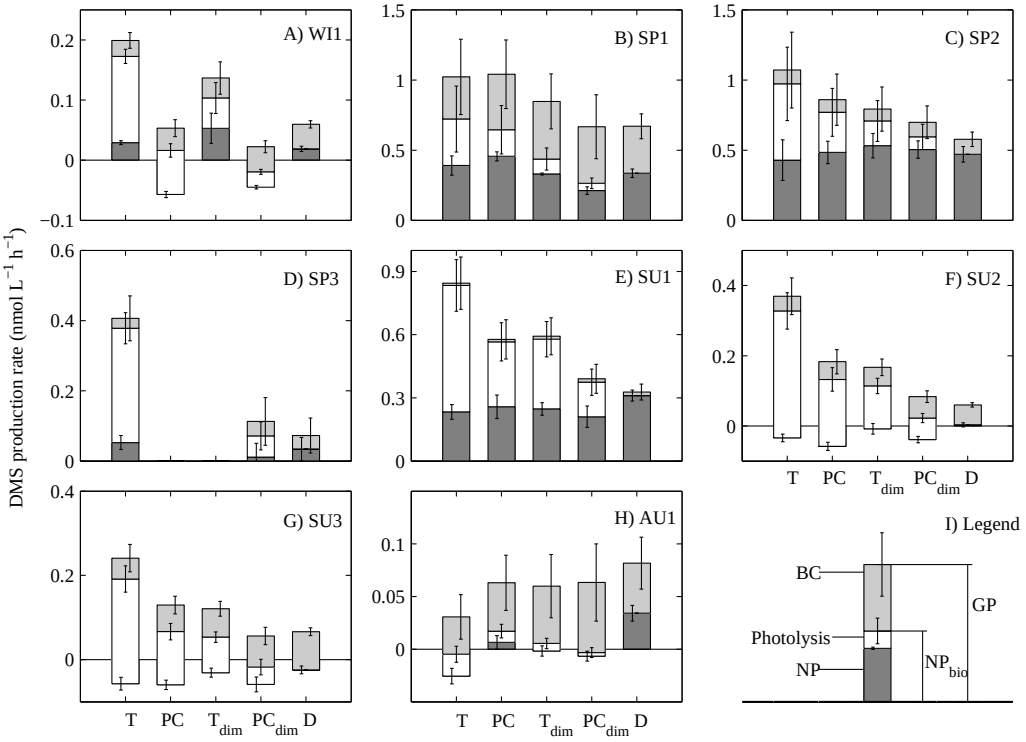

Figure 3.5: **DMS cycling rates under different spectral irradiance conditions** - (A-H) Gross DMS production (GP) rates in the eight experiments, and the contribution of each budget term used for its calculation, namely: net DMS production (NP), DMS photolysis, and bacterial DMS consumption (BC). Net biological DMS production (NP_{bio}) is $NP + Photolysis$. (I) Sketch showing how to interpret the color coding of the bars.

time (SP1 vs. SP2, and SU2 vs. SU3); and 3) in the three experiments were biological process bottles were duplicated (SU2-3 and WI1) the error between duplicates was as small as the analytical error ($<$ 5%), which indicates that the large incubation volumes (2.3 L) minimized artifacts by ensuring community-inclusive incubations (Galí et al., 2011).

3.3.6 Bacterial DMS consumption

Dark BC rates were highest in SP1 and SP2 (0.33 $\pm$ 0.15 and 0.11 $\pm$ 0.08 nmol L^{-1} h^{-1}, respectively) and lower in the other experiments (between 0.04 and 0.09 nmol L^{-1} h^{-1}), being virtually undetectable in SU1 (0.02 $\pm$ 0.03 nmol L^{-1} h^{-1}). BC rate constants, that is, BC rates normalized to the initial DMS ($BC/[DMS]_0$; d^{-1} units) were very similar to those found by

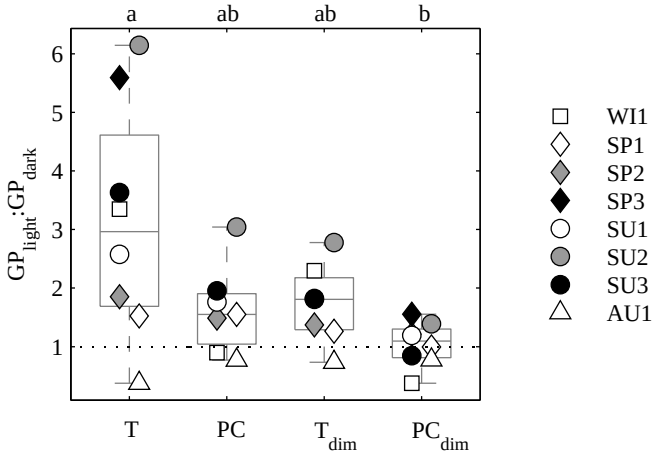

Figure 3.6: **Stimulation factor of gross DMS production in sunlit vs. dark incubations in each experiment** - The boxes encompass the first and third quartiles, with center in the median. Differences between treatments where significant in the ensemble of all experiments (Kruskal-Wallis $p < 0.05$), as deduced from multiple comparisons (post-hoc Tukey-Kramer test; indicated by different letters).

(Vila-Costa et al., 2008) both in magnitude and in terms of seasonal variation. The highest values were found in spring (around 1 d^{-1}) and the lowest in summer (around 0.3 d^{-1}). Only the WI1 sample, with 0.04 ± 0.01 nmol L^{-1} h^{-1} (0.3 d^{-1}), deviated from the general wintertime behavior (1.0 ± 0.4 d^{-1}) found by Vila-Costa et al. (2008).

3.3.7 Net biological and gross DMS production

NP_{bio} displayed a strong response to spectral irradiance. This resulted from adding irradiance-dependent photolysis rates to NP rates that were comparatively smaller and flat across the spectral irradiance gradient (Fig. 3.5 A-H). In all experiments but one (AU1), highest NP_{bio} occurred in the T bottles, followed by PC or T_{dim}. Samples exposed to mild irradiance (PC_{dim}) showed NP_{bio} rates very similar to those incubated in the dark. Gross DMS production (GP) rates, calculated as the sum of BC and NP_{bio} (Eq. 5), showed a pattern very similar to that of NP_{bio} (Fig. 3.5 A-H). Maximum GP rates in T bottles were found in SP1-2 and SU1 (0.84-1.07 nmol L^{-1} h^{-1}) followed by the remaining samples (0.22-0.46 nmol L^{-1} h^{-1}) and AU1 (< 0.05 nmol L^{-1} h^{-1}). Interestingly, the degree of GP stimulation by sunlight was highly variable despite the qualitatively consistent response (Fig. 3.6).

3.3.8 Sources of uncertainty

Our GP estimates had an average uncertainty of 24%, and the error was $< 33\%$ in 80% of the incubations ($n = 38$). The relative contribution of NP, photolysis (PH_{bio}) and BC to GP varied for each initial sample and treatment (Fig. 3.5). GP became more sensitive to the PH_{bio} term as spectral irradiance increased, while the importance of BC decreased. Across treatments, the error of PH_{bio} contributed on average 59, 52, 31, and 14% of the GP error in T, PC, T_{dim}, and PC_{dim}, respectively. BC contributed 30, 31, 39, 61 and 78% in T, PC, T_{dim}, and PC_{dim}, and D, respectively. The remaining 11 - 30% of the error was due to NP.

3.4 Discussion

Short-term modulation of community gross DMS production by meteorological forcing has been in the spotlight since the studies of Simó and Pedrós-Alió (1999a,b). These studies pointed out that photobiological processes mediated by vertical mixing could result in enhanced DMS yields. Indeed, our results show that gross DMS production can increase dramatically under full-spectrum midday irradiance. Yet, the strength and spectral behavior of the stimulation response are highly variable (Fig. 3.5 and 3.6). In the following paragraphs we will discuss how that this variability can be understood by analyzing the response of GP to spectral irradiance, and its relationship with the structure of the microbial community and its light exposure history.

3.4.1 Irradiance dependence of gross DMS production (GP)

The clearest outcome of our experiments is that sunlight-stimulated GP is irradiance-dependent. As shown in Fig. 3.5, the increase in GP across the spectral irradiance gradient is balanced by photolysis, producing the observed flat response of net DMS production (NP). Such response had been already reported by Toole et al. (2006) (see Fig. 9 of that paper), who envisioned the occurrence of radiation-driven GP but did not explore in detail the magnitude and photobiological basis of this process. Our GP stimulation estimate is clearly higher than the 1.3 – 1.8 range of the stimulation factor reported by Galí et al. (2011). In that study the samples were incubated during 24 – 29 h, spending less of the total incubation time at high irradiance. This suggests that highest GP occurs during the hours of harshest UVR-PAR exposure, and that the stimulation effect becomes relatively less important on a daily basis.

The lack of short-term effects of UVR on net DMS production contrasts with the strong seasonal relationship between UVR and DMS seasonality (Toole and Siegel, 2004). This appar-

ent paradox can be understood by the superposition of the short-term processes analyzed here and the seasonal succession of plankton communities towards enhanced DMS(P) dynamics in summer (Vila-Costa et al., 2008; Lizotte et al., 2012). In this context, sunlight-driven GP can provide the DMS surplus that compensates for photolysis in highly irradiated and stratified waters. This fits with the observation of no DMS depletion (or even net DMS increase) around noontime in studies where surface DMS was measured across diel cycles in summer (Gabric et al., 2008, see Chapter 5).

It is worth mentioning that the GP rates derived from our experimental design are incubation averages, which result from integrating dose-dependent nonlinear photolysis over time. At this stage, it is unclear whether GP rates are a function of the instantaneous photon flux (irradiance), of the cumulative UVR dose, or (most probably) both. Work is underway to better comprehend the kinetics of sunlight-dependent gross DMS production, and their dynamic relationship with vertical mixing (Neale et al., 2003).

3.4.2 GP and microbial community structure

The subset of samples exhibiting high NP and GP rates (SP1-2 and SU1) shared a number of characteristics, in some cases significantly different from the remaining samples (two-group Kruskal-Wallis test; $n = 8$; $df = 1$): elevated DMSPt concentrations ($p < 0.05$); high proportions of DMSP producers ($p < 0.05$), as deduced from the sum of coccolithophores, dinoflagellates and non-prasinophyte nanoflagellates (most of which were probably prymnesiophytes; Gutiérrez-Rodríguez et al. (2011)); and high proportions of bacterial clades putatively harboring DMSP cleavers Curson et al. (2011), like *Gammaproteobacteria* (specifically its sub-clade NOR5, $p < 0.05$), or *Roseobacter* (highest in SP1-3 but not in SU1). The *Bacteroidetes* clade was also more abundant in the SP1-2 and SU1 samples ($p < 0.05$). Another interesting feature was the significant correlation between DMSPt and leucine incorporation rate (Spearman's $r = 0.88$, $p < 0.01$). In summary, we could identify phyto- and bacterioplankton communities that were geared towards high DMS production, concurrent with high bacterial activity, possibly associated to active DMSP catabolism. However, elevated DMS production (SP1-2, SU1) did not co-occur with the strongest stimulation (SP3, SU2-3, and WI1), suggesting that the response to light was not determined by community structure.

3.4.3 Spectral response of GP

In our experimental approach GP responded, by definition, to irradiance weighted by the spectral shape of DMS photolysis (E^*). Therefore, we wanted to explore whether giving greater weights to other regions of the UVR spectrum would render better or worse prediction of GP rates by E^*. For that purpose we calculated, experiment by experiment, the correlation coefficients between GP and irradiance, weighted by the different spectral weighting functions (Fig. 3.2), or restricted to specific bands (UVB, UVA and PAR). Although we found substantial variability in the regions of the spectrum eliciting the strongest response, most experiments represented an average situation where wavelengths in the 320 – 340 nm band were the best predictors of radiation-dependent GP (Fig. 3.7A). This region coincides with the spectral peak of photosynthesis photoinhibition (which results from multiplying the action spectrum of photosynthesis inhibition and downwelling irradiance). This apparently surprising result stems from the fact that the action spectra of DMS photolysis and photosynthesis inhibition have remarkably similar shapes (Fig. 3.2C), and clearly points at phytoplankton as key players in sunlight-stimulated GP. Remarkably, Levine et al. (2012) recently reached a similar conclusion with a totally different approach in a time-series study in the Sargasso Sea. They found that potential DMS production by the algal fraction (> 1.2 μm), as deduced from in-vitro essays, was associated to the radiation dose at 340 nm in the upper mixed layer.

It can be argued that our results are too heavily influenced by our methodological assumptions. However, in some experiments, the trends encountered in GP were already apparent in net DMS production (NP), before photolysis was accounted for (PH_{bio} term). For example, in WI1, NP was significantly higher in T and T_{dim} than in PC and PC_{dim} (duplicate bottles; Kruskal-Wallis test, $p < 0.05$), indicating that a process specific to the UVB band influenced DMS production (Fig. 3.5A). As a result, UVB-shifted weighting functions worked best to predict GP rates in that experiment (Fig. 3.7). In SP1, conversely, NP was similarly high in the T and PC treatments (Fig. 3.5B and E), suggesting a more important role of UVA and PAR wavelengths. We also observed that, in some experiments, E^* did better at predicting GP than NP_{bio} (Fig. 3.7B), although the link between NP_{bio} and E^* was methodologically more direct. These results strengthen our view that biological weighting functions are appropriate to parameterize GP.

Due to varying experimental conditions and in situ radiation fields (Fig. 3.1), the comparison between experiments was not straightforward. For that reason, we took advantage of our

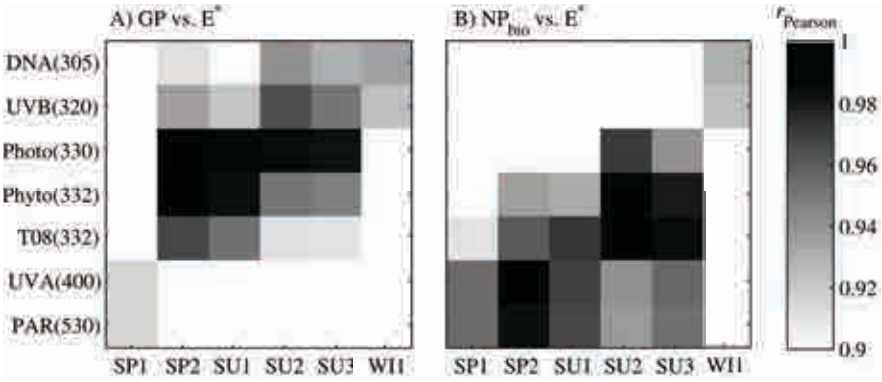

Figure 3.7: **Graphical representation of the correlation between DMS production in the light treatments and the corresponding weighted irradiance dose** - (A) gross DMS production; (B) net biological DMS production. Irradiance is represented as unweighted wavebands (UVB, UVA and PAR) or as UV irradiance weighted by different spectral functions (see Fig. 3.2). The weighting functions are sorted from shortwave- to longwave-shifted, and the peak wavelength of each action spectrum is indicated in parentheses. Experiment WI1 has been moved to the end of x-axis for an easier interpretation. Significance levels are $p < 0.01$ for $r > 0.99$, $p < 0.05$ for $r > 0.95$, and $p < 0.1$ for $r > 0.90$; $r < 0.90$ are not included; (n = 4 treatments).

experimental design to introduce a responsiveness index (R), defined as the relative increase in GP per unit of relative increase in weighted irradiance:

$$R = \frac{(GP_A - GP_B)/GP_B}{(E^*_A - E^*_B)/E^*_B} \tag{3.6}$$

The spectral irradiance was weighted using the spectral weighting function of DMS photolysis, and the subscripts A and B represent two hypothetical treatments. Spectral responsiveness (R_{spec}) was calculated from the comparison between T to PC and $\mathrm{T_{dim}}$ to $\mathrm{PC_{dim}}$ bottles. Analogously, total irradiance responsiveness (R_{tot}) was calculated from the comparison between T to $\mathrm{T_{dim}}$ and PC to $\mathrm{PC_{dim}}$.

For a given initial water sample, we found that the responsiveness to a spectral shift was of similar magnitude regardless the T and PC bottles compared had been incubated at high or dimmed irradiance. Similarly, the response to a shift in total irradiance (with the shape of spectrum held constant) was of similar magnitude between treatments, regardless the samples had been incubated in T or PC bottles (Fig. 3.8A). In other words, GP displayed a consistent response on a weighted irradiance basis. WI1 and SU2-3 exhibited stronger spectral responses ($R_{spec} > R_{tot}$), while SP1-2 showed similar R_{spec} and R_{tot}, and SU1 stronger response to total irradiance ($R_{tot} > R_{spec}$). These exploratory calculations (Fig. 3.7 and 3.8) suggest

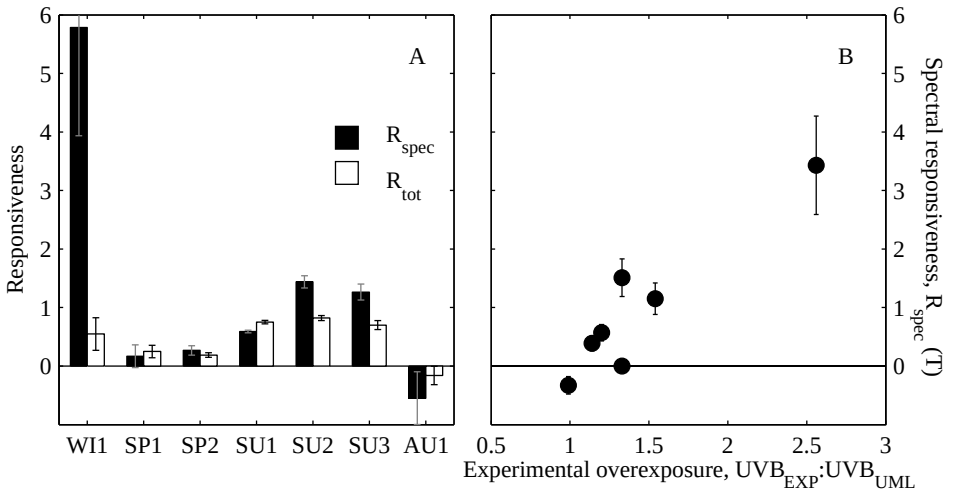

Figure 3.8: **'Irradiance responsiveness' of gross DMS production** - (A) Comparison between spectral responsiveness (R_{spec}) of gross DMS production vs. its responsiveness to total irradiance (R_{tot}). (B) Relationship between R_{spec} and experimental overexposure to UVB as compared to in situ conditions (see text for definitions).

that distinct processes, with different spectral sensitivity, might be responsible for the observed stimulation of GP.

3.4.4 Light exposure history

Although our experimental setup approximated quite reasonably the in situ irradiance conditions (Fig. 3.1), we were not equally successful in all the experiments. To assess the relationship between sunlight-stimulated GP and the radiative history of the planktonic community, we calculated an index of experimental overexposure, defined as the quotient between experimental and in situ irradiance for a particular radiation band. The underlying hypothesis was that exposing organisms to irradiances higher than those at which they are acclimated would elicit stronger responses. In congruence with this hypothesis, we found a suggestive relationship between R_{spec} in T bottles and the degree of experimental overexposure to UVB (Fig 3.8B) (Spearman's $r = 0.57$, $p = 0.11$; Pearson's $r = 0.70$, $p < 0.05$; $n = 7$). That is, the enhanced response due to inclusion of UVB was somewhat proportional to the degree of experimental overexposure to UVB with respect to the mixed-layer average. On the other hand, a less clear relationship was found between R_{tot} and the PAR (or UVA+PAR) overexposure (Spearman's $r = 0.57$, $p = 0.2$; Pearson's $r = 0.52$, $p = 0.23$; $n = 7$).

3.4.5 GP and phytoplankton photophysiology

DMS release may help phytoplankton cells maintain homeostasis at high UVR and PAR, as postulated by the overflow (Stefels, 2000) and antioxidant (Sunda et al., 2002) hypotheses. In stratified waters, nutrient depletion can act synergistically with UVR to enhance oxidative stress (Sunda et al., 2007). While not exclusive, these mechanisms should have distinct spectral profiles. Particularly, the antioxidant mechanism should be more responsive to the UV band, which is more effective at generating intracellular radicals (Lesser, 1996). Extant data suggest that DMS production by phytoplankton can increase by up to one order of magnitude due to UV stress (Sunda et al., 2002; Archer et al., 2010b). To explore how feasible was that phytoplankton supplied all the sunlight-stimulated GP (indeed, an extreme supposition), we calculated the amount of primary production channeled through GP. The estimated GP-carbon flux represented a non-negligible fraction of PPp, with a maximum of around 4% (SP1-2 and SU1) and an average ($\pm$ SE) of 1.9 $\pm$ 0.3 ($n = 30$). Furthermore, this fraction was higher in T and T_{dim} bottles than in their PC and PC_{dim} counterparts (by two-fold, on average; Kruskal-Wallis $p < 0.01$). Considering that phytoplankton can invest as much as 10% of C fixation in DMSP production (Simó and Dachs, 2002; Stefels et al., 2007), the observed GP-carbon flux should be affordable. It is intriguing, however, why such amount of DMS would be released without being oxidized by intracellular radicals.

A distinct feature of the antioxidant mechanism would be the up-regulation of intracellular DMSP concentrations. In this regard, only a few incubations (WI1, SP1, and SP3; T and/or PC_{dim} bottles) showed a strong increase in DMSPt concentrations (up to 90%; data not shown). In most incubations we observed slight changes in DMSPt, or even sharp DMSPt decreases (up to -70%), the latter indicating that DMSP synthesis could not keep up with DMSP loss processes.

3.4.6 GP and radiation-induced damage

So far, our results fit in the framework of the overflow and/or antioxidant hypotheses. But, if these physiological mechanisms were the predominant response promoting DMS production, why was the largest stimulation observed in SU2-3 and WI1 (Fig. 3.6), where potential algal DMS producers were not abundant (Fig. 3.3A)? In our view, an additional mechanism should be considered: radiation-induced phytoplankton cell damage. In this scenario, exposure to sublethal or lethal UVR doses would elicit an increase in the permeability of the cell

membrane and, eventually, trigger programmed cell death or necrosis (Bidle and Falkowski, 2004; Murik and Kaplan, 2009). This would make intracellular DMSP available to bacterial, algal extracellular, or dissolved DMS-producing enzymes, resulting in a more accidental (less physiologically-regulated) DMS production. This might have been the case in experiments SU2-3 and especially WI1, where the largest stimulation of GP and spectral responsiveness co-occurred with UVB overexposure.

3.4.7 GP and microbial interactions

A long-standing question in DMS cycling studies is resolving the relative importance of the different DMS production pathways. Few studies exist where the influence of grazing and viral lysis on DMS production was determined simultaneously. A culture study carried out by Evans et al. (2007) showed that grazing was more important a DMS production pathway than viruses. Studies done with natural communities demonstrate that grazing-mediated DMS production can represent a dominant pathway for DMS production (Saló et al., 2010). PAR-enhanced grazing and digestion rates in microzooplankton (Strom, 2001) may promote DMS production. On the other hand, UVR can worsen the feeding performance of some microzooplankton, alter the nutritional quality of prey, and modify population sizes through trophic cascade effects (Sommaruga, 2003). UVB can reduce viral infectivity and, in turn, viral infection can enhance the UVB resistance of some phytoplankton (Jacquet and Bratbak, 2003), thereby affecting viral infection-related DMS production. Moreover, UVR can potentially alter DMS-producing microbial interactions at the microscale, which are driven by chemotaxis (Seymour et al., 2010). Altogether, these facts suggest that grazing and viral lysis may play an important (yet uncertain) role in sunlight-stimulated GP, which clearly deserves further investigation. It should also be noted that food web-level effects are probably slower than individual physiological responses, and thus less relevant in our short incubations.

Once algal DMSP has been released by any of the processes discussed above it can be catabolized by bacteria. We can represent bacterial DMS production as the product of dissolved DMSP concentration (DMSPd; nmol L^{-1}), the rate constant of bacterial DMSPd consumption (dimension $time^{-1}$), and the bacterial DMS yield (%). As irradiance and UVR increase, the rate constant of DMSPd consumption decreases due to photoinhibiton (Slezak et al., 2001, 2007), and the bacterial DMS yield can either decrease or increase (Slezak et al., 2007; Valle et al., 2012). Due to these opposed changes, the DMSP cleavage capacity of the bacterial community cannot change dramatically (note that bacterial DMS yields rarely exceed 15%; Kiene and

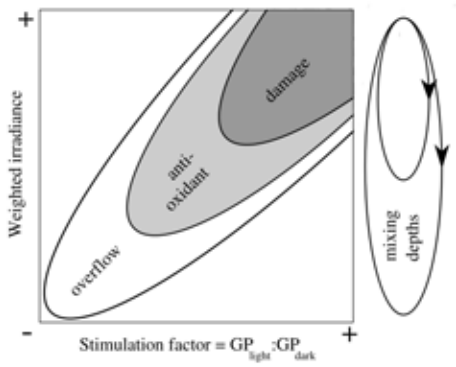

Figure 3.9: **Conceptual synthesis of the interaction between solar exposure and the stimulation of gross DMS production** - The scheme focuses on phytoplankton, since the roles played by bacteria, microzooplankton grazers and viruses are more uncertain.

Linn (2000); Valle et al. (2012). In addition, as UVR and PAR increase DMSP-consuming phytoplankton become more efficient competitors (Ruiz-González et al., 2012f). Therefore, bacterial DMS production ultimately relies on the active or accidental release of algal DMSP.

3.4.8 A conceptual framework for sunlight-stimulated GP

The microorganisms thriving in the surface ocean need to be able to cope with changes in the irradiance exposure regime. On one hand, vertical mixing results in a fluctuating irradiance exposure in the turbulent upper layer. On the other hand, diurnal heating and the ensuing stratification can trap a water parcel at the surface, exposing it to continuous high irradiance (our static incubations would resemble the second situation). Due to the spectral dependence of underwater light attenuation, an increase in total irradiance caused by shallow mixing will be accompanied by increasing proportions of shortwave UVR. The dynamic nature of light exposure is still poorly resolved in experimental settings, and its biogeochemical consequences are not well understood (Bertoni et al., 2011; Ross et al., 2011a,b). Our experimental setup, while not totally realistic, provided a first approximation towards understanding the photobiological bases of some DMS production pathways.

In the light of our results, we propose that the overflow and antioxidant mechanisms could be integrated in a wider overflow-antioxidant-damage continuum (Fig. 3.9), focused on the pivotal

role of phytoplankton DMS(P) release. For a given exposure to irradiance, each phytoplankton population will preferentially contribute to DMS production through overflow, antioxidant, or damage mechanisms, depending on its sunlight sensitivity, its constitutive photoprotection strategies and its DMSP-cleaving capacity. Along a gradient of increasing (weighted) irradiance, the three mechanisms will tend to occur simultaneously, with an increasing importance of damage-related processes and relatively weaker acclimation and repair mechanisms. The interplay between species-specific responses, and food-web processes will ultimately determine the variable response of GP to irradiance.

In summary, we have shown that gross DMS production is consistently stimulated by high irradiance and high proportions of shortwave UVR. This highlights the importance of measuring GP under realistic conditions, taking into account that the 'light' history of the planktonic community may determine its response to subsequent exposure. Phytoplankton photoinhibition or photodamage are identified as the most likely drivers of sunlight-induced GP. We encourage the use of spectral weighting functions to parameterize sunlight-stimulated GP, keeping always in mind the intricate nature of DMS production by microbial food webs.

Acknowledgments

We thank Ruben Sommaruga and Cristina Sobrino for kindly providing biological weighting functions, the Blanes sampling team for invaluable logistic help, Ramon Massana for the epifluorescence microscopy nanoplankton data, and Cèlia Marrasé for help with microphytoplankton data, colored dissolved organic matter (CDOM), and useful comments. We are also indebted with Andrés Gutiérrez-Rodríguez, who shared his expertise with the Fast Repetition Rate fluorometer. Two reviewers provided insightful comments. M.G. acknowledges the receipt of a Junta de Ampliación de Estudios (JAE) scholarship from the Consejo Superior de Investigaciones Científicas (CSIC). This work was supported by the (former) Spanish Ministry of Science and Innovation through the projects 'Organic matter sources, microbial diversity, and coastal marine pelagic ecosystem functioning (respiration and carbon use)' (MODIVUS) (Ciencias y Tecnologías Marinas-CTM2005-04795/MAR) and 'Surface mixing modulation of the exposure to solar radiation' (SUMMER) (CTM2008-03309/MAR). This is a contribution of the Research Group on Marine Biogeochemistry and Global Change and the Research Group on Aquatic Microbial Food Webs, supported by the Generalitat de Catalunya.

Chapter 4

Differential response of planktonic primary production, bacterial production, and dimethylsulfide production to vertically-moving and static incubations in UV-transparent summer stratified waters

Galí, M., Simó, R., Ruiz-González, C., Sarmento, H., Fuentes-Lema, A., Pérez, G., Royer, S.-J., and Gasol, J. M. In preparation for *Geophysical Research Letters*.

Abstract

Microbial plankton experience fluctuations in solar irradiance and its spectral composition as they are vertically moved by turbulence in the upper mixed layer (UML) of the oceans. Yet, biogeochemically-relevant processes other than primary production, like bacterial production or dimethylsulfide (DMS) production, are seldom measured in sunlight and even less in dynamic light fields. We did so in four experiments conducted in oligotrophic summer stratified Mediterranean waters, where a sample from the UML was incubated at three fixed depths plus a vertically-moving incubation. In addition, we assessed the response of the dominant picoplankton community (phyto- and bacterioplankton) with flow cytometric indicators. Dynamic light exposure caused a disruption of the inhibition and photoacclimation processes associated to ultraviolet radiation (UVR), which alleviated bacterial photoinhibition but did not favor primary production. Gross DMS production decreased sharply with depth in parallel to shortwave UVR, and displayed a dose-dependent response that mixing did not significantly disrupt.

4.1 Introduction

Characteristic response times of microbial plankton match the natural variability of light exposure, which changes with solar elevation, the passage of clouds, and vertical mixing (Gallegos and Platt, 1985). In transparent oceanic waters, exposure to high irradiance (photosynthetically available radiation, PAR) is accompanied by exposure to detrimental UVR (Vincent and Neale, 2000). Short-term irradiance fluctuations elicit fast and reversible responses (Roy, 2000), whereas continued exposure to high PAR and UVR may elicit permanent physiological changes, i.e., irreversible damage (Buma et al., 2001) or photoacclimation (Macintyre et al., 2002). Vertical mixing can have either a positive, neutral or negative effect on water column-integrated processes depending on the interplay between mixing times, damage and repair kinetics, and underwater attenuation of PAR and UVR (Neale et al., 2003). In the absence of repair mechanisms, damage will be proportional to cumulative exposure (i.e., dose-dependent); if moderate repair exists, mixing will alleviate the damage by allowing cells recover in the UVR shaded portion of the UML (Fig. 4.1), and damage will no longer be dose-dependent; if repair rates can completely counteract damage rates, vertical mixing will have neutral effects. Admittedly, these responses can change with exposure time.

The effects of dynamic light exposure have concerned the aquatic photosynthesis research community for almost 40 years (see Gallegos and Platt (1985) and references therein), and apparently contradictory findings have often been reached using either experimental or modeling approaches (Ross et al., 2011a,b). The knowledge on the photoresponse of (bacterial) heterotrophic activity is much more limited, but a number of studies suggest that significant stimulation effects driven by PAR may frequently occur (Moran et al., 2001; Church et al., 2004), as well as inhibitory effects due to UVR (Aas et al., 1996; Kaiser and Herndl, 1997). There is mounting evidence that UVR-resistance and photostimulation responses vary among bacterial phylogenetic groups (Agogué et al., 2005; Alonso-Sáez et al., 2006; Ruiz-González et al., 2012b), which might be partially related to the widespread occurrence of photoheterotrophic metabolisms in the ocean (Kolber et al., 2000; Béjà et al., 2000).

Besides carbon (and nutrient) cycling, solar radiation modulates the biogeochemical cycles of other elements. It has been recently shown that sunlight stimulates gross DMS production (Galí et al., 2011) in an irradiance- and spectrum-dependent manner (Chapter 3). The sulfur volatile DMS is produced by the enzymatic cleavage of the phytoplankton compound dimehtylsulfoniopropionate (DMSP) as a result of microbial food web interactions (Simó, 2004). Its

marine emission represents the main natural source of sulfur to the atmosphere (Lana et al., 2011) and has potential climate implications (Charlson et al., 1987, but see Quinn and Bates (2011)), which depend on its response to solar radiation (Vallina and Simó, 2007).

We designed an experiment where a single surface seawater sample was incubated in UVR-transparent bottles at three fixed optical depths, approximately corresponding to the water subsurface, the optical middle, and the bottom of the UML. An additional set of bottles was regularly moved up and down across the same depth range (and radiation gradient) (Fig. 4.1). Rather than simulating actual turbulent mixing experimentally (which is extremely difficult), vertical motion was applied as a perturbation of the photoinhibiton and photoacclimation processes occurring in stratified waters. The experimental design was aimed at answering two questions. The first is of photobiological nature: since the bottles incubated at the middle optical depth and the mixing ones received almost the same cumulative dose, should they display the same response? (which would imply that the measured processes were dose-dependent). The second question is biogeochemical as well as methodological: are the rates obtained from vertical integration of static bottles equivalent to those obtained in vertically-moving bottles in UVR-transparent and shallow-stratified waters?

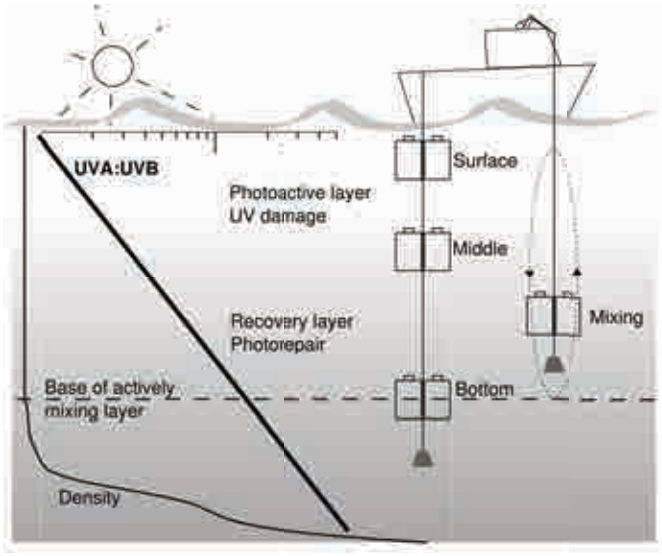

Figure 4.1: **Cartoon of the experimental design** - Vertically-moving and fixed-depth bottles were incubated in a spectral irradiance gradient

4.2 Methods

Seawater samples were taken pre-dawn in 20-30 L polycarbonate carboys. In the two first experiments (C1 and C2) the samples were taken from a boat at the Blanes Bay Microbial Observatory coastal site (BBMO; < 24 m depth; 0.5 miles offshore), brought to the lab, and incubated at the pier of Barcelona Olympic Harbor during 4 h centered on the solar noon. The second two experiments (O1 and O2) were done in the open Mediterranean during a 10 d Lagrangian cruise (R/V García del Cid). In these experiments the samples were incubated in situ, beginning 4 h before solar noon and ending 2 h after solar noon (with an intermediate sample taken after the first 2 h). In C1 and C2 mixing was applied by moving the bottle holders manually every 15 min, completing a mixing cycle every 60 min. In the ship-based experiments the mixing bottles were moved using the winch of the ship at the smallest possible vertical speed (3 – 4 cm s^{-1}), completing a cycle in 10–18 min. Since the waters were less transparent in the harbor than at the BBMO, in C1 and C2 the bottles were incubated at shallower depths to approximate the equivalent optical depths in situ. In practice, the incubations in all four experiments spanned an optical gradient larger than that in the UML (Table 4.1) once the attenuation due to the Teflon bottles (65% and 77% transmittance in the UVB and UVA) was taken into account. Mixed layer depths (MLD) were estimated from CTD temperature profiles, and defined by a > 0.2 °C deviation with respect to 1 m depth. Underwater radiation profiles were measured with a PUV-2500 (Biospherical) filter radiometer, which was also used to record subsurface irradiance during the incubations.

Primary production was measured as the ^{14}C incorporated into particles in 40 mL Teflon bottles inoculated with $NaH^{14}CO_3$ (Morán et al., 1999). Bacterial heterotrophic activity was estimated with the ^{3}H-leucine incorporation method (Kirchman et al., 1985; Smith and Azam, 1992) in 2 h post-exposure dark incubations. In the oceanic experiments, incubation-averaged leucine incorporation rates (LIR) where calculated as the time-weighted average of intermediate and final time incubations. Net biological DMS production was measured in 2.3 L Teflon bottles as outlined in Chapter 3. Gross DMS production was measured in the same way in additional bottles amended with 200 nmol L^{-1} dimethyldisulfide (Simó et al., 2000). All the processes were measured in duplicate bottles except DMS production rates, which require large incubation volumes (Chapters 2 and 3).

Flow citometry was used to enumerate picoplankton populations and to measure their performance at the single-cell level. The fluorescence per cell of different picophytoplankton pop-

Table 4.1: Summary of initial sample characteristics, ecosystem settings and experimental conditions.

Experiment code	Coastal 1 (C1)	Coastal 2(C2)	Oceanic 1 (O1)	Oceanic 2 (O2)
Date	27 Jul 2010	29 Jul 2010	16 Sep 2011	20 Sep 2011
Sampling position	41.67 N 2.81 E		40.9 N 2.67 E	40.9 N 2.44 E
Physical setting in the upper mixed layer				
SST (°C)	23.0	22.7	25.2	23.6
MLD (m)	4	3	7	16
Z 10% 320 nm	7	7	12	11
Z 10% 380 nm	20	20	38	32
Buoyancy frequency (h^{-1})	6.2 ± 1.7	8.8 ± 2.7	8.1 ± 2.8	4.9 ± 0.9
Wind speed (m s^{-1})	2.4 – 6.7	1.4 –7.1	0.3 – 4.8	1.0 – 9.5
UVB range (W m^{-2})	0.4 – 1.4	0.4 – 1.1	0.3 – 1.1	0.04 – 1.1
UVA range (W m^{-2})	22 – 37	21 – 31	19 – 30	9 – 30
PAR range (μE)	1100 – 1580	1010 – 1330	830 – 1360	410 – 1340
Experiment conditions				
Incubation depth (m)	0.3, 1, 3	0.5, 1.5, 3.5	0.5, 3, 11	0.5, 5.5, 18
Equiv. depth UVB (m)	1.3, 4, 10	1.3, 3.5, 6	2.5, 5, 13	2.5, 7, 20
Mixing time	60	60	18	10
UVB range (W m^{-2})	0.04 – 0.9	0.13 – 0.7	0.09 – 0.7	0.01 – 0.65
UVA range (W m^{-2})	4 – 28	9 – 24	11 – 23	5 – 22
PAR range (μE)	460 – 1930	600 – 1210	610 – 1360	320 – 1290
Initial sample characteristics				
DMS (nmol L^{-1})	7.5	8.5	2.1	2.1
DMSPt (nmol L^{-1})	23.0	18.5	18.2	19.6
Chl a (μg L^{-1})	0.24	0.25	0.08	0.08
Dominant phyto. (biomass)	PPeuk > Pro > Syn		Syn > PPeuk > Pro	
Bacteria (10^5 cells mL^{-1})	9.0	7.3	9.4	7.3
'Live' bacteria (%)	54	52	56	56
Biogeochemical process rates (min-max)				
PPp (nmol C L^{-1} h^{-1})	80 – 150	160 – 200	20 – 26	21 – 25
BP t_0 (pmol leu L^{-1} h^{-1})	32	21	36	18
BP (pmol leu L^{-1} h^{-1})	33 – 37	16 – 21	37 – 44	17 – 27
GP (nmol DMS L^{-1} h^{-1})	0.05 – 0.40	0.24 – 0.49	na	0.07 – 0.17
NP_{bio} (nmol DMS L^{-1} h^{-1})	0.03 – 0.32	0.18 – 0.44	0.02 – 0.10	0.04 – 0.16

ulations (normalized to their side scatter -SSC-, a proxy for cell size) was measured following (Marie and Partensky, 2006). Two subpopulations of heterotrophic bacterioplankton were distinguished based on the nucleic acid double staining protocol: 'live' bacteria and membrane-compromised ('dead') bacteria (Grégori et al., 2001).

All variables were normalized to the vertical integral of the fixed incubations within each experiment. After pooling the four experiments together we checked for significant differences among treatments. If the Bartlett's equal variance test was positive ($p > 0.05$) one-way ANOVA was used. Otherwise, a non-parametric Kruskal-Wallis ANOVA was performed. After a significant ANOVA ($p < 0.05$) multiple comparisons were done with the Tukey-Kramer test.

4.3 Results and discussion

The UML where the samples were taken from was in all cases exposed to high proportions of UVR, i.e. $>$ 10% of the subsurface UVB and UVA levels ($<$1 optical depth; Table 4.1). The phytoplankton community was typical of oligotrophic conditions, with low biomass dominated in all samples by the pico-sized fraction (*Prochlorococcus, Synechococcus* and picoeukaryotes).

Surface mixing was very shallow at the coastal site (3 – 4 m). In the oceanic setting, the UML deepened from 7 m (O1) to 16 m (O2) due to the passage of a storm (see SI). The fact that all experiments took place in soft wind conditions, and the relatively high values of the buoyancy frequency (or Brunt-Väisälä frequency) within the UML suggest that the mixed layer was not mixing actively at the time of the CTD casts (Table 4.1). If we assume that vertical diffusivities (K_z) in the UML interior were in the range 10^{-2} – 10^{-4} m^2 s^{-1} (Denman and Gargett, 1983; Ross et al., 2011b), it would take between ca. 0.25 and 100 h for a population of particles released at a single depth to diffuse across one optical depth in the UML (depending on the wavelengths and MLD considered; Gallegos and Platt (1985)). A similar range is obtained by calculating the mixing timescale as MLD^2/K_z as suggested by Ross et al. (2011a,b). The highest K_z might be representative of nighttime convective overturning, while the lowest K_z might be more representative of the daytime, when mixing was likely inhibited by solar heating (Brainerd and Gregg, 1995). From these calculations we can conclude that the simulated mixing times were considerably faster than the actual mixing times.

Particulate primary production (PPp) was moderately inhibited at the surface, optimal at the middle depth, and slightly lower at the bottom (Fig. 4.2A). With the exception of C1, PPp in mixing bottles resembled that in surface bottles and was 18% lower than in middle bottles

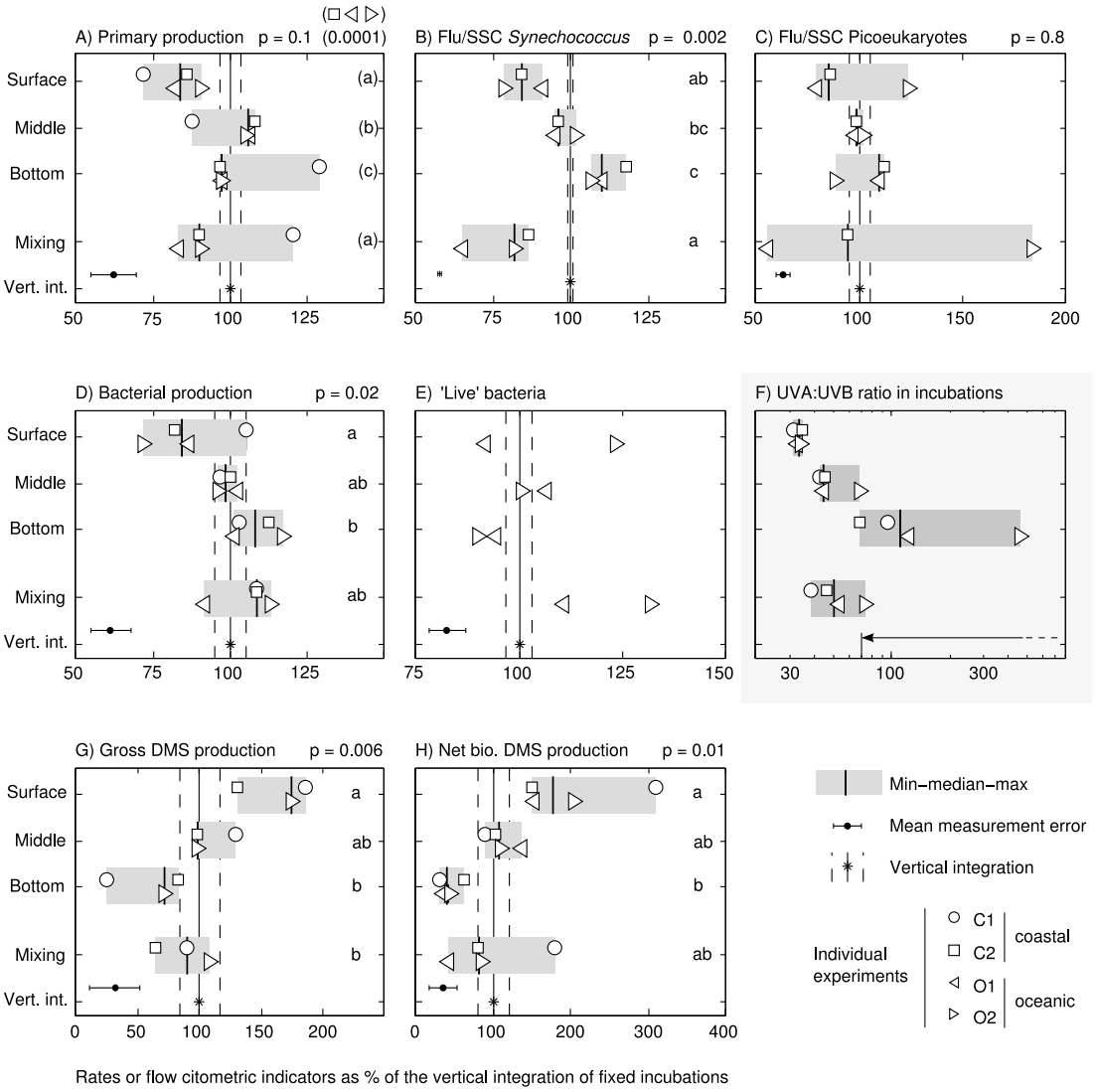

Figure 4.2: **Response of microbial plankton and biogeochemical process rates to irradiance gradients in static and vertically moving incubations** - C and S cycling rates (A, D, G and H), and flow cytometric indicators of picoplankton activity (B, C and E). The arrow in (F) indicates the UVA:UVB window where photolyase repair is more efficient, calculated from underwater UVR profiles according to Kaiser and Herndl (1997). Differences between treatments are represented by p-values of ANOVA tests followed by multiple comparisons. In (A), a test was performed on a subset of experiments that exhibited a more coherent response.

($p < 0.01$). As a result, vertically integrated PPp from fixed bottles generally exceeded that in mixing bottles by 10-17%(except in C1). This result contrasts with that obtained by Bertoni et al. (2011), who observed a neutral to positive effect of dynamic light exposure in coastal

Mediterranean waters in late spring. At the end of the incubations, the average fluorescence of *Synechococcus* and picoeukaryote cells was generally lowest at the surface and increased with depth (Fig. 4.2B, C). Again, fluorescence was lower than average in mixing bottles (although different patterns were observed for picoeukaryotes in O2). Similar responses could be observed for nanoeukaryotes in C2 and for *Prochloroccus* in O1 (data not shown), accompanied by marked decreases in *Prochlorococcus* cell counts (Sommaruga et al., 2005).

The decrease in fluorescence per cell may simultaneously result from photoacclimation (Macintyre et al., 2002, decrease in chlorophyll *a* to carbon ratios), a decrease in the fluorescence yield of photosystem II (Behrenfeld et al., 1998), and pigment bleaching (Vincent and Neale, 2000). In a first interpretation our results might indicate that the short surface exposure received by mixing bottles was enough to cause some irreversible inhibition, and that phytoplankton repair capacity was limited. However, the fact the surface inhibition was only moderate and that highest PPp occurred in the middle bottle suggests that their photosynthetic machinery was not geared to deal with fast changes in spectral irradiance. In concordance with this explanation, UV sunscreen compounds (most probably mycosporine-like aminoacids, MAAs) were frequently observed in the absorption spectra of surface phytoplankton. Moreover, in experiment O2 MAAs were detected at the end of the incubation only in surface bottles (Fig. 4.3), suggesting that the irradiance conditions experienced by mixing bottles were not harsh enough to induce (or maintain) MAAs synthesis.

Leucine incorporation rates (LIR) were significantly inhibited at the surface (by 14-28% except in C1) and increased with depth to find their optimum at the bottom of the mixed layer (Fig 2D). LIR in mixing bottles resembled those of bottom bottles in 3 out of 4 experiments, and were higher (though not significantly) than those in middle bottles and the vertical integral. This suggests that fast mixing favored recovery and photorepair over photodamage, an interpretation that is supported by the higher proportions of 'live' bacteria found in mixing bottles at the end of the incubations (O1 and O2 only; Fig. 4.2E). It is well known that photolyase enzymes use UVA and blue light to repair damaged DNA. According to Kaiser and Herndl (1997), optimal photoreactivation occurs in a certain window of UVA:UVB that, in our experiments, would roughly correspond to the bottom half of the UML (Fig. 4.2F). Besides the photoresponse 'inherent' to different bacterial populations, other factors have been invoked to explain the changes in bacterial activity under sunlight. For instance, exudation of labile organic matter by phytoplankton due to high PAR or grazing. In our experiments, no obvious patterns linking the response of LIR and PPp were found.

In addition to the post-exposure dark incubations, in C1 and C2 we measured LIR during the sunlit incubations, i.e., with the ^{3}H-leucine added into the exposed bottles (Fig. 4.4). In these 'in situ' incubations surface and mixing bottles displayed more similar degrees of inhibition. This indicates that some bacterial recovery took place during the dark post-exposure incubations, which therefore might not be the best choice when assessing the short-term effects of sunlight. Our study adds to the only previous study of bacterial production under dynamic light exposure (Bertoni et al., 2011), and agrees with it in that the effect of mixing was neutral to positive compared to fixed incubations.

Gross DMS production (GP) showed the strongest vertical gradient among the three processes, and increased by around three-fold between the bottom and the surface of the UML. Net biological DMS production, which is equivalent to GP minus bacterial DMS consumption, showed a similar pattern, which indicates that bacterial DMS consumption was relatively small compared to GP. Indeed, the vertical gradient of GP was evident only after the apparent DMS production in the incubations was corrected by photochemical DMS consumption, as discussed by Galí et al. (2011, and Chapter 3) (Fig. 4.5). Gross and net biological DMS production in mixing bottles were not significantly different from those in middle bottles, and not either from the vertical integral (Fig. 4.2G, H), although a slight trend towards lower GP in mixing bottles occurred in C1 and C2.

Gross DMS production results from the addition (and interaction) of several processes, namely: exudation of DMS by phytoplankton, and bacterial degradation of the DMSP released by healthy phytoplankton or by phytoplankton cells lysed as a results of grazing, viral infection, or cell death. In Chapter 2 it was shown that UVR stimulates gross DMS production in an irradiance-dependent manner, and that the stimulation is more effective at shorter (more energetic) UVR wavelengths. In that study the stimulation effect was attributed to phytoplankton DMS release caused by excess PAR (Stefels, 2000) and/or UVR stress (Sunda et al., 2002). Furthermore, it was suggested that lethal UVR exposure could promote DMS production by causing phytoplankton cell lysis. Overall, our results suggest that the UVR dose-dependence of GP holds in dynamic exposure regimes, and that GP is far more responsive to spectral irradiance gradients than primary or bacterial production. The different responses of PPp, LIR and GP to static and dynamic exposure indicate that DMS production cannot be obviously linked to neither autotrophic nor heterotrophic bulk activities.

We conclude that, in summer stratified UV-transparent waters, vertically-moving incubations *generally* caused (1) an adverse effect on particulate primary production concomitant with

reduced fluorescence per cell; (2) an alleviating effect on bacterial production photoinhibition, related to an increase in the proportion of active cells; (3) a neutral effect or slight reduction in gross DMS production, which was the process showing a clearer dose-response proportionality. These responses translated, in some experiments, into measurable deviations with respect to the vertically-integrated rates in the water column; in others, the effects were close to neutral or too small to be reliably detected. Incubating the samples at an intermediate optical depth appears as a reasonable (and convenient) solution for measuring leucine incorporation and gross DMS production, but not primary production, in UVR-transparent stratified UML waters. Our results call for a more systematic assessment of the consequences of dynamic light exposure on light-mediated biogeochemical processes in different oceanic regimes.

Acknowledgements

We thank the staff at Port Olímpic de Barcelona for their collaboration, and the crew of R/V García del Cid for their invaluable help in setting up the experiments during the SUMMER I cruise.

4.4 Supplementary information

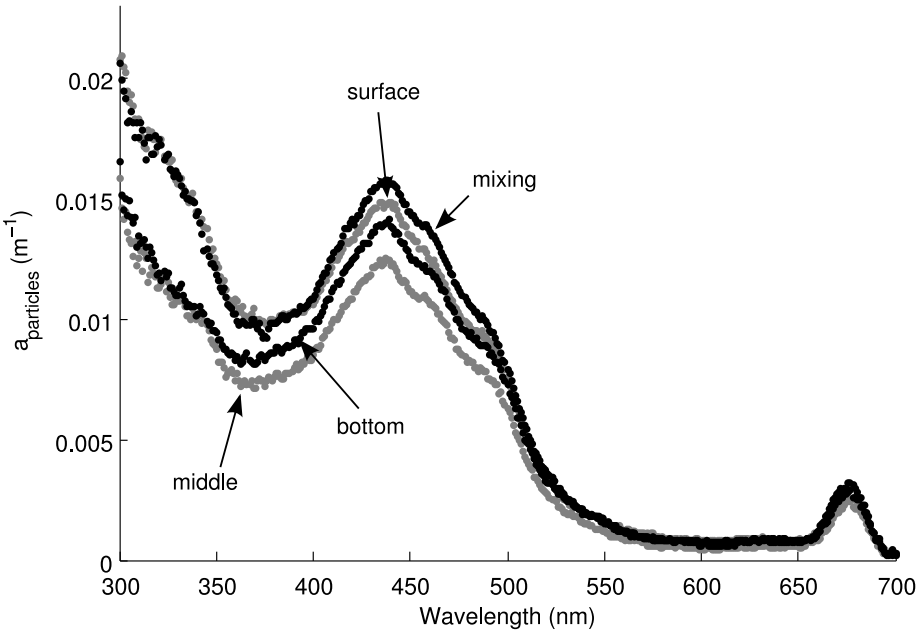

Figure 4.3: **Phytoplankton absorption spectra at the end of experiment O2 (SI)** - The spectra were measured by collecting particles on a GF/F filter (2 L volume filtered) in a spectrophotometer fitted with a black filter holder located just before the detector window. The method compared well against measurements performed with an integrating sphere. The UV-absorbing compounds appear clearly in bottles incubated at the surface or mixing within the UML

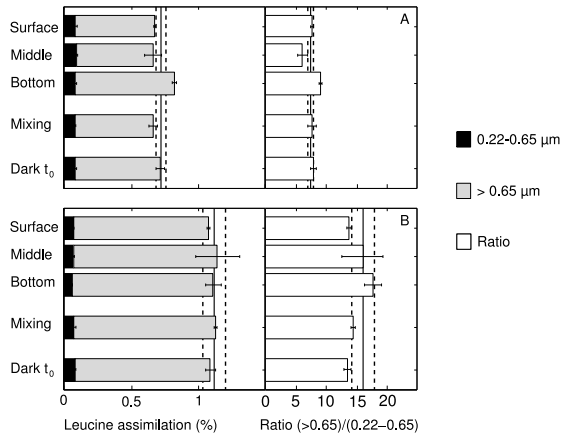

Figure 4.4: **Bacterial production measured by inoculating 40 mL Teflon bottles incubated 'in situ' (SI)** - Leucine incoropration was split in two size fractions. Large bacteria (those retained on a 0.65 μm-pore size filter) accounted for most heterotrophic activity, probably with a sizable contribution of cyanobacteria and photosynthetic picoeukaryotes (Ruiz-González et al., 2012f). (A) C1, (B) C2.

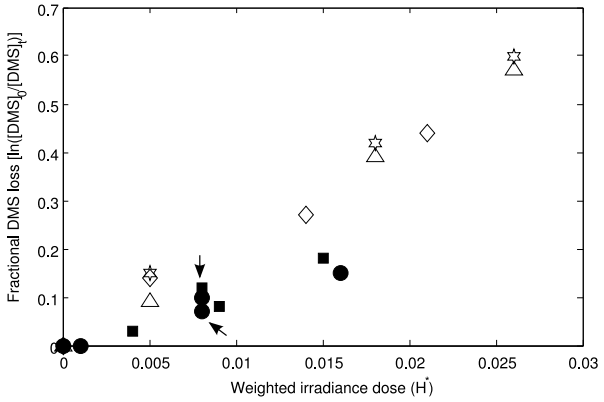

Figure 4.5: **DMS photolysis dose-response in fixed and vertically-moving incubations (SI)** - Teflon bottles were incubated in C1 and C2 at the three fixed depths and in a vertically-moving basket (filled symbols). The two types of incubation showed consistent dose-response behavior, and similar photolysis rates were found on the two sampling dates. Arrows indicate vertically moving incubations. Empty symbols: Dose-response of DMS photolysis in Teflon or quartz flasks incubated on board and withdrawn at different times (three different samples). Photolysis rate constants (on a weighted radiation dose basis, the k^*_{photo} defined in Chapter 3), were 22.4 and 11.2 at the coastal station and at the oceanic station, with R^2 of 0.92 and 0.99, respectively.

Chapter 5

Diel cycles of oceanic dimethylsulfide (DMS) cycling: microbial and physical drivers

Galí, M., Simó, R., Vila-Costa, M., Ruiz-González, C., Gasol, J. M., and Matrai, P. Under review in *Global Biogeochemical Cycles*.

Abstract

Dimethylsulfide (DMS) is a potential climate-active gas produced by marine microbial food webs, and its emission depends on the interplay between microbial activity and physical forcing in the oceanic upper mixed layer (UML). We investigated the diel cycling patterns of DMS and its precursor dimethylsulfoniopropionate (DMSP) in four experiments (28 to 48 h long) performed in meso- to ultraoligotrophic Mediterranean and Sargasso Sea waters. Samples taken every 4 or 6 h were analyzed for dimethylated sulfur pools and incubated to measure biotic and abiotic DMS(P) cycling rates, as well as primary production, bacterial production, and microbial DMSP consumption. The measured biological DMS cycling rates, photolysis, and ventilation, were extrapolated to the whole UML to calculate high temporal resolution DMS budgets and day vs. night budgets. In the three summer experiments, gross community DMS production (GP) increased by 2 to 3-fold from night- to daytime, peaking 0-4 h after solar noon, presumably due to phytoplankton radiative stress. This excess GP was balanced by higher photochemical and microbial sinks during the day, effectively buffering DMS concentrations. In the only winter experiment, GP exhibited completely opposed dynamics and peaked at nighttime in parallel to DMSP consumption, presumably due to grazing. Our data provide solid evidence of radiation-driven DMS production (and DMSP-to-DMS conversion yields) during summer stratification, and strongly suggest that diel variability should be taken into account in process studies, diagnostic, and prognostic models of DMS cycling.

5.1 Introduction

The dimethylated sulfur compound DMSP is produced in varying amounts by diverse marine phytoplankton groups (Stefels et al., 2007). Besides osmoregulation, intracellular DMSP serves distinct physiological functions related to environmental stress, particularly the response to high radiation levels and nutrient starvation (Stefels, 2000; Sunda et al., 2002, 2007). Planktonic DMSP metabolism is the main source of the volatile DMS, produced either through direct enzymatic DMSP cleavage by phytoplankton, or through DMSP transformations mediated by microbial food web interactions (Simó, 2004; Stefels et al., 2007). The latter involve bacterial DMSP catabolism, which may channel DMSP to DMS or divert it to other volatile and non-volatile compounds (Moran et al., 2012).

DMS emission plays an important role in aerosol formation, growth and chemistry with potential for influencing cloud microphysics in remote marine regions (Vallina et al., 2006; Andreae and Rosenfeld, 2008), to the point that it might induce significant radiative forcing at regional scales, and even drive a (controversial) plankton-climate feedback loop (Charlson et al., 1987; Quinn and Bates, 2011). Being DMS generally supersaturated in the ocean side respective to the atmosphere side, its emission depends largely on sea-surface DMS concentrations and wind speed. However, DMS ventilation generally represents a non-dominant sink, compared to the other competing DMS consumption pathways in the oceanic UML: microbial (bacterial) DMS consumption and photochemical oxidation (Simó, 2004; Toole et al., 2006). Thus, it follows that the interplay between biotic and abiotic DMS sinks and gross community DMS production within the UML determines how much DMS ends up in the marine troposphere.

Day-night alternation and the underwater light exposure regime (the latter modulated by meteorological variability and vertical mixing), exert an obvious rhythmic forcing on photochemical and photobiological processes (Doney et al., 1995). In turn, these may couple or uncouple, to amplify or buffer the diel oscillations of biogeochemical fluxes. Since light-driven processes are key in the biogeochemical cycling of DMS and its precursor DMSP (Toole et al., 2006; Galí et al., 2011; Levine et al., 2012) diel variability is to be expected; yet, studies aimed at understanding this relevant time scale are surprisingly scarce. Diel studies of DMS(P) cycling can also provide significant insight into coupled physical-microbial ecosystem functioning, given the important role of DMSP in planktonic metabolism (Kiene et al., 2000; Simó, 2004; Seymour et al., 2010), and the relevance of DMS(P) as model compounds. Here, we report four diel cycle experiments conducted in different oceanographic settings, revealing a marked diel

Table 5.1: General description of the four diel cycle experiments. See Bailey et al. (2008) and Gabric et al. (2008) for details on the trajectory of the Lagrangian drifters.

Experiment	Med winter (coastal)	Med summer (coastal)	Med summer (oceanic)	Sargasso su. (oceanic)
Abbreviation	CMEDwin	CMEDsum	MEDsum	SARGsum
Date	22 – 24 Mar 2004	18 – 20 Sep 2007	23 – 25 Sep 2007	31 Jul – 1 Aug 2004
Position	41º 40' N, 2º 48' E		40º 39' N, 2º 51' E	29º 1' N, 63º 36' W
Type	coastal	coastal	oceanic	oceanic
Trophic status	mesotrophic	oligotrophic	oligotrophic	ultraoligotrophic
lagrangian	no	no	no	yes
Bott. depth (m)	24	30	2000	>4000
Exp. duration (h)	48	48	48	28
Sampl. depth (m)	0.5	4	5	3
Type of incub.	Dark	Dark-light	Dark-light	Dark

variability of biotic and abiotic DMS cycling which translated into highly variable but balanced surface ocean DMS budgets.

5.2 Methods

5.2.1 Overview

We performed four diel cycle studies of 28-48 h duration, as summarized in Table 5.1. The wintertime study (CMEDwin) took place in March 2004 at the Blanes Bay Microbial Observatory (BBMO), a thoroughly studied NW Mediterranean coastal site. The remaining three studies were conducted in summer during oceanographic cruises to the Sargasso (Biocomplexity cruise on board the R/V Seward Johnson) and the Mediterranean Sea (MODIVUS cruise, R/V García del Cid). In the Sargasso Sea cruise, an anticyclonic eddy (named A2) was followed for 6 days by deploying Lagrangian drifters, and the diel cycle experiment (SARGsum) was conducted during the last two days. In the Mediterranean Sea cruise, a first experiment (CMEDsum) was conducted 1 km offshore from the regular BBMO sampling site, and a second at an open ocean station (MEDsum), located ca. 120 km south of the BBMO.

In CMEDwin surface seawater was sampled from a boat every 6 h and brought to the lab within 2 h for further processing. In the ship-based experiments sampling was done every 4 h from Niskin bottles attached to a CTD-rosette, and the samples were immediately processed. This said, all the experiments proceeded similarly: after taking aliquots to determine dimethylated sulfur concentrations and ancillary microbial parameters at time zero, incubation bottles were filled with unfiltered water and immediately incubated to measure biological sulfur cycling

rates plus autotrophic and heterotrophic microbial activities. All the biological process incubations (except otherwise noted) lasted for ca. 6 h and, thus, successive incubations overlapped. The samples were incubated in the dark at in situ temperature, either in a thermostatted chamber (CMEDwin) or in a tank with running seawater from the ship underway intake. In CMEDsum and MEDsum, additional incubations of whole- and 0.2 μm-filtered seawater were done in UV-transparent bottles during the day, to determine the response of microbial and photochemical processes to natural sunlight (see 2.5).

Some of the data used here, corresponding to the 2004 Sargasso Sea cruise, were already published (as noted throughout the paper). The reader is referred to the works by Bailey et al. (2008) and Gabric et al. (2008) for a comprehensive description of the oceanographic setting and DMS cycling during that cruise.

5.2.2 Oceanographic and meteorological data

Vertical profiles of conductivity (salinity) and temperature in the upper 200 m were obtained every 4 h with a CTD probe (Seabird 9/11 plus) equipped with sensors of chlorophyll fluorescence, turbidity, beam attenuation and dissolved oxygen. The SEASOFT software (Seabird) was used to calculate seawater density (σ_t) and to bin the profiles at 1 m intervals. Binned profiles were used to calculate the mixed layer depth (MLD), defined as the layer where a temperature difference < 0.02 °C occurred with respect to that at 4 m (Fig. 5.1) (4 m was the shallowest depth available in all CTD profiles). Alternative MLD criteria based on either temperature or density profiles were also explored, but we chose the 0.02°C criterion because it is more likely to capture the actively mixing layer and diurnal stratification events (Brainerd and Gregg, 1995; Gardner et al., 1999). In CMEDwin, lower resolution temperature profiles were obtained with a manual thermometer. In this case, we chose a 0.05°C criterion and 2 m as the reference depth, which rendered more robust MLD values.

Underwater irradiance profiles in six bands in the ultraviolet region (UV; 305, 313, 320, 340, 380 and 395 nm) and one integrated band for photosynthetically available radiation (PAR; 400-700 nm) were obtained by deploying a PUV 2500 radiometer (Biospherical) 2 to 4 h before and after the solar noon. Diffuse attenuation coefficients of downwelling cosine irradiance (K_d) were calculated from the linear regression between logarithm-transformed irradiance and depth (within the UML or a deeper, optically homogeneous surface layer). Meteorological data were recorded by either shipboard stations or a nearby land-based station (CMEDwin; Malgrat de Mar, Catalan Meteorological Service, SMC). During sunlit incubations, the PUV

2500 radiometer was placed inside the incubator to take a continuous record of downwelling irradiance (care was taken to use black incubation tanks to avoid upwards light reflection). By combining the time series of spectral irradiance, CTD-derived mixing depths, and underwater light attenuation, we obtained high temporal resolution time series of spectral irradiance and radiation doses within the UML. These were used to estimate in situ DMS photolysis and the effects of sunlight on microbial processes.

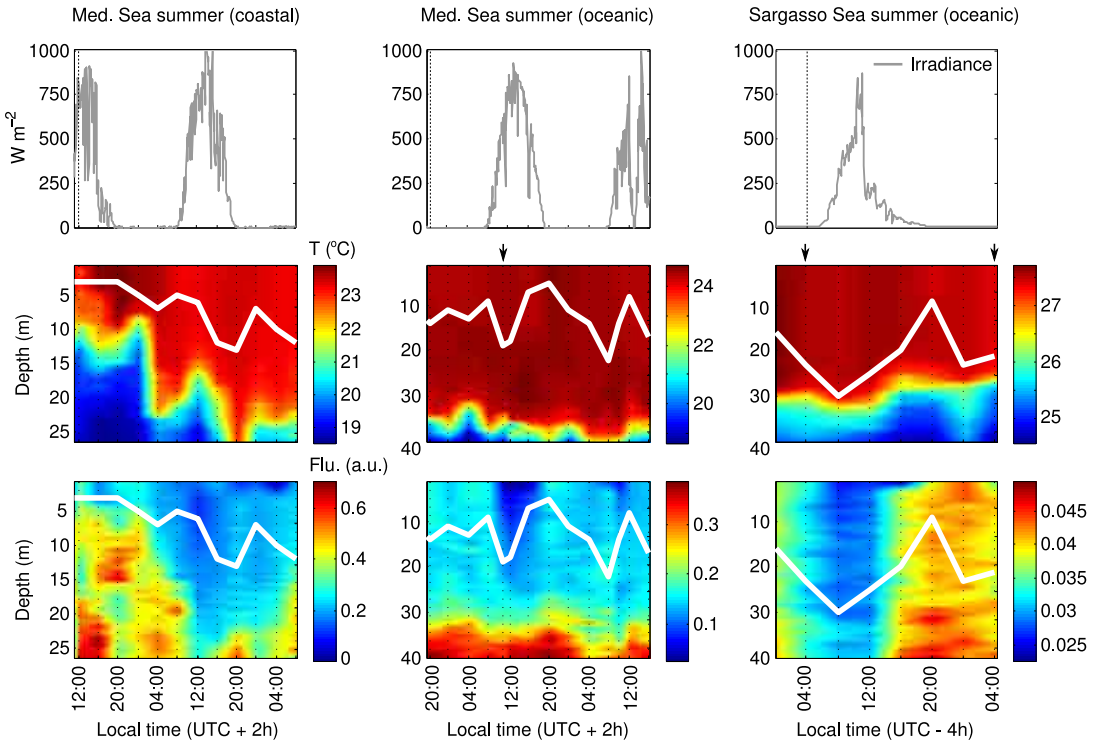

Figure 5.1: **Physical setting in the summert diel cycle experiments** - Total shortwave irradiance (first row), and verticaltemporal variability of temperature (second row) and fluorescence profiles (third row), plotted together with mixing layer depths (white line). Arrows indicate time points of DMS profiles (see Fig 7).

5.2.3 Chemical analyses and determination of microbial abundance

DMS was analyzed by purge and trap gas chromatography (GC) coupled to flame photometric detection (FPD), with a detection limit of ca. 3 pmol and analytical precision generally better than 5%. Total DMSP (DMSPt), comprising the particulate and dissolved pools (DMSPp and DMSPd), was analyzed as the DMS evolved by alkaline DMSP cleavage in whole water

samples, as described elsewhere (Simó et al., 1998; Saló et al., 2010). Chlorophyll *a* (Chl *a*) was determined fluorometrically after filtration onto GF/F filters and overnight extraction in acetone. Flow cytometry was used to enumerate heterotrophic bacteria after DNA staining with SybrGreen I (Gasol and del Giorgio, 2000), and pico- and nanophytoplankton populations in live samples (*Prochlorococcus*, *Synechococcus*, picoeukaryotes and nanoeukaryotes) (Marie and Partensky, 2006). Microphytoplankton species were identified and counted with an inverted microscope in the three Mediterranean Sea experiments.

5.2.4 Microbial activity parameters determined with radioisotope additions

Particulate primary production (PPp) was estimated from the uptake of $H^{14}CO_3$ addition following standard procedures (Morán et al., 1999). The irradiance levels were adjusted with neutral density screens, so that we could estimate the PPp rates corresponding to the average UML light levels. Since different incubation setups were employed in CMEDwin (artifical light shource), and (C)MEDsum and SARGsum (on-deck incubators), we will use the estimated PPp rates to explore possible relationships between microbial activities, but not to make quantitative inferences. Bacterial heterotrophic activity was estimated with the ^{3}H-leucine incorporation method (Kirchman et al., 1985). Triplicate samples plus one killed control were incubated in the dark for 2 h and processed by the centrifugation method of Smith and Azam (1992). Size-fractionated microbial DMSP assimilation into macromolecules (> 0.22, > 0.65 and > 3 μm fractions) was measured by trace additions of ^{35}S-DMSP, only in CMEDsum and MEDsum. The samples for DMSP assimilation were incubated in 50 ml quartz flasks (thus, under full spectrum sunlight during the day) and processed as explained elsewhere (Ruiz-González et al., 2012a).

5.2.5 GC-based DMS(P) cycling incubations

The inhibitor method (Wolfe and Kiene, 1993a; Simó et al., 2000) was employed to estimate gross community DMS production (GP) and bacterial DMS consumption rates (BC). Briefly, GP was calculated as the rate of DMS accumulation over time in bottles ammended with 200 nmol L^{-1} dimethyldisulfide (DMDS, final conc.). Net DMS production rates (NP) were determined in unamended bottles incubated in parallel, so that BC could be determined as the difference between GP and NP. Only initial and final concentrations were measured; previous work had shown that linear changes in concentration occur, particularly in short-term (<10

h) incubations (Simó et al., 2000; Saló et al., 2010). Darkened 2.9 L amber glass bottles were used for the dark incubations. Light incubations were done in 2.3 L Teflon bottles, which transmitted 65, 77 and 100%, respectively, of UVB, UVA and PAR irradiance. The bottles were additionally covered by one layer of neutral screen (62% transmission) to approximate the mean UML irradiance. Although no treatment replicates existed, the large incubation volumes ensured a community inclusive incubation which minimized the experimental error (Galí et al., 2011). *GP* and NP rates obtained in sunlight were corrected to account for photochemical DMS loss, using the photolysis rate constants measured in each experiment (see below) scaled to the radiation dose received by each incubation, following Galí et al. (2011).

Total microbial DMSP consumption was measured with the net-loss curve approach of *Simo2000* in the same whole water dark incubations where net DMS production was determined. Briefly, the logarithm of fractional DMSPt loss (final/initial) was divided by the incubation time. The resulting DMSPt consumption rate constant (h^{-1}) was multiplied by the DMSPt concentration in situ, yielding the consumption rate (nmol L^{-1} h^{-1}). Note that this measurement renders the amount of DMSP consumed by the whole community, that is, the sum of particulate and dissolved DMSP consumption. This allows calculating the community DMS yield as the quotient between *GP* and DMSPt consumption in %. Note that this yield differs from the DMS yield from microbial DMSPd consumption (Kiene and Linn, 2000). The DMSPt consumption rate was further combined with in situ DMSPt variations to estimate, by budgeting, the DMSPt production (Simó and Pedrós-Alió, 1999c).

Pseudo first-order DMS photolysis rate constants ($k_{photo,incub}$; h^{-1} units) were determined by incubating 0.2 μm-filtered water under subsurface irradiance in the on-deck incubator. In the Mediterranean Sea cruise, bulk photochemical DMS loss was estimated as described in Chapter 2, with the difference that gaseous DMS was added at concentrations up to 60 nmol L^{-1} to ensure better detection. In this DMS concentration range, first-order kinetics should be expected (Kieber et al., 1996). In the CMEDwin experiment no photolysis measurements were available. Thus, we decided to use an average wintertime photolysis rate constant obtained from published (Vila-Costa et al., 2008) and unpublished studies (Chapter 3), based on the observation of consistent seasonal patterns of DMS photolysis in this Mediterranean coastal site (see Chapter 6). In the Sargasso Sea cruise, $k_{photo,incub}$ were obtained with the ^{35}S-DMS tracer method (details in Bailey et al. (2008) and references therein).

Table 5.2: Summary of the ecosystem setting and sulfur cycling during the diel cycle experiments. Means and ranges (min-max) of usually 8-11 measurements are reported, unless < 5 measurements are available. SST: Sea Surface Temperature; $E_{d,hourlymax}$: maximum hourly total shortwave irradiance; $K_{d,PAR}$ and $K_{d,340}$: vertical attenuation coefficients of PAR and 340 nm radiation, respectively; MLD: mixed layer depth; SRD: Solar Radiation Dose index (Vallina and Simó, 2007); $UVB_{UML,max}$: maximum hourly UVB irradiance in the upper mixed layer; see text for other abbreviations.

Experiment	CMEDwin	CMEDsum	MEDsum	SARGsum
Meteorological and oceanographic data				
SST (°C)	12.6 (12.1 – 12.9)	23.6 (23.3 – 23.9)	24.7 (24.4 – 25.3)	27.5 (27.3 – 27.7)
Salinity	37.9 (37.1 – 38.4)	37.7 (37.6 – 37.9)	37.5 (37.4 – 37.6)	37.0 (36.8 – 37.1)
Wind speed (m s^{-1})	1.5 (0.5 – 3.2)	3.9 (0.3 – 9.9)	4.7 (0.04 – 14.6)	7.8 (0.8 – 13.5)
E_d hourly max (W m^{-2})	725	913	818	660
$K_{d,PAR}$ (m^{-1})	0.12	0.08 (0.05 – 0.12)	0.04	0.035
$K_{d,340}$ (m^{-1})	0.26	0.18 (0.12 – 0.29)	0.10	0.055
Z 10% 340 nm (m)	9	13 (8 – 17)	22	34
MLD (m)	10 (4 – 24)	7 (3 – 13)	14 (5 – 22)	21 (9 – 30)
SRD (W m^{-2})	98	123	139	67
$UVB_{UML,max}$ (W m^{-2})	0.42	0.8 (0.2 – 1.6)	0.5 (0.2 – 0.8)	0.55
NO_3^- + NO_2^- (μmol L^{-1})	2.7	0.63	0.09	< 0.02
Phosphate (μmol L^{-1})	0.2	0.02	0.03	< 0.01
Microbial community descriptors				
Dominant phyto.	Diat. > PPeuk	Syn > PPeuk	Syn > PPeuk	PPeuk > Syn
Chl a (μg L^{-1})	0.56	0.14	0.11	0.05 (0.035 – 0.061)
PPp (μmol C L^{-1} d^{-1})	0.76	0.48 (0 – 0.7)	0.5 (0 - 0.9)	0.02
Bacteria (10^9 cells L^{-1})	1.3	0.7	0.6	0.4
LIR (nmol leu L^{-1} d^{-1})	0.7	0.8 (0.2 – 1.6)	0.5 (0.2 – 0.8)	0.24 (0.10 – 0.46)
Sulfur pools and ratios				
DMS (nmol L^{-1})	1.5 (1.1 – 1.9)	3.1 (2.2 – 4.0)	4.0 (2.3 – 4.7)	3.1 (2.8 – 3.4)
DMSPt (nmol L^{-1})	36.1 (13.3 – 77.1)	18.1 (15.5 – 27.4)	16.9 (14.4 – 19.8)	8.0 (6.6 – 9.3)
DMS:DMSPt	0.05 (0.01 – 0.12)	0.18 (0.10 – 0.25)	0.20 (0.14 – 0.31)	0.40 (0.34 – 0.50)
DMS:Chl *a* (nmol μg^{-1})	2.8	14.1	36.4	74 (58 – 102)
DMSPt:Chl *a* (nmol μg^{-1})	33	135	155	180 (143 – 206)
Biotic DMS(P) cycling				
k DMSPt prod (d^{-1})	1.9 (0 – 4.1)	1.0 (0 – 2.0)	0.9 (0.3 – 2.5)	0.8 (0.3 – 1.5)
k DMSPt cons. dark (d^{-1})	1.6 (0.5 – 2.7)	0.9 (0.3 – 1.6)	0.9 (0 – 1.8)	0.4 (0 – 1.0)
k DMS *GP* dark (d^{-1})	1.6 (0.2 – 3.9)	0.6 (0 – 1.6)	0.5 (0 – 1.0)	1.0 (0 – 1.8)
k DMS *GP* light (d^{-1})		0.8 (0 – 2.3)	0.7	
k DMS *BC* dark (d^{-1})	1.3 (0 – 2.8)	0.5 (0 – 0.8)	0.5 (0.2 – 1.0)	0.7 (0 – 1.6)
k DMS *BC* light (d^{-1})		0.4 (0 – 0.7)	0.4	
Abiotic DMS cycling (upper mixed layer mean)				
k DMS photo. (d^{-1})	0.25 (0 – 1.3)	0.07 (0 – 4.5)	0.06 (0 – 0.35)	0.03 (0 – 0.28)
k DMS vent. (d^{-1})	0.04 (0 – 0.07)	0.29 (0.01 – 1.4)	0.12 (0 –0.75)	0.19 (0.02 – 0.53)

5.2.6 Sulfur cycling budgets in the UML

Sulfur cycling budgets were calculated by extrapolating the measured DMS cycling rates (GP, BC and photolysis) and the parameterized DMS ventilation to the whole upper mixed layer. We assumed homogeneous DMS concentrations and biological activity throughout the mixing layer. At any time interval, the DMS budget equation has the form (Gabric, 2001):

$$\frac{[DMS]}{dt} = GP - BC - k_{photo,UML}[DMS] - \frac{k_w[DMS]}{MLD} + Transport \tag{5.1}$$

Photolysis and ventilation rates were calculated as the product of in situ DMS concentration and the respective rate constants (k's, which are a function of meteorological forcing) and averaged throughout the UML as explained in the following paragraphs. GP and BC rates were directly obtained from the incubations, lagged by two hours from the sampling time. This time lag was chosen for all the experiments because it represented a good compromise between the sampling time and the length of the incubations. Lagged correlations showed that the best fit between diagnosed and in situ net DMS production generally occurred at around 2 h lag, and always between 0 and 4 h. We used the rates determined in sunlight when possible (CMEDsum and MEDsum). The DMS budgets were calculated at 5 min temporal resolution, and temporally averaged afterwards to obtain 30 min budgets and daytime vs. nighttime budgets (with the exception of CMEDwin, where only hourly meteorological measurements were available). For this purpose, the minutely meteorological time series from the shipboard stations were decimated to a frequency of $(5\ \mathrm{min})^{-1}$. DMS concentrations, MLD, and biological DMS cycling rates (all determined at 4 h frequency) were linearly interpolated to match the same time interval.

To obtain the UML-averaged photolysis rate constants ($k_{photo,UML}$), experimentally determined $k_{photo,incub}$ were normalized to the average shortwave irradiance received during the incubation and then scaled to the UML-averaged scalar irradiance at time t ($E_{o,UML}$; for clarity, time is omitted from the notation):

$$k_{photo,UML} = k_{photo,incub}\frac{E_{o,UML}}{E_{o,incub}} \tag{5.2}$$

$E_{o,UML}$ was calculated as the vertical integral of exponentially decreasing irradiance in the UML (Vallina and Simó, 2007). We assumed that photolysis propagated downwards with the attenuation coefficient of 340 nm (instead of that centered at PAR), because this wavelength has been shown to represent reasonably the spectral peak of DMS photolysis in UV-transparent

surface waters (Toole et al., 2003). Scalar irradiance was calculated from downwelling irradiance ($E_{d,UML}$), corrected by the cosine of underwater radiance (μ) to better take into account the tridimensional light field:

$$E_{o,UML} = \frac{E_{d,UML}}{\mu} \tag{5.3}$$

Our calculations indicated that a value of $\mu = 0.80$ was a good approximation for the wavelengths and the optical characteristics of the waters under study (Bannister, 1992; Morel and Gentili, 2004). In this approach, we assumed that the radiation band causing the majority of DMS photolysis at the water subsurface was linearly related to above-water total shortwave irradiance, which was supported by simultaneous pyranometer and PUV 2500 measurements ($R^2 = 0.96$, data not shown). Assuming a non-linear dependence instead, which is more consistent with current knowledge of atmospheric radiative transfer, did not impact our budgets appreciably.

DMS sea-air flux was calculated as the product of seawater DMS concentrations and the transfer velocity (k_w), after accounting for the temperature-dependent Schmidt number (Saltzman et al., 1993). k_w (m h^{-1}) was parameterized as a linear function of wind speed (U; m s^{-1}), according to Marandino et al. (2009):

$$k_w = 0.46U - 0.24 \tag{5.4}$$

We chose this parameterization based on recent evidence for a linear wind-speed dependence of k_w for wind speeds up to 14 m s^{-1} (Huebert et al., 2010; Marandino et al., 2009). k_w was set to 0 in the few occasions when U was <0.52 m s^{-1}, which would produce negative k_w. In our dataset, 0-3.4% of minutely U were <0.5 m s^{-1}, and 83-98% of the values fell in the 1 – 9 m s^{-1} wind speed range (for which eq. 5.4 was obtained). The surface flux was divided by MLD to obtain average volumetric ventilation rates.

Vertical DMS transport was estimated only in the oceanic experiments, and treated as a constant term in the budgets due to the lack of measurements with adequate spatial-temporal resolution. Turbulent diffusion can be estimated as the product of the vertical DMS gradient and vertical diffusivity (K_z) at the base of the UML. Although the vertical transport term has been generally assumed to make a negligible contribution to UML DMS budgets, it can become sizable when the UML undergoes diel variations, periodically entraining deeper waters with different DMS content (Bailey et al., 2008). In the MEDsum diel cycle, we combined

the only DMS profile available with the output of model simulations (O. Ross, pers. comm.), including depth-resolved vertical diffusivity, to make order-of-magnitude estimates of vertical DMS diffusion. In SARGsum, we used the estimates made by Bailey et al. (2008) for the entire Lagrangian study of the eddy A2, based on model simulations of vertical mixing and the DMS profiles measured every 4 h. In CMEDwin and CMEDsum no vertical DMS profiles were measured, so no estimations were made.

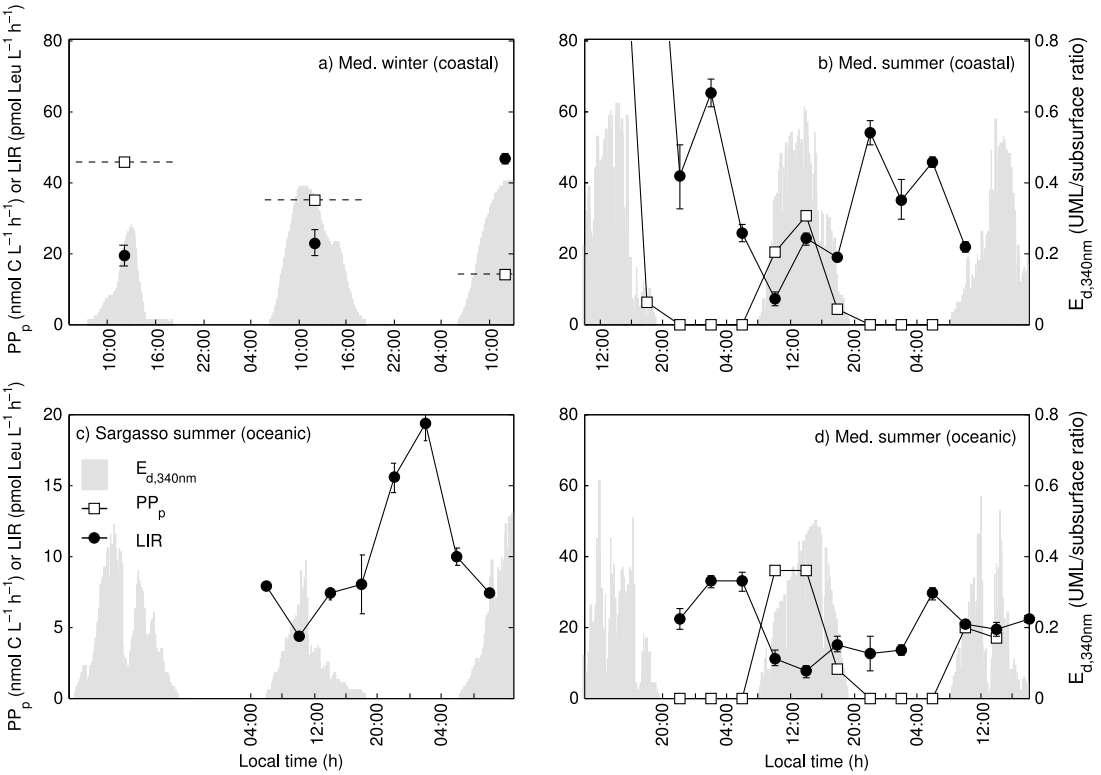

Figure 5.2: **Diel changes in particulate primary production and leucine incorporation rates** - In (A) the estimated mixed-layer average PPp during the daytime is shown. The gray shade represents the ratio of UV radiation (340 nm) averaged within the mixed layer with respect to that at the water subsurface. Error bars correspond to triplicate LIR measurements.

5.3 Results

5.3.1 Oceanographic settings and Lagrangianity of the sampling

The four experiments covered one order of magnitude in phytoplanton biomass (measured as Chl *a*), from the average 0.56 μg L^{-1} in CMEDwin to the 0.11-0.14 μg L^{-1} in the Mediterranean

summer and 0.05 μg L^{-1} in the Sargasso Sea eddy (see ranges in Table 6.2). Algal biomass was dominated by diatoms and prasinophytes in CMEDwin (a rather typical situation at BBMO in late winter, Gutiérrez-Rodríguez et al. (2011)), whereas *Synechoccoccus* and photosynthetic picoeukaryotes, in varying proportions, dominated the summer assemblages (Table 6.2; supplementary information). Bacterial counts decreased in parallel to the trophic status but to a minor extent. Sizable inorganic nutrient pools could be measured only in CMEDwin.

In terms of 'Lagrangianity', the coastal experiments (CMEDwin and CMEDsum) displayed higher hydrographic variability. This was evident in the excursions displayed by the temperature-salinity diagrams during the final 12 h of CMEDwin and the initial 12 h of CMEDsum (supplemenary information). Conversely, the oceanic experiments showed more compact temporal T-S traces. This was expected in SARGsum, which was Lagrangian by design. Yet, we also observed quasi-Lagrangian behavior in MEDsum and in the last 36 h of CMEDsum. The T-S diagrams were used to exclude from further calculations and budgets those measurements that were judged as excessively affected by water mass transitions (the first two time points of CMEDsum).

Contrasting dynamics in the vertical stratification regime were found in winter vs. summer and coastal vs. oceanic experiments (Table 6.2; Fig. 5.1). In CMEDwin we found a quasi-mixed vertical profile (temperature differences $<0.5^{o}$C from top to bottom depths), which sometimes showed a very subtle surface thermal stratification. In CMEDsum mixed layer depths (MLD) reflected a water-mass transition, from a deep water intrusion event (upwelling) initially found to a thicker surface layer of warm water with more oceanic conditions (Fig. 5.1). Both oceanic experiments displayed similar stratification regimes, with a marked seasonal thermocline and a shallower actively mixing layer, which underwent diurnal thermal stratification and nighttime convective overturning.

5.3.2 Autotrophic and heterotrophic activities

Experiment-averaged particulate primary production (PPp) was highest in CMEDwin (0.76 μmol C L^{-1} d^{-1}), with lower values in CMEDsum and MEDsum (around 0.50 μmol C L^{-1} d^{-1}), and lowest values at SARGsum (0.02 μmol C L^{-1} d^{-1}; this rate is suspected to be unrealistically low). Leucine incorporation rates (LIR; a proxy for bacterial heterotrophic production) were highest at the coastal sites (0.71 and 0.81 nmol Leu L^{-1} d^{-1} during CMEDsum and CMEDwin respectively), with lower values during MEDsum and SARGsum (0.48 and 0.24 nmol Leu L^{-1}

d^{-1} respectively). While the diel variation in primary production (PPp) was obviously light-dependent, we found that bacterial heterotrophic activity (LIR) also underwent pronounced diel variations, with a drastic nighttime increase in the three summer experiments (by 9-fold at CMEDsum and 4.5-fold at both MEDsum and SARGsum, Fig. 5.2). The diel pattern of LIR reflected an increase in the activity per cell, because bacterial numbers underwent much smaller variations (data not shown).

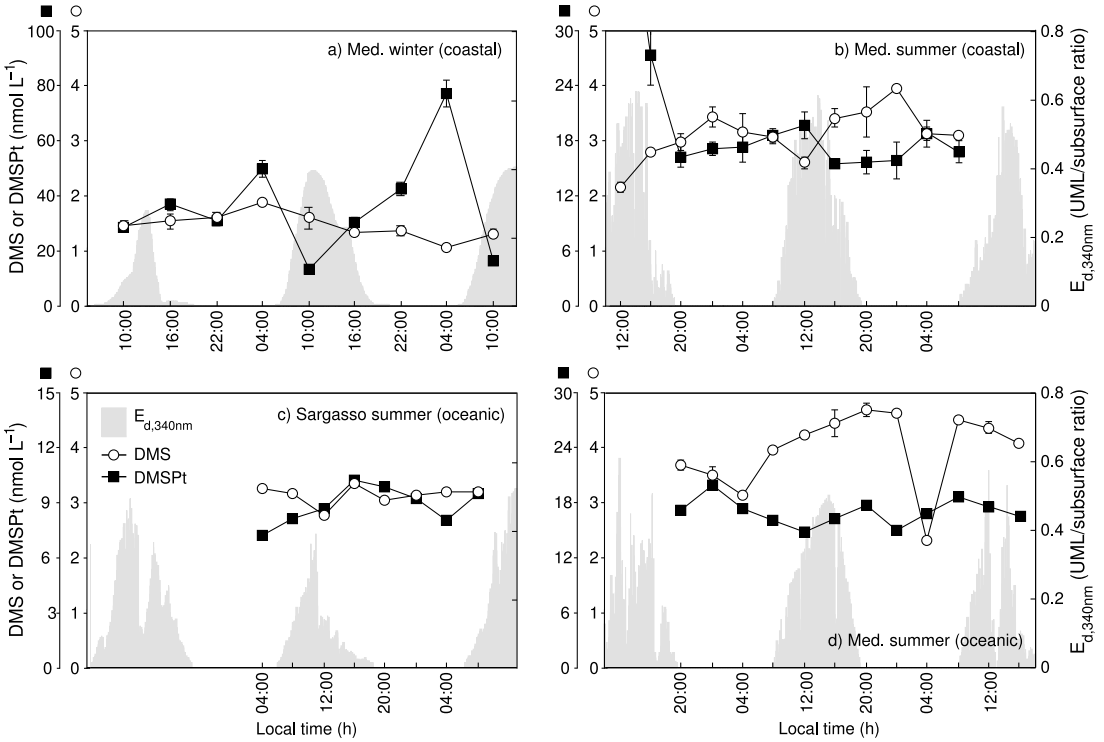

Figure 5.3: **Diel changes in total DMSP (DMSPt) and DMS pools** - The gray shade represents the ratio of UV radiation averaged within the mixed layer with respect to that at the water subsurface. Error bars correspond to duplicate analyses.

5.3.3 DMS and DMSPt pools

Experiment-averaged DMSPt concentrations ranged between a minimum of 8 nmol L^{-1} in SARGsum and a maximum of 36 nmol L^{-1} in CMEDwin, while DMS ranged between 1.5 (CMEDwin) and 4 nmol L^{-1} (MEDsum). Thus, compared to the order-of-magnitude differences in Chl *a* between experiments, DMSPt and especially DMS spanned a narrower range (Table 6.2). DMS and DMSPt pools underwent minor variations during the diel cycles (Fig.

5.3), with a coefficient of variation about the mean (CV) <20%. The exception was the broad variability observed for DMSPt during CMEDwin (CV = 53%), with marked DMSPt peaks at night. Diel DMSPt patterns were less clear in the summer experiments, with a tendency towards net daytime accumulation and nigthtime consumption. Regular diel variations of DMS could only be observed in CMEDsum, with midday troughs and midnight peaks. In MEDsum lowest DMS levels occurred at 04:00 on the two consecutive nights (but see 4.3). In SARGsum a slight surface depletion was observed at solar noon.

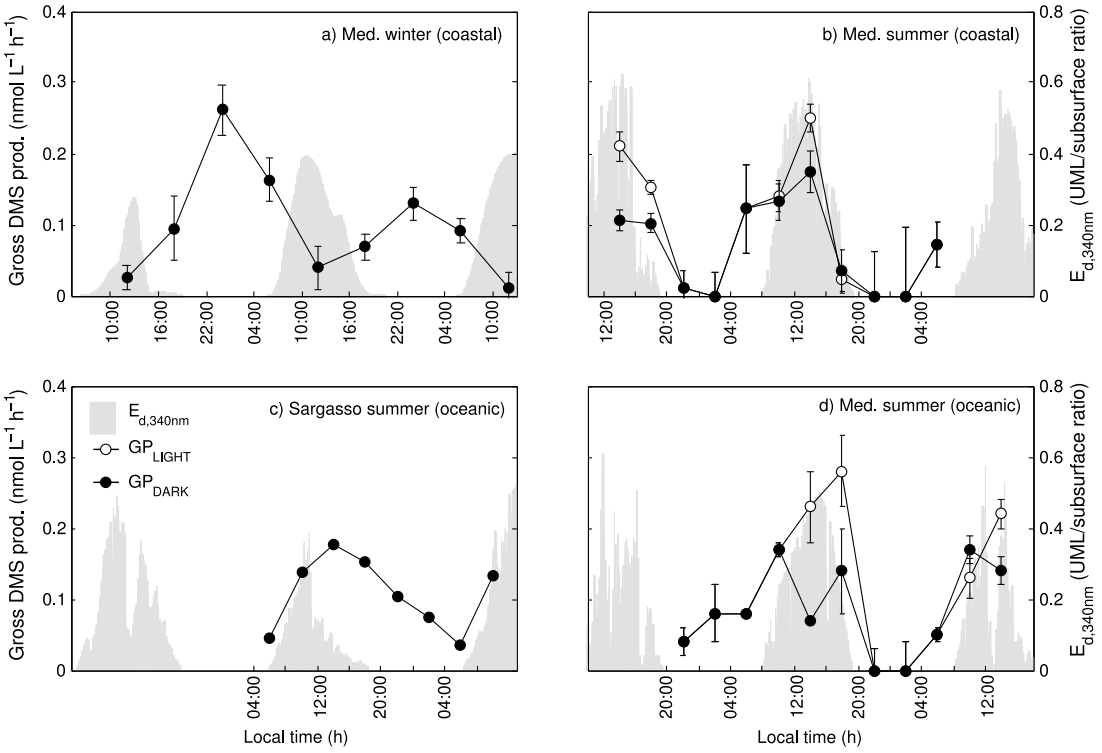

Figure 5.4: **Diel changes in gross DMS production** - Measurements done in the dark and in sunlight are represented with filled and open symbols, respectively (see text). The gray shade represents the ratio of UV radiation averaged within the mixed layer with respect to that at the water subsurface. Error bars correspond to the analytical error of single incubations.

5.3.4 Gross DMS production and community DMSP metabolism

[24] Gross DMS production (GP) displayed broad and regular diel variations in the dark incubations (Fig. 5.4), with opposite patterns found in winter and summer. Nevertheless, the four diel cycles displayed surprisingly similar GP rates, with experiment averages ranging 0.07 – 0.11

nmol L^{-1} h^{-1}. In CMEDwin *GP* peaked at night and was lowest in the morning. Conversely, in the three summer experiments *GP* peaked at solar noon or shortly after, decreased during the night, and started increasing again around dawn. In the sunlit incubations (CMEDsum and MEDsum), *GP* was generally equal or higher (up to three-fold) than in their dark counterparts, with an average stimulation of 52%. Considering the whole 48 h sampling, light-driven stimulation resulted in an average *GP* 30- 36% over the average dark *GP*, a figure that compares well with the range reported in Galí et al. (2011).

CMEDwin displayed the highest average DMSPt consumption rates (2.2 nmol L^{-1} h^{-1}) followed by MEDsum and CMEDsum (ca. 0.7 nmol L^{-1} h^{-1}) and SARGsum (0.3 nmol L^{-1} h^{-1}). DMSPt consumption also underwent day-night variations (Fig. 5.5). These were especially evident in CMEDwin and SARGsum, both displaying nightime peaks and daytime troughs. Conversely, DMSPt consumption was slightly higher during the day in CMEDsum and MEDsum, clearly peaking around noon in CMEDsum. In SARGsum, we had the opportunity to compare our DMSPt consumption estimates to the DMSPd consumption rates (Gabric et al., 2008) obtained by the ^{35}S-DMSP radiotracer method. The average DMSPd consumption in the two samples taken at 04:00 (3 m depth) was 0.16 nmol L^{-1} h^{-1}, and the corresponding DMSPt consumption we obtained in the same samples was 0.5 nmol L^{-1} h^{-1}. This indicates that about one third of the consumed DMSP was cycled through the dissolved pool, a figure that compares well with the average year-round value of ca. 50% found at the BBMO site by Vila-Costa et al. (2008).

The experiment-averaged DMS yields (the quotient of *GP* to DMSPt consumption) were minimum in CMEDwin (5%) and maximum in SARGsum (41%), with intermediate values (around 10%) in CMEDsum and MEDsum. Distinct diel patterns of DMS yield emerged depending on the covariation (or the lack thereof) between *GP* and DMSPt consumption. While no obvious diel patterns were found in CMEDwin, daytime peaks of DMS yield were observed in the three summer experiments, though with variable amplitude. It should be noted that the yields reported here were calculated with DMSPt consumption and *GP* measured in the dark. It is unknown whether solar radiation would have stimulated community DMSPt consumption to the same extent as *GP*, therefore modifying DMS yields.

DMSPd assimilation into macromolecules, as measured with ^{35}S-DMSP additions, represented a minor sink for DMSP, with an average of 4.8 and 2.7% in CMEDsum and MEDsum, respectively, and little diel variability (Fig. 5.5). Thus, assimilation might have been an even smaller sink compared to the totality of DMSPt cycled. DMSP assimilation was dominated by

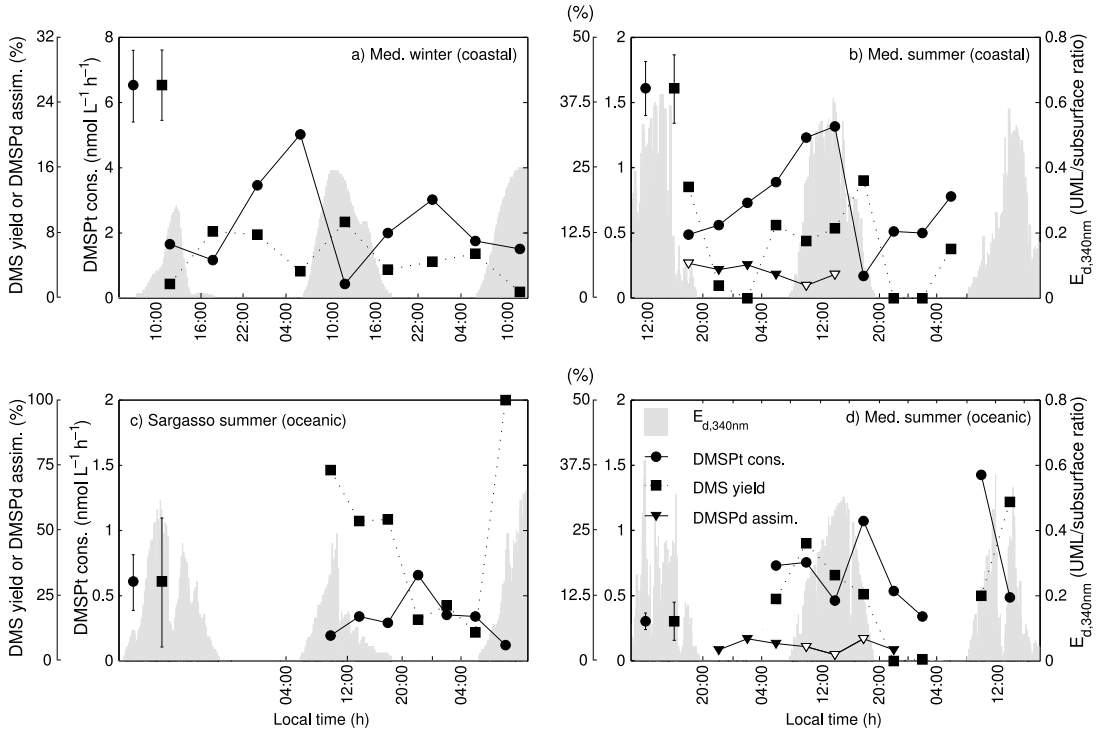

Figure 5.5: **Diel changes in total DMSP consumption, DMS yield and radiolabelled DMSP assimilation** - Measurements done in the dark and in sunlight are represented with filled and open symbols, respectively (see text). For clarity, only average errors (analytical error of single incubations) are shown for each variable and experiment (not available for DMSP assimilation). The gray shade represents the ratio of UV radiation averaged within the mixed layer with respect to that at the water subsurface.

the >0.65 μm organisms or particles (81-97%), probably non DMSP-producing phytoplankton (Vila-Costa et al., 2006b) and attached bacteria.

5.3.5 Bacterial DMS consumption

As found for GP, experiment-averaged dark bacterial DMS consumption (BC) spanned quite a small range (0.06 to 0.09 nmol L^{-1} h^{-1}), but exhibited distinct diel patterns from one experiment to another (Fig. 5.6). Dark BC peaked during the central hours of the day in MEDsum or at dusk in SARGsum, with pre-dawn minima in both experiments. Instead, dark BC showed no clear diel variations in CMEDwin and CMEDsum. In those experiments where BC was simultaneously measured in the dark and in sunlight (CMEDsum and MEDsum), inhibition was generally observed (5 samples), although some incubations showed no light effects (3 samples) or even stimulation (1 sample).

5.3.6 DMS photolysis

In CMEDsum, MEDsum and SARGsum, where the subsurface photolysis rate constants were determined experimentally, $k_{photo,max}$ were 0.049, 0.040, and 0.025 h^{-1}, respectively (SARGsum value taken from Gabric et al. (2008)). In CMEDwin, a value of 0.13 h^{-1} was used, with an associated uncertainty of about ± 50%. The daytime averages of DMS photolysis in the UML (that is, after accounting for underwater radiation fields, in situ DMS concentrations and mixing depths) were 0.044, 0.041, 0.047 and 0.008 nmol L^{-1} h^{-1} in CMEDwin, CMEDsum, MEDsum and SARGsum, respectively. The value obtained for SARGsum (0.10 nmol L^{-1} d^{-1}) is consistent with that obtained by *Bailey2008* (0.20 nmol L^{-1} d^{-1}), since the former corresponds to an overcast day and the latter to the less cloudy conditions that prevailed during the anticyclonic eddy sampling.

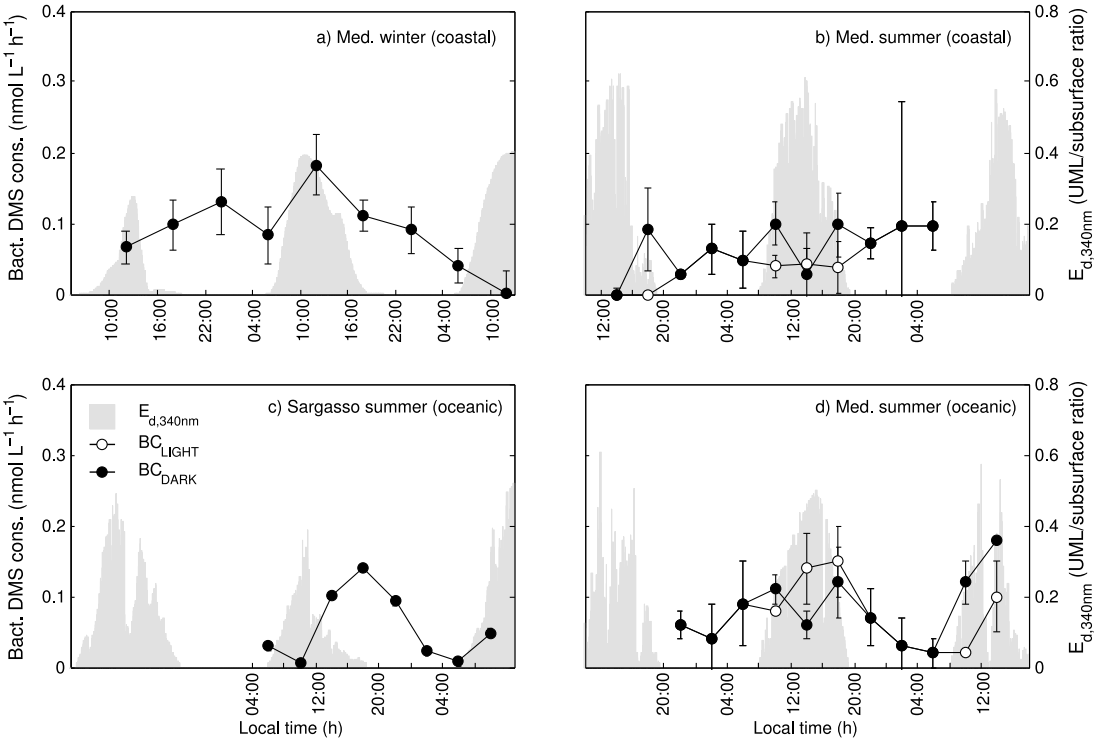

Figure 5.6: **Diel changes in microbial DMS consumption** - Measurements done in the dark and in sunlight are represented with filled and open symbols, respectively (see text). The gray shade represents the ratio of UV radiation averaged within the mixed layer with respect to that at the water subsurface. Error bars correspond to the propagated analytical error of non-amended and dimethyldisulfide-amended single bottle incubations.

5.3.7 DMS ventilation

Average sea-air transfer velocities (k_w) were 1.3, 15.2, 6.8 and 5.3 cm h^{-1} in CMEDwin, CMEDsum, MEDsum and SARGsum, respectively. These values correspond to sea-air fluxes raging from 0.02 μmol m^{-2} h^{-1} in CMEDwin to 0.47 μmol m^{-2} h^{-1} in SARGsum (0.5 – 11.3 μmol m^{-2} d^{-1}). Converted to volumetric fluxes in the UML, these figures become 0.002, 0.025, 0.038 and 0.020 nmol L^{-1} h^{-1} in CMEDwin, CMEDsum, MEDsum and SARGsum, respectively. The use of the Marandino et al. (2009), Huebert et al. (2010) or Nightingale et al. (2000) k_w vs. wind speed relationships had a relatively small impact on DMS fluxes. In SARGsum, our flux estimate (parameterized according to Marandino et al. (2009)) was in good agreement (14% difference) with the estimates based on eddy covariance measurements reported by Bailey et al. (2008).

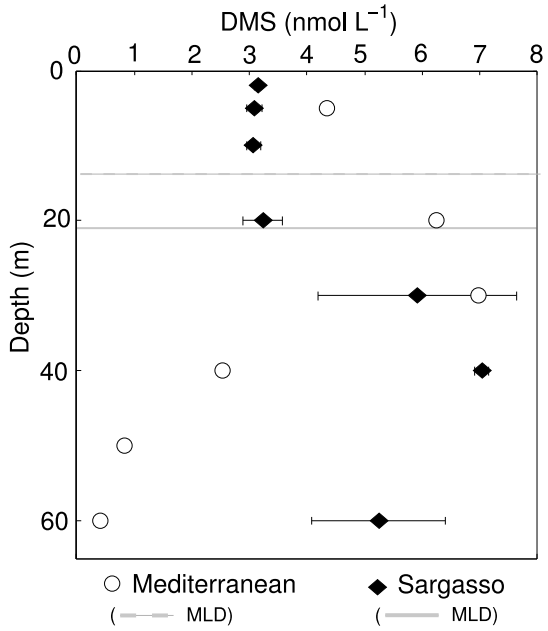

Figure 5.7: **Vertical DMS profiles in the Mediterranean and Sargasso Sea oceanic experiments** - Horizontal lines represent the average mixed layer depth at the time the profiles were measured. Error bars in the Sargasso Sea profile represent the range of two profiles measured at 04:00 local time.

5.3.8 Vertical DMS flux

Vertical DMS profiles were measured at the two oceanic stations, both showing a peak in the thermocline (30 – 40 m) of ca. 7 nmol L^{-1} (Fig. 5.7). In MEDsum, DMS concentrations

became hardly detectable below 65 m, the depth of the deep chlorophyll maximum. A similar but less vertically-compressed profile was observed in the Sargasso Sea eddy, with <1 nmol L^{-1} concentrations below 100 m depth (deep chlorophyll maximum around 150 m). These profiles resulted in a DMS gradient at the base of the UML of about 0.30 (SARGsum) or 0.50 μmol m^{-4} (MEDsum). Combining this gradient with vertical diffusivities of the order 10^{-5} to 10^{-4} m^2 s^{-1} (estimated to be similar at both sites) yielded an upwards DMS flux of 0.08 $\pm$ 0.06 and 0.12 $\pm$ 0.08 nmol L^{-1} d^{-1} in SARGsum and MEDsum, respectively. These figures (note the d^{-1} units) are negligible compared to the other budget terms. Nevertheless, Bailey et al. (2008) found that accounting for the entrainment of DMS due to diurnal stratification/mixing cycles increased the upwards flux to 0.34 $\pm$ 0.06 nmol L^{-1} d^{-1}. Entrainment might have been of similar magnitude in MEDsum, because it showed mixing dynamics and vertical DMS distribution similar to SARGsum.

5.4 Discussion

The four ocean settings represented a considerable biogeochemical gradient, clearly reflected in the dimethylated sulfur pools and their microbial cycling (Table 6.2). Combined with the diel sampling scheme, this provided an extraordinary testbed for hypotheses regarding the biotic/abiotic regulation of DMS cycling.

5.4.1 Factors controlling gross DMS production and the fate of DMSP

Microbial DMSP cycling occurs through a tangled network of microbial interactions (Simó, 2004; Stefels et al., 2007) and follows diverse biochemical pathways (Curson et al., 2011; Moran et al., 2012). We took an integrative approach where all the DMSP cycling pathways eventually releasing DMS were encompassed (Simó et al., 2000). This has the advantage of better constraining gross DMS production for budgeting and modeling exercises, and the drawback that the contribution of each single production process can only be guessed from indirect evidence. In our approach, gross DMS production can be modulated by changing either DMSPt consumption, DMS yields, or both. Noteworthy, we found a similar pattern of diel GP modulation in the three summer experiments, which contrasted with the winter experiment, hinting at the existence of distinct DMS production regimes at the diel scale. The dayt to night differences in GP rates were significant in all 4 experiments (Kruskal-Wallis p <0.03). In CMEDsum, MEDsum, and SARGsum, GP was driven by DMS yields (Table 6.3) rather than by DMSPt consumption

Table 5.3: Day night differences in DMS yield (%) from consumed DMSPt.

Experiment	CMEDwin	CMEDsum	MEDsum	SARGsum
Overall mean (range)	4.8 (0.7 – 9.3)	9.3 (0 – 22.5)	13.2 (0 – 30.2)	46.7 (10.4 – 100)
Daytime average ± sd (n)	4.6 ± 1.7 (*5*)	17.0 ± 5.8 (*4*)	18.8 ± 7.6 (*5*)	69.9 ± 22.0 (*4*)
Nighttime average ± sd (n)	5.1 ± 0.9 (*4*)	4.2 ± 7.5 (*6*)	4.0 ± 6.6 (*3*)	15.8 ± 5.3 (*3*)
Day:night factor	0.9	4.0	4.8	4.4
p (Kruskal-Wallis test)	0.81	**0.03**	**0.01**	**0.03**

(Fig. 5.8). This was most evident in SARGsum, where the lower DMSPt consumption during the day was more than compensated by a sharp increase of the DMS yield (reaching 73-100%). In the case of CMEDsum and MEDsum, the concerted increase during the day of both DMS yield (by a 4 to 4.8 factor) and DMSPt consumption (by a 1.2 to 1.6 factor) contributed to rise GP. In CMEDwin, conversely, the nighttime increase in DMSPt consumption, combined with low yields over the diel cycle, translated into nighttime GP peaks (Table 6.3, Fig. 5.8).

The summertime GP diel pattern could result from different scenarios. Among them, DMS release by radiation-stressed phytoplankton appears to be the most feasible. In this scenario, DMS production enzymes would have been up- regulated during the day by phytoplankton cells undergoing oxidative stress (Sunda et al., 2002) or requiring an overflow mechanism for excess reducing power (Stefels, 2000). Nutrient starvation could have acted synergistically with light exposure to enhance DMS production (Sunda et al., 2007). While a few studies have reported on daytime increases of the DMS(P) pools linked to algal physiology in natural assemblages (Belviso, 2000; Sunda et al., 2005; Yang et al., 2008), to our knowledge only one study has reported a daytime increase of GP (Merzouk et al., 2004), which was attributed to dinoflagellate vertical migration in an estuarine area. Since we did not detect dinoflagellate migration (supplementary information), our study would be the first to show a clear link between light exposure dynamics and gross DMS production rates at physiologically meaningful time scales in a natural microbial community. This provides clear field evidence for both the antioxidant and overflow hypotheses, which have hitherto been largely based on culture studies (e.g., Archer et al. (2010b)).

Supporting the algal stress hypothesis, we observed that bulk chlorophyll fluorescence was clearly depleted in surface waters during the hours of strongest irradiance in the oceanic experiments (Fig. 5.1), indicating reduced photosynthetic competency and/or dissipation of excess irradiance through photoprotective mechanisms (Sakshaug et al., 1997). Moreover, in MEDsum we observed higher GP in sunlit incubations during a high-irradiance day, when UV stress was

further enhanced by diurnal stratification, than in the following day, with lower irradiance and deeper mixing due to the passage of a storm (Fig. 1 and 4). This seemed to result from harsher light exposure, particularly higher proportions of shortwave UV (i.e., higher UVB:UVA ratios), both prior to sampling and during the incubations. In CMEDsum and MEDsum, both dark and light GP were significantly correlated to primary production (Spearman rank correlation; p <0.05), linking DMS production with photosynthesis physiology. In SARGsum, conversely, the best predictor of dark GP was the UV dose in the UML during the 4 h prior to sampling (p <0.01; see supplementary information), pointing at cumulative UV stress as the driver.

Besides direct algal DMS production from the particulate pool, other sources of DMS include DMSP release by phytoplankton and its transformation by bacterial enzymes or by dissolved algal enzymes (note that in some algal strains physical disruption is required to put in contact DMSP and its cleavage enzymes (Wolfe and Steinke, 1996; Evans et al., 2007). Again, DMSP release can occur through various pathways: active DMSP exudation (Stefels, 2000) or cell disruption by grazing, viral lysis or UV-triggered cell death (Veldhuis et al., 2001; Bidle and Falkowski, 2004). In our view, the latter process is more likely to explain the observed pattern in UV-transparent waters in summer. Although we cannot rule out some contribution of light-enhanced grazing (Jakobsen and Strom, 2004) or even viral lysis, the relationship between the latter two processes and solar radiation is ambiguous (Ochs, 1997; Jacquet and Bratbak, 2003). On the other hand, microzooplankton grazing appears to be the most plausible explanation for the nighttime increase of GP found in CMEDwin. Recently, Ruiz-González et al. (2012e) reported higher ingestion rates of picoeukaryotes by heterotrophic nanoflagellates during the night (causing stimulation of bacterial activity) in a study done at the same site (BBMO) and in similar conditions as the CMEDwin experiment.

DMS production from released DMSP could have been further enhanced during the day if the bacterial yield was light-dependent. Recently, Valle et al. (2012) found evidence of PAR-stimulated bacterial DMSPd consumption and bacterial DMS yields, associated to PAR-decreased DMSP assimilation. The assimilation measurements we performed in CMEDsum and MEDsum are in keeping with this observation. Although total assimilation showed little diel variability (Fig. 5.5), assimilation by the <0.65 μm size fraction (free-living bacteria) was lower during the day, clearly paralleling leucine uptake in MEDsum (Spearman's $r = 0.75$; p <0.10). This could indicate a lower assimilation yield resulting from lower carbon demand (hence sulfur) during the day. All in all, the mechanism proposed by Valle et al. (2012) is unlikely to supply all the excess GP observed in our study, due to UV inhibition of bacterial

DMSPd consumption (Slezak et al., 2007). Also, note that bacterial DMS yields from DMSPd rarely exceed 15% (Kiene and Linn, 2000; Lizotte et al., 2012), whereas yields from DMSPt can reach values >90% (Simó and Pedrós-Alió, 1999a; Simó et al., 2000, this study).

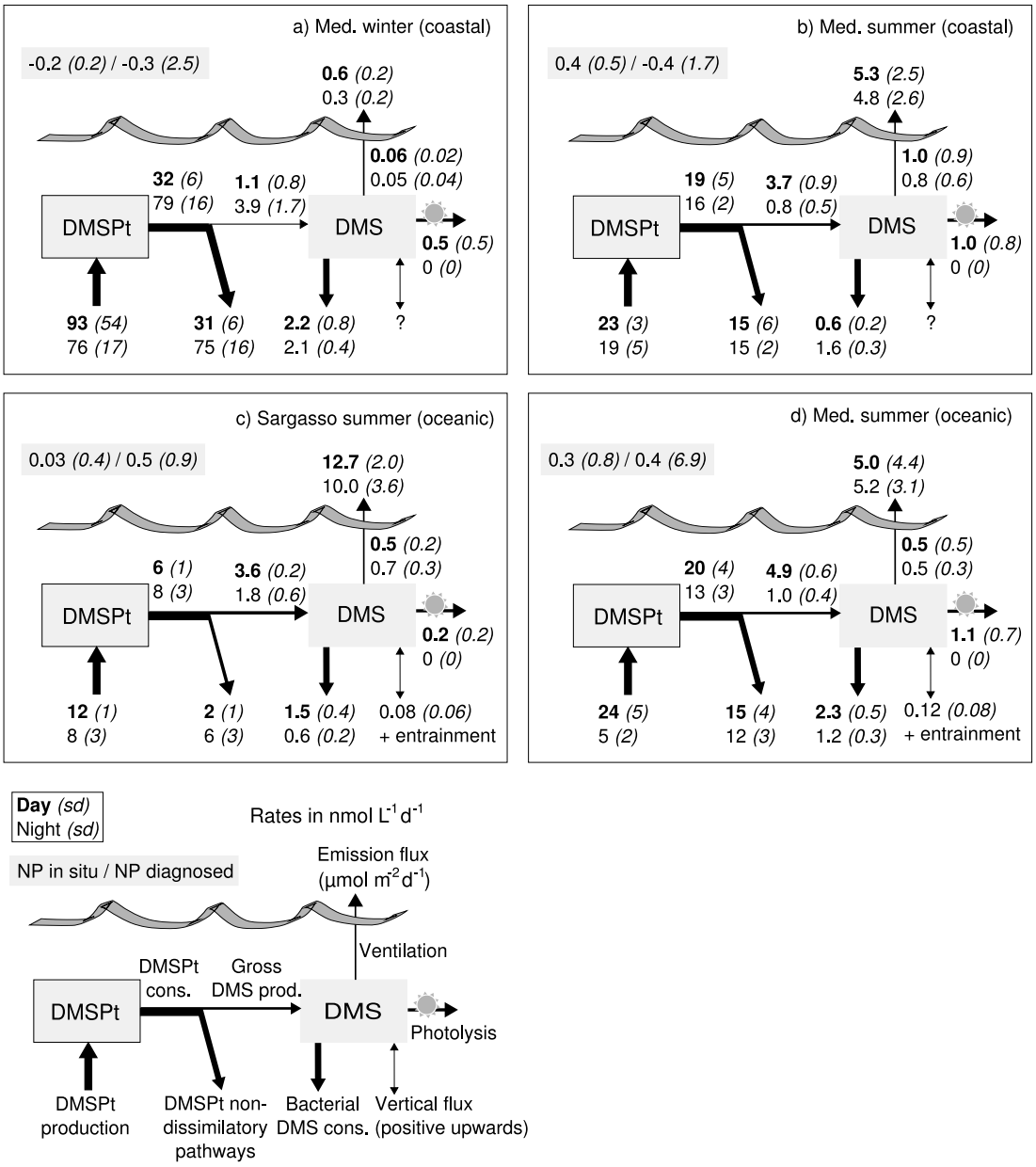

Figure 5.8: **Day versus night budgets of DMS cycling in the upper mixed layer** - Values in parentheses are the standard deviation (sd) of biological process incubations ($3 < n < 6$) or that of 5-minute resolution budgets in the case of abiotic DMS sinks (DMS photolysis and ventilation). Order-of-magnitude estimates of vertical DMS transport are also given, with no day-night distinction.

Last, but not least, we can consider the role of circadian rhythms. The diel gene expression patterns of several microbial plankton are regulated by molecular clocks (Hastings, 1961; Mackey and Golden, 2007; Corellou et al., 2009), which help cells anticipate environmental variability and adequately phase sensitive processes like cell division (Vaulot and Marie, 1999). Consistently, a recent metatranscriptomics study (Poretsky et al., 2009) identified a switching between housekeeping genes at night and photophysiology-related genes during the day. DMS(P) metabolism might be regulated in such a manner if it effectively prevented radiative stress. In CMEDsum and MEDsum GP rose significantly already in the pre-dawn sample (04:00), or in the 08:00 sample, when surface waters had barely seen any radiation, indicating a possible role of circadian rhythms. However, it is intriguing why phytoplankton should start releasing DMS instead of accumulating intracellular DMSP before radiative stress set in. Another explanation is that different processes were causing the pre-dawn rise in GP and the afternoon GP peak.

5.4.2 Factors controlling bacterial DMS consumption

According to current knowledge, UV inhibition should tend to decrease BC during the day. However, this effect should show up with different intensity depending on (1) whether the samples are incubated in the dark or in sunlight and (2) the length of the incubation compared to the recovery time. In CMEDsum, the relief from UV inhibition elicited some recovery of BC in the 16:00 samples incubated in the dark, whereas the same samples incubated in full sunlight remained inhibited. The 08:00 sample incubated in the light showed also inhibition, and the 12:00 samples, which came from rather high UV waters and suffered the harshest exposure, showed equally low BC rates in both dark and light incubations (perhaps indicating no recovery). In MEDsum, relative dark-light inhibition was observed during day 2, whereas on day 1 we observed no significant inhibition or even stimulation in the 12:00 sample. The relative dark-light inhibition we observed should be viewed with some caution since the inhibitor method is less precise than the ^{35}S-DMS tracer method for determining BC.

Perhaps more relevant than the inhibition response described above is the observation of regularly higher BC around noon or dusk in the oceanic experiments, with the more extreme variation found in the most oligotrophic system (SARGsum). Although counter-intuitive, this pattern can be explained within the framework of bacterioplankton-phytoplankton coupling combined with recent studies of bacterial DMS metabolism. It has been postulated that in oceanic environments, far from coastal carbon sources, pelagic bacteria rely on the labile carbon

excreted by phytoplankton. The tighter coupling between primary producers and heterotrophs would render stronger diel fluctuations of bacterial heterotrophic production (Fuhrmanl et al., 1985; Gasol et al., 1998), as we observed in CMEDsum, MEDsum and SARGsum (Fig. 5.2). Recent studies have shown that there are few bacterial taxa able to grow on DMS as the sole carbon source (Vila-Costa et al., 2006a). Instead, a broader diversity of bacteria can oxidize DMS to DMSO to obtain energy, provided they have an alternative C source (Vila-Costa et al., 2006a; Green et al., 2011; Hatton et al., 2012). Remarkably, a study by del Valle et al. (2007) indicated that DMS to DMSO oxidation prevailed in the sunlit UML in the Sargasso Sea. This observation can be interpreted as DMS oxidation rates being carbon-limited, therefore peaking at the optimum of labile carbon supply -UV inhibition permitting.

5.4.3 Short-term microbial/meteorological variability and DMS budgets

Biological and abiotic DMS cycling rates indicated that DMS removal was dominated by bacterial DMS consumption in all four experiments (44-78% on a daily basis), in line with previous reports (see compilation in Simó (2004)). Nevertheless, the average budgets enclosed a rich short-term variability, and each consumption term became dominant during short periods, as shown in Fig. 5.9. Notably, DMS concentration rarely underwent sudden fluctuations, because the excess daytime gross DMS production was compensated by photolysis and, more unexpectedly, bacterial consumption. Thus, the resulting net DMS turnover rates, both observed and diagnosed (Fig. 5.8), were always far smaller than the gross DMS turnover rates. At this point it has to be acknowledged that biological DMS cycling processes, if light-dependent, should have been also depth-dependent as well. However, the assumption of an homogeneous upper mixed layer, both in terms of microbial activity and DMS pools (Fig. 5.7), seemed to produce reasonable budgets (Fig. 5.8).

The diel variability of vertical DMS transport remains unresolved in our study. There are indications that its contribution could be higher than generally assumed when day-night cycles of stratification-convection combine with a sub-pycnocline DMS peak (Bailey et al., 2008). Yet, the close correspondence we found between in situ and budget-derived net DMS production (Fig. 5.8), without any need to invoke vertical transport, indicates the contrary. Indirect evidence of DMS entrainment from deeper layers could be deduced if a positive correlation existed between MLD and DMS concentration. Such correlation was found to be significant only in CMEDsum (Spearman $r = 0.64$, $p < 0.05$). However, the increasing trend of DMS

(0.4 nmol L^{-1} d^{-1}, or 13% d^{-1}) was small compared to its diel amplitude ($\pm$ 0.6 nmol L^{-1}), and possibly associated to the transition from upwelling to oceanic conditions (supplemenary information). In MEDsum, lowest DMS levels were measured at 04:00 on two consecutive nights. The minimum was especially marked during the second night (2.3 nmol L^{-1}), concurrent with a convective mixing event. Still, the sudden drop in DMS concentration could be explained only if the underlying waters had had inconceivably low DMS levels. This low concentration could neither be explained by instrumental misfunctioning, measured cycling processes, or water-mass Lagrangianity considerations.

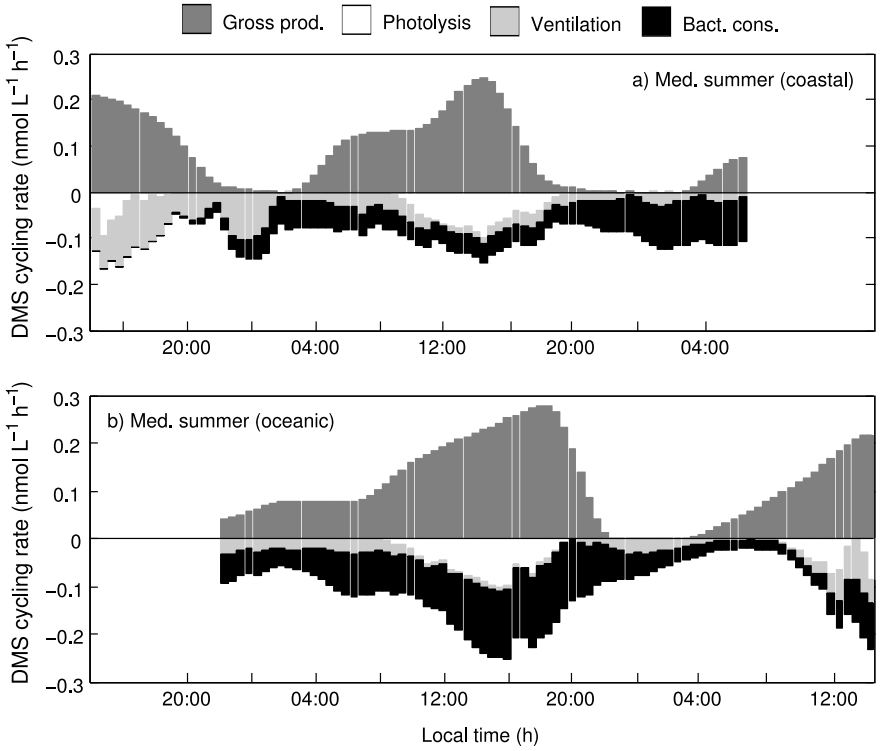

Figure 5.9: **Idealized DMS budgets in the upper mixed layer at 30 min. resolution in the Mediterranean summer experiments** - The budgets reflect the combined impact of meteorological variability and biological responses. These budgets were calculated assuming that vertical DMS transport was negligible.

Diel variability has also consequences for diagnostic modeling of gross DMS production. In this approach, GP is estimated by budgeting simultaneous measurements of net in situ DMS evolution and biotic and abiotic DMS sinks during a Lagrangian sampling scheme. The anticyclonic eddy A2 was object of one such studies (Bailey et al., 2008), which diagnosed an average GP of 0.68 $\pm$ 0.09 nmol L^{-1} d^{-1} in the upper 20 m (roughly, the UML). This

figure is 3 to 4 times lower than the average 2.6 ± 1.3 nmol L^{-1} d^{-1} (n = 8) of our diel cycle SARGsum (performed during the last day of the 6-day Lagrangian period), where *GP* was directly measured with the inhibitor method. In the Lagrangian study, bacterial DMS consumption was measured, with the ^{35}S-DMS method, with daily frequency in 3 m depth samples from the 04:00 CTD casts (pre-dawn). The rate constants measured at that time of the day (and used by Bailey et al. (2008)) were 0.13 ± 0.08 d^{-1}, comparing relatively well with the 0.24 ± 0.10 d^{-1} that we obtained with the DMDS inhibition method in the corresponding pre-dawn samples. Thus, microbial DMS consumption rates determined at too low frequency could have caused the underestimation of diagnosed *GP* by Bailey et al. (2008).

5.4.4 Insights into dimethylated sulfur cycling regimes

DMSPt:Chl *a* ratios are a good indicator of how shifted are planktonic communities to dimethylated sulfur processing (Stefels et al., 2007; Simó et al., 2009). In the wide trophic states included in our work, DMSPt:Chl *a* varied by 6-fold, from 33 nmol μg^{-1} (CMEDwin) to 180 nmol μg^{-1} (SARGsum). Likewise, average community DMS yields (i.e., the % of DMSPt consumed resulting in DMS production) ranged between 5 and 47%. Experiment-averaged DMS:DMSPt ratios, which can be regarded as an 'ecosystem DMS yield' resulting from both biotic and abiotic factors, spanned a similar range (0.05 to 0.40), suggesting they are a good proxy for process-based DMS yields. In parallel, both DMSP and DMS specific turnover slowed down as we progressed towards more oligotrophic (and DMS rich) environments. A recent study suggested that the GP:DMSPt ratio could be a useful shortcut to predict gross DMS production (Herrmann et al., 2012), arguing that it is relatively invariant across ecosystems with a value about 0.06 ± 0.01 d^{-1}. Our results suggest that this index, conceptually close to the DMS yield, is far from constant, since we have observed GP:DMSPt ratios (mean ± sd) as variable as 0.07 ± 0.06 d^{-1} (CMEDwin), 0.10 ± 0.10 d^{-1} (CMEDsum), 0.15 ± 0.15 d^{-1} (MEDsum) and 0.29 ± 0.14 d^{-1} (SARGsum). The GP:DMSPt index deserves further exploration, but the emphasis should be placed at understanding its variability.

Toole and Siegel (2004) proposed a classification of DMS cycling regimes, distinguishing between a bloom regime typical of high latitudes, where DMS correlates to phytoplankton biomass, and a stress regime typical of low latitudes, where DMS is negatively correlated to phytoplankton biomass (the 'summer paradox' areas of Simó and Pedrós-Alió (1999a)). Altogether, the picture drawn by the four diel cycle experiments provides an explanation for the decoupling between DMS and plankton biomass (Lizotte et al., 2012), a feature that remains

difficult to represent in prognostic DMS models (Le Clainche et al., 2010). For a given amount of DMSP consumed, if the DMS yield increases proportionally more than the DMS consumption rate constants, DMS will reach a steady state at higher concentrations. The fact that DMS consumption rate constants rather seemed to decrease with increasing oligotrophy would tend to accentuate this pattern.

In our view, oceanic DMS cycling could be divided into high- and low-DMS-yield situations, both of which can potentially occur in environments with high or low biomass and/or DMSPt. In low oxidative stress situations (nighttime, winter mixing) bacterial DMS production may prevail, with low associated yields. In high stress situations, direct DMS exudation from the particulate pool seems to dominate DMS production, and much higher DMS yields can be attained. During the last years much research has focused on understanding the so-called bacterial switch (Simó, 2001; Moran et al., 2012), by which bacteria divert a lower or higher amount of consumed DMSP to the DMS production pathway(s). Now there is compelling evidence that an important share of gross DMS production originates from particulate DMSP cycling, and that radiative forcing is required to reproduce this feature in mechanistic models (Toole et al., 2008; Vallina et al., 2008; Vogt et al., 2010). Therefore, ecosystem-level studies should evaluate total DMSP turnover, ideally, simultaneously with DMSPd turnover (Vila-Costa et al., 2008). Understanding the distinct modes of operation of the oceanic DMS cycle will require disentangling their intricate relationship with microzooplankton grazing, viral lysis, phytoplankton cell death, and even the relative importance of attached vs. free-living bacteria, all of this in the context of plankton photophysiology.

Acknowledgements

We thank the crews and scientists who made possible the Biocomplexity and Modivus (Sargasso and Mediterranean Sea) cruises on board the R/V Seward Johnson and R/V Garcia del Cid, respectively, as well as the Blanes Bay Microbial Observatory sampling team. Irene Forn provided invaluable help in the Sargasso Sea cruise. We also thank Oliver Ross for providing physical model simulations, and Jaume Piera for thoughtful comments. M.G. acknowledges the receipt of a CSIC JAE scholarship. This work was supported by the (former) Spanish Ministry of Science and Innovation through the projects 'Organic Matter sources, microbial DIVersity, and coastal marine pelagic ecosystem functioning (respiration and carbon USe)' (MODIVUS; CTM2005-04795/MAR) and 'SUrface Mixing Modulation of the Exposure to solar Radiation'

(SUMMER; CTM2008-03309/MAR), and by the NSF Biocomplexity funding program through OPP-0083078. This is a contribution of the Research Group on Marine Biogeochemistry and Global Change and the Research Group on Aquatic Microbial Food Webs, supported by the Generalitat de Catalunya.

5.5 Supplementary information

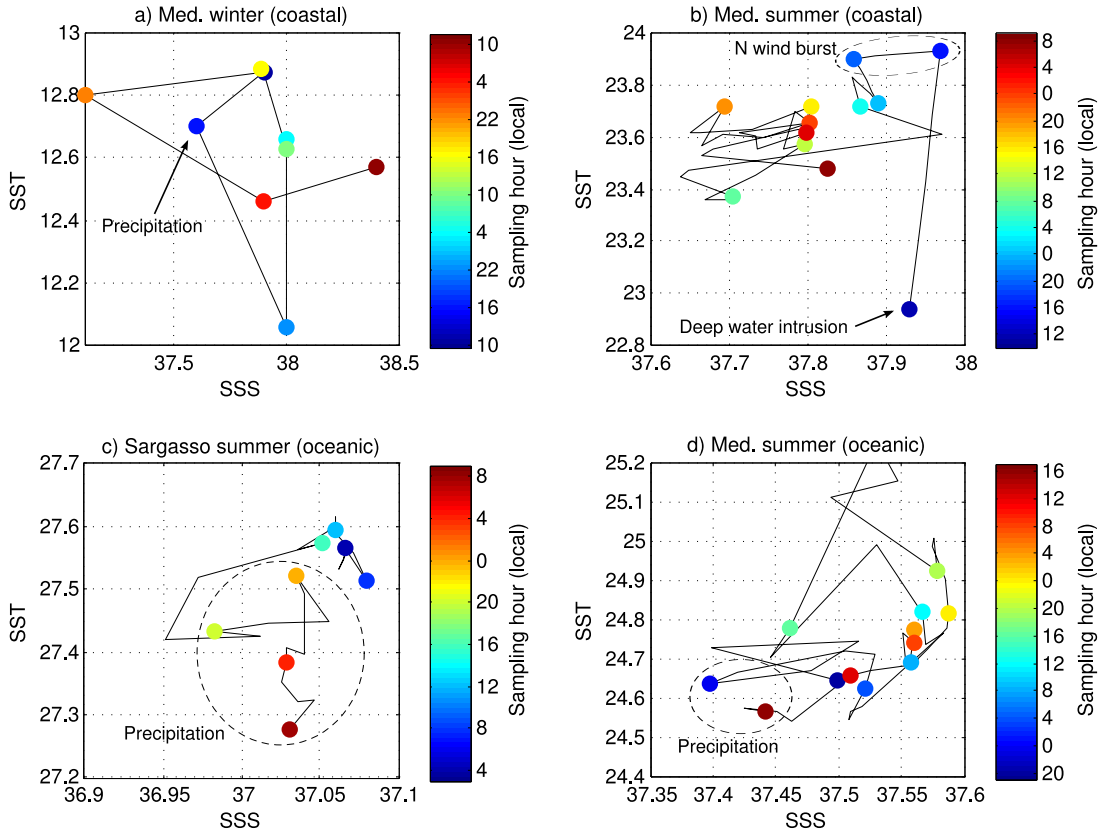

Figure 5.10: **Analysis of sampling Lagrangianity by means of temperature-salinity (TS) diagrams (SI)** - The sampling points are superimposed on the TS temporal traces, with the color code indicating sampling time. Precipitation events causing a freshening of surface waters are shown (A, C and D), as well as the deep water intrusion followed by a N wind burst that occurred at the beginning of CMEDsum (B).

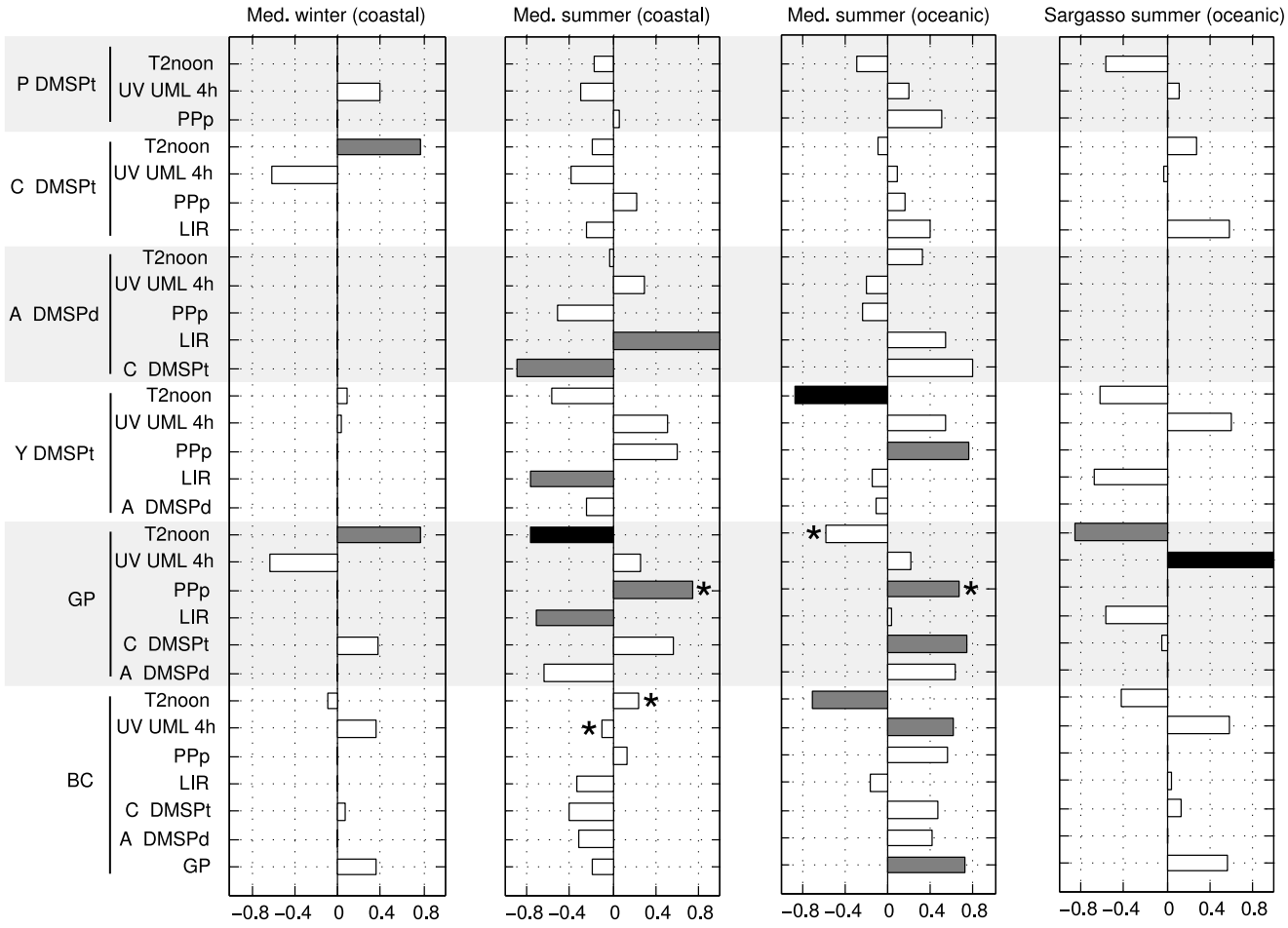

Figure 5.11: **Cross-correlations (non-parametric Spearman rank correlation) between biological sulfur cycling rates and other microbial activities (SI)** - Black bars: $p < 0.01$ (correlation significant at the 99% confidence level); gray bars: $p < 0.05$; white bars: $p > 0.05$. DMSPt production showed overall week correlations, so it was not included as a predictor variable.

Table 5.4: Composition of the phytoplankton communities. [a]Biomass estimates indicated that diatoms dominated in this samples (Gutiérrez-Rodríguez et al., 2011).

Experiment	CMEDwin	CMEDsum	MEDsum	SARGsum
Prochlorococcus (10^5 cells L^{-1})	130	180	170	
Synechococcus (10^5 cells L^{-1})	14.7	540	240	27
Picoeukaryotes (10^5 cells L^{-1})	74	13	5.4	3.8
Nanoeukaryotes (10^5 cells L^{-1})	9.4	3.6	1.3	1.4
Dinofalegellates (10^2 cells L^{-1})	[a]	15	51	
Diatoms (10^2 cells L^{-1})	[a]	22	3.4	

Table 5.5: Day vs. night comparison of dinoflagellates abundance. Means, standard errors and number of samples where dinoflagellates were counted. Day samples are those taken at 08:00, 12:00 and 16:00 (local time), and dark samples at 20:00, 00:00 and 04:00.

Experiment	CMEDsum	MEDsum
Day mean ± se (n)	1520 ± 490 (*3*)	5200 ± 810 (*6*)
Night mean ± se (n)	1470 ± 270 (*2*)	4960 ± 770 (*6*)

Chapter 6

General discussion: A meta-analysis of oceanic DMS cycling

6.1 Overview and rationale

The results presented and discussed in the preceding chapters allowed us to better comprehend the effect of solar radiation on gross DMS production and oceanic DMS budgets. However, these results may be better understood if they are properly placed among the existing DMS literature. Since the CLAW hypothesis was postulated (25 years ago), the picture of oceanic DMS(P) cycling has become increasingly complex. If we are to succeed at modeling its present, past and future behavior we will need to (1) identify a reduced number of measurable variables that describe DMS(P) cycling, and (2) establish which of these variables will be more critically shaping the DMS(P) cycle in different oceanic biomes. The performance of prognostic DMS(P) cycling models may be optimized if their outputs are constrained by well-defined emergent properties and easy-to-measure index variables. In response to these needs, we started assembling a comprehensive database of previously published studies, centered on upper ocean DMS(P) budgets, which allowed us to conduct a meta-analysis. A *Plankton Functional Types* (PFTs; Le Quéré et al. (2005); Boyd et al. (2010)) approach was taken in order to define characteristic modes of operation of the DMS(P) cycle. We also collected ancillary data (when available) in order to re-assess the relationships between upper ocean physics, the biogeochemical cycles of dimethylated sulfur, carbon, and nutrients, and the microbial processes that drive them.

6.2 Constructing a literature data compilation on oceanic DMS cycling

A database was created by extracting gross DMS production rates (generally coupled to bacterial DMS consumption rates) from 26 studies (see SI). Data from another > 30 papers were also utilized, either to complement DMS(P) cycling rates or because they contained ancillary variables. Thus, what was initially designed as a database centered on gross DMS production (GP) soon turned into a DMS(P) cycling database, encompassing DMSP production, DMSP consumption and the fate of consumed DMSP, and the biotic and abiotic sinks of DMS. When we could not access the primary data, we extracted the information contained in tables and digitized the figures using the open source application G3Data Graph Analyzer. Since the upper mixed layer (UML) is the depth horizon that regulates ocean-atmosphere exchange, the analysis focused only on UML samples, although measurements from below the UML were also included. Only data from natural planktonic communities, plus one iron fertilization experiment, were included. Occasionally, we also made some use of microcosm studies.

GP rates included in the database fell onto two main categories: directly and indirectly determined. Directly determined *GP* rates were defined as those obtained with the inhibitor technique (see section 6.7.1). Indirectly determined *GP* rates were defined as those estimated by budgeting. Given the DMS budget equation

$$\frac{[DMS]}{dt} = GP - BC - Photolysis - Ventilation + Transport \tag{6.1}$$

GP can be estimated if the other budget terms are known. Since the transport term is generally one order of magnitude smaller than the other terms (Gabric, 2001), it can be omitted. The equation can be further simplified by assuming that the net DMS change is zero: $\frac{d[DMS]}{dt} = 0$. Such assumption is generally valid, i.e., introduces an acceptable and unbiased error (as will be shown in section 6.4). This leaves us with a simplified budget equation:

$$GP = BC + Photolysis + Ventilation \tag{6.2}$$

Each entry of the database contained the following groups of variables:

- Sample metadata: date (day of the year), latitude, longitude, sampling depth and depth horizon (UML or below).
- Dimethylated sulfur pools (nmol L^{-1}): DMS, DMSPd, DMSPp and DMSPt.
- Rates (nmol L^{-1} d^{-1}) and rate constants (d^{-1}) of microbial DMSP(d,p,t) cycling.
- Yields of DMSP(d,t) to DMS conversion.
- Rates (nmol L^{-1} d^{-1}) and rate constants (d^{-1}) of biotic and abiotic DMS cycling.
- Physiochemical environmental parameters: temperature, salinity, nitrate+nitrite concentration, and mixed layer depth (MLD).
- Microbial plankton community descriptors: phytoplankton biomass (Chl *a*, μg L^{-1}), particulate primary production (μmol C L^{-1} d^{-1}), and bacterial production (^{3}H-leucine incorporation rate, LIR, nmol Leu L^{-1} d^{-1}).
- Predefined classification categories and methodological descriptors (*see* next section).

Table 6.1: Descriptive statistics in the whole dataset: mean, median, minimum, quantiles, maximum, and data counts

Variable	Mean	Median	Min	5%	25%	75%	95%	Max	*n*
Mixed Layer Depth (m)	24.4	21.0	1	3	11	30	64	88	*264*
Sea surface temperature (°C)	15.5	12.7	-1.8	-0.2	10.1	24.7	27.7	30.0	*387*
Salinity	34.49	34.50	12.00	29.95	32.90	36.70	37.90	38.27	*369*
Nitrate + nitrite (µmol L^{-1})	3.7	0.6	0.00	0.01	0.1	6.5	15.0	25.0	*257*
Chlorophyll *a* (µg L^{-1})	1.1	0.5	0.02	0.04	0.14	1.3	4.9	13.3	*344*
Primary production (µmol C L^{-1} d^{-1})	1.7	1.3	0.13	0.24	0.7	2.1	5.3	8.6	*99*
Bacterial production (nmol Leu L^{-1} d^{-1})	1.4	0.7	0.00	0.08	0.31	1.6	5.3	32.1	*189*
DMSPt (nmol L^{-1})	45.8	24.5	2.6	7.5	14.0	47.7	130.1	924	*318*
k DMSPt production (d^{-1})	1.0	0.7	0.0	0.1	0.4	1.2	2.5	7	*99*
k DMSPt consumption (d^{-1})	1.3	0.8	0.0	0.3	0.6	1.4	4.3	9.8	*116*
k DMSPp consumption (d^{-1})	0.6	0.5	0.2	0.3	0.4	0.7	0.9	1.0	*28*
k DMSPd consumption (d^{-1})	4.6	3.0	0.7	1.1	1.8	6.2	11.6	31.0	*115*
Yield DMSPt to DMS (%)	18	12	0	0	5	22	54	100	*122*
Yield DMSPd to DMS (%)	11.3	9.3	1.0	3.4	6.6	15.5	21.0	32.3	*79*
DMS (nmol L^{-1})	5.8	3.0	0.2	0.6	1.4	4.8	15.9	216	*357*
K_{cr} (d^{-1})	1.37	0.88	0.00	0.00	0.47	1.5	3.9	22.2	*261*
K_{bc} (d^{-1})	0.94	0.55	0.00	0.03	0.25	1.0	2.2	16.4	*254*
K_{phto} (d^{-1})	0.31	0.19	0.00	0.00	0.07	0.31	1.2	2.4	*79*
K_{vrel} (d^{-1})	0.09	0.06	0.00	0.00	0.01	0.13	0.3	0.67	*97*
DMS:DMSPt	0.15	0.10	0.01	0.02	0.04	0.20	0.40	2.81	*300*
GP:DMSPt (d^{-1})	0.13	0.09	0.00	0.00	0.06	0.17	0.36	0.92	*202*
DMS:Chl *a*	18.2	6.8	0.00	0.0	1.7	19	74	262	*207*
GP:Chl *a*	18.7	7.7	0	0	1.9	24	73	216	*326*
DMSPt:Chl *a*	102	73	2.3	7.7	32	134	319	790	*307*

6.3 Characterization of the dataset

In this section we will evaluate the distribution of the samples among predefined categories, and characterize the statistical distribution of the most relevant variables (Table 6.1). This will help establishing strategies for the posterior statistical analyses.

The primary data were classified into the categories listed below:

- Domain: coastal or oceanic.
- Season (astronomic): winter, spring, summer, or autumn.
- Study type: time-series, transect/cross system, Lagrangian, or diel (day-night) cycle.
- Method used to determine GP: direct (using either chloroform, methyl-butyl ether (MBE), or DMDS as inhibitor) or indirect.
- Light conditions in which biological rates were determined: dark or light.

In addition, the data were split along continuous variables: by latitude band ($< 20^{o}$, 20^{o}-40^{o}, 40^{o}-60^{o}, or $> 60^{o}$) and by Chl a concentration (0.01-0.1, 0.1-1, and > 1 μg L^{-1}). This exercise showed that the samples were biased towards summer, temperate (40^{o}-60^{o}), and moderately productive (Chl a of 0.1-1 1 μg L^{-1}) conditions, with an astonishing scarcity of process measurements in the equatorial belt. The partition between the coastal and oceanic domains was numerically equilibrated, as well as the distribution of samples among study types. However, on an areal basis the dataset was obviously biased towards coastal and shelf locations.

Despite the sampling bias mentioned above, the dataset covered a wide range of marine environments (Table 6.1, Fig. 6.12) and represented all main oceanic biomes: polar, westerlies, trade winds, and coastal, as defined by Longhurst et al. (1995). For example, temperature ranged -1.8-30 ^{o}C (median of 13.6 ^{o}C), and Chl a ranged three orders of magnitude, from 0.02 to 13.3 μg L^{-1} (median of 0.50 μg L^{-1}). The median DMS concentration (3.0 nmol L^{-1}) was slightly higher than the global median found in the updated DMS climatology of Lana and coauthors (2.0 nmol L^{-1}), which is expectable given the summer bias of the data (Lana et al., 2011, 2012). Median DMSPt concentrations (23 nmol L^{-1}) were slightly lower than those reported by Kettle and coauthors (32 nmol L^{-1}). Overall, our relatively small dataset seems to be reasonably representative of the most frequent oceanic conditions. This statistical information, summarized in Table 6.1, provides a valuable reference for observational and modeling studies.

The reference time frame used in the database is one day. In the case of the diel cycle studies, where several samples had been taken and incubated every day, the samples were treated as individual rates or averaged to produce a single daily datum depending on the purpose of the analysis. In the inhibitor-based studies we assumed that the incubations were representative of a one day period and of the entire UML. In the case of budget-derived GP, we carefully checked that the budgets had been calculated for a 1-d period and averaged within the UML. Most GP measurements included in the database (or BC measurements used for budgeting) where done in the dark ($> 90\%$) using the inhibitor technique (around 80 %), with DMDS (Fig. 6.12). When dark and light rates had been measured simultaneously, only the dark rates were included in the analysis. In approximately one third of budgeting-based studies ($< 10\%$ of the total) bacterial DMS consumption (BC) was measured only in the light. We assumed that this would cause a small difference, since BC was vertically integrated within the UML (which reduces the weight of the photoinhibiton effect) and then added to photolysis and ventilation.

It may seem inappropriate to use a database composed mainly of dark GP rates after finding that direct solar exposure has a strong impact on GP (Chapters 2-5). By means of the meta-analysis we will try to address some methodological aspects concerning the measurement of GP, and to reconcile the observation of sunlight-stimulated GP with the macroscale patterns of DMS(P) cycling and their drivers.

6.4 Preprocessing of the data and statistical analysis work flow

The original data, which we will call the *samples* subset, contained 245 individual GP measurements, most of which were paired with BC measurements ($n = 230$). A higher level subset called the *means* subset ($n = 44$) was created by averaging a variable number of individual samples (always $n > 3$) within each study, following (Baines and Pace, 1991). This subset was created to check the robustness of the trends observed in the samples subset, at the cost of reducing the number of observations, thus, the statistical significance. We generally followed the grouping criteria adopted by the authors. Otherwise, a group of samples was defined by having a coefficient of variation (CV) $< 60\%$ in at least two of the following four variables: DMS concentration, GP, GP:DMSPt, and GP:Chl *a*. If the above conditions were not met, which was generally due to a lack of data, the samples were grouped subjectively or, else, no mean was calculated.

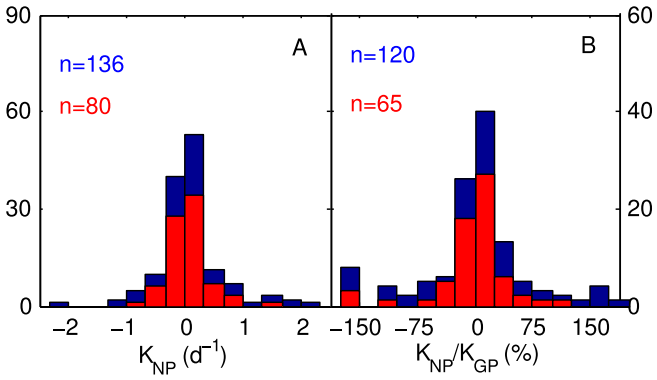

Figure 6.1: **Statistical distribution of in situ net DMS production and its magnitude with respect to gross DMS production** - (A) net DMS production rate constant (k_{NP}) and (B) its quotient to the gross DMS production rate constant (k_GP). Blue columns: all data; red columns: time frame equal or $>$ 24 h (see text for details)

To further avoid biases derived from unequal spatio-temporal coverage, site-specific features, or method-specific pitfalls, the variables of interest were binned in intervals defined by different independent variables (x). For example, the medians of the GP:DMSPt ratio were calculated for bins of latitude, temperature, salinity, nitrate-nitrite, Chl *a*, MLD, solar radiation dose (SRD). The binning intervals of each x variable were optimized to find a compromise between the number of observations contained in each bin and the regular spacing between bin centers. When necessary, the x variables were log-transformed. We acknowledge that binning is a rather drastic way of smoothing out natural variability, but binned data may reveal patterns that are not obvious in the raw dataset.

Prior to analyze the trends in gross DMS production, it was necessary to evaluate our main assumption: that net DMS production (NP) was generally zero on a daily basis. To this end, we calculated in-situ NP in Lagrangian studies where the same water mass had been sampled daily. We also included in the calculation the measurements made on two consecutive days at the BBMO on a monthly basis during 2003-04. In addition, NP was calculated in shorter and longer time periods (4, 6 and 12 h, and up to two weeks), to find the timescales at which wider DMS fluctuations occur within the meteorological time frame (see 6.7.6). As shown by the histogram in Fig. 6.1A, NP was generally well constrained around 0, with a median of 0.015 d^{-1} and 2/3 of the values comprised between -0.18 and 0.27 d^{-1} on a daily basis. To further asses the error and possible bias derived from our assumption, we calculated the quotient k_{NP}/k_{GP} in all those samples where these variables were simultaneously available (Fig. 6.1B). Again,

this quotient showed a rather symmetric distribution with median 0.03 and 2/3 of the values comprised in the ± 0.24 interval. This means that our assumption caused no bias and that it carried an acceptable error (< 25% in 2/3 of the occasions), that is, an error much smaller than the > 2 orders of magnitude spanned by the GP rates. It has to be noted that the GP rates calculated by budgeting were only ca. 20% of the total.

Another issue we faced when assembling the database concerned the calculation of the integrated solar radiation dose (SRD, W m^{-2}) in the upper mixed layer. The SRD index is calculated using the 24 h average of total shortwave irradiance reaching the sea surface ($E_{d,o+}$), the depth of the mixed layer (MLD), and underwater PAR attenuation ($K_{d,PAR}$), following Vallina and Simó (2007):

$$SRD = \frac{1}{K_{d,PAR}MLD}(1 - e^{-K_{d,PAR}MLD}) \tag{6.3}$$

Only a few studies reported SRD, whereas a few more reported $E_{d,o+}$ and/or $K_{d,PAR}$, and the majority of them reported MLD. Since we found interesting to add SRD as an explanatory variable, we calculated it whenever the primary variables were available. We assumed that MLDs provided by the authors were correct, and did not homogenize them by using a single calculation criterion (Brainerd and Gregg, 1995). In those studies where $K_{d,PAR}$ was not available, it was calculated according to the model of Morel and Maritorena (2001) for case 2 waters, as updated in Morel et al. (2007). The daily irradiance at the top of the atmosphere (TOA) was calculated using a standard astronomical model (Brock, 1981). Vallina and Simó (2007) used an average atmospheric transmission factor of 0.5 to convert TOA irradiance to that at the sea surface ($E_{d,o+}$). In our dataset, the direct comparison between modeled and observed $E_{d,o+}$ gave an average atmospheric transmission of 0.53. Thus, in those studies where $E_{d,o+}$ had to be estimated we used this atmospheric transmission factor.

We took different statistical approaches depending on the questions being posed:

- Multivariate analysis was used to describe emergent patterns, by means of principal components analysis (PCA), and to classify the samples in coherent groups (e.g., PFTs) by means of hierarchical clustering.
- Parametric (Pearson) and non-parametric (Spearman) correlation analyses were used to find relationships between variable pairs within different subsets of the data.
- Multiple linear regression (also in its stepwise version) was used to explore the explanatory power of a set of predictor variables on the variables of interest.

- Parametric and non-parametric (Kruskal-Wallis) analyses of variance (ANOVA), followed by post-hoc multiple comparisons when needed (Tukey-Kramer test), were used to verify the differences between the different PFTs and among sample subsets.

6.5 Emergent properties: Multivariate analyses and PFT classification by clustering

A PCA was performed on the *samples* subset to depict their variability on a reduced dimension space. In this analysis, each diel cycle study was treated as a single datum so that site-specific variability was not confounded with diel variability. The variables included in the analysis were selected in a way that maximized the fraction of explained variance while keeping the highest possible number of observations (rows; $n = 147$). Since PCA requires that the data matrix has no missing values, and some variables were not available for all the observations, increasing the number of variables (columns) caused a reduction in the number of complete data rows (see Fig. 6.13). The eight variables included were: latitude, days to/from summer solstice (D2SS, a negative proxy for light), mixed layer depth (MLD), sea surface temperature, Chl *a*, DMS, DMSPt, and GP. The latter four variables were log-transformed to render them symmetrically distributed (since they were strongly right-skewed), and the whole data matrix was standardized before performing the PCA. Only primary and independently measured variables were used, and the collinearity between them was checked by calculating the variance inflation factor ($VIF = 1/(1 - R^2)$). The highest correlation (r) between variable pairs was 0.69 for DMS vs. GP; this would result in a VIF = 1.9, which is far below the threshold VIF < 5 proposed by Legendre and Legendre (1998). The first two components, PC1 and PC2, explained 53% and 19% of the variance, respectively. From the third component on the variance explained decayed more or less exponentially (Fig. 6.14) and with a less steep slope, which is characteristic of random noise (Wilks, 1995). Thus, we decided to retain only the first two components.

The PCA revealed different modes of variability of DMS(P) cycling in plankton communities (Fig. 6.2). PC1 reflected the increase in phytoplankton biomass (Chl *a*) and DMSPt associated to high latitudes, a signal dominated by subpolar and polar haptophyte blooms. PC2 retained information associated to the light and mixing regime. The three main factors determining light availability loaded with high positive coefficients on PC2, namely Chl *a* (which directly affects water transparency; Morel and Maritorena (2001)), distance from the summer solstice, and MLD. Thus, negative values of PC2 are associated to elevated light (PAR and UVR) doses

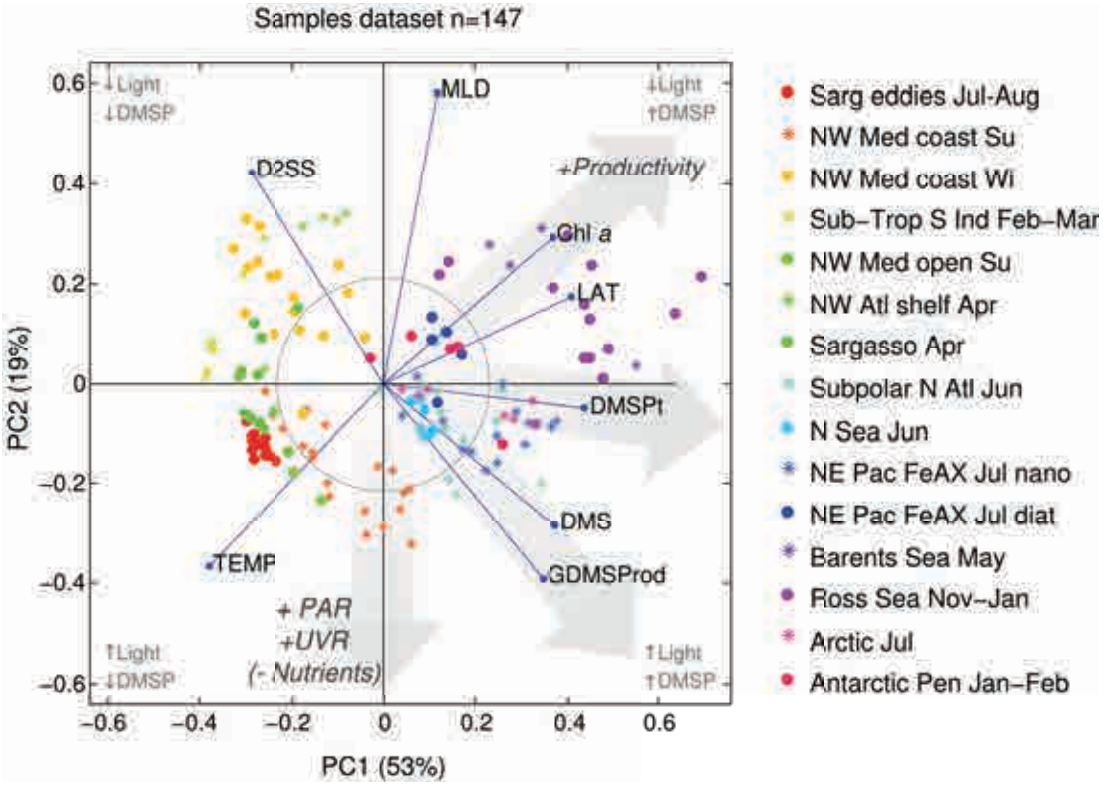

Figure 6.2: **Principal Components Analysis of DMS cycling** - D2SS: days to summer solstice; MLD: mixed layer depth; LAT: latitude; GDMSProd: gross DMS production; TEMP: temperature; see text for other abbreviations

in the UML, generally concurrent with stratification-derived nutrient scarcity. Regarding gross DMS production, an interesting interpretation was obtained by looking at the two orthogonal axes that formed an angle of about 45° with PC1 and PC2 (which is equivalent to rotating the axes). In this way, we could identify a *phytoplankton productivity* and a *DMS production* axis. The productivity axis was defined by high temperature at one extreme (indicative of stably-stratified, nutrient-poor subtropical waters), and high Chl *a* and latitude at the opposed extreme. Orthogonal to this axis was found an axis defined by high DMS concentration and gross DMS production at one extreme, and low light at the other. Therefore, DMS levels and gross DMS production are independent of the trophic status on the plane defined by PC1-PC2, which explains the majority of the total variance. This provides further evidence of the covariation between DMS and light exposure irrespective of latitude and phytoplankton production regime, a well known emergent property of marine DMS variability (Vallina and Simó, 2007; Lana et al., 2012).

When the PCA was performed on the more reduced *means* subset, essentially the same pattern was obtained, with similar projections of the variables onto PC1 and PC2 and 74% of the variance explained. Very similar PCAs were also obtained when only the GP rates derived from DMDS inhibition (which made up the majority of the measurements) were considered. Alternative PCAs were performed by including the following variables in different combinations and in a stepwise manner: salinity, nitrate+nitrite, particulate primary production rates (PPp), and leucine incorporation rates (LIR). As observed before, adding new variables produced a decrease in the number of valid observations, but did not increase the fraction of variance explained or unveil any new patterns. Salinity covaried with temperature ($R^2 = 0.40$), and nitrate+nitrite concentration was well predicted by a linear combination of temperature and MLD ($R^2 = 0.58$), with higher nitrate+nitrite in cold and deeply-mixed waters. Nitrate+nitrite appeared orthogonal (uncorrelated) to DMS on the PC1-PC2 plane, but opposed in the PC2-PC3 plane, which points to a marginal role of nitrogen limitation stress in enhancing DMS dynamics. Alternatively, a possible important role of nitrogen limitation would have been better captured by the mixing/light axis (PC2). Adding PPp or LIR did not render a better representation of DMS(P) cycling either, with both variables covarying mainly with Chl *a*. From this exercise we concluded that the patterns revealed by the PCA are robust.

We also performed the PCA substituting GP and DMS by k_{GP} ($k_{GP} = GP/[DMS]$). In this alternative PCA a smaller fraction of the variance could be explained by PC1 and PC2 (65%) and most of the variability of k_{GP} was associated to PC3. This indicates that DMS turnover is not correlated to the other variables, a pattern that will be explored in more detail in sections 6.7.1 and 6.7.6.

According to the PCA, DMS(P) cycling can be partitioned into four quadrants characterized by high/low DMSPt and high/low stress. Highest DMS production (and concentration) occurs in high-DMSPt communities suffering radiation- and nutrient- derived oxidative stress. The DMSPt vector sits half-way between the productivity and the radiative stress vectors, but closer to the former. In other words, highest DMSPt levels are found at the optimum between phytoplankton biomass and radiative stress, in accordance with its putative physiological roles (Stefels, 2000; Sunda et al., 2002). Notably, highest DMSPt levels are not matched by highest DMS. This pattern resembles that occurring seasonally in nutrient-limited, temperate to subtropical oceans where the peak of surface DMSPt precedes that of DMS by approximately 2 months (Simó and Pedrós-Alió, 1999c). It is also remarkable that similar levels of DMS production can occur in samples where DMSPt differs by almost one order of magnitude, for example,

the coastal Mediterranean in late spring or early summer and the Ross Sea during *Phaeocystis antarctica* blooms. Here, it has to be noted that in the Ross Sea study done by Delvalle et al. (2009) no reliable DMSPt measurements were available (see Rellinger et al. (2009); del Valle et al. (2011), and DMSPt had to be estimated by assuming a DMSPt:Chl *a* ratio of 40 nmol/μg (a reasonable value according to Stefels et al. (2007). This estimation was made because we found especially interesting to include that study in the PCA. In the other only study reporting DMS cycling in the Ross Sea (DiTullio et al., 2003) DMS concentrations and production rates were arguably overestimated (del Valle et al., 2009). On the other hand, excluding the study by Del Valle *d*id not change appreciably the patterns described above.

Going a step further in the task of classifying the observations, we performed a hierarchical cluster analysis on the same matrix used as input for the PCA. Euclidean distances were used as the distance metric, and the cluster tree was calculated by means of the unweighted average distance method. In Fig. 6.3, a 'heat map' showing the relative value of each variable is displayed besides the cluster tree, making it easier to interpret which variables were critical in defining each subcluster. Based on the results of these analyses, on previous literature, and on subjective (experience-based) criteria, we decided to group the observations in four categories or PFTs (Table 6.2): diatom-dominated communities, picophytoplankton-dominated communities, mixed phytoplankton blooms, and *Phaeocystis* blooms. Phytoplankton community composition was chosen as the primary factor determining the DMS(P) cycling regime. This does not mean that phytoplankton alone can explain DMS(P) distribution and cycling, but that the phytoplankton community reflects the underlying physical forcing that shapes the diversity and functioning of the microbial food web. In addition, the composition of the phytoplankton community is far more frequently reported than the identity of co-occurring bacteria and microzooplankton.

It should be noted that the PFTs approach seeks a functional classification, rather than a taxonomical one. Indeed, some phylogenetic groups are associated with a defined mode of bioegeochemical functioning. This is the case of blooming diatom species, which occur in well-mixed nutrient- and Fe-rich environments, producing intense C export. Diatoms (except for the sea-ice associated ones; Levasseur et al. (1994)) are also known for their low DMS(P) production. On the other hand, some phylogenetic groups are widespread among different PFTs, most remarkably the DMSP-rich haptophytes (= prymnesiophytes): they can form massive blooms in polar and eutrophic coastal waters (genus *Phaeocystis*), but can also be dominant components of subtropical and temperate pico-sized communities (Liu et al., 2009;

Cuvelier et al., 2010; Jardillier et al., 2010) as well as major players in mixed phytoplankton blooms occurring in temperate to subpolar regions. A good example of the latter would be *Emiliania huxleyi* blooms, where haptophytes often share with autotrophic dinoflagellates their influence on DMS(P) dynamics (Simó and Dachs, 2002; Steinke et al., 2002).

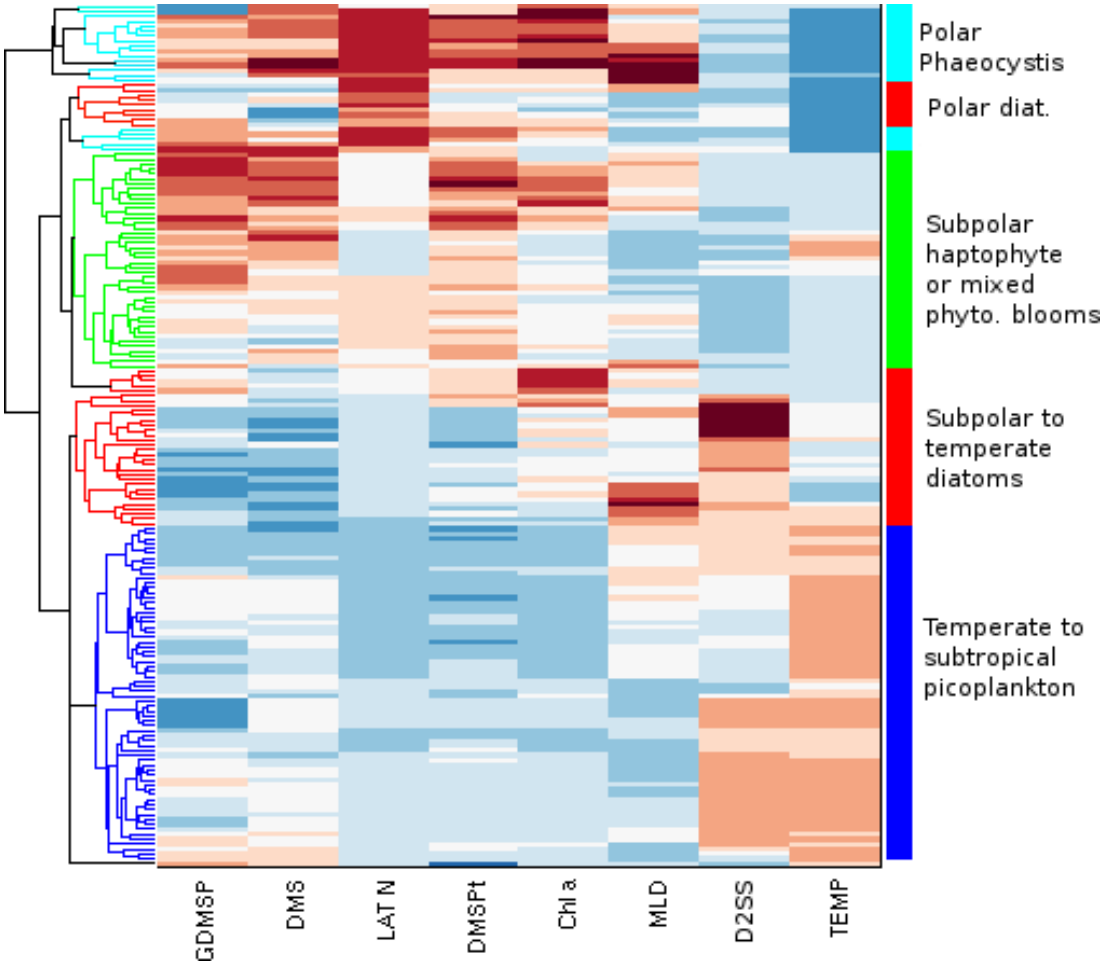

Figure 6.3: **Cluster tree employed to classify the samples with the Plankton Functional Types approach** - The colors in the heat map indicate low (blue) or high (red) values of the variables specified in the x-axis. Abbreviations as in Fig. 6.2

Table 6.2: Descriptive statistics as per PFT: median values are reported, and the letters indicate significant differences deduced from a posthoc Tukey test, following a significant KruskalWallis ANOVA ($p < 0.05$).

Phytoplankton functional group	Picoplankton		Mixed		Diatoms		Polar Hapto		*p*
Mixed Layer Depth (m)	26	*ab*	20	*a*	22	*b*	18	*ab*	*0.01*
Sea surface temperature (°C)	24.7	*a*	11.3	*b*	9.2	*b*	0.0	*c*	*0*
Salinity	36.2	*a*	34.2	*b*	33.0	*b*	34.3	*b*	*0*
Nitrate + nitrite (µmol L^{-1})	0.2	*a*	5.4	*b*	2.2	*b*	15.0	*c*	*0*
Chlorophyll *a* (µg L^{-1})	0.12	*a*	0.6	*b*	1.4	*c*	2.0	*c*	*0*
Primary production (µmol C L^{-1} d^{-1})	1.1		1.5		1.7				*0.470*
Bacterial production (nmol Leu L^{-1} d^{-1})	0.4	*a*	1.1	*b*	1.6	*b*	0.7	*ab*	*3E-07*
DMSPt (nmol L^{-1})	13.3	*a*	46	*b*	26	*c*	95	*b*	*0*
k DMSP prod (d^{-1})	0.7		0.5		0.8				*0.25*
k DMSPt consumption (d^{-1})	0.7		0.6		0.6		1.1		*0.33*
k DMSPp consumption (d^{-1})	0.5	*ab*	0.5	*a*	0.9	*b*			*0.01*
k DMSPd consumption (d^{-1})	2.0	*a*	3.1	*b*	2.9	*ab*			*0.045*
Yield DMSPt to DMS (%)	19	*a*	15	*a*	5	*b*	22	*ab*	*2E-03*
Yield DMSPd to DMS (%)	7		9		14				*0.07*
DMS (nmol L^{-1})	2.2	*a*	4.1	*b*	1.1	*a*	9.9	*c*	*8E-16*
K_{GP} (d^{-1})	0.7	*a*	1.1	*b*	1.4	*ab*	1.0	*ab*	*0.03*
K_{BC} (d^{-1})	0.3	*a*	0.5	*b*	0.7	*b*	0.6	*b*	*1E-03*
K_{photo} (d^{-1})	0.23	*a*	0.20	*a*	0.08	*b*	0.10	*b*	*0.03*
K_{vent} (d^{-1})	0.10		0.09		0.02		0.06		*0.06*
DMS:DMSPt	0.14	*a*	0.08	*b*	0.05	*b*	0.07	*ab*	*2E-05*
GP:DMSPt (d^{-1})	0.10		0.10		0.07		0.10		*0.052*
DMS:Chl *a*	23	*a*	5	*b*	1	*c*	8	*b*	*0*
GP:Chl *a*	17	*a*	7	*b*	1	*c*	3	*b*	*0*
DMSPt:Chl *a*	130	*a*	66	*b*	13	*c*	76	*b*	*0*

6.6 Factors regulating DMSP production, food web transformations, and DMS production yields

6.6.1 Community DMSP production

DMS(P) production is species- and even strain-specific. Yet, oxidative stress can enhance intracellular DMSP concentrations by a factor as large as inter-specific differences (Sunda et al., 2002, 2007; Bucciarelli and Sunda, 2003). Therefore, the implicit or explicit combination of both factors should do particularly well at predicting DMSP levels in the upper ocean. This has been confirmed by prognostic biogeochemical models, which showed that modulation of the internal DMSP quota by diagnosed radiative stress was essential to reproduce DMSP seasonality (Vallina et al., 2008; Vogt et al., 2010; Steiner et al., 2011), while implicitly representing phytoplankton succession. In our dataset, two community-level indicators of the DMSP production capacity have been explored: the DMSPt:Chl *a* ratio and the fraction of PPp invested in DMSP production: PP_{DMSP}:PPp (%, in carbon currency).

The first indicator is an easy-to-measure concentration ratio, and has been proposed as an indicator of how shifted are microbial communities towards DMSP catabolism (Simó et al., 2009). DMSP is mostly found in the particulate fraction (Kiene and Slezak, 2006) in phytoplankton cells, but also as untransformed DMSP retained by grazers (Tang and Simó, 2003; Saló et al., 2009) and DMSP-consuming heterotrophs and autotrophs (Kiene and Linn, 2000; Vila-Costa et al., 2006a; Archer et al., 2011). DMSPt:Chl *a* is also affected by photoacclimation, as phytoplankton thriving in well-lit mixed layers reduce their Chl *a* content relative to carbon (Macintyre et al., 2002). The PFTs partition shows clear and significant differences in DMSPt:Chl *a* among groups (Table 6.2), with picoplankton displaying one order of magnitude higher DMSPt:Chl *a* than diatoms, and the other two groups falling in an intermediate position. Clearly, a much larger database exists from where to obtain globally representative DMSPt:Chl *a* estimates. Nevertheless, the values shown in Tables 6.2 and 6.3 indicate that the PFTs partition is relevant.

Indeed, PP_{DMSP}:PPp provides a more direct assessment of the autotrophic investment on DMSP, but it is more difficult to measure. In our dataset, about 40 measurements of DMSPt synthesis were obtained by the net-loss curve approach (Simó et al., 2000) combined with budgeting in Lagrangian settings (e.g. Simó and Dachs (2002)), while the remaining 30 measurements were obtained in dilution grazing experiments (Archer et al., 2001; Saló et al., 2010). Measurements done with the two methods were well distributed among PFTs. It is worth

Table 6.3: Dimethylated sulfur fluxes as % of primary production (in carbon currency) in the different PFTs: from DMSP production to DMS emission.

PFT	Picoplankton		Mixed		Diatoms		*Phaeocystis*		*p*
DMSPt prod	8.2	a	7.2	ab	2.74	b			0.04
GP	0.52	a	0.58	a	0.11	b	0.69	a	$7x10^{-6}$
Emission flux	0.13	ab	0.03	ab	0	a	0.2	b	0.02

noting that PP_{DMSP}:PPp obtained with the net-loss curve method are potentially larger: DMSPt synthesis accounts for particulate DMSP production but also for the DMSP released to the dissolved phase, so it would be more consistent to normalize it to the total carbon fixation (dissolved + particulate). Despite possible inconsistencies between methods, we observed significant differences among PFTs, with picoplankton and mixed phytoplankton investing a median of 7.5% of particulate carbon fixation on DMSP, and diatoms a median of 2.7% (Table 6.3). Although a usual upper limit for PP_{DMSP}:PPp is set at 10%, we find 1/4 of PP_{DMSP}:PPp values above 10%, most of them $< 25\%$. While some values may actually be off, it is possible that some phytoplankton communities are investing more than 10% of PPp in DMSP under certain conditions, which requires that the actual DMSP-producing species are possibly investing $> 20\%$. According to culture studies such big values are not unfeasible: A DMSP-carbon (DMSP-C) quota as big as 36% was observed in the dinoflagellate *Alexandrium minutum* (Berdalet et al., 2011), and Stefels et al. (2007) reported a mean $\pm$ sd of $11 \pm 16\%$ for dinoflagellates.

The data from this literature compilation call for an upwards revision of intracellular DMSP quotas in phytoplankton. The weak but significant positive correlation between the DMSPt:Chl *a* ratio and PP_{DMSP}:PPp in our dataset supports this notion (Spearman's $r = 0.36$, $p = 0.011$). The DMSP-C investment observed in diatom-dominated communities is particularly difficult to reconcile with the widely used DMSP-C quotas and DMSPt:Chl *a* ratios proposed by Stefels et al. (2007), and fits with previous studies suggesting that diatoms contribute more than generally assumed to the DMSPp pool (Steiner and Denman, 2008, and references therein). Indeed, blooming diatoms can be accompanied by DMSP-producing species. For example, in the BBMO the prasinophyte *Micromonas* is often found accompanying diatom blooms (Gutiérrez-Rodríguez et al., 2011), a situation where it might contribute a large share of the DMSP produced. Nevertheless, intracellular DMSP quotas derived from non-stressed cultures, growing in nutrient-replete and soft PAR conditions, might lay at the lower end. As usual, there is an alternative (and compatible) interpretation: that intracellular DMSP is being recycled faster

than the average turnover of cellular carbon, therefore contributing relatively more to the C flux than to the C pool. Either case, algal DMSP synthesis requires further attention, and newly developed methods may be helpful in accomplishing this task (Stefels et al., 2009).

6.6.2 Food web DMSP transformations

In the original CLAW hypothesis, DMS was thought to be largely a result of direct exudation by phytoplankton. Although this mechanism was shown to be relevant (though more complex than originally thought) in certain phytoplankton species, the paradigm of DMS production tipped during the nineties towards a potentially key role of bacteria. This was formally expressed by means of the 'sulfur demand hypothesis' of Kiene et al. (2000) and synthesized by the concept of the 'bacterial switch' (Simó, 2001), which suggest that bacteria produce DMS only when their S requirements have been met by assimilating a sufficient amount of DMSP-derived MeSH or other S sources like methionine (Zubkov et al., 2003; Tripp et al., 2008). Although the S demand hypothesis proved useful to interpret bacterial DMSP catabolism in large blooms (Merzouk et al., 2006, 2008; Lizotte et al., 2009) or certain oceanic regions (Royer et al., 2010), it did not seem to hold when tested on a seasonal basis in studies done in summer-paradox regions using different molecular approaches (Vila-Costa et al., 2007; Levine et al., 2012).

The distinction between dissolved and particulate pools, which, as many size-fractionated measurements usually done in oceanography, is basically operational (Verdugo et al., 2004), shaped the way we currently think about DMS production. In the last decade a lot of efforts have been devoted to elucidating the role of bacterial DMSP metabolism on DMS production, encouraged by the 'omics' revolution occurred in microbial oceanography (Moran et al., 2012). In this approach, bacterial DMS production was generally assumed to arise from the dissolved pool. At the same time grew the awareness that other food-web interactions (viral lysis and microzooplankton grazing) might have a profound influence on DMS production (Hill et al., 1998; Archer et al., 2001; Simó, 2001), and it was realized that the relative importance of DMS production pathways was very sensitive to the partitioning between dissolved and particulate DMSP (Archer et al., 2002). The importance of DMSPd-based DMS production, however, is lately being downplayed by successive downwards revisions of the fraction of DMSP available to bacterioplankton (Kiene and Slezak, 2006, Kiene, pers. comm.). In addition, bacterioplankton have to compete for DMSPd with non DMSP- producing phytoplankton (Vila-Costa et al., 2006b; Ruiz-González et al., 2012f,c). This, and observations of light (UVR) and oxidative stress-induced DMS release by phytoplankton (Hefu and Kirst, 1997; Sunda et al., 2007), which

are well rooted on physiological grounds (Stefels, 2000; Sunda et al., 2002), are tipping the paradigm back to the key role of DMS production from the 'particulate' pool.

Indeed, results from Chapters 2, 3 and 4 add to mounting evidence of the key role of stress-induced algal DMS release, which is also supported by some recent modeling works (Toole et al., 2008; Vallina et al., 2008; Vogt et al., 2010). Furthermore, our results indicate that processes controlling the turnover of the particulate pool must be understood if we are to mechanistically predict gross DMS production. We also showed that, besides the 'classical' DMSP-releasing processes (namely grazing and viral lysis), radiation-induced phytoplankton cell damage should be taken into account (Chapters 3 and 4). Still, the microscale picture of DMS production is surely more complex than our schematic representations and depends on multiple interactions between grazers, phytoplankton cells of varied physiological condition, and bacteria. In fact, from our results it is not possible to conclude whether sunlight-stimulated DMS production arises mostly from intracellular or extracellular, algal or bacterial enzymes, all of them probably working in close vicinity to the DMSP source (Seymour et al., 2010). Moreover, the sign of the interaction between UV-stress and grazing is largely unknown.

There is growing evidence that metabolic capabilities are not evenly distributed among pelagic bacteria, with different genotypes and phenotypes possibly associated to the free-living and particle-attached lifestyles (Cottrell and Kirchman, 2000; Giovannoni et al., 2005; González et al., 2008, but see also Mou et al. (2008)). Bacteria occupying different niches may utilize DMSP-sulfur differently (Tripp et al., 2008), and may also differ in the way they cope with radiative stress or utilize light (Ruiz-González et al., 2012b). Bacterioplankton succession is an evident feature at the temperate BBMO site, with *Roseobacter* (*Alphaproteobacteria*) and *Bacteroidetes* showing higher affinity for productive and DMSP-rich spring phytoplankton blooms, *Gammaproteobacteria* appearing related to high DMS production (and consumption) rates in late spring, and SAR-11 (*Alphaproteobacteria*) showing a marked preference for late summer oligotrophy (Fig. 6.15). These groups have shown varying affinities for DMSP in distinct oceanic regions (Vila-Costa et al., 2007; Ruiz-González et al., 2012a), and also different tendencies for demethylation, DMS production, and DMS oxidation (González et al., 1999; Vila-Costa et al., 2006a; Green et al., 2011; Hatton et al., 2012; Moran et al., 2012).

Although the dissolved vs. particulate dichotomy is more operational than conceptual, it is difficult to detach from it when it comes to field measurements; the measurements that will be feeding models sooner or later. For this reason we will use our PFTs approach to define different scenarios of DMSP metabolism. The DMSP turnover k's portray a fast-cycling DMSPd pool

(most frequently 2-6 d^{-1}) and a DMSPp pool that turns over as fast as phytoplankton cells (0.4-0.7 d^{-1}). The relatively similar turnover of DMSPp among PFTs is consistent with a meta-analysis of microzooplankton grazing (Calbet and Landry, 2004), which found only minor differences in phytoplankton mortality (generally 0.4-0.5 d^{-1}) across different oceanic regimes (Table 6.2). This clearly points to microzooplankton grazing as the main factor determining DMSP consumption. The values spanned by DMSPt turnover k's (0.6-1.4 d^{-1}) reflect the combination of DMSPd and DMSPp turnover k's in a proportion relative to the size of the respective DMSP pools (Table 6.2). More formally, a simple mass balance shows that the total DMSP flux (nmol L^{-1} d^{-1}) in a water volume must be equal to the flux of DMSPp + DMSPd:

$$k_{DMSPt}[DMSPt] = k_{DMSPd}[DMSPd] + k_{DMSPp}[DMSPp] \tag{6.4}$$

The partition between DMSPp and DMSPd is quite uncertain, but we know that the sum of both fractions equals DMSPt, so that we can express eq. 6.4 as a function of DMSPt:

$$k_{DMSPt}[DMSPt] = k_{DMSPd}fd[DMSPt] + k_{DMSPp}fp[DMSPt] \tag{6.5}$$

where fd and fp are the fraction of DMSPt found in the dissolved and particulate pools, respectively. DMSPt is a factor in all terms, so it can be dropped from the equation. Since we know that $fd + f\text{p} = 1$, we can subsitute fp in eq. 6.5:

$$k_{DMSPt} = k_{DMSPd}fd + k_{DMSPp}(1 - fd) \tag{6.6}$$

If we know the value of all k's, we can find the value of fd. The result of this exercise using the median k's in the global dataset (Table 6.1) is $fd = 0.12$, which is a reasonable value although slightly too high (Kiene and Slezak, 2006). Presumably more realistic values of 0.09 and 0.06 are obtained using the picoplankton and mixed PFTs subsets (Table 6.2), even though a non-sense value of -0.11 is obtained from the diatoms subset (which suffers from a lower number of observations). In *Phaeocystis* blooms it is not possible to estimate fd because not enough k_{DMSPd} measurements are available.

The DMSP budget can be turned into a gross DMS production DMS budget by multiplying each of the terms in eq. 6.5 by the DMSP to DMS conversion yield (Y) in each of the pools:

$$GPt = GPd + GPp \tag{6.7}$$

that is,

$$k_{DMSPt}[DMSPt]Y_{DMSPt} = k_{DMSPd}fd[DMSPt]Y_{DMSPd} + k_{DMSPp}fp[DMSPt]Y_{DMSPp} \tag{6.8}$$

which can be simplified to:

$$k_{DMSPt}Y_{DMSPt} = k_{DMSPd}fdY_{DMSPd} + k_{DMSPp}fpY_{DMSPp} \tag{6.9}$$

From eq. 6.7 and 6.8 we can estimate the fraction of GP derived from each pool as a function of fd, assuming that fd is the main factor causing uncertainty, and for each PFT:

$$\frac{GPd}{GPt} = fd\frac{k_{DMSPd}Y_{DMSPd}}{k_{DMSPt}Y_{DMSPt}} \tag{6.10}$$

As shown in Fig. 6.4A, the slope of this expression $(k_{DMSPd}Y_{DMSPd})/(k_{DMSPt}Y_{DMSPt})$ can be interpreted as the potential of each community type for producing DMS from the dissolved pool, given the median k's and yields.

From eq. 6.9, we can further try to estimate the DMS yield from consumed DMSPp (Y_{DMSPp}) as a function of fd (Fig 5B):

$$Y_{DMSPp} = \frac{k_{DMSPt}Y_{DMSPt} - fdk_{DMSPd}Y_{DMSPd}}{(1-fd)k_{DMSPp}} \tag{6.11}$$

The above equation has a y-intercept equal to the maximum Y_{DMSPp} attainable by each PFT, once the values of the k's and yields are fixed as specified in Table 6.2. Although we do not know the exact values of fd, recent studies generally suggest that $fd > 0.1$ are not feasible in most oceanographic conditions. Thus, we can estimate the most probable values for GPd/GPt and Y_{DMSPp} in each of the PFTs.

The results of this mass-balance analysis provide a framework for systematizing oceanic DMS production regimes, based on the fact that different microbial communities have markedly different DMS production profiles. The differences are mainly governed by the significantly different k_{DMSPd} and Y_{DMSPt} (or Y_{DMSPp}) among PFTs, while k_{DMSPt} (or k_{DMSPp}) and Y_{DMSPd} are more homogeneous among PFTs. According to these results, diatom dominated communities have the lowest DMS yields from intracellular DMSP and the highest potential for bacterial DMS production from DMSPd, due to the co-occurrence of low algal DMSP cleavage capacity and high k_{DMSPd} (Table 6.2). The opposite is true for low-biomass picoplankton-dominated communities, where the highest Y_{DMSPp} occur in combination with low k_{DMSPd}. Mixed phytoplankton and *Phaeocystis*-dominated communities are found in between, in congruence with

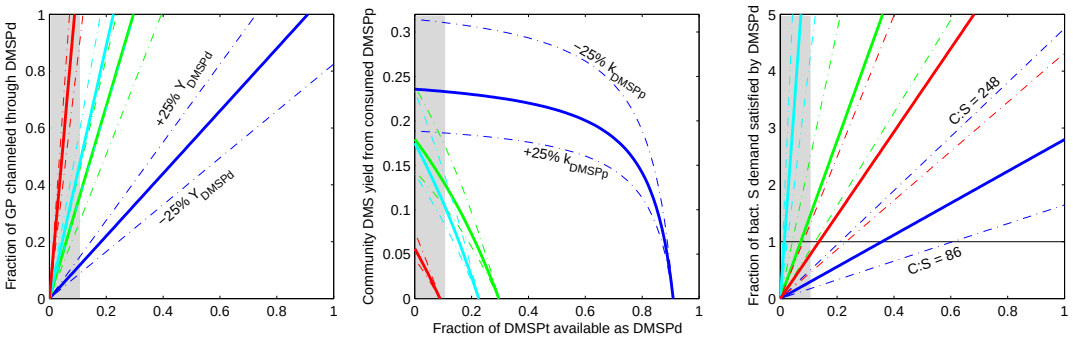

Figure 6.4: **DMSP metabolism in the different PFTs** - The shaded area indicates the most probable values of fd, the fraction of DMSPt available as DMSPd. Color coding as in Fig. 6.3. See text for definitions and abbreviations.

their intermediate position in the stress axis of the PCA (Fig. 6.2). Remarkably, the patterns encountered in the discrete PFT classification also show up as significant trends when analyzed with a binning approach: k_{DMSPd} increases with trophic status and decreases with SRD, while Y_{DMSPt} shows the opposed trends (Fig. 6.5). Therefore, we can conclude that community DMS yields (Y_{DMSPt}) are regulated by the interplay between algal DMSP cleavage capacity (likely modulated by radiative and nutrient stress), and bacterial DMSPd consumption capacity (likely a function of total bacterial activity). The significant correlation between bulk bacterial activity, as measured by LIR, and k_{DMSPd} ($r = 0.48$, $p < 10^{-5}$) supports the latter notion.

In agreement with our assessment of the potential of DMSPp and DMSPd as DMS sources, different studies indicate that DMSP cleavage capacity associated to particles is generally greater than that occurring in the dissolved phase (Cantin et al., 1999; Scarratt et al., 2000; Levine et al., 2012). Indeed, DMS cleavage in the algal phycosphere or in close vicinity to microzooplankton grazers might be operationally assigned to the DMSPp fraction. If this was the case, the fraction of the DMSP flux occurring through bacteria would be greater than generally assumed and, hence, the fraction of algal DMSP available to bacteria. We can try to constrain these numbers by calculating the bacterial sulfur demand satisfied by DMSP as a function of fd (Fig. 6.4C). In this calculation we need to assume a mean value for many variables: we set the leucine to carbon conversion factor to the widely used 1.55 kg C mol leu^{-1} (Simon and Azam, 1989; Alonso-Sáez et al., 2007); the bacterial growth efficiency to 0.13 (del Giorgio et al., 2011); the values of k_{DMSPd}, Y_{DMSPd}, and DMSPt, which also affect the calculation, are chosen according to the medians in Table 6.2; finally, we assume that 80% of the DMSPd

is consumed by bacteria, the remainder being taken up by phytoplankton (Vila-Costa et al., 2006a). The molar carbon:sulfur ratio in bacteria is identified as the main uncertainty, ranging between 86 (Fagerbakke et al., 1996) and 248 (del Valle et al., 2007). These calculations suggest that fd between 0 and 0.1 are sufficient for satisfying bacterial S needs in all PFTs except in picoplankton-dominated communities. In the framework of the S demand hypothesis, this is consistent with the slightly lower Y_{DMSPd} generally found in such communities (Table 6.2). Testing this hypothesis requires, however, a better knowledge of the several variables involved that describe bacterial carbon metabolism.

Modulation of Y_{DMSPd} by nutrient availability has been proposed as an alternative explanation of the summertime DMS peak in summer-paradox and non-summer-paradox regions. Steiner and Denman (2008) found that modulation of bacterial DMS yields by nutrient availability in the NE Pacific improved the performance of their model. However, both the microbial consumption rate constant of DMSPd (5.5 d^{-1}) and the Y_{DMSPd} (0.2) used in that study are at the high end, thus overestimating the influence of DMSPd metabolism on DMS production. Conversely, the proportion of DMSP 'consumed' by grazing or cell lysis tat is released as DMS (0.05 to 0.08) lays at the low end of probable values (Fig. 6.4B). Similarly, Polimene et al. (2011) argued that enhancement of bacterial DMS yields by nutrient limitation was more important than phytoplankton stresss in producing the seasonal DMSP/DMS decoupling in the Sargasso Sea. Again, their findings appear to rely on: (1) too high DMSPd concentrations (at least by one order of magnitude), and (b) a too low phytoplankton DMS exudation rate constant. Such exudation rate constants may occur in cells growing in culture (Laroche et al., 1999), but may be unrealistically low for stressed picophytoplankton in the Sargasso Sea summer (Fig. 6.4B). Finally, the temporal evolution of Y_{DMSPd} in iron addition experiments also argues against the nutrient-regulated bacterial yield hypothesis. In those experiments, Y_{DMSPd} decreased in parallel to nutrient exhaustion caused by iron-stimulated diatom growth (Merzouk et al., 2006; Lizotte et al., 2009). The arguments developed in this paragraph and the paragraphs above leave only a marginal role for bacterial DMSPd to DMS conversion yields as the explanation for broad scale patterns of DMS production.

There is a need to understand the evolutionary utility of bacterial DMSP-cleaving enzymes, and the relationship between bacterial lifestyles and their metabolic capabilities regarding the use of DMS(P,O), which will be inevitably linked to the cycles of organic carbon and organic/inorganic nutrients. Mutualistic and symbiotic relationships between bacteria and algae or grazers might play a relevant role (Johnston et al., 2008) and, perhaps, the decomposition of

DMSP and its metabolites should rather be seen as a tightly coordinated microbial consortium rather than as separate functional boxes.

6.6.3 Indicators of ecosystem DMS yield

Several variables would have to be measured in process studies to appropriately describe DMS(P) cycling. However, this task may not be affordable on many occasions. The meta-analysis provides a unique opportunity to define easy-to-measure diagnostics of DMS(P) cycling. These diagnostics can also be applied to constrain model outputs in those regions where process measurements are scarce. Our dataset indicates that DMS:DMSPt ratio appears as a robust diagnostic of community DMS yield (Y_{DMSPt}). In Table 6.1 it can be seen that the quantiles of both variables are rather coincident between the 5% quantile and the median, meaning that they have similar statistical distributions. Moreover, both variables exhibit similar trends when they are binned according to trophic status (yields decrease with increasing Chl *a* or nitrate+nitrite) or mixing-irradiance regime (yields increase with MLD shoaling and increasing SRD; Fig. 6.5). The somewhat smoother trends of DMS:DMSPt are probably due to the larger amount of data available in each bin. Similarly consistent but even broader trends are found when GP is normalized to Chl *a*, as a result of phytoplankton photoacclimation (as discussed for the DMSPt:Chl *a* ratio). The GP:DMSPt ratio has also been proposed as a useful indicator of DMS(P) cycling. Diagnostic modeling studies done in the Sargasso Sea and in the coastal Antarctic peninsula found rather similar GP:DMSPt (Bailey et al., 2008; Herrmann et al., 2012), which lead the authors to the conclusion that this ratio is quite invariant across oceanic biomes, allowing them to infer global DMS production rates. Supporting their view, we observe that GP:DMSPt is not significantly different among the PFTs (Table 6.2). Yet, now we can say that this apparent uniformity results from the combination of diverging tendencies in the rate constants and yields of total DMSP consumption (Fig 6). On the other hand, our global median for gross DMS production is 50% higher than the 0.06 $\pm$ 0.01 d^{-1} suggested by Herrmann et al. (2012), and GP:DMSPt displays significant trends when plotted against MLD or SRD bins (Fig. 6.5).

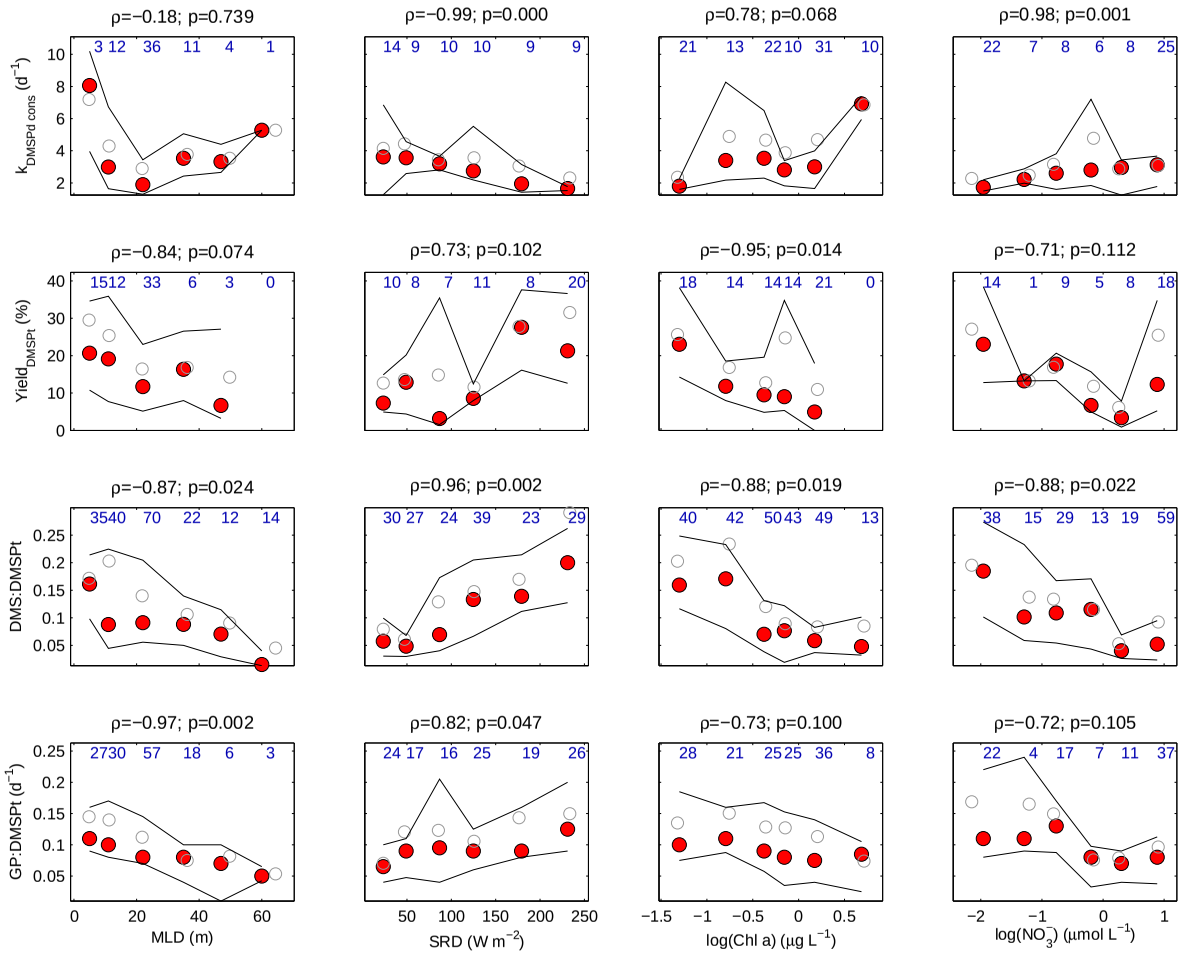

Figure 6.5: **Binned data scatterplots of DMSP metabolism rate constants (and process indicators) against environmental variables** - Red dots: bin medians; gray circles: bin means. The intervals are the 25 and 75% quantiles, and the blue numbers indicate the n of each bin; Pearson correlation ρ's and p's are shown.

6.7 Factors regulating DMS cycling

In this section we will evaluate how the interplay between DMS sources and sinks, as modulated by environmental factors, determines DMS turnover. Although in the previous section we have been able to identify distinct DMS production regimes, we know that the GP rates and associated bacterial DMS consumption (BC) rates were obtained from dark incubations and with different methods. Moreover, as demonstrated in Chapter 5, once-a-day sampling can cause underestimation or overestimation of daily GP and BC if diel variability patterns are ignored. We will first try to address these methodological issues and their impact on the observed patterns, and will conclude with a general model of oceanic DMS(P) cycling.

6.7.1 Are there methodological differences between methods used to measure gross DMS production and bacterial DMS consumption?

As discussed by Saló et al. (2010), chosing the inhibitor or the radiotracer (Kiene and Linn, 2000) method may depend on whether the focus is on DMS production or consumption. In the inhibitor approach, a seawater sample is amended with a compound that inhibits bacterial DMS consumption and incubated for several hours, usually 8 – 24, so that the rate of DMS accumulation over time renders GP. Net biological DMS production is obtained from parallel unamended incubations, and the difference between both rates renders bacterial DMS consumption (BC). In the seminal paper by (Kiene and Bates, 1990) chloroform was the inhibitor used. However, chloroform was shown to cause release of DMSP and thus overestimation of GP and BC (Wolfe and Kiene, 1993a; Simó et al., 2000). Subsequent studies suggested that methyl-butyl ether (MBE; Visscher and Taylor (1993)), dimethyldisulfide (DMDS), or dimethylselenide (DMSe; Simó et al. (2000)) provided more realistic estimates, and MBE (at 30 μmol L^{-1}) and DMDS (at 200 nmol L^{-1}) have since become the inhibitors of choice. Another concern raised by the inhibitor technique relates to the inhibition efficiency. Although total inhibition is not achievable on theoretical grounds, the underestimation of GP might well lay within the measurement error interval if the inhibitor:DMS molar ratio is high enough. Decrease of the inhibition efficiency with time has been reported in a few occasions (van Duyl, 1998; Simó et al., 2000). However, there is a larger number of incubations, done in extremely different environments, where inhibition was shown to hold for longer than 24 h (Wolfe et al., 1999; Galí and Simó, 2010; Galí et al., 2011).

To answer the question posed at the beginning of this section we performed a three-way ANOVA, where the factors *method*, *PFT* and *domain* were hypothesized to affect k_{GP} and k_{BC}. Models with two-factor interactions could not be evaluated, since some terms were not full-rank. The four methods considered were *inhibitor-DMDS*, *inhibitor-chloroform*, *inhibitor-MBE* and *budgeting* (for k_{GP}) or *radiotracer* (for k_{BC}); the four PFTs were those explained in previous sections; and the *coastal/shelf* and *oceanic* areas were considered as the two domains. It has to be noted that this ANOVA might suffer from heteroscedasticity (non-homogeneity of the variance) and by the unbalanced number of observations in each group. In addition, the fact the measurements were done with different methods in different regions and times of the year may confound the interpretation. We performed the ANOVA on different subsets, the *samples* and the *means*, and on untransformed and log-transformed data. Among the different combinations, the log-transformed means subset was the only where the variances of the different groups were homogeneous enough, as indicated by Bartlett's test $p > 0.05$.

The ANOVA results did not allow us to conclude whether different methods rendered significantly different k_{GP}'s (Table 6.5, SI). None of the three factors had significant effects ($p > 0.3$), although a larger fraction of the variance, as indicated by the sum of squares, was associated with both method and PFT factors. Nevertheless, mean DMS turnover (k_{GP}) was on average 30% smaller when determined by budgeting compared to the global average of the three inhibitors. Note that most budgeting studies were based on ^{35}S-DMS radiotracer loss rates. The ANOVA of k_{BC}'s indicated that both method ($p = 0.0008$) and domain ($p = 0.014$) had significant effects (Table 6.6, SI). Mean k_{BC}'s were 35% smaller in radiotracer studies compared to inhibitor studies, and 40% slower DMS consumption was found in oceanic areas compared to shelf areas.

Thus, a tendency seems to exist towards measuring slightly faster DMS production and consumption with the inhibitor methods. This tendency can be directly examined in a couple of studies where DMDS inhibition and radiotracer-based budgeting were used simultaneously, both done in the Sargasso Sea. In the first case (R/V Oceanus, April 2002), k_{GP} was on average 30 ± 17% smaller when determined with radiotracer. In the second study (R/V Seward Johson, July-August 2004), k_{GP} was 66% smaller when determined with radiotracer on the same samples (pre-dawn, 04:00 local time). In the latter study, however, GP and BC rates exhibited a marked variability when measured with DMDS inhibition over a diel cycle (SARGsum diel cycle in Chapter 4). We can also examine how well compared the DMDS GP measurements done on the pre-dawn samples to those done over a diel cycle in the (RV/ Seward Johnson

study). In this case, we observed no obvious difference between the average of 8 incubations over a diel cycle (0.83 d^{-1}) and the GP measured daily during the previous 6 days (0.75 ± 0.10 d^{-1}). The diel cycle DMDS incubations lasted ca. 6 h, whereas the daily incubations lasted about 12-15 h. These comparisons lead us to the conclusion that longer incubation times may be integrating a portion of the diel variability which is intrinsic to the samples (as they were incubated in the dark). On the other hand, radiotracer incubations are arguably more precise and, due to the shorter incubation time, may suffer less from bottle effects. However, if not performed with sufficient temporal resolution over the diel cycle, may cause significant bias in the estimation of daily BC and budget-derived daily GP.

6.7.2 Factors regulating gross DMS production (GP)

So far, we have discussed about DMS production patterns deduced from dark incubations. However, in Chapters 3 and 4 we have demonstrated that GP is irradiance dose-dependent when measured in static incubations. In Chapter 4 we have shown that this dependence can be modified by vertical motion, presumably because the cells spend sufficient time in conditions that allow recovery and photorepair from UV-inflicted damage, and/or not enough time in subsurface waters to accumulate irreversible damage. These findings indicate that in summer stratified waters stress mechanisms may prevail (Chapter 5). Moreover, the results from Chapter 5 reconcile the order-of-magnitude difference found between short-term (hours, Chapter 3 and 4) and long-term (one day, Chapter 2) sunlight-induced GP stimulation. We place our highest estimate of daily radiation-driven stimulation of GP at 30 – 40%, while the lowest estimate may approach 0 in deep actively-mixing layers. It is important to note that reproducing a realistic light exposure in incubations, which requires taking into account the radiation exposure history of the sample (Chapter 3), is crucial to obtain realistic GP rates. In many occasions, stimulation may lay within the error intervals of GP measurements. However, the stimulation effect may be seasonally and regionally large, which underlines the need for improving current methodologies. We would like to note that stress-driven GP likely occurs in summer paradox regions but also at higher latitudes, where stratification is promoted by mesoscale structures (e.g. eddies; Mahadevan et al. (2012) or by ice melt (Chapter 1). However, in high planktonic biomass conditions typical of higher latitudes, the stratification effect caused by phytoplankton heat dissipation (Manizza et al., 2005) may be offset by the diminished water transparency due to phytoplankton themselves.

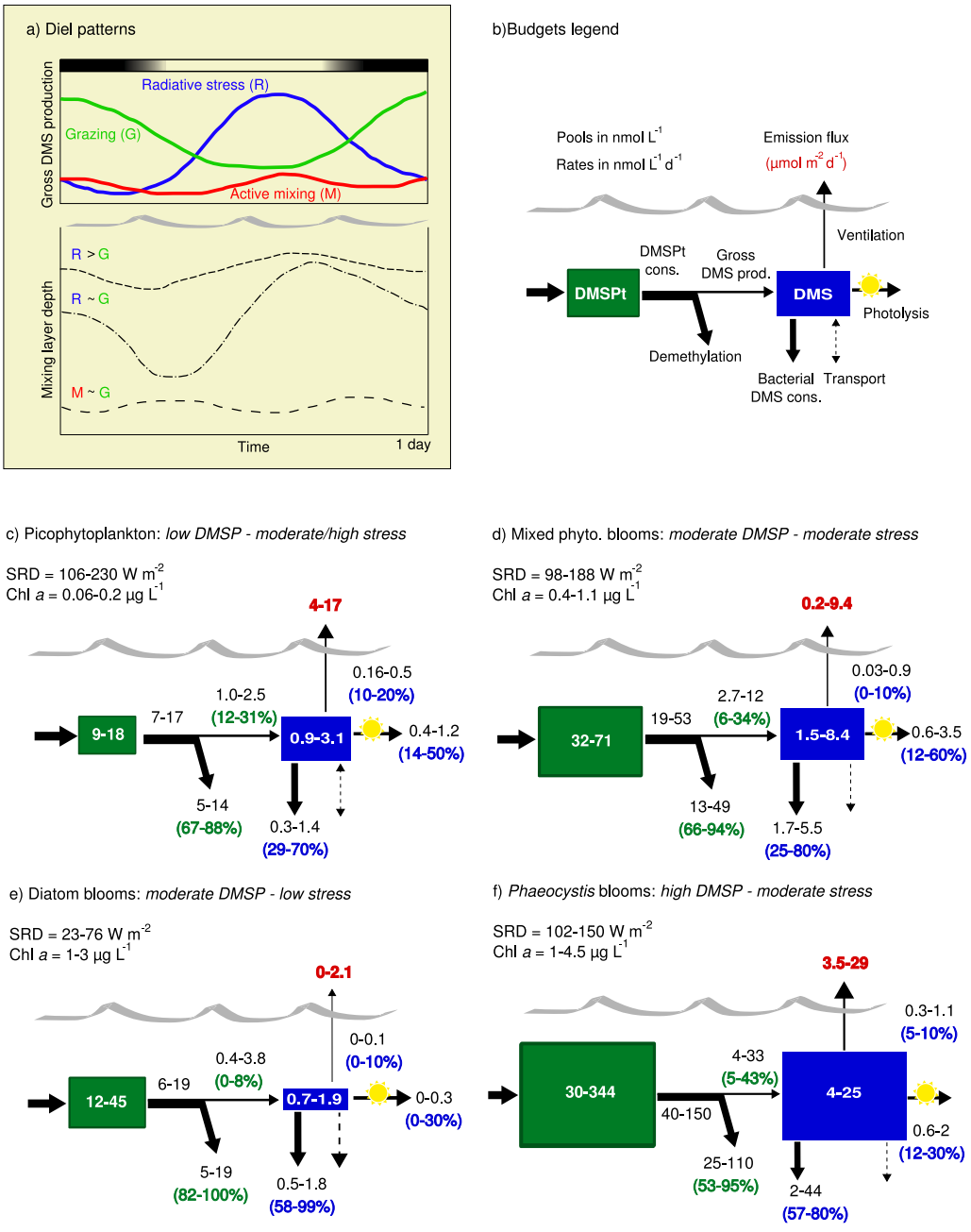

Figure 6.6: **Statistically-deduced DMS budgets in different microbial communities (defined by the Phytoplankton Functional Types)** - (A) proposed diel patterns of gross DMS production, according to mixing regime and the dominant effect of grazing, radiative stress, or 'background' DMS production. (B – F), DMS budgets in different PFTs. The ranges are the 25 – 75% quantiles.

Microzooplankton grazing appears as another key factor controlling GP (Archer et al., 2001; Saló et al., 2010). Since DMSP cleavage enzymes are isolated from their substrate in some phytoplankton species (Wolfe and Steinke, 1996), cell disruption may sometimes be a prerequisite for DMS production. The other food-web process causing cell disruption, viral lysis, is thought to contribute relatively less than grazing to DMS production (Evans et al., 2007). According to the observations made in Chapter 5, grazing may be particularly important under conditions of moderate to low radiative stress. Protist microzooplankton grazers are characterized by sharing similar sizes and growth rates with their prey, which allows them to readily exploit blooming pico- and nanophytoplankton. It is believed that most primary production is consumed by micrograzers due to this tight coupling (Calbet and Landry, 2004), which would also explain why blooms are generally formed by large phytoplankton populations superimposed on a background of small phytoplankton (Li, 2002). Colonial *Phaeocystis* blooms are probably the most relevant exception, as micrograzers do not seem to feed efficiently on large colonies (Schoemann et al., 2005). It has been hypothesized that mixing can disrupt the coupling between phytoplankton prey and micrograzers by diluting the community thereby decreasing encounter rates. This mechanism can be important only if mixing entrains waters with smaller predator and prey abundance into the UML (Behrenfeld, 2010).

In Figure 6A, we propose a conceptual scheme relating vertical mixing and the occurrence of stress- and grazing-dominated GP. Unfortunately, too little is known yet on the interaction between radiative stress and grazing to predict even its sign. This interaction is related to a controversial question in plankton ecology: could UVR-induced damage be the main cause of phytoplankton mortality in highly irradiated waters, as suggested by some studies (Llabrés et al., 2010)? Or even: could UVR promote grazing on phytoplankton cells that have damaged (and leaky) cell membranes, by enhancing chemotactic behavior of microzooplankton? In any case, there is a need for a better knowledge of how UVR modulates microbial interactions (Sommaruga, 2003).

6.7.3 Factors regulating bacterial DMS consumption (BC)

Bacterial DMS consumption is generally found to be tightly coupled to GP (Simó, 2004). Indeed, GP and DMS, in this order, are the best predictors of BC, although there is considerable scatter in these relationships (Fig. 6.7). With the inhibitor method, BC rates and GP rates are methodologically correlated, since BC is calculated as the difference between GP and net biological DMS production. However, there are indications that the strong correlation generally

found between GP and BC is not an artifact. For example, in Chapter 1 we showed that GP and BC became uncoupled in the Arctic summer only in the shallowest mixed layers, and attributed this observation to bacterial photoinhibition. Strong photoinhibiton of BC has been measured in samples exposed to subsurface irradiance (Toole et al., 2006; Kieber et al., 2007). In the binned data scatterplots, lowest k_{BC} occur at high SRDs (Fig. 6.8). It should be noted that these relationships arise from dark incubations, which implies that bacterial DMS consumers do not recover completely from photoinhibition in incubations that last several hours. Possibly, even clearer trends would be observed if the BC rates were representative of the average daily photoinhibiton. The dynamic response of BC photoinhibiton to light deserves further exploration.

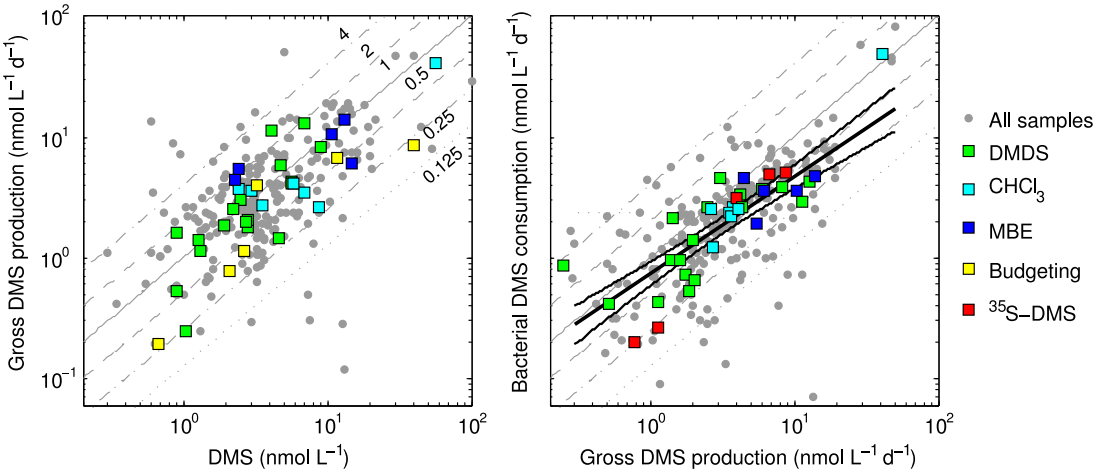

Figure 6.7: **Coupling between biological DMS consumption and production** - (A) relationship between gross DMS production and DMS concentration, and (B) bacterial DMS consumption and gross DMS production. Straight gray lines on the background represent equal turnover lines (d^{-1}). Regression lines and the slope error intervals corresond to the gray dots (*samples* subset).

It has been suggested that enzyme kinetics may limit bacterial DMS consumption (Wolfe and Kiene, 1993b), thereby explaining DMS build-up in blooms of strong DMS producers. For instance, del Valle et al. (2009) found saturation to occur at around 25 nmol DMS L^{-1} in the Ross Sea *Phaeocystis* bloom, and other studies in warmer waters also report saturations at 10 to 30 nmol DMS L^{-1} (Kiene and Service, 1991; Wolfe and Kiene, 1993b; Ledyard and Dacey, 1996; Wolfe et al., 1999). These were determined by DMS additions to incubations, and therefore represent assessments of the rapid response of DMS consumers to DMS pulses. We evaluated whether these kinetic observations are reflected in general patterns of BC, by regressing BC

rates against GP rates. In a log-log regression of the form $log(BC) = a + b(log(BC))$, a slope smaller than 1 would indicate that, as GP increases, BC increases proportionally less. In the samples subset, with DMS concentrations up to 50 nmol L^{-1}, we found a slope of 0.80 ± 0.11 (95% confidence interval, CI). Using a robust regression algorithm instead of ordinary least squares yielded a slope of 0.92 (standard error = 0.04). However, when the same analysis was performed on the means subset, we did not find a significant trend, with slopes of 0.84 (CI of ± 0.19) and 0.98 (standard error = 0.09) using ordinary least squares and robust regression, respectively. Therefore, there is subtle yet inconclusive evidence that bacterial DMS consumers contribute proportionally less to DMS removal at very high DMS concentrations, which seldom occur in open ocean environments.

Further insight into biological DMS removal dynamics can be obtained by looking at the temporal evolution of k_{BC} during the development and decline of blooms. Microcosm experiments indicate that bacterial DMS consumers respond with a time lag of few days or even longer to a sudden increase in DMS production (Zubkov et al., 2004; Pinhassi et al., 2005). In the Ross Sea, del Valle et al. (2009) found that k_{BC} lagged by a few weeks the rise in DMS production. A less clear increase of k_{BC}, lagging the pulse of DMS production by almost two weeks, was observed in an iron fertilization experiment (Merzouk et al., 2006). In the latter example, highest k_{BC} occurred simultaneously with the replacement of nanophytoplankton by diatoms as dominant phytoplankton. Studies conducted in recent years suggest that bacterial DMS oxidation is carried out by diverse bacteria with different metabolic capabilities. While only very specialized methylotrophs are able to grow on DMS as the sole substrate (Vila-Costa et al., 2006a; Schäfer, 2007), a wider array of taxa might be able to derive energy from DMS oxidation provided they have an alternative carbon source (Vila-Costa et al., 2006a; Green et al., 2011; Hatton et al., 2012). Labile carbon in the open ocean is thought to derive mostly from phytoplankton and grazer activity. If co-metabolic DMS oxidation prevails in the upper ocean, we can speculate that changes in phytoplankton community structure, phytoplankton exudation, grazing activity, and other factors causing cell lysis like viral attack and UVR-induced cell death, will entail temporal and spatial variations in bacterial DMS consumption. The diel cycles of bacterial DMS consumption observed in Chapter 5 point to this direction.

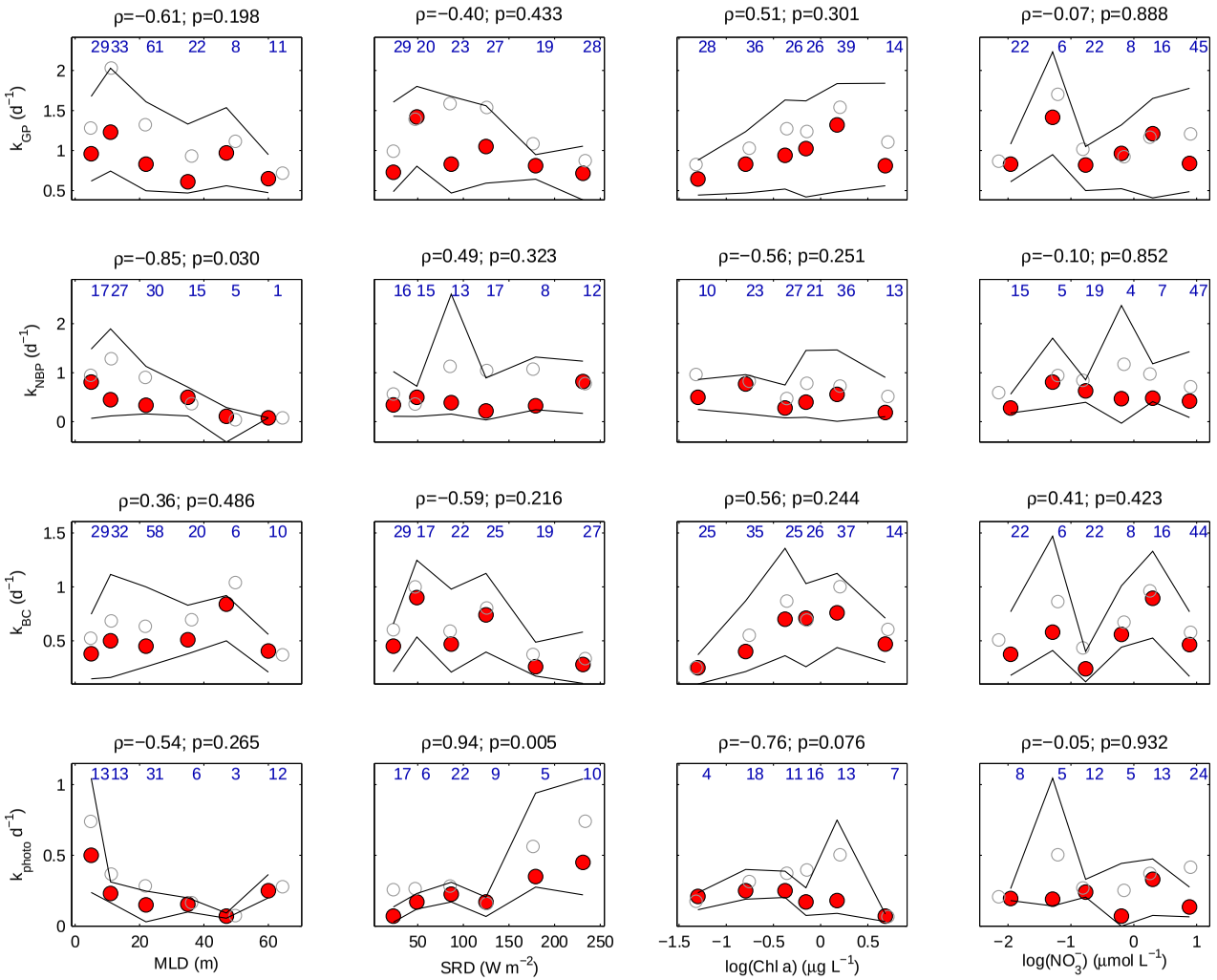

Figure 6.8: **Binned data scatterplots of DMS cycling against environmental variables** - As Fig. 6.5, but for DMS k's.

6.7.4 Factors regulating DMS photolysis

DMS photolysis is a photosensitized process, which means that DMS cannot absorb actinic radiation itself, but reacts with the oxidants produced by other photoreactive compounds known as photosensitizers (chiefly, CDOM and nitrate). Due to its spectral dependence, which is well approximated by a negative exponential (Toole et al., 2003; Bouillon, 2004; Deal et al., 2005), the decrease of photolysis with depth is driven by the attenuation of UVR (Toole et al., 2003). The spectral peak of DMS photolysis will occur at longer wavelengths as we move deeper in the water column, because shortwave UV wavelengths are attenuated faster than longwave UV. Since UVR attenuates within the few meters to tens of meters of the water column, the weight of photolysis on DMS budgets will decrease with increasing mixing depths. These general patterns are reflected in the binned data scatterplot as a positive correlation between SRD and k_{photo} (Fig. 6.8).

When it comes to predict the spatio-temporal variability of DMS photolysis, the time-based k_{photo} allows only a very crude understanding of the chemical processes that drive it. Some studies have shown that nitrate can promote DMS photolysis in a concentration dependent manner (Bouillon, 2004; Toole and Siegel, 2004). However, DMS photolysis quantum yields appear to be highly variable, even at the same nitrate concentration (Toole and Siegel, 2004), which indicates that differences in the chemical composition and photoreactivity of the CDOM pool probably have a bigger effect on DMS photolysis efficiency. To evaluate this variability, we collected all the DMS photolysis rate constants ($time^{-1}$) we were able to find in the literature and normalized them to the corresponding total shortwave irradiance (W m^{-2}) at the water subsurface (which was deduced as outlined in section 6.4 when necessary). In this approach, we assumed that total shortwave irradiance (typically measured by pyranometers, 300-3000 nm) was linearly related, across latitudes, to the spectral irradiance in the UV range at the water subsurface. This assumption carries an acceptable error, although the relationship between broadband irradiance and specific bands is affected by changes in atmospheric radiative transfer, which mainly depends on atmospheric pathlength and total ozone column. Due to spectral variations in UV attenuation, such relationship would not hold deeper in the water column, or when comparing different radiation bands vertically integrated in the UML. A further assumption was that different measurement techniques (i.e. ^{35}S-DMS radiotracer or bulk DMS), filtration procedures (0.7 μm nominal cutoff glass fiber filters and 0.2 μm pore filters), and incubation vessels (quartz or teflon) yielded comparable results. Previous tests indicate that these assumptions carry an error $< 30\%$ (Kieber et al., 1996; Toole and Siegel, 2004, Galí,

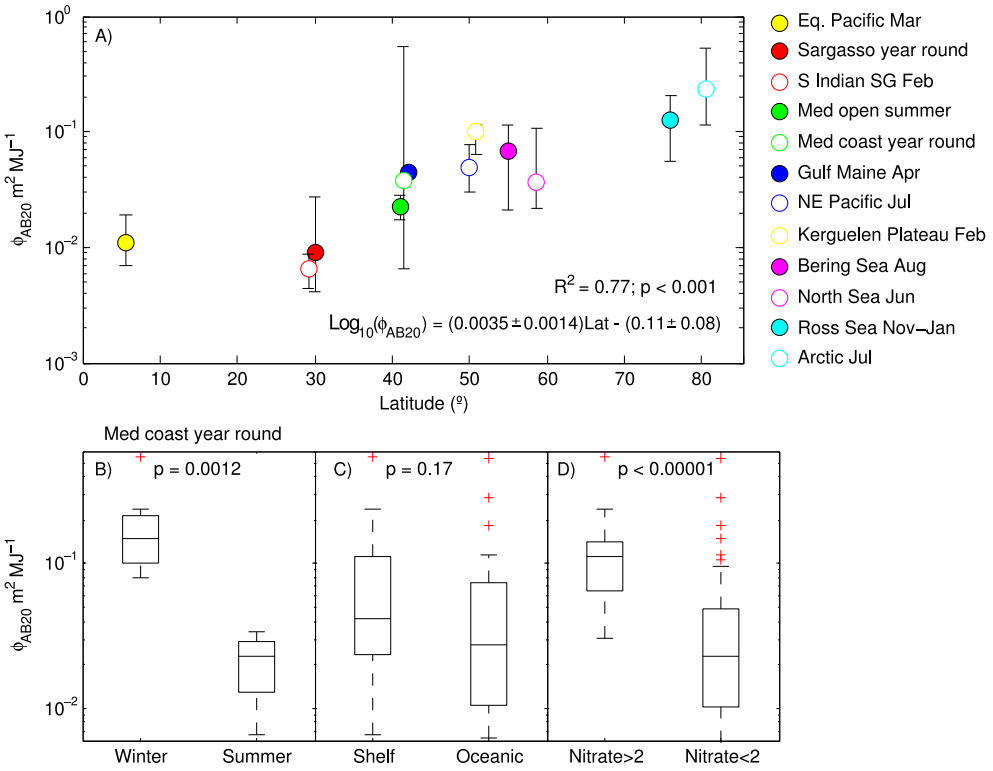

Figure 6.9: **Latitudinal, spatial and temporal trends in apparent quantum yields of DMS photolysis** - (A) Latitudinal trend (data from the equatorial region excluded); and comparison between (B) winter and summertime in the northwest Mediterranean, (C) shelf and oceanic locations at latitudes ¡ 60°, and (D) samples containing nitrate concentrations higher or lower than 2 μmol L^{-1}.

unpublished). Finally, we also assumed that photolysis was dose dependent, i.e., that k_{photo} did not decrease as the irradiation progressed (the so-called reciprocity assumption). Reciprocity was confirmed in irradiations spanning a time period relevant to our analysis (e.g. the central 8 h of the day) in highly irradiated Mediterranean waters (Chapter 4), although it might not hold when irradiating less photobleached CDOM. A temperature correction factor was applied, assuming the temperature dependence found by (Toole et al., 2003), so that all photolysis rate constants were normalized to 20°C. After the appropriate unit conversions, we obtained what we will call the 'apparent broadband quantum yields', $\phi_{AB,20}$,in units of m^2 MJ^{-1}.

$\phi_{AB,20}$ varied over two orders of magnitude and displayed a clear latitudinal gradient, with an exponential increase found between 30 and 80 degrees ($R^2 = 0.77$; $p < 0.001$; $n = 11$) (Fig. 6.8A). As expected, the latitudinal trend seemed to break between tropical and equatorial latitudes, likely due to equatorial upwelling. We also evaluated the effect of other sources of

variability in $\phi_{AB,20}$: seasonality, coastal-open ocean gradients, and nitrate concentration. The effect of seasonality could be evaluated only at two locations: the Sargasso Sea and the coastal NW Mediterranean. In the Sargasso, $\phi_{AB,20}$ increased by approximately 3-fold from summer to winter. In the coastal NW Mediterranean, a 7-fold increase was found between summer (May to September) and winter (October to April) (Fig. 6.8B). However, this wider seasonality was partly due to a higher degree of continental influence in winter (Vila-reixach et al., 2012). These differences remained significant when no temperature normalization was applied. When we split the dataset between shelf and oceanic locations (excluding polar seas), we found 1.5-fold higher median $\phi_{AB,20}$ on continental shelves (although not significantly; Fig. 6.8C). The gradients we observed are consistent with latitudinal trends in CDOM optical properties (Siegel, 2002; Nelson et al., 2007), as well as coastal-open ocean gradients, which are exacerbated at the cores of the subtropical gryes. We attribute the gradients in $\phi_{AB,20}$ to changes in CDOM photoreactivity caused by photobleaching of autocthonous and terrigenous CDOM (Vahatalo, 2004), shaped by solar irradiance, water transparency and stratification (Del Vecchio, 2002).

The median $\phi_{AB,20}$ of the subset of samples containing $> 2\mu$mol NO_3^- L^{-1} was 5-fold that of the samples with nitrate < 2 (Fig. 6.8D), clearly supporting the role of nitrate as photosensitizer. However, nitrate could not explain the latitudinal gradient, since samples containing very different nitrate concentrations exhibited similar $\phi_{AB,20}$. The clearest example of this was found by examining the differences between $\phi_{AB,20}$ in Antarctic waters (15-29 μmol NO_3^- L^{-1}), which are not affected by continental runoff , and Arctic waters (< 1 μmol NO$_3$extsuperscript- L^{-1}), which are characterized by a strong influence of Arctic river outflow carrying highly colored and photoreactive CDOM (Bélanger et al., 2006). As expected, $\phi_{AB,20}$ was higher in the Fram Strait area (Arctic), with 0.28 ± 0.18 m^2 MJ^{-1}, than in the Ross Sea (Antarctica), with 0.13 ± 0.04 m^2 MJ^{-1}. Furthermore, Arctic stations classified as Polar Surface Water had higher $\phi_{AB,20}$ (0.29-0.54 m^2 MJ^{-1}) than those classified as Atlantic Water (0.11-0.19 m^2 MJ^{-1}) (Galí and Simó, 2010), the latter having potentially less continental influence (Hansell et al., 2004). A similar example was found at lower latitudes (50-60^o): similar $\phi_{AB,20}$ were found on the Kerguelen Plateau (21.5 μmol NO_3^- L^{-1}), in the NE Pacific (3-10 μmol NO_3^- L^{-1}), Bering Sea (1-4.5 μmol NO_3^- L^{-1}) and the North Sea (< 1 μmol NO$_3$extsuperscript- L^{-1}). This strongly suggests that CDOM quality is the primary factor determining DMS photolysis efficiency (as noted by Toole and Siegel (2004)), and leaves nitrate with a secondary role.

6.7.5 Factors regulating DMS transport and sea-air flux

. The UML may export or import DMS from/to the waters underneath depending on the DMS gradient through the pycnocline and the vertical turbulent diffusivity. When a sub-pycnocline DMS peak exists, like in summertime Sargasso Sea profiles (Dacey et al., 1998), the UML will receive a net input. This situation may occur in other regions with shallow stratification and a much deeper euphotic layers. On the contrary, the sub-pycnocline layer will probably act as a DMS sink in more deeply mixed waters, where the highest DMS concentrations occur in the UML (e.g., del Valle et al. (2009); Archer et al. (2010a). Estimates of vertical DMS transport generally agree in that vertical DMS transport is negligible compared to the other budget terms. Still, we underline the need of better constraining vertical DMS fluxes by means of actual measurements of turbulent diffusivity and fine-scale DMS gradients in distinct ocean settings. This task could be facilitated by high resolution DMS analytical systems (Tortell, 2005; Saltzman et al., 2009) used in profiling mode, for instance, by pumping seawater from different depths.

Similarly, subsurface DMS gradients appear as a potential factor biasing estimates of the sea-air DMS flux. Although it is common practice to calculate sea-air flux using parameterizations based on wind speed and DMS concentration at 'surface' depths ranging from 3 m down to 10 m, some studies have shown that pronounced gradients develop in the first centimeters of the water subsurface during calm conditions (Chapter 1; Zemmelink et al. (2005)). Such gradients may add uncertainty to the inherently uncertain sea-air flux parameterizations, and may bias direct gas transfer measurements (Marandino et al., 2008).

Finally, it is crucial to define the right mixed or mixing layer or, in other words, to identify the processes and timescales that are relevant to each depth horizon. The impact of DMS transport on UML budgets will change significantly depending on the thickness of the layer where these fluxes are shared. For example, Bailey et al. (2008) found that diurnal cycles of stratification and convection periodically entrained DMS from the pycnocline to the UML. This flux was one order of magnitude higher than turbulent diffusion, and therefore able to cause a significant bias to the budgets if the sampling scheme had missed it. High resolution DMS measurements should help detect DMS transport pulses and quantify their importance.

6.7.6 Upper mixed layer DMS budgets: the DMS buffer

Fig. 6.6C-F provides a clear example that very similar DMS budgets can be found in contrasting oceanic ecosystems. As suggested by previous studies and reviews (Simó, 2004), BC is the main

DMS sink in the UML and, as a consequence, has more potential to influence DMS budgets than photolysis, ventilation, and vertical transport. The meta-analysis supports the hypothesis that solar radiation is the major factor producing uncoupling between *GP* and BC. Bacterial photoinhibition combined with UVR-driven stimulation of *GP* enhances net biological DMS production (Chapter 3). However, as solar exposure increases, photolysis can compete with *BC* as the main DMS sink (Fig. 6.8), at the same time that atmospheric ventilation increases due to shallower stratification. As pointed out in Chapters 1 and 5, the alternation between dominant DMS sinks dampens DMS oscillations at the timescale associated with meteorological variability (hours to several days). In fact, DMS undergoes larger fluctuations in 12 h periods than on a daily time frame (Fig. 6.10).

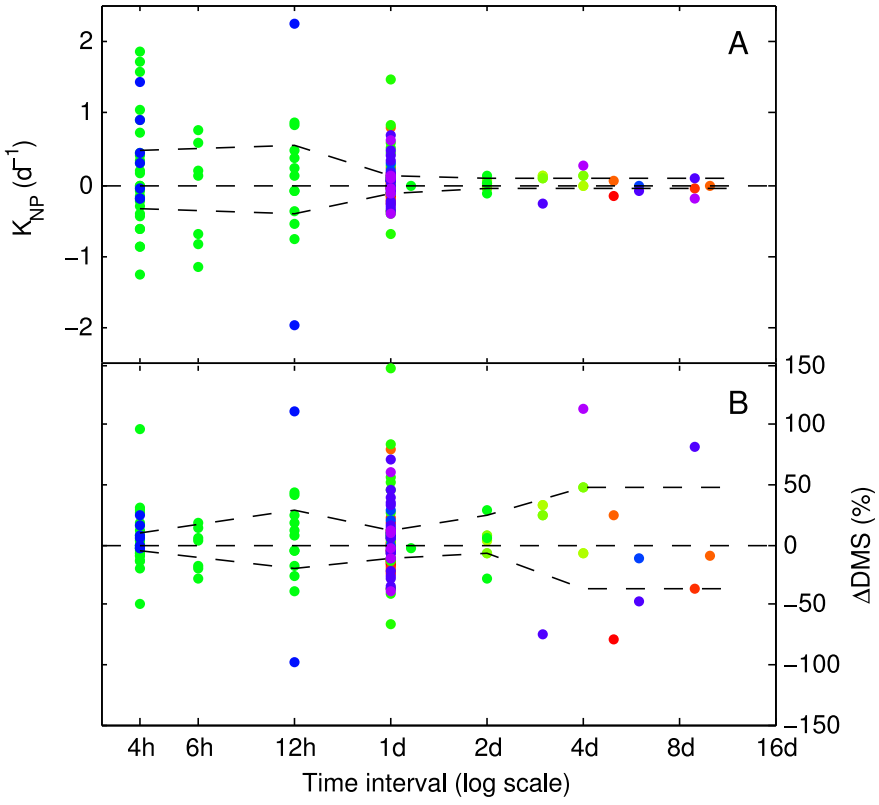

Figure 6.10: **Fluctuations of DMS at different temporal scales** - (A) net DMS production rate constant, (B) % net DMS change. Color coding indicates different studies. Dashed lines indicate the 25 - 75% quantiles, which help to appreciate the real variability.

Besides the short-term buffering effects, other buffer mechanisms (also due to solar radiation and the associated stratification) operate seasonally or across latitudes. For example,

the highest photolysis yields per radiation unit occur in the coldest and less irradiated waters, whereas in the cores of subtropical gyres low photochemical yields counteract the strong irradiation (Fig. 6.9). It is worth noting that nitrate, rather than buffering DMS dynamics, tends to exacerbate seasonal and spatial DMS gradients by promoting DMS photolysis and the growth of weak DMS(P) producers (diatoms). However, the high biomass attained in diatom blooms may counteract the low DMS yields and high DMS photolysis rates. Besides, high nitrate in stratified waters may promote *Phaeocystis* blooms, in which case nitrate acts as buffer too. The overall result of the several feedbacks and buffer mechanisms is that DMS turnover occurs in a narrow time frame (Tables 6.1 and 6.3), with a mean turnover time of 1.1 d and 95% confidence bounds at 0.25 and 4.5 d (deduced from fitting $\ln(k_{GP})$ with a logistic distribution).

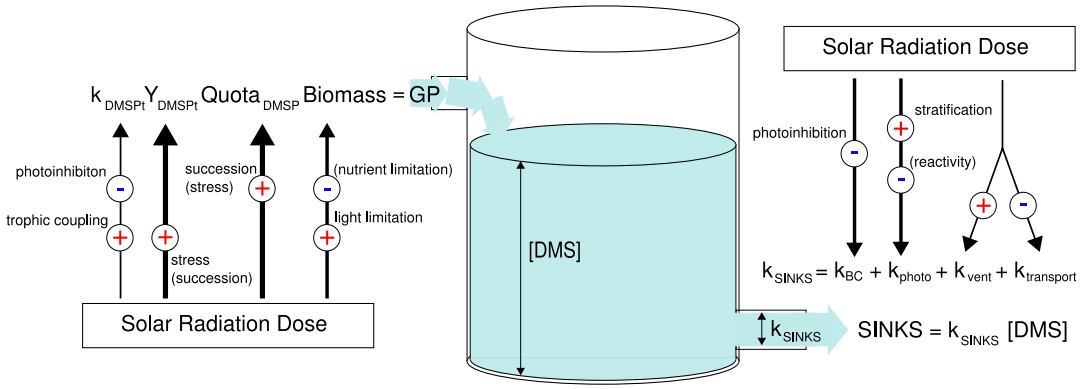

Figure 6.11: **Hydrodynamic analogy to explain how DMS concentrations are regulated. Short-term steady states result from forcing factors acting at the seasonal to diel time scale** - See text for a detailed description and interpretation.

So, if DMS concentrations do not undergo dramatic changes in the short term, why DMS generally increases into summer and overall shows such a marked seasonal pattern (Dacey et al., 1998; Simó and Pedrós-Alió, 1999a; Vila-Costa et al., 2008; Lana et al., 2012)? Since the k of total DMS loss (k_{LOSS}) has limited capacity of regulating DMS concentrations, we argue that the response is to be found in gross DMS production, as illustrated with the hydrodynamics analogy in Fig. 6.11. DMS concentrations (the fluid level in the bucket) depend on the dynamic balance between sources (GP) and losses (sum of the sinks). The discharge at the outlet ($LOSS = k_{LOSS}[DMS]$) depends on the diameter of the outlet tube (k_{LOSS}) and the pressure produced by the height of the fluid ('DMS level'). If the outlet tube has a fixed diameter, the discharge will depend entirely on the height of the fluid. If an increase in the inlet discharge

Table 6.4: Example of how the short-term steady state DMS is modulated by an increase in solar radiation dose (SRD). Realistic values of the factors contributing to DMS production and DMS consumption have been used. Chl *a* in μg L^{-1}; DMS and DMSPt in nmol L^{-1}; *k*'s in d^{-1}.

Variable	@ SRD = 100 W^{-2}	Fraction (%)	Factor	@ SRD = 200 W^{-2}	Fraction
Chl *a* (μg L_{-1})	0.5		0.2	0.1	
DMSPt:Chl *a*	30		3	150	
k_{DMSPt}	0.8		1	0.8	
Y_{DMSPt}	0.08		3	0.24	
GP	**0.9**			**2.8**	
k_{BC}	0.55	69	0.65	0.36	49
k_{photo}	0.19	24	1.5	0.29	39
k_{vent}	0 .06	8	1.5	0.09	12
k_{LOSS}	0.80	100		0.73	100
Steady state DMS	**1.2**			**3.8**	

(GP) forces the steady state, the height of the fluid will increase until it exerts sufficient pressure to cause a discharge through the outlet equivalent to the new GP. The opposite response will occur when the inlet discharge (GP) decreases. An what regulates GP? We can represent it as the product of phytoplankton biomass, their average DMSP quota, the k of DMSPt consumption (k_{DMSPt}) and the DMS yield from consumed DMSPt (Y_{DMSPt}). Each of these factors exhibits a different response to solar radiation and its indirect effects caused by stratification. But, if the overall response of GP to an increase in solar exposure is stronger than that of the k_{LOSS}, GP will be the main factor controlling the 'DMS level', as illustrated by the calculations in Table 6.4.

In other words, as the seasons progress from winter to summer with an increase in sunlight exposure: (a) GP rates (bucket inflow rates) increase by the concurrence of succession to stronger DMSP-producers and physiological stress, while (b) the constant rate of total DMS loss (bucket outlet section) remains relatively steady by the buffering interplay among BC, photolysis and, to a lesser extent, ventilation. As a result, DMS concentration (fluid level in the bucket) increases. The opposite occurs as the seasons progress back into winter.

6.8 Recommendations for future oceanic DMS(P,O) cycling studies

Based on the results of this meta-analysis and on recent advances in marine biogeochemistry we can identify a few research questions for the years (or decades) to come:

- Will the changes in upper ocean stratification, warming, and acidification, affect plankton biogeography, and thus productivity regimes and dimethylated sulfur cycling?
- Will the changes in (C)DOM inputs (terrestrial and autochtonous), combined with changes in ocean stratification and circulation, entail changes in their microbial and photochemical processing? Will this translate into altered UV transparency of surface waters, thereby modifying UV-mediated processes, and change the photoreactivity of CDOM?
- Will the changes in sea-ice extent and thickness in polar oceans turn them into stronger or weaker DMS producers?

Answering these questions may be facilitated by improving the design and spatio-temporal coverage of observational studies that will inform the next generation of models.

6.8.1 Observational studies

The burst of 'omics' approaches is shedding light into the evolutionary and biochemical complexities of DMS(P) cycling. However, in what concerns quantitative assessment of biogeochemical processes, it is currently no more than promising. In our view, the simultaneous assessment of the functional diversity of the microbial community and the bulk rates of DMS(P,O) cycling in different oceanic settings would enhance our predictive capacity. The combination of developing isotope tracer methods (Asher et al., 2011; Oduro et al., 2012) with molecular and 'omics' approaches will surely yield new insights in the near future.

Although bulk methods are not well suited for resolving the microscale intricacies of DMS production, they provide robust estimates of ecosystem-level processes, which are badly needed for parameterizing or fine-tuning the models. Based on the meta-analysis and the findings reported in previous chapters we can make the following recommendations:

- *Constraining DMSP synthesis.* There is limited knowledge of the response of DMSP synthesis to environmental stress, particularly UVR. Direct measurements of gross DMSP production (Stefels et al., 2009) will help constrain it.

- *Understanding particulate DMSP cycling.* A better understanding of what regulates the turnover of the whole DMSP pool is needed. Dilution experiments, though time and water consuming, appear as a reliable method for the simultaneous assessment of the turnover of phytoplankton biomass and the DMSP-producing populations due to grazing (Archer et al., 2001; Saló et al., 2010). Measuring total DMSPt consumption by the net loss-curve method (Simó et al., 2000) appears both as a complement and as a simple substitute when grazing experiments cannot be performed.

- *Disentangling dissolved vs. particulate DMS production.* There is an astonishing scarcity of studies where the turnover k's of dissolved and total DMSP and the corresponding DMS yields are simultaneously assessed. Though operational, the distinction between the dissolved vs. particulate (or dissolved vs. total) pathways for DMS production seems to have an ecological meaning which needs to be disentangled.

- *Constraining DMS cycling.* To better characterize DMS cycling and its response to sunlight, GP, BC, and DMS photolysis should be measured in different mixing regimes. The new generation of automated systems for DMS analysis opens up a new world of high spatio-temporal resolution description of DMS dynamics.

- *Resolving diel variability.* Diel variability in DMS and DMSP cycling must be taken into account, since it may often be as large as month-to-month variability.

- *Monitoring long-term trends.* More time-series studies are needed to understand the seasonal beat that generates most of the DMS(P,O) variability. Multi-year and multi-decadal time-series will be invaluable in the near future, even more if they are accompanied by an accurate description of meteorological forcing, underwater radiation climate, and the overall biogeochemical functioning.

- *Combining multiple approaches.* It is desirable that DMS(P,O) cycling rates are measured with more than one approach in each study. For example, GP can be simultaneously estimated with the inhibitor technique and by budgeting or diagnostic modeling.

- *Understanding DMSO cycling.* The possible dual role of DMSO in the dimethylated sulfur cycling, acting both as the product and the precursor of DMS, requires further research. While DMSO production by bacterial and photochemical DMS oxidation (Vila-Costa et al., 2006a; del Valle et al., 2007; Delvalle et al., 2009; Hatton et al., 2012) and algal

DMSP catabolism (Simó et al., 1998; Simó and Vila-Costa, 2006; Hatton and Wilson, 2007) is beginning to be understood, the same cannot be said about the fate of dissolved DMSO.

- *The very basics.* When describing DMS variability is the only goal, adding easy and inexpensive measurements of DMSPt and extracted Chl *a* will multiply the value of the DMS data and provide robust indicators of the actual cycling processes.

In the last decade the annual production of DMS(P,O) cycling process studies has oscillated between 3-8 studies per year (mean of ca. 5), with a worrying decline in the last few years compared to 2007-2008. Moreover, most of the papers have been produced by a few research groups. Meanwhile, modeling studies have maintained a stream of about 2.3 papers per year. Since models are no better than the data they rely upon, more comprehensive process studies are needed, particularly in areas like the equatorial belt, the southern ocean, and the rapidly changing polar ecosystems.

6.8.2 Model studies

Diagnostic DMS models already benefit from up-to-date climatologies of surface DMS, vertical mixing, nutrients, and meteorological forcing. Thus, our recommendations focus on prognostic models, aiming at improving current model representations of DMS(P) cycling but, equally important, at testing hypotheses.

- *Parameterize radiative (or oxidative) stress.* Reproducing the summer paradox requires decoupling DMS(P) dynamics from 'phytoplankton dynamics' (Le Clainche et al., 2010). We argue that this has to be achieved at two distinct levels: seasonal phytoplankton succession and daily radiative stress. The seasonal component can be simulated by means of the PFT approach (Vogt et al., 2010) and/or by modulating the average community DMSP quota (Vallina et al., 2008). Either approach is valid as far as it captures the natural variability. The daily stress component allows modulating DMS yields as a function of vertical mixing and irradiance, which may require resolving the diel variability or at least accounting for it.

- *Explicitly represent (heterotrophic) bacterial activity.* Our meta-analysis shows that bacterial DMSP consumption rates are more critical than bacterial yields in shaping the DMS production regimes. An explicit representation of the heterotrophic use of DMSP

and organic carbon, their physiological ties, and their modulation by sunlight, may help understand how the actual 'bacterial switch' operates. Recognizedly, this suffers from limited knowledge of the controls acting on osmoheterotrophic organisms (e.g. bottom-up vs. top-down control, amount of active vs. inactive bacteria, or bacterial growth efficiency).

- *Refine the parameterization of DMS photolysis.* In the sensitivity analysis carried out by Vogt et al. (2010), uncertainty in photolysis rates was the most critical factor affecting DMS budgets among the DMS sinks (production processes appeared to be even more important). The trends encountered in this meta-analysis, together with a more accurate representation of underwater irradiance fields, can be readily implemented in prognostic DMS models.

- *Optimize model outputs with known emerging properties.* Compounded state variables (DMS:Chl *a*, DMSPt:Chl *a*, DMS:DMSPt), process indicators (GP:DMSPt, *GP*:Chl *a*), and community yields show robust trends across ocean regimes. Likewise, the modes of variability identified by the PCA are ecologically meaningful. The models' ability to reproduce these patterns could show at a glance how well the model captures the complex network of underlying interactions.

6.9 Supplementary information

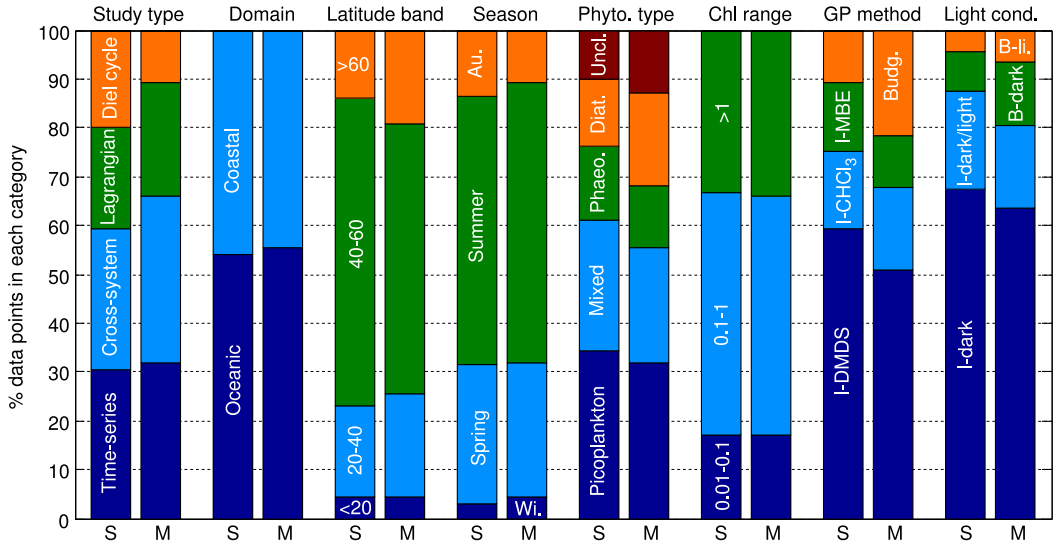

Figure 6.12: **Distribution of the data among predefined categories (SI)** - S stands for the *samples* and M for the *means* subset.

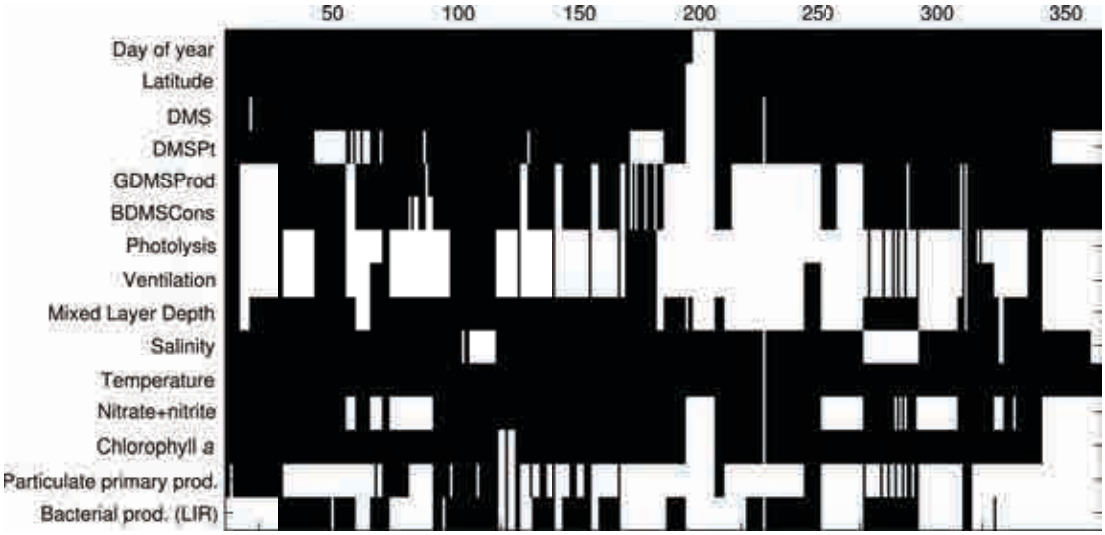

Figure 6.13: **Overlap between the variables included in the meta-analysis (SI)** - White areas indicate missing data (*means* subset).

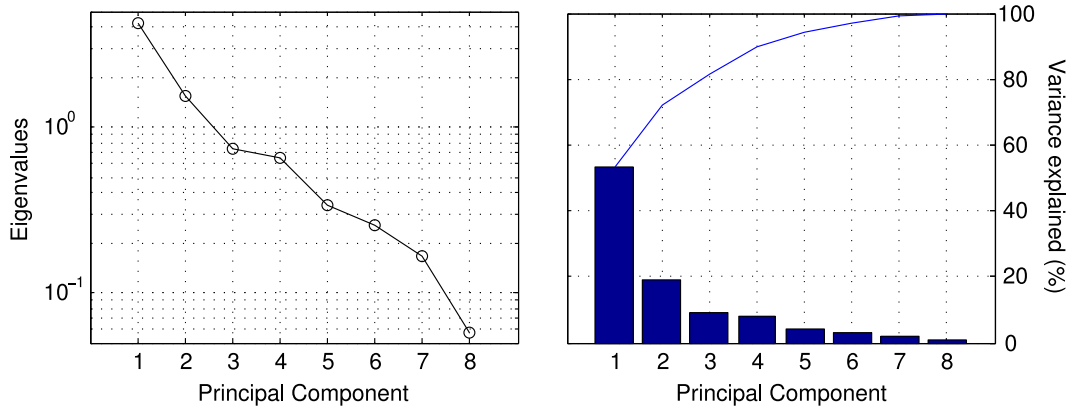

Figure 6.14: **Variance explained by the principal components (SI)** - Log-eigenvalue (left) and scree plot (right) of the PCA.

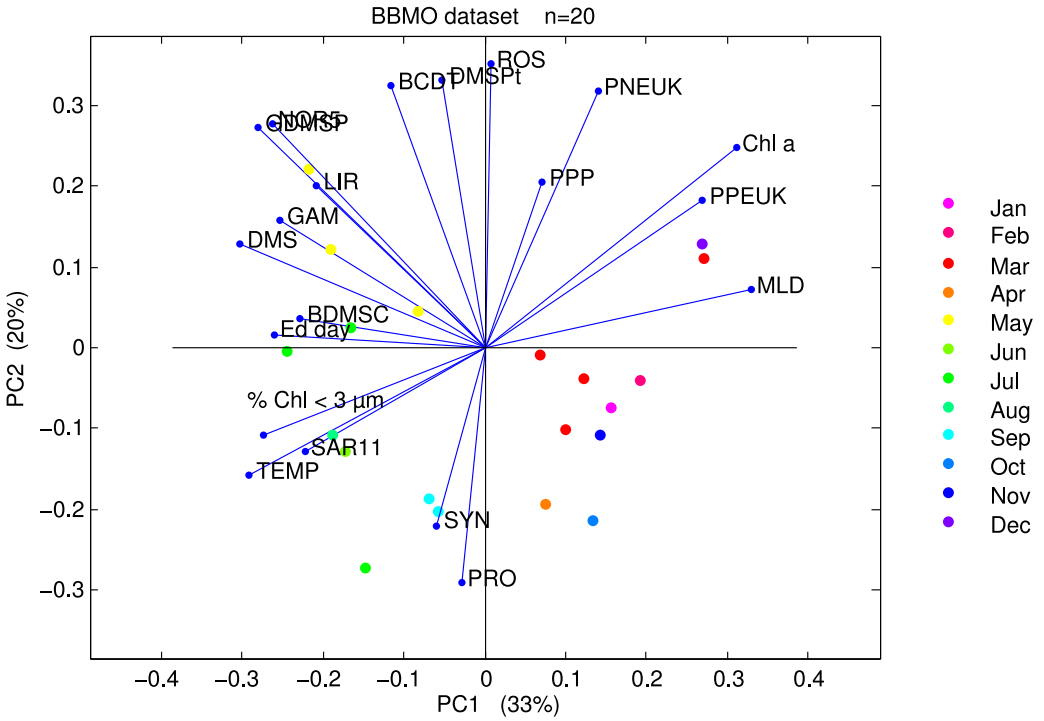

Figure 6.15: **PCA analysis of DMS(P) cycling and picoplankton communities in the Blanes Bay Microbial Observatory** - GAM: *Gammaproteobacteria*, which includes the sub-clade NOR5; ROS (*Roseobacter*), and SAR11 are *Alphaproteobacteria*; BCDT: *Bacteroidetes*; PRO: *Prochlorococcus*; SYN: *Synechococcus*; PPEUK: phototrophic picoeukaryotes; PNEUK: phototrophic nanoeukaryotes; GDMSP: gross DMS production; BDMSC: bacterial DMS consumption; other abbreviations defined in the text.

Table 6.5: Three-factor ANOVA of bacterial DMS consumption rate constants

Source	Sum Sq.	$d.f.$	Mean Sq.	F	p
Method	1.13	3	0.38	0.91	0.4478
PFT	1.09	3	0.36	0.88	0.4643
Domain	0.3	1	0.3	0.73	0.3995
Error	12.86	31	0.41		
Total	16.62	38			

Table 6.6: Three-factor ANOVA of bacterial DMS consumption rate constants

Source	Sum Sq.	$d.f.$	Mean Sq.	F	p
Method	6.87	3	2.29	7.39	0.0008
PFT	0.88	3	0.29	0.94	0.4331
Domain	2.12	1	2.12	6.84	0.0138
Error	9.3	30	0.31		
Total	19.69	37			

Chapter 7

Conclusions

- The changes in radiation fields, regulated by vertical mixing and by the differential attenuation of solar wavelengths in seawater, have a strong impact on oceanic DMS budgets (*Chapters 1-6*).

- Gross DMS production (GP) is stimulated by solar radiation in a dose- and spectrum-dependent manner. However, sunlight-stimulated GP is mirrored by DMS photolysis on the short term, which prevents net DMS accumulation. The response of GP to shifts in spectral irradiance is frequently one order of magnitude larger than the photoinhibiton of autotrophic and heterotrophic production. The relationship between the light (UV) exposure history of the microbial community and their subsequent response to further UV exposure might be critical. (*Chapters 2-5*).

- Oceanic DMS cycling shows pronounced day-night (diel) variability. In stratified waters, with deep UV penetration and nutrient scarcity, GP, bacterial DMS consumption, and DMS photolysis are all modulated by the light exposure regimes. Failing to take into account the diel variability can cause significant deviations in DMS budgets (*Chapter 5*).

- The depth of the upper mixed layer regulates the relative importance of bacterial or photochemical oxidation as the main DMS sinks, as well as the impact of sea-air DMS flux and vertical transport in the water column. Across oceanic biomes, the rate constants of total DMS loss exhibit little variability. This leaves to gross DMS production the key regulatory role of oceanic DMS concentrations (*Chapters 1, 5 and 6*).

- In turn, gross DMS production depends on DMSP concentrations and the yield of DMSP to DMS conversion. While the first depends on plankton biogeography and seasonal succession, the second is mainly modulated by short-term radiative (or oxidative) stress. Assessing the turnover of the whole DMSP pool (dissolved and particulate) is critical to understand what drives DMS production (*Chapters 5 and 6*).

Open questions

- The physiological meaning of UV-stress induced DMS production by phytoplankton is still enigmatic. The fact that large amounts of DMS are released without having been oxidized intracellularly calls into question its antioxidant function. The role of UV-induced cell disruption, causing DMSP release and subsequent cleavage to DMS, requires further assessment.

- The role of bacteria, (micro)zooplankton grazers and viruses in UV-stimulated DMS production remains to be elucidated. The interaction between grazing-promoted DMS production and UV radiation needs more attention.

- The relative importance of algal and bacterial DMSP cleavage enzymes is not yet understood. This requires a better knowledge of microscale interactions and the trophic coupling of phyto- and bacterioplankton, probably linked to the phylogenetic identity of the microorganisms.

- At larger scales, the abundance and photoreactivity of CDOM seem to play a critical role: on one hand, CDOM attenuates UV radiation; on the other hand, it promotes DMS photolysis. The photoreactivity of CDOM, related to the degree of photobleaching it has suffered, causes order-of-magnitude variations in DMS photolysis quantum yields. Changes in CDOM due to modifications of oceanic circulation and plankton biogeography might impact DMS cycling.

Bibliography

Aas, P., Lyons, M., Pledger, R., Mitchell, D., and Jeffrey, W. (1996). Inhibition of bacterial activities by solar radiation in nearshore waters and the Gulf of Mexico. *Aquatic Microbial Ecology*, 11:229–238.

Agogué, H., Joux, F., Obernosterer, I., and Lebaron, P. (2005). Resistance of Marine Bacterioneuston to Solar Radiation. *Applied and environmental microbiology*, 71(9):5282–5289.

Agustí, S. and Llabrés, M. (2007). Solar radiation-induced mortality of marine picophytoplankton in the oligotrophic ocean. *Photochemistry and photobiology*, 83(4):793–801.

Alonso-Sáez, L., Gasol, J. M., Aristegui, J., Vilas, J. C., Duarte, C. M., Agustí, S., and Agust, S. (2007). Large-scale variability in surface bacterial carbon demand and growth efficiency in the subtropical northeast Atlantic Ocean. *Limnology and oceanography*, 52(2):533–546.

Alonso-Sáez, L., Gasol, J. M., Lefort, T., Hofer, J., and Sommaruga, R. (2006). Effect of natural sunlight on bacterial activity and differential sensitivity of natural bacterioplankton groups in northwestern Mediterranean coastal waters. *Applied and environmental microbiology*, 72(9):5806–5813.

Alonso-Sáez, L., Vázquez-Domínguez, E., Cardelús, C., Pinhassi, J., Sala, M. M., Lekunberri, I., Balagué, V., Vila-Costa, M., Unrein, F., Massana, R., Simó, R., and Gasol, J. M. (2008). Factors Controlling the Year-Round Variability in Carbon Flux Through Bacteria in a Coastal Marine System. *Ecosystems*, 11(3):397–409.

Anderson, S. P., Weller, R. A., and Lukas, R. B. (1996). Surface buoyancy forcing and the mixed layer of the Western Pacific Warm Pool: Observations and 1D model results. *Journal of Climate*, 9:3056–3085.

Andreae, M. O. (1980). Dimethylsulfoxide in marine and freshwaters. *Limnology and Oceanography*, 25(6):1054–1063.

Andreae, M. O. and Crutzen, P. J. (1997). Atmospheric Aerosols: Biogeochemical Sources and Role in Atmospheric Chemistry. *Science*, 276(5315):1052–1058.

Andreae, M. O. and Rosenfeld, D. (2008). Aerosol cloud precipitation interactions. Part 1. The nature and sources of cloud-active aerosols. *Earth-Science Reviews*, 89:13–41.

Archer, S., Safi, K., Hall, A., Cummings, D., and Harvey, M. (2010a). Grazing suppression of dimethylsulphoniopropionate (DMSP) accumulation in iron-fertilised, sub-Antarctic waters. *Deep Sea Research Part II: Topical Studies in Oceanography*.

Archer, S., Tarran, G., Stephens, J., Butcher, L., and Kimmance, S. (2011). Combining cell sorting with gas chromatography to determine phytoplankton group-specific intracellular dimethylsulphoniopropionate. *Aquatic Microbial Ecology*, 62(2):109–121.

Archer, S. D., Gilbert, F., Nightingale, P., Zubkov, M., Taylor, a., Smith, G., and Burkill, P. (2002). Transformation of dimethylsulphoniopropionate to dimethyl sulphide during summer in the North Sea with an examination of key processes via a modelling approach. *Deep Sea Research Part II: Topical Studies in Oceanography*, 49(15):3067–3101.

Archer, S. D., Ragni, M., Webster, R., Airs, R. L., and Geider, R. J. (2010b). Dimethyl sulfoniopropionate and dimethyl sulfide production in response to photoinhibition in Emiliania huxleyi. *Limnology and Oceanography*, 55(4):1579–1589.

Archer, S. D., Widdicombe, C. E., Tarran, G. A., Rees, A. P., and Burkill, P. H. (2001). Production and turnover of particulate dimethylsulphoniopropionate during a coccolithophore bloom in the northern North Sea. *Aquatic Microbial Ecology*, 24:225–241.

Asher, E. C., Dacey, J. W. H., Mills, M. M., Arrigo, K. R., and Tortell, P. D. (2011). High concentrations and turnover rates of DMS, DMSP and DMSO in Antarctic sea ice. *Geophysical Research Letters*, 38(L23609):1–5.

Bailey, K., Toole, D. A., Blomquist, B., Najjar, R., Huebert, B., Kieber, D. J., Kiene, R. P., Matrai, P., Westby, G., and del Valle, D. (2008). Dimethylsulfide production in Sargasso Sea eddies. *Deep Sea Research Part II: Topical Studies in Oceanography*, 55(10-13):1491–1504.

Baines, S. B. and Pace, M. L. (1991). The production of dissolved organic matter by phytoplankton and its importance to bacteria : pattterns across marine and freshwater systems across marine Patterns. 36(6):1078–1090.

Bannister, T. T. (1992). Model of the mean cosine of underwater radiance and estimation of underwater scalar irradiance. *Limnology and Oceanography*, 37(4):773–780.

Barnes, I., Becker, K. H., and Mihalopoulos, N. (1994). An FTIR product study of the photooxidation of dimethyl disulfide. *Journal of Atmospheric Chemistry*, 18(3):267–289.

Bates, T. S., Charlson, R. J., and Gammon, R. H. (1987). Evidence for the climatic role of marine biogenic sulphur. *Nature*, 329:319–321.

Bates, T. S., Lamb, B. K., Guenther, a., Dignon, J., and Stoiber, R. E. (1992). Sulfur emissions to the atmosphere from natural sourees. *Journal of Atmospheric Chemistry*, 14(1-4):315–337.

Behrenfeld, M. and Boss, E. (2003). The beam attenuation to chlorophyll ratio: an optical index of phytoplankton physiology in the surface ocean? *Deep Sea Research Part I: Oceanographic Research Papers*, 50(12):1537–1549.

Behrenfeld, M. J. (2010). Abandoning Sverdrup's Critical Depth Hypothesis on phytoplankton blooms. *Ecology*, 91(4):977–989.

Behrenfeld, M. J. and Falkowski, P. G. (1997). Photosynthetic rates derived from satellite-based chlorophyll concentration. *Limnology and Oceanography*, 42(1):1–20.

Behrenfeld, M. J., Prasil, O., Kolber, Z. S., Babin, M., and Paul, G. (1998). Compensatory changes in Photosystem II electron turnover rates protect photosynthesis from photoinhibition. *Photosynthesis Research*, 58:259–268.

Béjà, O., Aravind, L., Koonin, E. V., Suzuki, M. T., Hadd, A., Nguyen, L. P., Jovanovich, S. B., Gates, C. M., Feldman, R. A., Spudich, J. L., Spudich, E. N., and DeLong, E. F. (2000). Bacterial Rhodopsin: Evidence for a New Type of Phototrophy in the Sea. *Science*, 289(5486):1902–1906.

Bélanger, S., Xie, H., Krotkov, N., Larouche, P., Vincent, W. F., and Babin, M. (2006). Photomineralization of terrigenous dissolved organic matter in Arctic coastal waters from 1979 to 2003: Interannual variability and implications of climate change. *Global Biogeochemical Cycles*, 20(4):1–13.

Bell, T. G., Malin, G., Kim, Y.-N., and Steinke, M. (2007). Spatial variability in DMSP-lyase activity along an Atlantic meridional transect. *Aquatic Sciences*, 69:320–329.

Bell-Pedersen, D., Cassone, V. M., Earnest, D. J., Golden, S. S., Hardin, P. E., Thomas, T. L., and Zoran, M. J. (2005). Circadian rhythms from multiple oscillators: Lessons from diverse organisms. *Nature Reviews Genetics*, June:1–13.

Belviso, S. (2000). Diel variations of the DMSP-to-chlorophyll a ratio in Northwestern Mediterranean surface waters. *Journal of Marine Systems*, 25(2):119–128.

Belviso, S., Bopp, L., Moulin, C., Orr, J. C., Anderson, T. R., Aumont, O., Chu, S., Elliott, S., Maltrud, M. E., and Simó, R. (2004). Comparison of global climatological maps of sea surface dimethyl sulfide. *Global Biogeochemical Cycles*, 18(3).

Berdalet, E., Llaveria, G., and Simó, R. (2011). Modulation of dimethylsulfoniopropionate (DMSP) concentration in an Alexandrium minutum (Dinophyceae) culture by small-scale turbulence: A link to toxin production? *Harmful Algae*, 11:88–95.

Bertoni, R., Jeffrey, W. H., Pujo-Pay, M., Oriol, L., Conan, P., and Joux, F. (2011). Influence of water mixing on the inhibitory effect of UV radiation on primary and bacterial production in Mediterranean coastal water. 73:377–387.

Bidle, K. D. and Falkowski, P. G. (2004). Cell death in planktonic, photosynthetic microorganisms. *Nature reviews. Microbiology*, 2(8):643–655.

Bird, D. F. and Kalff, J. (1986). Bacterial grazing by planktonic lake algae. *Science*, 231(4737):493–5.

Bordewijk, J. A., Slaper, H., Reinen, H. A. J. M., and Schlamann, E. (1995). Total solar radiation and the influence of clouds and aerosols on the biologically effective UV. *Geophysical Research Letters*, 22(16):2151–2154.

Bouillon, R., Lee, P. A., Demora, S., Levasseur, M., and Lovejoy, C. (2002). Vernal distribution of dimethylsulphide, dimethylsulphoniopropionate, and dimethylsulphoxide in the North Water in 1998. *Deep Sea Research Part II: Topical Studies in Oceanography*, 49(22-23):5171–5189.

Bouillon, R.-C. (2004). Determination of apparent quantum yield spectra of DMS photodegradation in an in situ iron-induced Northeast Pacific Ocean bloom. *Geophysical Research Letters*, 31(6):1–4.

Bouillon, R.-C. and Miller, W. L. (2005). Photodegradation of dimethyl sulfide (DMS) in natural waters: laboratory assessment of the nitrate-photolysis-induced DMS oxidation. *Environmental science & technology*, 39(24):9471–7.

Boyd, P. W., Jickells, T., Law, C. S., Blain, S., Boyle, E. A., Buesseler, K. O., Coale, K. H., Cullen, J. J., de Baar, H. J. W., Follows, M., Harvey, M., Lancelot, C., Levasseur, M., Owens, N. P. J., Pollard, R., Rivkin, R. B., Sarmiento, J., Schoemann, V., Smetacek, V., Takeda, S., Tsuda, A., Turner, S., and Watson, A. J. (2007). Mesoscale iron enrichment experiments 1993-2005: synthesis and future directions. *Science*, 315(5812):612–7.

Boyd, P. W., Strzepek, R., Fu, F., and Hutchins, D. a. (2010). Environmental control of open-ocean phytoplankton groups: Now and in the future. *Limnology and Oceanography*, 55(3):1353–1376.

Brainerd, K. E. and Gregg, M. C. (1995). Surface mixed and mixing layer depths. *Deep Sea Research Part I: Oceanographic Research Papers*, 42(9):1521–1543.

Brimblecombe, P. and Shooter, D. (1986). Photo-oxidation of dimethylsulphide in aqueous solution. *Marine Chemistry*, 19:343–353.

Broadbent, A. D. and Jones, G. B. (2004). DMS and DMSP in mucus ropes, coral mucus, surface films and sediment pore waters from coral reefs in the Great Barrier Reef. *Marine and Freshwater Research*, 55(8):849.

Brock, T. D. (1981). Calculating solar radiation for ecological studies. *Ecological Modelling*, 14(1-2):1–19.

Brugger, A., Slezak, D., Obernosterer, I., and Herndl, G. J. (1998). Photolysis of dimethylsulfide in the northern Adriatic Sea: Dependence on substrate concentration, irradiance and DOC concentration. *Marine Chemistry*, 59(3-4):321–331.

Bucciarelli, E. and Sunda, W. G. (2003). Influence of CO2, nitrate, phosphate, and silicate limitation on intracellular dimethylsulfoniopropionate in batch cultures of the coastal diatom Thalassiosira pseudonana. *Limnology and Oceanography*, 48(6):2256–2265.

Buma, a. G., Helbling, E. W., de Boer, M. K., and Villafañe, V. E. (2001). Patterns of DNA damage and photoinhibition in temperate South-Atlantic picophytoplankton exposed to solar ultraviolet radiation. *Journal of photochemistry and photobiology. B, Biology*, 62(1-2):9–18.

Calbet, A. and Landry, M. R. (2004). Phytoplankton growth, microzooplankton grazing, and carbon cycling in marine systems. 49(1):51–57.

Calbet, A., Trepat, I., Almeda, R., Saló, V., Saiz, E., Movilla, J. I., Alcaraz, M., Yebra, L., and Simó, R. (2008). Impact of micro- and nanograzers on phytoplankton assessed by standard and size-fractionated dilution grazing experiments. *Aquatic Microbial Ecology*, 50:145–156.

Calbó, J., Pagès, D., and González, J.-A. (2005). Empirical studies of cloud effects on UV radiation: A review. *Reviews of Geophysics*, 43(RG2002):1–28.

Cantin, G., Levasseur, M., Schultes, S., and Michaud, S. (1999). Dimethylsulfide (DMS) production by size-fractionated particles in the Labrador Sea. *Aquatic Microbial Ecology*, 19:307–312.

Carmack, E. (2007). The alpha/beta ocean distinction: A perspective on freshwater fluxes, convection, nutrients and productivity in high-latitude seas. *Deep Sea Research Part II: Topical Studies in Oceanography*, 54(23-26):2578–2598.

Charlson, R., Lovelock, J., Andreae, M., Warren, S., and Others (1987). Oceanic phytoplankton, atmospheric sulphur, cloud albedo and climate. *Nature*, 326(6114):655–661.

Chisholm, S. W. (1992). Phytoplankton size. In Falkowski, P. G. and Woodhead, A. D., editors, *Primary Productivity and Biogeochemical Cycles in the Sea*, volume 02139, pages 213–237. Plenum Press, New York.

Church, M. J., Ducklow, H. W., and Karl, D. M. (2004). Light dependence of [3H]leucine incorporation in the oligotrophic North Pacific ocean. *Applied and environmental microbiology*, 70(7):4079–87.

Corellou, F., Schwartz, C., Motta, J.-p., and Djouani-tahri, E. B. (2009). Clocks in the Green Lineage: Comparative Functional Analysis of the Circadian Architecture of the Picoeukaryote Ostreococcus. *The Plant Cell*, 21(November):3436–3449.

Corn, M., Belviso, S., Partensky, F., Simon, N., Christaki, U., and Fukai, E. (1996). Origin and importance of picoplanktonic DMSP. In Kiene, R. P., Visscher, P. T., Keller, M. D., and

Kirst, G. O., editors, *Biological and environmental chemistry of DMSP and related sulfonium compounds*, pages 191–201.

Cottrell, M. T. and Kirchman, D. L. (2000). Natural Assemblages of Marine Proteobacteria and Members of the Cytophaga-Flavobacter Cluster Consuming Low- and High-Molecular-Weight Dissolved Organic Matter. *Applied and Environmental Microbiology*, 66(4):1692–1697.

Cunningham, G. B., Strauss, V., and Ryan, P. G. (2008). African penguins (Spheniscus demersus) can detect dimethyl sulphide, a prey-related odour. *The Journal of experimental biology*, 211(Pt 19):3123–7.

Curson, A. R. J., Todd, J. D., Sullivan, M. J., and Johnston, A. W. B. (2011). Catabolism of dimethylsulphoniopropionate: microorganisms, enzymes and genes. *Nature reviews. Microbiology*, 9(12):849–59.

Cuvelier, M. L., Allen, A. E., Monier, A., McCrow, J. P., Messié, M., Tringe, S. G., Woyke, T., Welsh, R. M., Ishoey, T., Lee, J.-H., Binder, B. J., DuPont, C. L., Latasa, M., Guigand, C., Buck, K. R., Hilton, J., Thiagarajan, M., Caler, E., Read, B., Lasken, R. S., Chavez, F. P., and Worden, A. Z. (2010). Targeted metagenomics and ecology of globally important uncultured eukaryotic phytoplankton. *Proceedings of the National Academy of Sciences of the United States of America*, 107(33):14679–84.

Dacey, J. W., Howse, F. A., Michaels, A. F., and Wakeham, S. G. (1998). Temporal variability of dimethylsulfide and dimethylsulfoniopropionate in the Sargasso Sea. *Deep Sea Res. I*, 45:2085–2104.

de Boyer Montégut, C. (2004). Mixed layer depth over the global ocean: An examination of profile data and a profile-based climatology. *Journal of Geophysical Research*, 109(C12):1–20.

Deal, C., Kieber, D. J., Toole, D. A., Stamnes, K., Jiang, S., and Uzuka, N. (2005). Dimethylsulfide photolysis rates and apparent quantum yields in Bering Sea seawater. *Continental Shelf Research*, 25(15):1825–1835.

Decelle, J., Probert, I., Bittner, L., Desdevises, Y., Vargas, C. D., Galí, M., Simó, R., and Not, F. (2012). Original mode of symbiosis in open ocean plankton. *Proceedings of the National Academy of Sciences of the United States of America*.

del del Valle, D., Kieber, D. J., Bisgrove, J., and RP (2007). Light-stimulated production of dissolved DMSO by a particle-associated process in the Ross Sea, Antarctica. *Limnology and*, 52(6):2456–2466.

del Giorgio, P. a., Condon, R., Bouvier, T., Longnecker, K., Bouvier, C., Sherr, E., and Gasol, J. M. (2011). Coherent patterns in bacterial growth, growth efficiency, and leucine metabolism along a northeastern Pacific inshore-offshore transect. *Limnology and Oceanography*, 56(1):1–16.

del Giorgio, P. A. and Duarte, C. M. (2002). Respiration in the open ocean. *Nature*, 420(November):379–384.

del Valle, D., Kieber, D. J., and Kiene, R. P. (2007). Depth-dependent fate of biologically-consumed dimethylsulfide in the Sargasso Sea. *Marine Chemistry*, 103(1-2):197–208.

del Valle, D., Kieber, D. J., Toole, D. A., Brinkley, J., and Kiene, R. P. (2009). Biological consumption of dimethylsulfide (DMS) and its importance in DMS dynamics in the Ross Sea, Antarctica. *Limnology and Oceanography*, 54(3):785–798.

del Valle, D. a., Slezak, D., Smith, C. M., Rellinger, A. N., Kieber, D. J., and Kiene, R. P. (2011). Effect of acidification on preservation of DMSP in seawater and phytoplankton cultures: Evidence for rapid loss and cleavage of DMSP in samples containing Phaeocystis sp. *Marine Chemistry*, 124(1-4):57–67.

Del Vecchio, R. (2002). Photobleaching of chromophoric dissolved organic matter in natural waters: kinetics and modeling. *Marine Chemistry*, 78(4):231–253.

Delvalle, D., Kieber, D. J., Toole, D. A., Bisgrove, J., and Kiene, R. P. (2009). Dissolved DMSO production via biological and photochemical oxidation of dissolved DMS in the Ross Sea, Antarctica. *Deep Sea Research Part I: Oceanographic Research Papers*, 56(2):166–177.

Denman, K. L. and Gargett, A. E. (1983). Time and space scales of vertical mixing in the upper ocean. *Limnology and Oceanography*, 28(5):801–815.

DiTullio, G. R., Jones, D. R., and Geesey, M. E. (2003). Dimethylsulfide dynamics in the Ross Sea during austral summer. *Antarctic Research Series*, 78:279–294.

Doney, S. C., Abbott, M. R., Cullen, J. J., Karl, D. M., and Rothstein, L. (2004). From genes to ecosystems : the oceans new frontier. *Frontiers in Ecology*, 2(9):457–466.

Doney, S. C., Najjar, R. G., and Stewart, S. (1995). Photochemistry , mixing and diurnal in the upper ocean cycles. *Photochemistry*, pages 341–369.

Dusenberry, J. a., Olsen, R. J., and Chisholm, S. W. (1999). Frequency distributions of phytoplankton single-cell fluorescence and vertical mixing in the surface ocean. *Limnology and Oceanography*, 44(2):431–435.

DAsaro, E. a. (2002). Turbulent Vertical Kinetic Energy in the Ocean Mixed Layer. *Journal of Physical Oceanography*, 31(12):3530–3537.

Estrada, M. (1996). Primary production in the northwestern Mediterranean *. *Production*, 60:55–64.

Evans, C., Kadner, S. V., Darroch, L. J., Wilson, W. H., Liss, P. S., and Malin, G. (2007). The relative significance of viral lysis and microzooplankton grazing as pathways of dimethylsulfoniopropionate (DMSP) cleavage : An Emiliania huxleyi culture study. *Methods*, 52(3):1036–1045.

Fagerbakke, K. M., Heldal, M., and Norland, S. (1996). Content of carbon, nitrogen, oxygen, sulfur and phosphorus in native aquatic and cultured bacteria. *Aquatic Microbial Ecology*, 10:15–27.

Field, C. B., Behrenfeld, M. J., Randerson, J. T., and Falkowski, P. G. (1998). Primary Production of the Biosphere: Integrating Terrestrial and Oceanic Components. *Science*, 281:237–240.

Follows, M. J., Dutkiewicz, S., Grant, S., and Chisholm, S. W. (2007). Emergent biogeography of microbial communities in a model ocean. *Science*, 315(5820):1843–1846.

Franklin, D., Steinke, M., Young, J., Probert, I., and Malin, G. (2010). Dimethylsulphoniopropionate (DMSP), DMSP-lyase activity (DLA) and dimethylsulphide (DMS) in 10 species of coccolithophore. *Marine Ecology Progress Series*, 410:13–23.

Fuhrmanl, J. A., Eppley, R. W., Hagstrom, A., and Azam, F. (1985). Diel variations in bacterioplankton, phytoplankton, and related parameters in the Southern California Bight. *Marine Ecology Progress Series*, 27:9–20.

Gabric, a. (2001). Modeling the biogeochemical cycle of dimethylsulfide in the upper ocean: a review. *Chemosphere - Global Change Science*, 3(4):377–392.

Gabric, A., Matrai, P., Kiene, R. P., Cropp, R., Dacey, J., DiTullio, G., Najjar, R., Simó, R., Toole, D. A., and DelValle, D. (2008). Factors determining the vertical profile of dimethylsulfide in the Sargasso Sea during summer. *Deep Sea Research Part II: Topical Studies in Oceanography*, 55(10-13):1505–1518.

Gabric, A. J., Matrai, P. a., and Vernet, M. (1999). Modelling the production and cycling of dimethylsulphide during the vernal bloom in the Barents Sea. *Tellus B*, 51(5):919–937.

Gabric, A. J., Qu, B., Matrai, P., and Hirst, A. C. (2005). The simulated response of dimethylsulfide production in the Arctic Ocean to global warming. *Tellus B*, 57(5):391–403.

Gage, D. A., Rhodes, D., Nolte, K. D., Hicks, W. A., Leustek, T., Cooper, A. J. L., and Hanson, A. D. (1997). A new route for synthesis of dimethylsulfoniopropionate in marine algae. *Nature*, 387(26):891–894.

Galí, M., Saló, V., Almeda, R., Calbet, A., and Simó, R. (2011). Stimulation of gross dimethylsulfide (DMS) production by solar radiation. *Geophysical Research Letters*, 38(15):1–5.

Galí, M. and Simó, R. (2010). Occurrence and cycling of dimethylated sulfur compounds in the Arctic during summer receding of the ice edge. *Marine Chemistry*.

Gallegos, C. L. and Platt, T. (1985). Vertical advection of phytoplankton and productivity estimates: a dimensional analysis. *Marine Ecology Progress Series*, 26(1982):125–134.

Garcia-Pichel, F. (1994). A model for internal self-shading in planktonic organisms and its implications for the usefulness of ultraviolet sunscreens. *Limnology and Oceanography*, 39(7):1704–1717.

Gardner, W., Gundersen, J., Richardson, M., and Walsh, I. (1999). The role of seasonal and diel changes in mixed-layer depth on carbon and chlorophyll distributions in the Arabian Sea. *Deep Sea Research Part II: Topical Studies in Oceanography*, 46(8-9):1833–1858.

Gasol, J. M. and del Giorgio, P. A. (2000). Using flow cytometry for counting natural planktonic bacteria and understanding the structure of planktonic bacterial communities. *Scientia Marina*, 64(2):197–224.

Gasol, J. M., del Giorgio, P. A., and Duarte, C. M. (1997). Biomass distribution in marine planktonic communities. *Limnology and Oceanography*, 42(6):1353–1363.

Gasol, J. M., Doval, M. D., Pinhassi, J., Calderón-Paz, J. I., Guixa-Boixareu, N., Vaqué, D., and Pedrós-Alió, C. (1998). Diel variations in bacterial heterotrophic activity and growth in the northwestern Mediterranean Sea. *Marine Ecology Progress Series*, 164:107–124.

Gasol, J. M., Pinhassi, J., Alonso-sáez, L., Ducklow, H., Herndl, G. J., Koblí, M., Labrenz, M., Luo, Y., Morán, X. A. G., Reinthaler, T., and Simon, M. (2008). Towards a better understanding of microbial carbon flux in the sea. *Aquatic Microbial Ecology*, 53(September):21–38.

Giovannoni, S. J., Tripp, H. J., Givan, S., Podar, M., Vergin, K. L., Baptista, D., Bibbs, L., Eads, J., Richardson, T. H., Noordewier, M., Rappé, M. S., Short, J. M., Carrington, J. C., and Mathur, E. J. (2005). Genome streamlining in a cosmopolitan oceanic bacterium. *Science*, 309(5738):1242–5.

Gómez-Consarnau, L., González, J. M., Coll-Lladó, M., Gourdon, P., Pascher, T., Neutze, R., Pedrós-Alió, C., and Pinhassi, J. (2007). Light stimulates growth of proteorhodopsin-containing marine Flavobacteria. *Nature*, 445(January):210–213.

González, J. M., Fernández-Gómez, B., Fernàndez-Guerra, A., Gómez-Consarnau, L., Sánchez, O., Coll-Lladó, M., Del Campo, J., Escudero, L., Rodríguez-Martínez, R., Alonso-Sáez, L., Latasa, M., Paulsen, I., Nedashkovskaya, O., Lekunberri, I., Pinhassi, J., and Pedrós-Alió, C. (2008). Genome analysis of the proteorhodopsin-containing marine bacterium Polaribacter sp. MED152 (Flavobacteria). *Proceedings of the National Academy of Sciences of the United States of America*, 105(25):8724–9.

González, J. M., Kiene, R. P., and Moran, M. a. (1999). Transformation of sulfur compounds by an abundant lineage of marine bacteria in the alpha-subclass of the class Proteobacteria. *Applied and environmental microbiology*, 65(9):3810–9.

Gordon, H. R. (2008). Can the Lambert-Beer Law Be Applied to the Diffuse Attenuation Coefficient of Ocean Water? *Limnology and Oceanography*, 34(8):1389– 1409.

Green, D. H., Shenoy, D. M., Hart, M. C., and Hatton, A. D. (2011). Coupling of dimethylsulfide oxidation to biomass production by a marine flavobacterium. *Applied and environmental microbiology*, 77(9):3137–40.

Grégori, G., Citterio, S., Ghiani, A., Labra, M., Sgorbati, S., Brown, S., and Denis, M. (2001). Resolution of viable and membrane-compromised bacteria in freshwater and marine waters

based on analytical flow cytometry and nucleic acid double staining. *Applied and Environmental Microbiology*, 67:4662–4670.

Gueymard, C. A., Myers, D., and Emery, K. (2003). Proposed reference irradiance spectra for solar energy systems testing. *Solar Energy*, 73(6):443–467.

Gutiérrez-Rodríguez, A., Latasa, M., Scharek, R., Massana, R., Vila, G., and Gasol, J. M. (2011). Growth and grazing rate dynamics of major phytoplankton groups in an oligotrophic coastal site. *Estuarine, Coastal and Shelf Science*, 95(1):77–87.

Häder, D.-P., Kumar, H. D., Smith, R. C., and Worrest, R. C. (2007). Effects of solar UV radiation on aquatic ecosystems and interactions with climate change. *Photochemical & photobiological sciences*, 6(3):267–85.

Hansell, D. a., Kadko, D., and Bates, N. R. (2004). Degradation of terrigenous dissolved organic carbon in the western Arctic Ocean. *Science*, 304(5672):858–861.

Harada, H., Rouse, M.-A., Sunda, W., and Kiene, R. P. (2004). Latitudinal and vertical distributions of particle- associated dimethylsulfoniopropionate (DMSP) lyase activity in the western North Atlantic Ocean. *Canadian Journal of Fisheries and Aquatic Sciences*, 61:700–711.

Hastings, J. W. (1961). A Persistent Daily Rhythm in Photosynthesis. *The Journal of General Physiology*, 45(1):69–76.

Hatton, A. D. (2002). Influence of photochemistry on the marine biogeochemical cycle of dimethylsulphide in the northern North Sea. *Deep-Sea Research II*, 49:3039–3052.

Hatton, A. D., Darroch, L., and Malin, G. (2004). The role of dimethylsulphoxyde in the marine biogeochemical cycle of dimethylsulphide. *Oceanography and Marine Biology*, 42:29–56.

Hatton, A. D., Shenoy, D. M., Hart, M. C., Mogg, A., and Green, D. H. (2012). Metabolism of DMSP, DMS and DMSO by the cultivable bacterial community associated with the DMSP-producing dinoflagellate Scrippsiella trochoidea. *Biogeochemistry*, 110(1-3):131–146.

Hatton, A. D. and Wilson, S. T. (2007). Particulate dimethylsulphoxide and dimethylsulphoniopropionate in phytoplankton cultures and Scottish coastal waters. *Aquatic Sciences*, 69(3):330–340.

Hefu, Y. and Kirst, G. O. (1997). Effect of UV- radiation on DMSP content and DMS formation of Phaeocystis antarctica. *Polar Biology*, 18(6):402–409.

Hellebust, J. A. and Lewin, J. (1972). Transport systems for organic acids induced in the marine pennate diatom, Cylindrotheca fusiformis. *Canadian Journal of Microbiology*, 18(2):225–233.

Herrmann, M., Najjar, R. G., Neeley, A. R., Vila-Costa, M., Dacey, J. W., DiTullio, G. R., Kieber, D. J., Kiene, R. P., Matrai, P. a., Simó, R., and Vernet, M. (2012). Diagnostic modeling of dimethylsulfide production in coastal water west of the Antarctic Peninsula. *Continental Shelf Research*, 32:96–109.

Hill, R. W., White, B. A., Cottrell, M. T., and Dacey, J. W. H. (1998). Virus-mediated total release of dimethylsulfoniopropionate from marine phytoplankton: a potential climate process. *Aquat. Microb. Ecol*, 14:1–6.

Hojerová, E., Mašín, M., Brunet, C., Ferrera, I., Gasol, J. M., and Koblížek, M. (2011). Distribution and growth of aerobic anoxygenic phototrophs in the Mediterranean Sea. *Environmental microbiology*, 13(10):2717–25.

Howard, E. C., Henriksen, J. R., Buchan, A., Reisch, C. R., Bürgmann, H., Welsh, R., Ye, W., González, J. M., Mace, K., Joye, S. B., Kiene, R. P., Whitman, W. B., and Moran, M. A. (2006). Bacterial taxa that limit sulfur flux from the ocean. *Science*, 314(5799):649–52.

Huebert, B. J., Blomquist, B. W., Yang, M. X., Archer, S. D., Nightingale, P. D., Yelland, M. J., Stephens, J., Pascal, R. W., and Moat, B. I. (2010). Linearity of DMS transfer coefficient with both friction velocity and wind speed in the moderate wind speed range. *Geophysical Research Letters*, 37(1):0–4.

IPCC (2007). Climate change 2007: synthesis report. Contribution of Working Groups I, II and III to the Fourth Assessment Report of the Intergovernmental Panel on Climate Change. Technical report, IPCC, Geneva.

Jacquet, S. and Bratbak, G. (2003). Effects of ultraviolet radiation on marine virus-phytoplankton interactions. *FEMS microbiology ecology*, 44(3):279–89.

Jakobsen, H. H. and Strom, S. L. (2004). Circadian cycles in growth and feeding rates of heterotrophic protist plankton. *Limnology and Oceanography*, 49(6):1915–1922.

Jardillier, L., Zubkov, M. V., Pearman, J., and Scanlan, D. J. (2010). Significant CO2 fixation by small prymnesiophytes in the subtropical and tropical northeast Atlantic Ocean. *The ISME journal*, 4(9):1180–92.

Jeffrey, S., MacTavish, H., Dunlap, W., Vesk, M., and Groenewoud, K. (1999). Occurrence of UVA- and UVB-absorbing compounds in 152 species (206 strains) of marine microalgae. *Marine Ecology Progress Series*, 189(1992):35–51.

Jerlov, N. G. (1976). *Marine Optics*, volume 0. Elsevier Oceanography Series.

Johannessen, O. M., Bengtsson, L., Miles, M. W., Kuzmina, S. I., Semenov, V. A., Alekseev, G. V., Nagurnyi, A. P., Zakharov, V. F., Bobylev, L. P., Petterson, L. H., Hasselmann, K., and Cattle, H. P. (2004). Arctic climate change: observed and modelled temperature and sea-ice variability. *Tellus A*, 56(4):328–341.

Johnston, A. W. B., Todd, J. D., Sun, L., Nikolaidou-Katsaridou, M. N., Curson, A. R. J., and Rogers, R. (2008). Molecular diversity of bacterial production of the climate-changing gas, dimethyl sulphide, a molecule that impinges on local and global symbioses. *Journal of experimental botany*, 59(5):1059–67.

Kaiser, E. and Herndl, G. J. (1997). Rapid Recovery of Marine Bacterioplankton Activity after Inhibition by UV Radiation in Coastal Waters. *Applied and environmental microbiology*, 63(10):4026–4031.

Keller, M. D. (1989). Dimethyl sulfide production in marine phytoplankton. In Saltzman, E. S. and Cooper, W. J., editors, *Biogenic sulfur in the environment*, volume no. 393, pages 167–182. ACS Symposium series, New York.

Keller, M. D., Kiene, R. P., Matrai, P. A., and Bellows, W. K. (1999a). Production of glycine betaine and dimethylsulfoniopropionate in marine phytoplankton. I. Batch cultures. *Marine Biology*, 135(2):237–248.

Keller, M. D., Kiene, R. P., Matrai, P. A., and Bellows, W. K. (1999b). Production of glycine betaine and dimethylsulfoniopropionate in marine phytoplankton. II. N-limited chemostat cultures. *Marine Biology*, 135(2):249–257.

Kettle, A. J., Andreae, M. O., Amouroux, D., Andreae, T. W., Bates, T. S., Berresheim, H., Bingemer, H., Boniforti, R., Curran, M. A. J., DiTullio, G. R., Helas, G., Jones, G. B.,

Keller, M. D., Kiene, R. P., Leck, C., Levasseur, M., Malin, G., Maspero, M., Matrai, P., McTaggart, A. R., Mihalopoulos, N., Nguyen, B. C., Novo, A., Putaud, J. P., Rapsomanikis, S., Roberts, G., Schebeske, G., Sharma, S., Simó, R., Staubes, R., Turner, S., and Uher, G. (1999). A global database of sea surface dimethylsulfide (DMS) measurements and a procedure to predict sea surface DMS as a function of latitude, longitude, and month. *Global Biogeochemical Cycles*, 13(2):399.

Kieber, D. J., Jiao, J., Kiene, R. P., and Bates, T. S. (1996). Impact of dimethylsulfide photochemistry on methyl sulfur cycling in the equatorial Pacific Ocean. *Journal of Geophysical Research*, 101(C2):3715–3722.

Kieber, D. J., Toole, D. A., Jankowski, J. J., Kiene, R. P., Westby, G. R., del Valle, D., and Slezak, D. (2007). Chemical light meters for photochemical and photobiological studies. *Aquatic Sciences*, 69(3):360–376.

Kiene, R. P. and Bates, T. S. (1990). Biological removal of dimethyl sulphide from sea water. *Nature*, 345(21 June):702–705.

Kiene, R. P., Hoffmann Williams, L., and Walker, J. (1998). Seawater microorganisms have a high affinity glycine betaine uptake system which also recognizes dimethylsulfoniopropionate. *Aquatic Microbial Ecology*, 15(Galinski 1995):39–51.

Kiene, R. P., Linn, L., and Bruton, J. (2000). New and important roles for DMSP in marine microbial communities. *Journal of Sea Research*, 43:209–224.

Kiene, R. P. and Linn, L. J. (2000). The fate of dissolved dimethylsulfoniopropionate (DMSP) in seawater: tracer studies using 35S-DMSP. *Geochimica et Cosmochimica Acta*, 64(16):2797–2810.

Kiene, R. P., Linn, L. J., González, J., Moran, M. a., and Bruton, J. a. (1999). Dimethylsulfoniopropionate and methanethiol are important precursors of methionine and protein-sulfur in marine bacterioplankton. *Applied and environmental microbiology*, 65(10):4549–58.

Kiene, R. P. and Service, S. K. (1991). Decomposition of dissolved DMSP and DMS in estuarine waters: dependence on temperature and substrate concentration. *Marine Ecology Progress Series*, 76:1–11.

Kiene, R. P. and Slezak, D. (2006). Low dissolved DMSP concentrations in seawater revealed by small volume gravity filtration and dialysis sampling. *Limnol. Oceanogr.: Methods*, 4:80–95.

Kirchman, D., K'nees, E., and Hodson, R. (1985). Leucine incorporation and its potential as a measure of protein synthesis by bacteria in natural aquatic systems. *Appl. Envir. Microbiol.*, 49(3):599–607.

Kirk, J. T. O. (1994). *Light and Photosynthesis in Aquatic Ecosystems*. Cambridge University Press, Cambridge, 2nd edition.

Kolber, Z. (2007). Energy Cycle in the Ocean: Powering the Microbial World. *Oceanography*, (June):79–88.

Kolber, Z., Van Dover, C., Niederman, R., and Falkowski, P. (2000). Bacterial photosynthesis in surface waters of the open ocean. *Nature*, 407:177 – 179.

Lana, A., Bell, T. G., Simó, R., Vallina, S. M., Ballabrera-Poy, J., Kettle, A. J., Dachs, J., Bopp, L., Saltzman, E. S., Stefels, J., Johnson, J. E., and Liss, P. S. (2011). An updated climatology of surface dimethlysulfide concentrations and emission fluxes in the global ocean. *Global Biogeochemical Cycles*, 25(1):GB1004.

Lana, A., Simó, R., Vallina, S. M., and Dachs, J. (2012). Re-examination of global emerging patterns of ocean DMS concentration. *Biogeochemistry*, 110(1-3):173–182.

Laney, S. R. (2003). Assessing the error in photosynthetic properties determined with Fast Repetition Rate fluorometry. *Limnology and Oceanography*, 48(6):2234–2242.

Large, W. G., Mcwilliams, J. C., and Doney, S. C. (1994). Oceanic vertical mixing: A review and a model with a nonlocal boundary layer parameterization. *Reviews of Geophysics*, 32(4):363–403.

Laroche, D., Vézina, A., Levasseur, M., Gosselin, M., Stefels, J., Keller, M. D., Matrai, P., and Kwint, R. (1999). DMSP synthesis and exudation in phytoplankton:a modeling approach. *Marine Ecology Progress Series*, 180:37–49.

Lasternas, S. and Agustí, S. (2010). Phytoplankton community structure during the record Arctic ice-melting of summer 2007. *Polar Biology*, 33(12):1709–1717.

Lasternas, S., Agustí, S., and Duarte, C. (2010). Phyto- and bacterioplankton abundance and viability and their relationship with phosphorus across the Mediterranean Sea. *Aquatic Microbial Ecology*, 60(2):175–191.

Le Clainche, Y., Vézina, A., Levasseur, M., Cropp, R. A., Gunson, J. R., Vallina, S. M., Vogt, M., Lancelot, C., Allen, J. I., Archer, S. D., Bopp, L., Deal, C., Elliott, S., Jin, M., Malin, G., Schoemann, V., Simó, R., Six, K. D., and Stefels, J. (2010). A first appraisal of prognostic ocean DMS models and prospects for their use in climate models. *Global Biogeochemical Cycles*, 24(3):1–13.

Le Quéré, C., Harrison, S. P., Prentice, I. C., Buitenhuis, E. T., Aumont, O., Bopp, L., Claustre, H., Da Cunha, L. C., Geider, R., Giraud, X., and Others (2005). Ecosystem dynamics based on plankton functional types for global ocean biogeochemistry models. *Global Change Biology*, 11(11):2016–2040.

Leck, C. (2005). Source and evolution of the marine aerosolA new perspective. *Geophysical Research Letters*, 32(19):28–31.

Ledyard, K. M. and Dacey, J. W. H. (1996). Microbial cycling of DMSP and DMS in coastal and oligotrophic seawater. *Limnology and Oceanography*, 41(1):33–40.

Lee, P. A. and de Mora, S. J. (1999). Intracellular Dimethylsulfoxide (Dmso) in Unicellular Marine Algae: Speculations on Its Origin and Possible Biological Role. *Journal of Phycology*, 35(1):8–18.

Legendre, P. and Legendre, L. (1998). *Numerical Ecology*.

Lesser, M. (1996). Acclimation of phytoplankton to UV-B radiation:oxidative stress and photoinhibition of photosynthesis are not prevented by UV-absorbing compounds in the dinoflagellate Prorocentrum micans. *Marine Ecology Progress Series*, 132:287–297.

Lesser, M. P. (2006). Oxidative stress in marine environments: biochemistry and physiological ecology. *Annual review of physiology*, 68(3):253–78.

Levasseur, M. (2011). Ocean science: If Gaia could talk. *Nature Geoscience*, 4(6):351–352.

Levasseur, M., Gosselin, M., and Michaud, S. (1994). A new source of dimethylsulfide (DMS) for the arctic atmosphere: ice diatoms. *Marine Biology*, 121(2):381–387.

Levine, N. M., Varaljay, V. a., Toole, D. a., Dacey, J. W. H., Doney, S. C., and Moran, M. A. (2012). Environmental, biochemical and genetic drivers of DMSP degradation and DMS production in the Sargasso Sea. *Environmental microbiology*.

Li, J., Liu, Z., Tan, C., Guo, X., Wang, L., Sancar, A., and Zhong, D. (2010). Dynamics and mechanism of repair of ultraviolet-induced (6-4) photoproduct by photolyase. *Nature*, 466(7308):887–890.

Li, W. K. W. (2002). Macroecological patterns of phytoplankton in the northwestern North Atlantic Ocean. *Nature*, 419(September):154–157.

Liss, P. S. (2007). Trace gas emissions from the marine biosphere. *Philosophical transactions. Series A, Mathematical, physical, and engineering sciences*, 365(1856):1697–704.

Litchman, E. and Klausmeier, C. A. (2008). Trait-Based Community Ecology of Phytoplankton. *Annual Review of Ecology, Evolution and Systematics*, 39:615–639.

Liu, H., Probert, I., Uitz, J., Claustre, H., Aris-Brosou, S., Frada, M., Not, F., and de Vargas, C. (2009). Extreme diversity in noncalcifying haptophytes explains a major pigment paradox in open oceans. *Proceedings of the National Academy of Sciences of the United States of America*, 106(31):12803–8.

Lizotte, M., Levasseur, M., Kudo, I., Suzuki, K., Tsuda, A., Kiene, R. P., and Scarratt, M. G. (2009). Iron-induced alterations of bacterial DMSP metabolism in the western subarctic Pacific during SEEDS-II. *Deep Sea Research Part II: Topical Studies in Oceanography*, 56(26):2889–2898.

Lizotte, M., Levasseur, M., Michaud, S., Scarratt, M. G., Merzouk, A., Gosselin, M., Pommier, J., Rivkin, R. B., and Kiene, R. P. (2012). Macroscale patterns of the biological cycling of dimethylsulfoniopropionate (DMSP) and dimethylsulfide (DMS) in the Northwest Atlantic. *Biogeochemistry*.

Llabrés, M., Agustí, S., Alonso-Laita, P., and Herndl, G. (2010). Synechococcus and Prochlorococcus cell death induced by UV radiation and the penetration of lethal UVR in the Mediterranean Sea. *Marine Ecology Progress Series*, 399(Roy 1999):27–37.

Longhurst, a. (1995). Seasonal cycles of pelagic production and consumption. *Progress In Oceanography*, 36(2):77–167.

Longhurst, A. (2007). *Ecological Geography of the Sea*. Academic Press, 2nd edition.

Longhurst, A., Sathyendranath, S., Platt, T., and Caverhill, C. (1995). An estimate of global primary production in the ocean from satellite radiometer data. *Journal of Plankton Research*, 17(6):1245–1271.

Lovelock, J. (1995). *The Ages of Gaia: A Biography of Our Living Earth*.

Lovelock, J. E., Maggs, R. J., and Rasmussen, R. A. (1972). Atmospheric Dimethyl Sulphide and the Natural Sulphur Cycle. *Nature*, 237(5356):452–453.

Lovelock, J. E. and Margulis, L. (1974). Atmospheric homeostasis by and for the biosphere: the gaia hypothesis. *Tellus*, 26(1-2):2–10.

Macintyre, H. L., Kana, T. M., Anning, T., and Geider, R. J. (2002). Photoacclimation of photosynthesis irradiance response curves and photosynthetic pigmentspigments in microalgae and cyanobacteria. 38(July 2000):17–38.

Mackey, S. R. and Golden, S. S. (2007). Winding up the cyanobacterial circadian clock. *Trends in microbiology*, 15(9):318–388.

Mahadevan, A., D'Asaro, E., Lee, C., and Perry, M. J. (2012). Eddy-driven stratification initiates North Atlantic spring phytoplankton blooms. *Science*, 337(6090):54–8.

Malin, G. and Kirst, G. O. (1997). Algal Production of Dimethyl Sulfide and Its Atmospheric Role1. *Journal of Phycology*, 33(6):889–896.

Manizza, M., Quéré, C. L., Watson, A. J., and Buitenhuis, E. T. (2005). Bio-optical feedbacks among phytoplankton, upper ocean physics and sea-ice in a global model. *Geophys. Res. Lett.*

Mann, K. H. and Lazier, J. R. N. (2006). *Dynamics of Marine Ecosystems: Biological-Physical Interactions in the Oceans*. Blackwell, 3rd edition.

Marandino, C. A., Bruyn, W. J. D., Miller, S. D., and Saltzman, E. S. (2009). Open ocean DMS air/sea fluxes over the eastern South Pacific Ocean. *Atmospheric Chemistry and Physics*, 9:345–356.

Marandino, C. a., De Bruyn, W. J., Miller, S. D., and Saltzman, E. S. (2008). DMS air/sea flux and gas transfer coefficients from the North Atlantic summertime coccolithophore bloom. *Geophysical Research Letters*, 35(23):1–5.

Margalef, R. (1978). Life-forms of phytoplankton as survival alternatives in an unstable environment. *Oceanologica Acta*, 1(4):493–509.

Margalef, R. (1997). *Our biosphere*. Ecology Institue.

Marie, D. and Partensky, F. (2006). Analyse de micro-organismes marins. In Ronot, X., Grunwald, D., Mayol, J. F., and Boutonnat, J., editors, *La cytométrie en flux*, pages 211–233. Lavoisier.

Matrai, P., Vernet, M., and Wassmann, P. (2007). Relating temporal and spatial patterns of DMSP in the Barents Sea to phytoplankton biomass and productivity. *Journal of Marine Systems*, 67(1-2):83–101.

Matrai, P. a. and Keller, M. D. (1994). Total organic sulfur and dimethylsulfoniopropionate in marine phytoplankton: intracellular variations. *Marine Biology*, 119(1):61–68.

Matrai, P. A. and Vernet, M. (1997). Dynamics of the vernal bloom in the marginal ice zone of the Barents Sea: Dimethyl sulfide and dimethylsulfoniopropionate budgets. *Journal of Geophysical Research*, 102(96):22965–22979.

McGillis, W. R. (2005). US SOLAS: Science Implementation Strategy. Technical report, US SOLAS.

Menden-Deuer, S. and Lessard, E. J. (2000). Carbon to volume relationships for dinoflagellates, diatoms, and other protist plankton. *Limnology and Oceanography*, 45(3):569–579.

Merzouk, A., Levasseur, M., Scarratt, M., Michaud, S., and Gosselin, M. (2004). Influence of dinoflagellate diurnal vertical migrations on dimethylsulfoniopropionate and dimethylsulfide distribution and dynamics (St . Lawrence Estuary , Canada) 1. 720(September 2002):712–720.

Merzouk, a., Levasseur, M., Scarratt, M., Michaud, S., Lizotte, M., Rivkin, R., and Kiene, R. P. (2008). Bacterial DMSP metabolism during the senescence of the spring diatom bloom in the Northwest Atlantic. *Marine Ecology Progress Series*, 369:1–11.

Merzouk, a., Levasseur, M., Scarratt, M., Michaud, S., Rivkin, R., Hale, M., Kiene, R. P., Price, N., and Li, W. (2006). DMSP and DMS dynamics during a mesoscale iron fertilization experiment in the Northeast PacificPart II: Biological cycling. *Deep Sea Research Part II: Topical Studies in Oceanography*, 53(20-22):2370–2383.

Moran, M. A., Reisch, C. R., Kiene, R. P., and Whitman, W. B. (2012). Genomic Insights into Bacterial DMSP Transformations. *Annual Review of Marine Science*, 4(1):523–542.

Morán, X. A. G., Gasol, J. M., Arin, L., and Estrada, M. (1999). A comparison between glass fiber and membrane filters for the estimation of phytoplankton POC and DOC production. *Marine Ecology Progress Series*, 187:31–41.

Moran, X. A. G., Massana, R., and Gasol, J. M. (2001). Light Conditions Affect the Measurement of Oceanic Bacterial Production via Leucine Uptake. *Applied and Environmental Microbiology*, 67(9):3795–3801.

Morel, A. and Gentili, B. (2004). Radiation transport within oceanic (case 1) water. 109(C06008).

Morel, a., Huot, Y., Gentili, B., Werdell, P., Hooker, S., and Franz, B. (2007). Examining the consistency of products derived from various ocean color sensors in open ocean (Case 1) waters in the perspective of a multi-sensor approach. *Remote Sensing of Environment*, 111(1):69–88.

Morel, A. and Maritorena, S. (2001). Bio-optical properties of oceanic waters: A reappraisal. *Journal of Geophysical Research*, 106(C4):7163–7180.

Morel, A. and Prieur, L. (1977). Analysis of Variations in Ocean Color. *Limnology and Oceanography*, 22(4):709–722.

Moritz, R. E., Bitz, C. M., and Steig, E. J. (2002). Dynamics of Recent Climate Change in the Arctic. *Science*, 297(2002):1497–1502.

Mou, X., Sun, S., Edwards, R. a., Hodson, R. E., and Moran, M. A. (2008). Bacterial carbon processing by generalist species in the coastal ocean. *Nature*, 451(7179):708–11.

Murik, O. and Kaplan, A. (2009). Paradoxically, prior acquisition of antioxidant activity enhances oxidative stress-induced cell death. *Environmental microbiology*, 11(9):2301–2309.

Neale, P. J., Helbling, E. W., and Zagarese, H. E. (2003). MODULATION OF UVR EXPOSURE AND EFFECTS BY VERTICAL MIXING AND ADVECTION. In *UV effects in aquatic organisms and ecosystems*, chapter 4.

Neale, P. J. and Kieber, D. J. (2000). Assessing Biological and Chemical Effects of UV in the Marine Environment : Spectral Weighting Functions. *Issues in Environmental Science and Technology*, (14).

Nejstgaard, J. C., Tang, K. W., Steinke, M., Dutz, J., Koski, M., Antajan, E., and Long, J. D. (2007). Zooplankton grazing on Phaeocystis: a quantitative review and future challenges. *Biogeochemistry*, 83(1-3):147–172.

Nelson, N., Siegel, D., Carlson, C., Swan, C., Smethiejr, W., and Khatiwala, S. (2007). Hydrography of chromophoric dissolved organic matter in the North Atlantic. *Deep Sea Research Part I: Oceanographic Research Papers*, 54(5):710–731.

Nevitt, G. a. (2008). Sensory ecology on the high seas: the odor world of the procellariiform seabirds. *The Journal of experimental biology*, 211(Pt 11):1706–13.

Nightingale, P. D., Malin, G., Law, C. S., Watson, A. J., Liss, P. S., Liddicoat, M., Boutin, J., and Upstill-Goddard, R. C. (2000). In situ evaluation of air-sea gas exchange parameterizations using novel conservative and volatile tracers. *Global Biogeochemical Cycles*, 14(1):373–387.

Ochs, C. a. (1997). Effects of UV radiation on grazing by two marine heterotrophic nanoflagellates on autotrophic picoplankton. *Journal of Plankton Research*, 19(10):1517–1536.

Oduro, H., Van Alstyne, K. L., and Farquhar, J. (2012). Sulfur isotope variability of oceanic DMSP generation and its contributions to marine biogenic sulfur emissions. *Proceedings of the National Academy of Sciences of the United States of America*, 109(23):9012–6.

Orellana, M. V., Matrai, P. A., Leck, C., Rauschenberg, C. D., Lee, A. M., and Coz, E. (2011). Marine microgels as a source of cloud condensation nuclei in the high Arctic. *Proceedings of the National Academy of Sciences of the United States of America*, 108(33):13162–13167.

Oubelkheir, K., Claustre, H., Sciandra, A., and Babin, M. (2005). Bio-optical and biogeochemical properties of different trophic regimes in oceanic waters. *Limnology and Oceanography*, 50(6):1795–1809.

Pernthaler, A., Pernthaler, J., and Amann, R. (2002). Fluorescence In Situ Hybridization and Catalyzed Reporter Deposition for the Identification of Marine Bacteria. *Society*, 68(6):3094–3101.

Piera, J. (2001). *Signal processing of microstructure profiles: integrating turbulent spatial scales in aquatic ecological modeling*. PhD thesis, Universitat de Girona.

Pinhassi, J., Simó, R., González, J., and Vila-Costa, M. (2005). Dimethylsulfoniopropionate turnover is linked to the composition and dynamics of the bacterioplankton assemblage during a microcosm phytoplankton bloom. *Applied and*, 71(12):7650–7660.

Polimene, L., Archer, S. D., Butenschön, M., and Allen, J. I. (2011). A mechanistic explanation of the Sargasso Sea DMS summer paradox. *Biogeochemistry*, 110(1-3):243–255.

Polovina, J. J., Howell, E. a., and Abecassis, M. (2008). Ocean's least productive waters are expanding. *Geophysical Research Letters*, 35(3):2–6.

Poretsky, R. S., Hewson, I., Sun, S., Allen, A. E., Zehr, J. P., and Moran, M. A. (2009). Comparative day/night metatranscriptomic analysis of microbial communities in the North Pacific subtropical gyre. *Environmental Microbiology*, 11(6):1358–75.

Quinn, P. K. and Bates, T. S. (2011). The case against climate regulation via oceanic phytoplankton sulphur emissions. *Nature*, 480(7375):51–6.

Reisch, C. R., Stoudemayer, M. J., Varaljay, V. A., Amster, I. J., Moran, M. A., and Whitman, W. B. (2011). Novel pathway for assimilation of dimethylsulphoniopropionate widespread in marine bacteria. *Nature*, 473(7346):208–11.

Rellinger, A. N., Kiene, R. P., del Valle, D. a., Kieber, D. J., Slezak, D., Harada, H., Bisgrove, J., and Brinkley, J. (2009). Occurrence and turnover of DMSP and DMS in deep waters of the Ross Sea, Antarctica. *Deep Sea Research Part I: Oceanographic Research Papers*, 56(5):686–702.

Reynolds, C. S. (1994). The long, the short and the stalled: on the attributes of phytoplankton selected by physical mixing in lakes and rivers. *Hydrobiologia*, 289(1-3):9–21.

Ross, O. N., Geider, R. J., Berdalet, E., Artigas, M. L., and Piera, J. (2011a). Modelling the effect of vertical mixing on bottle incubations for determining in situ phytoplankton dynamics. I. Growth rates. *Marine Ecology Progress Series*, 435:13–31.

Ross, O. N., Geider, R. J., and Piera, J. (2011b). Modelling the effect of vertical mixing on bottle incubations for determining in situ phytoplankton dynamics. II. Primary production. *Marine Ecology Progress Series*, 435:33–45.

Roy, S. (2000). The strategies for minimization of UV damage. In de Mora, S. J., Demers, S., and Vernet, M., editors, *The Effects of UV Radiation in the Marine Environment*, chapter 3, pages 177–205. Cambridge University Press, Cambridge.

Royer, S.-J., Levasseur, M., Lizotte, M., Arychuk, M., Scarratt, M. G., Wong, C., Lovejoy, C., Robert, M., Johnson, K., Pena, A., Michaud, S., and Kiene, R. P. (2010). Microbial dimethylsulfoniopropionate (DMSP) dynamics along a natural iron gradient in the northeast subarctic Pacific. *Limnology and Oceanography*, 55(4):1614–1626.

Rudels, B., Bjfrk, G., Nilsson, J., and Winsor, P. (2005). The interaction between waters from the Arctic Ocean and the Nordic Seas north of Fram Strait and along the East Greenland Current: results from the Arctic Ocean-02 Oden expedition. *Journal of Marine Systems*, 55:1–30.

Ruiz-González, C., Galí, M., Gasol, J. M., and Simó, R. (2012a). Sunlight effects on the DMSP-sulfur and leucine assimilation activities of polar heterotrophic bacterioplankton. *Biogeochemistry*, pages 1–18.

Ruiz-González, C., Galí, M., Lefort, T., Cardelús, C., Simó, R., and Gasol, J. M. (2012b). Annual variability in light modulation of bacterial heterotrophic activity in surface northwestern Mediterranean waters. *Limnology and Oceanography*, 57(5):1376–1388.

Ruiz-González, C., Galí, M., Sintes, E., Herndl, G. J., Gasol, J. M., and Simó, R. (2012c). Sunlight Effects on the Osmotrophic Uptake of DMSP-Sulfur and Leucine by Polar Phytoplankton. *PLoS ONE*, 7(9):e45545.

Ruiz-González, C., Lefort, T., Galí, M., Montserrat Sala, M., Sommaruga, R., Simó, R., and Gasol, J. M. (2012d). Seasonal patterns in the sunlight sensitivity of bacterioplankton from Mediterranean surface coastal waters. *FEMS microbiology ecology*, 79(3):661–74.

Ruiz-González, C., Lefort, T., Massana, R., Simó, R., and Gasol, J. M. (2012e). Diel changes in bulk and single-cell bacterial heterotrophic activity in winter surface waters of the northwestern Mediterranean Sea. *Limnology and Oceanography*, 57(1):29–42.

Ruiz-González, C., Simó, R., Vila-Costa, M., Sommaruga, R., and Gasol, J. M. (2012f). Sunlight modulates the relative importance of heterotrophic bacteria and picophytoplankton in DMSP-sulphur uptake. *The ISME journal*, 6(3):650–9.

Sakshaug, E., Bricaud, a., Dandonneau, Y., Falkowski, P. G., Kiefer, D. a., Legendre, L., Morel, a., Parslow, J., and Takahashi, M. (1997). Parameters of photosynthesis: definitions, theory and interpretation of results. *Journal of Plankton Research*, 19(11):1637–1670.

Saló, V., Simó, R., and Calbet, A. (2010). Revisiting the dilution technique to quantify the role of microzooplankton in DMS(P) cycling: laboratory and field tests. *Journal of Plankton Research*, 32(9):1255–1267.

Saló, V., Simó, R., Vila-Costa, M., and Calbet, A. (2009). Sulfur assimilation by Oxyrrhis marina feeding on a 35S-DMSP-labelled prey. *Environmental microbiology*, 11(12):3063–72.

Saltzman, E. S., Bruyn, W. J. D., Lawler, M. J., Marandino, C. A., and Mccormick, C. A. (2009). A chemical ionization mass spectrometer for continuous underway shipboard analysis of dimethylsulfide in near-surface seawater. *Ocean Science*, 5:537–546.

Saltzman, E. S., King, D. B., Holmen, K., and Leck, C. (1993). Experimental Determination of the Diffusion Coefficient of Dimethylsulfide in Water. *Journal of geophysical Research*, 98(C)):16481–16486.

Scarratt, M., Cantin, G., Levasseur, M., and Michaud, S. (2000). Particle size-fractionated kinetics of DMS production: where does DMSP cleavage occur at the microscale. *Journal of Sea Research*, 43:245–252.

Schäfer, H. (2007). Isolation of Methylophaga spp. from marine dimethylsulfide-degrading enrichment cultures and identification of polypeptides induced during growth on dimethylsulfide. *Applied and environmental microbiology*, 73(8):2580–91.

Schlesinger, W. H. (1997). *Biogeochemistry: an analysis of global change.* Number Ed. 2. Academic Press.

Schoemann, V., Becquevort, S., Stefels, J., Rousseau, V., and Lancelot, C. (2005). Phaeocystis blooms in the global ocean and their controlling mechanisms: a review. *Journal of Sea Research*, 53(1-2):43–66.

Setlow, R. B. (1974). The wavelengths in sunlight effective in producing skin cancer: a theoretical analysis. *Proceedings of the National Academy of Sciences of the United States of America*, 71(9):3363–6.

Seymour, J. R., Simó, R., Ahmed, T., and Stocker, R. (2010). Chemoattraction to Dimethylsulfoniopropionate Throughout the Marine Microbial Food Web. *Science*, 329(5989):342–345.

Siegel, D. a. (2002). Global distribution and dynamics of colored dissolved and detrital organic materials. *Journal of Geophysical Research*, 107(C12):1–14.

Simó, R. (2001). Production of atmospheric sulfur by oceanic plankton: biogeochemical, ecological and evolutionary links. *Trends in Ecology & Evolution*, 16(6):287–294.

Simó, R. (2004). From cells to globe : approaching the dynamics of DMS(P) in the ocean at multiple scales. *Canadian Journal of Fisheries and Aquatic Sciences*, 61:673–684.

Simó, R. (2011). The role of marine microbiota in short-term climate regulation. In Duarte, C. M., editor, *The Role of Marine Biota in the Functioning of the Biosphere*, chapter 5, pages 107–130. Fundación BBVA.

Simó, R. and Dachs, J. (2002). Global ocean emission of dimethylsulfide predicted from biogeophysical data. *Global Biogeochemical Cycles*, 16(4).

Simó, R., Grimalt, J. O., and Albaigés, J. (1996). Sequential Method for the Field Determination of Nanomolar Concentrations of Dimethyl Sulfoxide in Natural Waters. *Analytical Chemistry*, 68(9):1493–1498.

Simó, R., Hatton, A., Malin, G., and Liss, P. (1998). Particulate dimethyl sulphoxide in seawater:production by microplankton. *Marine Ecology Progress Series*, 167:291–296.

Simó, R. and Pedrós-Alió, C. (1999a). Role of vertical mixing in controlling the oceanic production of dimethyl sulphide. *Nature*, 402(25 November):396–99.

Simó, R. and Pedrós-Alió, C. (1999b). Short-term variability in the open ocean cycle of dimethylsulfide. *Global Biogeochemical Cycles*, 13(4):1173.

Simó, R. and Pedrós-Alió, C. (1999c). Short-term variability in the open ocean cycle of dimethylsulfide. *Global Biogeochemical Cycles*, 13(4):1173–1181.

Simó, R., Pedrós-Alió, C., Malin, G., and Grimalt, J. O. (2000). Biological turnover of DMS, DMSP and DMSO in contrasting open-sea waters. *Marine Ecology Progress Series*, 203:1–11.

Simó, R. and Vila-Costa, M. (2006). Ubiquity of algal dimethylsulfoxide in the surface ocean: Geographic and temporal distribution patterns. *Marine Chemistry*, 100(1-2):136–146.

Simó, R., Vila-Costa, M., Alonso-Sáez, L., Cardelús, C., Guadayol, O., Vázquez-Domínguez, E., and Gasol, J. (2009). Annual DMSP contribution to S and C fluxes through phytoplankton and bacterioplankton in a NW Mediterranean coastal site. *Aquatic Microbial Ecology*, 57:43–55.

Simon, M. and Azam, F. (1989). Protein content and protein synthesis rates of planktonic marine bacteria. *Marine Ecology Progress Series*, 51:201–213.

Sinha, V., Williams, J., Meyerhöfer, M., Riebesell, U., Paulino, a. I., and Larsen, a. (2007). Air-sea fluxes of methanol, acetone, acetaldehyde, isoprene and DMS from a Norwegian fjord following a phytoplankton bloom in a mesocosm experiment. *Atmospheric Chemistry and Physics*, 7(3):739–755.

Slezak, D., Brugger, A., and Herndl, G. J. (2001). Impact of solar radiation on the biological removal of dimethylsulfoniopropionate and dimethylsulfide in marine surface waters. *Aquat. Microb. Ecol*, 25:87–97.

Slezak, D., Kiene, R. P., Toole, D. A., Simó, R., and Kieber, D. J. (2007). Effects of solar radiation on the fate of dissolved DMSP and conversion to DMS in seawater. *Aquatic Sciences*, 69:377–393.

Smith, D. C. and Azam, F. (1992). A simple, economical method for measuring bacterial protein synthesis rates in seawater using 3H-leucine. *Marine Microbial Food Webs*, 6(2):107–114.

Sobrino, C., Neale, P. J., Montero, O., and Lubian, L. M. (2005). Biological weighting function for xanthophyll de-epoxidation induced by ultraviolet radiation. *Physiologia Plantarum*, 125(1):41–51.

Sommaruga, R. (2003). UVR and its effects on species interactions. *UV effects in aquatic organisms and*, pages 4–26.

Sommaruga, R., Hofer, J. S., Alonso-Saez, L., and Gasol, J. M. (2005). Differential sunlight sensitivity of picophytoplankton from surface Mediterranean coastal waters. *Applied and Environmental Microbiology*, 71(4):2154–2157.

Spielmeyer, A., Gebser, B., and Pohnert, G. (2011). Investigations of the uptake of dimethylsulfoniopropionate by phytoplankton. *ChemBioChem*, 12:2276–2279.

Spiese, C., Kieber, D. J., Nomura, C., and Kiene, R. P. (2009). Reduction of dimethylsulfoxide to dimethylsulfide by marine phytoplankton. *Limnology and Oceanography*, 54(2):560–570.

Stefels, J. (2000). Physiological aspects of the production and conversion of DMSP in marine algae and higher plants. *Journal of Sea Research*, 43:183–197.

Stefels, J., Dacey, J. W., and Elzenga, J. T. M. (2009). In vivo DMSP-biosynthesis measurements using stable-isotope incorporation and proton-transfer-reaction mass spectrometry (PTR-MS). *Limnology and Oceanography: Methods*, 7:595–611.

Stefels, J. and Dijkhuizen, L. (1996). Characteristics of DMSP-lyase in Phaeocystis sp. (Prymnesiophyceae). *Marine Ecology Progress Series*, 131:307–313.

Stefels, J., Dijkhuizen, L., and Gieskes, W. (1995). DMSP-lyase activity in a spring phytoplankton bloom off the Dutch coast, related to Phaeocystis sp. abundance. *Marine Ecology Progress Series*, 123(1991):235–243.

Stefels, J., Steinke, M., Turner, S. M., Malin, G., and Belviso, S. (2007). Environmental constraints on the production and removal of the climatically active gas dimethylsulphide (DMS) and implications for ecosystem modelling. *Biogeochemistry*, 83:245–75.

Stefels, J. and van Boekel, W. H. M. (1993). Production of DMS from dissolved DMSP in axenic cultures of the marine phytoplankton species Phaeocystis sp. *Marine Ecology Progress Series*, 97:11–18.

Steiner, N. and Denman, K. (2008). Parameter sensitivities in a 1-D model for DMS and sulphur cycling in the upper ocean. *Deep Sea Research Part I: Oceanographic Research Papers*, 55(7):847–865.

Steiner, N. S., Robert, M., Arychuk, M., Levasseur, M. L., Merzouk, A., Peña, M. A., Richardson, W. a., and Tortell, P. D. (2011). Evaluating DMS measurements and model results in the Northeast subarctic Pacific from 19962010. *Biogeochemistry*, 110(1-3):269–285.

Steinke, M., Malin, G., Gibb, S. W., and Burkill, P. H. (2002). Vertical and temporal variability of DMSP lyase activity in a coccolithophorid bloom in the northern North Sea. *DeepSea Research II*, 49:3001–3016.

Stroeve, J., Serreze, M., Drobot, S., Gearheard, S., Holland, M., Maslanik, J., Meier, W., and Scambos, T. (2008). Arctic Sea Ice Extent Plummets in 2007. *Eos, Transactions (American Geophysical Union)*, 89(2):13–14.

Strom, S. L. (2001). Light-aided digestion, grazing and growth in herbivorous protists. *Aquatic Microbial Ecology*, 23:253–261.

Sunda, W., Kieber, D. J., Kiene, R. P., and Huntsman, S. (2002). An antioxidant function for DMSP and DMS in marine algae. *Nature*, 418(6895):317–20.

Sunda, W., Litaker, R., Hardison, D., and Tester, P. (2005). Dimethylsulfoniopropionate (DMSP) and its relation to algal pigments in diverse waters of the Belize coastal lagoon and barrier reef system. *Marine Ecology Progress Series*, 287:11–22.

Sunda, W. G., Hardison, R., Kiene, R. P., Bucciarelli, E., and Harada, H. (2007). The effect of nitrogen limitation on cellular DMSP and DMS release in marine phytoplankton: climate feedback implications. *Aquatic Sciences*, 69(3):341–351.

Sverdrup, H. U., Johnson, M. W., and Fleming, R. H. (1942). *The Oceans Their Physics, Chemistry, and General Biology*. Prentice-Hall, New York.

Tang, K. and Simó, R. (2003). Trophic uptake and transfer of DMSP in simple planktonic food chains. *Aquatic Microbial Ecology*, 31:193–202.

Tartarotti, B., Laurion, I., and Sommaruga, R. (2001). Large Variability in the Concentration of Mycosporine-Like Amino Acids among Zooplankton from Lakes Located across an Altitude Gradient. *Limnology and Oceanography*, 46(6):1546–1552.

Taylor, J. R. (1997). *An introduction to error analysis*. University Science Books, New York.

Todd, J. D., Rogers, R., Li, Y. G., Wexler, M., Bond, P. L., Sun, L., Curson, A. R. J., Malin, G., Steinke, M., and Johnston, A. W. B. (2007). Structural and regulatory genes required to make the gas dimethyl sulfide in bacteria. *Science*, 315(5812):666–9.

Toole, D. A., Kieber, D. J., Kiene, R. P., Siegel, D. a., and Nelson, N. B. (2003). Photolysis and the dimethylsulfide (DMS) summer paradox in the Sargasso Sea. *Limnology and Oceanography*, 48(3):1088–1100.

Toole, D. A. and Siegel, D. A. (2004). Light-driven cycling of dimethylsulfide (DMS) in the Sargasso Sea: Closing the loop. *Geophysical Research Letters*, 31(9):5–8.

Toole, D. A., Siegel, D. A., and Doney, S. C. (2008). A light-driven, one-dimensional dimethylsulfide biogeochemical cycling model for the Sargasso Sea. *Journal of Geophysical Research*, 113:1–20.

Toole, D. A., Slezak, D., Kiene, R. P., Kieber, D. J., and Siegel, D. A. (2006). Effects of solar radiation on dimethylsulfide cycling in the western Atlantic Ocean. *Deep Sea Res. I*, 53:136–153.

Tortell, P. D. (2005). Dissolved gas measurements in oceanic waters made by membrane inlet mass spectrometry. *Limnology and Oceanography: Methods*, 3:24–37.

Tripp, H. J., Kitner, J. B., Schwalbach, M. S., Dacey, J. W. H., Wilhelm, L. J., and Giovannoni, S. J. (2008). SAR11 marine bacteria require exogenous reduced sulphur for growth. *Nature*, 452(7188):741–4.

Unrein, F., Massana, R., Alonso-sa, L., and Gasol, J. M. (2007). Significant year-round effect of small mixotrophic flagellates on bacterioplankton in an oligotrophic coastal system. *Archaea*, 52(1):456–469.

Vahatalo, A. V. (2004). Photochemical and microbial decomposition of chromophoric dissolved organic matter during long (months?years) exposures. *Marine Chemistry*, 89(1-4):313–326.

Valle, D. A., Kiene, R. P., and Karl, D. M. (2012). Effect of visible light on dimethylsulfoniopropionate assimilation and conversion to dimethylsulfide in the North Pacific Subtropical Gyre. *Aquatic Microbial Ecology*, 66:47–62.

Vallina, S. M. and Simó, R. (2007). Strong relationship between DMS and the solar radiation dose over the global surface ocean. *Science*, 315(5811):506–8.

Vallina, S. M., Simó, R., Anderson, T. R., Gabric, A., Cropp, R., and Pacheco, J. M. (2008). A dynamic model of oceanic sulfur (DMOS) applied to the Sargasso Sea: Simulating the dimethylsulfide (DMS) summer paradox. *Journal of Geophysical Research*, 113:1–23.

Vallina, S. M., Simó, R., and Gassó, S. (2006). What controls CCN seasonality in the Southern Ocean? A statistical analysis based on satellite-derived chlorophyll and CCN and model-estimated OH radical and rainfall. *Global Biogeochemical Cycles*, 20(1):1–13.

Vallina, S. M., Simó, R., and Manizza, M. (2007). Weak response of oceanic dimethylsulfide to upper mixing shoaling induced by global warming. *Proceedings of the National Academy of Sciences of the United States of America*, 104(41):16004–9.

Van Alstyne, K. L., Schupp, P., and Slattery, M. (2006). The distribution of dimethylsulfoniopropionate in tropical Pacific coral reef invertebrates. *Coral Reefs*, 25(3):321–327.

van Bergeijk, S., Schönefeldt, K., Stal, L., and Huisman, J. (2002). Production and consumption of dimethylsulfide (DMS) and dimethylsulfoniopropionate (DMSP) in a diatom-dominated intertidal sediment. *Marine Ecology Progress Series*, 231:37–46.

van Duyl, F. (1998). Biological control of short-term variations in the concentration of DMSP and DMS during a Phaeocystis spring bloom. *Journal of Sea Research*, 40(3-4):221–231.

Vaulot, D. and Marie, D. (1999). Diel variability of photosynthetic picoplankton in the equatorial Pacific. *Journal of Geophysical Research*, 104(C2):3297–3310.

Veldhuis, M., Kraay, G., and Timmermans, K. (2001). Cell death in phytoplankton: correlation between changes in membrane permeability, photosynthetic activity, pigmentation and growth. *European Journal of Phycology*, 36(2):167–177.

Verdugo, P., Alldredge, A. L., Azam, F., Kirchman, D. L., Passow, U., and Santschi, P. H. (2004). The oceanic gel phase: a bridge in the DOMPOM continuum. *Marine Chemistry*, 92(1-4):67–85.

Vila-Costa, M., Del Valle, D. a., González, J. M., Slezak, D., Kiene, R. P., Sánchez, O., and Simó, R. (2006a). Phylogenetic identification and metabolism of marine dimethylsulfide-consuming bacteria. *Environmental microbiology*, 8(12):2189–200.

Vila-Costa, M., Kiene, R. P., and Simó, R. (2008). Seasonal variability of the dynamics of dimethylated sulfur compounds in a coastal northwest Mediterranean site. *Limnology and Oceanography*, 53(1):198–211.

Vila-Costa, M., Pinhassi, J., Alonso, C., Pernthaler, J., and Simó, R. (2007). An annual cycle of dimethylsulfoniopropionate-sulfur and leucine assimilating bacterioplankton in the coastal NW Mediterranean. *Environmental microbiology*, 9(10):2451–63.

Vila-Costa, M., Simó, R., Harada, H., Gasol, J. M., Slezak, D., and Kiene, R. P. (2006b). Dimethylsulfoniopropionate uptake by marine phytoplankton. *Science*, 314(5799):652–4.

Vila-reixach, G., Gasol, J. M., Cardelús, C., and Vidal, M. (2012). Seasonal dynamics and net production of dissolved organic carbon in an oligotrophic coastal environment. *Marine Ecology Progress Series*, 456:7–19.

Vincent, W. F. and Neale, P. J. (2000). Mechanisms of UV damage to aquatic organisms. In de Mora, S. J., Demers, S., and Vernet, M., editors, *The Effects of UV Radiation in the Marine Environment*, chapter 6, pages 149–176. Cambridge University Press, Cambridge.

Visscher, P. T. and Taylor, B. F. (1993). A new mechanism for the aerobic catabolism of dimethyl sulfide. *Applied and environmental microbiology*, 59(11):3784–9.

Vogt, M., Vallina, S. M., Buitenhuis, E. T., Bopp, L., and Le Quéré, C. (2010). Simulating dimethylsulphide seasonality with the Dynamic Green Ocean Model PlankTOM5. *Journal of Geophysical Research*, 115(C6):1–21.

Webb, W. L., Newton, M., and Starr, D. (1974). Carbon dioxide exchange of Alnus rubra. *Oecologia*, 17(4):281–291.

Welsh, D. T. (2000). Ecological significance of compatible solute accumulation by micro-organisms: from single cells to global climate. *FEMS microbiology reviews*, 24:263–290.

Wilks, D. S. (1995). *Statistical Methods in the Atmospheric Sciences*. Academic Press.

Wolfe, G. (2000). The chemical defense ecology of marine unicellular plankton: constraints, mechanisms, and impacts. *The Biological Bulletin*, 198(2):225–44.

Wolfe, G. and Kiene, R. P. (1993a). Effects of methylated, organic, and inorganic substrates on microbial consumption of dimethyl sulfide in estuarine waters. *Applied and environmental microbiology*, 59(8):2723–2726.

Wolfe, G. and Kiene, R. P. (1993b). Radioisotope and chemical inhibitor measurements of dimethyl sulfide consumption rates and kinetics in estuarine waters. *Marine ecology progress series. Oldendorf*, 99:261–269.

Wolfe, G. V., Levasseur, M., Cantin, G., and Michaud, S. (1999). Microbial consumption and production of dimethyl sulfide (DMS) in the Labrador Sea. *Aquatic Microbial Ecology*, 18:197–205.

Wolfe, G. V. and Steinke, M. (1996). Grazing-Activated Production of Dimethyl Sulfide (DMS) by Two Clones of Emiliania huxleyi. *Limnology and Oceanography*, 41(6):1151–1160.

Yang, G.-p., Jing, W., Kang, Z., Zhang, H., and GS (2008). Spatial variations of dimethylsulfide and dimethylsulfoniopropionate in the surface microlayer and in the subsurface waters of the South China Sea during springtime. *Marine environmental*, 65:85–97.

Yin, F., Grosjean, D., Flagan, R. C., and Seinfeld, J. H. (1990a). Photooxidation of dimethyl sulfide and dimethyl disulfide. II: Mechanism evaluation. *Journal of Atmospheric Chemistry*, 11(4):365–399.

Yin, F., Grosjean, D., and Seinfeld, J. (1990b). Photooxidation of dimethyl sulfide and dimethyl disulfide. I: Mechanism development. *Journal of Atmospheric Chemistry*, 11(4):309–364.

Yoch, D. (2002). Dimethylsulfoniopropionate: its sources, role in the marine food web, and biological degradation to dimethylsulfide. *Applied and Environmental Microbiology*, 68(12):5804–5815.

Yoch, D., Ansede, J., and KS (1997). Evidence for intracellular and extracellular dimethylsulfoniopropionate (DMSP) lyases and DMSP uptake sites in two species of marine bacteria. *Applied and environmental*, 63(8):3182–3188.

Zemmelink, H., Houghton, L., Sievert, S., and NM (2005). Gradients in dimethylsulfide, dimethylsulfonio-propionate, dimethylsulfoxide, and bacteria near the sea surface. *MARINE ECOLOGY-*, 295(3):33–42.

Zepp, R. G., Erickson, D. J., Paul, N. D., and Sulzberger, B. (2007). Interactive effects of solar UV radiation and climate change on biogeochemical cycling. *Photochemical & photobiological sciences : Official journal of the European Photochemistry Association and the European Society for Photobiology*, 6(3):286–300.

Zhang, T. and Hsu-Kim, H. (2010). Photolytic degradation of methylmercury enhanced by binding to natural organic ligands. *Nature geoscience*, 3(7):473–476.

Zimmer-Faust, R., de Souza, M. P., and Yoch, D. C. (1996). Bacterial Chemotaxis and its Potential Role in Marine Dimethylsulfide Production and Biogeochemical Sulfur Cycling. *Limnology and Oceanography*, 41(6):1330–1334.

Zubkov, M., Linn, L., Amann, R., and Kiene, R. P. (2004). Temporal patterns of biological dimethylsulfide (DMS) consumption during laboratory-induced phytoplankton bloom cycles. *Marine Ecology Progress*, 271:77–86.

Zubkov, M. V., Fuchs, B. M., Tarran, G. A., Burkill, P. H., and Amann, R. (2003). High Rate of Uptake of Organic Nitrogen Compounds by Prochlorococcus Cyanobacteria as a Key to Their Dominance in Oligotrophic Oceanic Waters High Rate of Uptake of Organic Nitrogen Compounds by Prochlorococcus Cyanobacteria as a Key to Their Dominance in. *Appl. Envir. Microbiol.*, 69(2):1299–1304.